Investigation of Instability of a Single Crystal Organic –Inorganic Hybrid Perovskites Used for Photovoltaic Solar Application.

Hessa A. Alsalmah

A thesis submitted to De Montfort University

in partial fulfilment of the requirements for the

degree of Doctor of Philosophy (PhD)

Emerging Technologies Research Centre

De Montfort University, Leicester, UK

2020

Author's Declaration

I declare that the work presented in this thesis was conducted according to De Montfort University regulations. No part herein has been submitted for the purposes of any other qualification at any other academic institution. Permission should be sought for any copying or use, wholly or in part, except for academic purposes or private study, providing the author is acknowledged. The work in this thesis is my own work unless stated otherwise.

Acknowledgements

First and foremost, without any hesitation my gratitude is to Allah for allowing me to complete this research. Special thanks to my supervisors Professor Shashi Paul and Dr Iulia Salaoru, without their patience and guidance this work would not have been possible. A heartfelt appreciation also goes to the technical staff and my colleagues at the university who have been a great help and inspiration.

A loving thanks goes to my husband, Mr. Suleman Alwheepy, who has supported me wholly and I could not have achieved this work without him, and my children Saara, Mohammad, Baadr, Pyadr and Yaser for their patience and understanding throughout the study. Last but certainly not least, I would like to thank my best friends for their never-ending encouragement and support.

Abstract

Due to the problem of global warming, there is an increasing need to gain energy from renewable resources. Development of renewable technologies requires consideration of efficient and reliable materials. Halide hybrid perovskites as a single crystal have been shown to efficient materials for photonic applications which include photovoltaic devices and photodetectors. However, the research lacks understanding of stability mechanisms of these materials under light and temperature found in normal operating conditions. The structural stability of these materials directly affects their electrical properties which are a functional requirement of photonic devices. Therefore, towards the widespread adoption of these materials it was necessary to investigate stability mechanisms of methylammonium lead bromide ($MAPbBr_3$) as a single crystal alone under heat and light conditions using thermal and optical measurements, and as a photonic device structure measuring the effects of heat, light and electrical current using IV measurements.

The research contributes new insights into material stability for $MAPbBr_3$ single crystal. The findings reveal that the application of heat, light, and electrical current, as normal operating factors, have significant effects on material stability and hence performance. A number of different stability mechanisms were identified and a deeper insight into the behaviour of $MAPbBr_3$ single crystal as a device structure was revealed. The research contributed to understanding the role of the interface between the single crystal active layer and electrode materials as having significant influence on stability mechanisms. Understanding the material has important implications for the use of $MAPbBr_3$ as a single crystal in application as a photonic device.

Table of Contents

Tables of Figures

List of Tables

Chapter1: Overview of Research

Chapter1: Overview of Research

1.1 Motivation

Energy today is one of the basic requirements of economic and social development and has become an indispensable aspect for improvement in the quality of life. However, the use of energy has significant environmental impacts. Therefore, it is necessary to provide sufficient and secure renewable energy sources that responds to the needs of the global economy while at the same time protecting the environment.

Although there is wide range of energy sources available, fossil fuels including, coal, oil and natural gas, can be considered the main sources of energy that are used these days. In fact, the consumption of fossil fuels is more than 85% globally, while non-fossil sources including hydroelectric, nuclear, geothermal, solar, tidal, wind, and waste, including biogas represent the rest [1].

This imbalance causes environmental problems and therefore, there is a clear need for renewable energy sources and a need to develop technology in this area. This would include the consideration and development of new, more efficient, technologies taking advantage of novel materials and approaches for further development.

1.1.1 Overview of Fossil Fuel

Fossil fuels originate from the remains of organic matter that accumulated over millions of years. These remains have been processed by micro-organisms which lead to the formation of coal, oil and gas [2,3]. Coal is the main mainstay of power generation in the world, as seen in

Figure 1.1. Discovery of natural oil and gas in 19th and 20th centuries made gas the second source for electricity generation and oil the preferred energy source for the transportation sector [4,5]. However, fossil fuels are not a sustainable source of energy in the long term. Moreover, usage of fossil fuels leads to an increase in the concentration of carbon dioxide and other gases which are responsible for many environmental problems, such as global temperatures and acidification of the oceans. Mainly greenhouse gases (carbon dioxide and chlorofluorocarbons) absorb and reflect the infrared radiation which cause increase in the temperature of earth [6]. This global warming would have a harmful impact on the environment including melting of the polar ice caps, rising sea levels, and desertification [7]. To limit increase in global temperatures, 196 countries in the world agreed at the United Nations conference on climate change in 2015, that reducing CO_2 emissions to ~50% by 2050 is a goal required to avoid damage in the future [8]. In June 2019, the UK parliament passed legislation that requires the UK to be a '"net zero" emitter of greenhouse gases by 2050 towards its commitment to the 2016 Paris Agreement. This agreement cannot be effective unless fossil fuels are substituted with alternative, renewable energy sources.

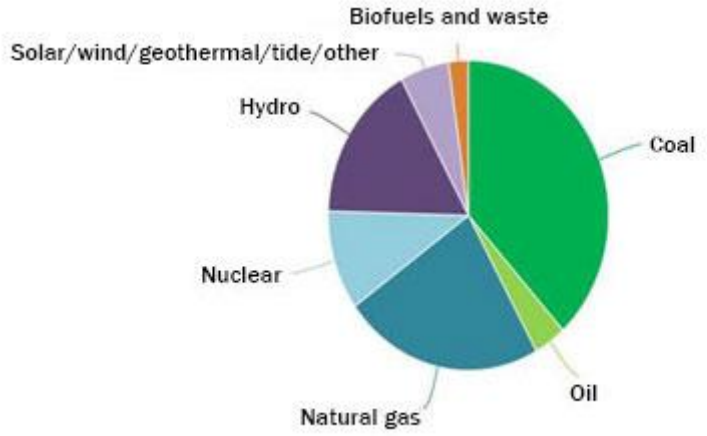

Figure 01.1: Summary of the generated electricity from seven different energy sources in 2016. The data are taken from IEA electricity information, December 2018 [5].

1.1.2 Fossil Fuel Alternatives

Fossil fuel alternatives refer to any energy is produced from sources other than fossil fuels such as geothermal, wind, nuclear, biomass and solar. They are a better choice compared with fossil fuels because they are renewable and environmentally friendly. Nuclear energy is a clean and effective source used to generate electricity, where up to 10 % of the world's electricity was generated by nuclear power in 2015 [5]. However, nuclear waste disposal, which is extremely harmful to flora and fauna, is the fundamental reason behind restriction of nuclear power as an energy source [9].

Alternative energy should come from resources that are renewable. Hence, exploitation of natural source of energy such as wind, sunlight, thermal energy, sea currents and hydro power to create electrical energy have become alternative pillars of exploration. Hydroelectric power is a reliable and safe source of energy; however, it is limited to geographic locations because its construction is in areas that meet the required conditions for such power plants. Furthermore, although hydroelectric power is environmentally friendly it might have environmental consequences such as changes in river levels and an increase in droughts [10]. Another alternative energy source is from wind turbines. Their use has grown rapidly, however, their production of energy is not consistent or unpredictable and depends on daily or seasonal weather, which makes management of electricity production difficult [11]. On the other hand, geothermal and tidal energy are sources of sustainable energy that have predictable output; however, they have very expensive installation costs [12].

The sun is the most abundant and available source of renewable energy because of its stable life, over 4.6 billion years. It is composed of electromagnetic radiation including ultra-violet

(UV), visible light and infra-red (IR) radiation. In fact, the average solar energy production from one square meter of the earth's surface under AM1.5 condition is around 1 KW/m^2 . The sun's energy can meet present power requirements more than 10,000 times over if it is harnessed properly [13]. In addition, it is worth to note that it has diverse applications. Solar energy can be used to produce electricity through photonic devices or solar thermal devices. Therefore, this thesis will focus on solar energy as a renewable energy source.

Semiconductors are increasingly being investigated and adopted for use in photonic devices and include materials such as silicon and germanium. One group of semiconductor materials that are increasingly being explored in photonic devices are perovskites, these organic – inorganic materials offer excellent properties for such devices, however, they are prone to instability and their use requires an understanding of their stability under normal operating conditions. Therefore, the focus of this research is the stability or degradation mechanisms of perovskite, namely, $MAPbBr_3$. Furthermore, this material in a single crystal form offers a more uniform structure with few bulk defects which significantly increases its efficiency in photonic devices, and thus, $MAPbBr_3$ in a single crystal form is investigated for stability under light and heat conditions as a photonic device or as a crystal alone towards contributing to the knowledge that can be used of this material for further exploitation into useful technology .

1.2 Aim and Objectives

To reveal and understand mechanisms of material stability of $MAPbBr_3$ single crystal alone and as a device under light and heat conditions.

Objectives

- Growth of high quality $MAPbBr_3$ single crystal.
- To establish material properties through thermal, optical and electrical characterization techniques.
- Investigation of optimal electrode material for consistent testing and reduction of contact resistance to further reveal stability mechanisms.
- Investigate the effect of light and heat on optical – electrical properties of $MAPbBr_3$ single crystal within a device structure and as a single crystal alone.
- Investigate stability mechanisms of photodetectors and photovoltaic devices with $MAPbBr_3$ single crystal.

1.3 Contributions of this Study

The main contribution of the research is an in-depth understanding of stability and associated degradation mechanisms of $MAPbBr_3$ single crystal alone and when it is used as a part of PV device and photodetectors using reverse bias. The stability of hybrid halide perovskites, while having excellent optical absorption properties, has received little investigation partly due to a

lack of understanding of stability mechanisms of these materials in photonic devices. While ion migration is known to be a leading factor of degradation of polycrystalline materials, this research was the first to address the degradation of $MAPbBr_3$ as a single crystal. Within this main contribution are a number of contributions revealed through a detailed understanding of such mechanisms.

The research contributed an in-depth understanding of the role of the interface and interface materials, namely electrode material and the single crystal itself and the association between the two. Specifically, this included a greater understanding the role of charge extraction rates as it is essential factor in achieving the overall stability mechanism. A related contribution here was the identification of silver as an electrode material for optimal low contact resistance. Furthermore, verification of the process of surface degradation was contributed through identification of the loss of organic and inorganic components from the single crystal.

In revealing phase changes for $MAPbBr_3$ single crystal under various temperatures, itself a contribution of this research, a further contribution was that the length of exposure was significant in effecting such phase changes in $MAPbBr_3$ single crystal specifically. Furthermore, this study also contributes that these phase transitions were at higher temperatures. Another contribution in relation to heat and associated mechanisms was that an increase in temperature resulted in changing the material from a semi-conductor to a conductor.

Finally, the research contributed to understanding the effect of solar spectrum covers wavelengths ranging from UV to IR regions on the $MAPbBr_3$ single crystal as it was observed that unlike previous studies, light by itself has no effect on single crystal alone. However, the

research also contributed that light did have a mediating effect on material stability when the single crystal used as part of PV device and photodetectors .

1.4 Thesis Organisation

The thesis is divided into nine chapters. Chapter 2 is concerned with an overview of Hybrid Halide Perovskite. Chapter 3 presents the Hybrid Halide Perovskite application and stability. The fabrication and various characterisation techniques used in this work is described in Chapter 4, while the results and discussion are presented in Chapter 5, 6,7 and 8. A summary of the major outcomes from this research and suggestions for future works are introduced in chapter 9.

It is important to note that due to the Covid 19 pandemic both photo detectors and solar cells were included up to chapter six which involved the selection of electrode materials for the devices to be tested. However, chapters seven and eight, which involved testing for heat and light respectively, only involved the photodetector device as development of the solar cell device was not possible due to closure of the labs.

1.5 Work Presented at Conference

1-‘‘Thermal behaviour of lead bromide perovskite single crystal’’, H. alsalmah, I. Salaoru, and S.Paul, Methods and applications of crystal structure prediction: Faraday Discussion, 11/07/2018 to 13/07/2018, Murray Edwards College, Cambridge, UK.

2-‘‘Investigation of thermally decomposing in lead bromide single crystal perovskite.’’, H. Alsalmah, I. Salaoru, and S.Paul, Nature Conference: Minerals and Materials for a sustainable future, 11-3 September, 2018.), Trondheim, Norway.

1.6 References

[1] International energy agency, "Estimates for global fossil-fuel consumption subsidies", Iea.org, 2016. [Online]. Available: https://www.iea.org/newsroom/energysnapshots/estimates-for-global-fossil-fuel-consumption-subsidies.html. [Accessed: 20- Dec- 2018].

[2] M. Teichmüller, " The genesis of coal from the viewpoint of coal petrology, " International journal of coal geology, vol 12, no 1-4, pp. 1-87, 1989.

[3] M. Halbouty, "Giant oil and gas fields of the decade 1978-1988: Introduction," 1978.

[4] R. Heinberg and D. Fridley, Our renewable future: Laying the path for one hundred PercClean energy, Island Press, pp. 35-43, 2016.

[5] International energy agency, Electricity Information, Iea.org, 2016. [online]. Available at: https://www.iea.org/statistics/electricity/ [Accessed 20 Dec. 2018]

[6] T. R. Karl and K. E. Trenberth," Modern global climate change," Science (New York, N.Y.), vol 302, no 5651, pp. 1719-1723, Dec 5 2003.

[7] L. G. Thompson, "Climate change: The evidence and our options," The behaviour analyst, vol 33, no 2, pp. 153-170, 2010.

[8] S. Birch and M. Valencia, "UN Climate Change Conference Paris 2015", United Nations Sustainable Development, 2015. [Online]. Available: https://www.un.org/sustainabledevelopment/cop21/. [Accessed: 20- Dec- 2018].

[9] R. Prăvălie and G. Bandoc, "Nuclear energy: Between global electricity demand, worldwide decarbonisation imperativeness, and planetary environmental implications, " Journal of environmental management, vol 209, pp. 81-92, 2018.

[10] B. Stoll, J. Andrade, S. Cohen, G. Brinkman and C. B. Martinez-Anido, Hydropower modeling challenges, 2017.

[11] J.F. Manwell, J.G. McGowan and A.L. Rogers, " Wind energy explained: Theory, design and application," John Wiley & Sons, pp 23-45, 2010.

[12] J. Twidell and T. Weir, "Renewable energy resources, " Routledge, pp. 445-514, 2015.

[13] National Research Council, "Solar influences on global change, " National Academies Press, 1994.

Chapter 2: Overview of Hybrid Halide Perovskites

Chapter 2: Overview of Hybrid Halide Perovskites

This chapter will provide an overview of perovskite materials, including types and their characteristics. In addition, there is an extensive description of hybrid halide perovskites used in photovoltaic devices, considered as semiconductor materials, through their composition structure, their symmetries and phase changes as well as their optical and electrical properties. Furthermore, there is an overview of fabrication methods including the deposition of perovskite thin film and the growth of perovskite single crystals.

2.1 Semiconductor Materials

Generally, conductors, insulators and semiconductors are the main classes for solid-state materials. Most optoelectronic devices employ semiconductor materials which act as insulators at low temperatures, but upon the application of energy (heat), behave as conductors. At room temperature, semiconductors have an intermediate electrical conductivity in the range of 10^{-6} to 10^{5} $ohm^{-1}m^{-1}$. However, the flow electrons and holes can be controlled by adding impurities. Therefore, semiconductor materials can be divided into two groups, namely; intrinsic semiconductors and extrinsic semiconductors. Intrinsic semiconductors can be made from pure semiconductor material such as silicon and germanium, where the number of holes in the valence band and electrons in the conduction band are the same. As result, they possess a high resistance at room temperature, and hence poor electrical conduction. In contrast, adding

impurities to the intrinsic semiconductor material is known an extrinsic semiconductor material. These impurities create a deficiency or excess of electrons which alter their conductivity.

2.2 Perovskites

Perovskites, as intrinsic semiconductors, are an abundant material in nature which attract the attention of material scientists. In modern technologies, perovskites are important because of a variety of their structures which can be exploited to exhibit a range of interesting physical properties. These properties include superconductivity at high temperatures [1], ferroelectricity [2], and metal insulator transition [3]. In addition, it is possible to modify their structure, hence their properties, by changing their composition [4]. Therefore, perovskite materials have shown promise for use in a number of applications.

2.2.1 Discovery of Perovskite Materials

The term ‘perovskite’ was named after Lev Perovski, a Russian mineralogist who discovered a perovskite mineral ($CaTiO_3$) in 1839. Perovskites are solid materials and their structure is based on a ceramic precursor. Since Goldschmidt successfully produced the first synthetic perovskite at the University of Oslo, the term of perovskite has become used as a description for the family of compounds that have a similar type of crystal structure as calcium titanium oxide ($CaTiO_3$) [5]. The structure of the perovskites was reported by Helen Dick Megaw in 1945 who characterised the crystal structure of both $CaTiO_3$ and $BaTiO_3$ using x-ray diffraction [6].

2.2.2 Perovskite General Structure

The perovskite structure is ABX_3 whereby A is the monovalent cation, B is the smaller metal, in diameter, divalent cation, and X represents the anions. The B cation and X anions come together to form octahedrons that connect together forming cubic voids. Hence, the crystal structure of perovskite compounds has a three-dimensional network of corner-sharing BX_6 octahedrons with cation A with 12-fold coordinated anions as shown in Figure 2.1. Furthermore, the structure can incorporate most metal ions with a significant number of different anions. As a result, perovskite structure is considered one of the most frequently encountered structures in solid state chemistry [7].

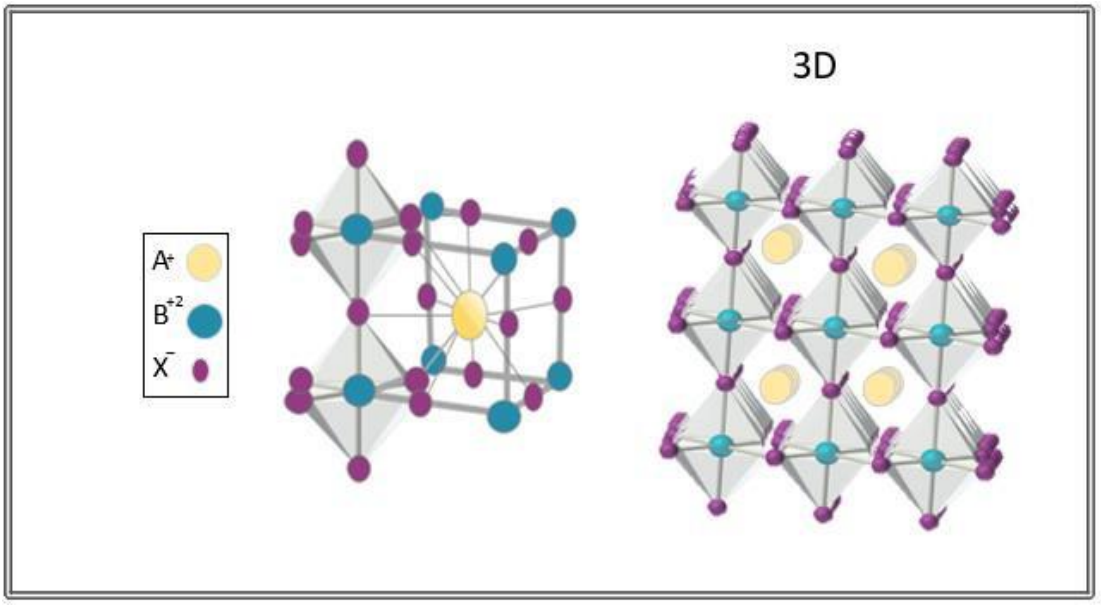

Figure 02.1:An ideal cubic perovskite structure ABX_3 where A+2 ions in the 12-fold cavities set in the centre of the cubic structure with 3 D net of corner sharing BX_6 octahedra

Charge balancing can be obtained in various ways based on the formal stoichiometry of the perovskite structure where the overall charge must be electrically neutral ($q^A + q^B = -3q^X$). For this reason, there are two main types of perovskite, namely, metal oxide perovskites and metal halide perovskites. For the former, metal oxide perovskites, the valence of the two metal cations should have a total value of six, ($q^A+q^B = -3q^O=6$). These types of perovskite can have any of the following compositions: I-V-O_3, II-IV-O_3 and III-III-O_3 which means they have elements from groups I, II, III, IV from the periodic table, examples of these include $KTaO_3$, $CaCrO_3$ and $GdFeO_3$. Alternatively, metal halide perovskites have only one possible composition which is a I- II-VII_3 whereby the two cations should have a total value of three, ($q^A+q^B = -3q^X=3$). For metal halide perovskites, the monovalent metal can be replaced by an organic cation which should have the same charge as the inorganic divalent metal cation [8].

However, the perovskite structure in figure 2.1 is rarely achieved at room temperature. The significant factor that can cause the distortion of perovskite structure is the size in terms of diameter of the elements. For example, in order to get a three-dimensional (3D) perovskite network, selection of a molecular cation is limited by the void size inside the enclosed octahedral. If the size of A cation is too large, then the perovskite structure is broken. Furthermore, a transition in the dimensionality of the perovskites exhibit unique chemical and physical properties, for example, the symmetry-breaking characteristics of oxide-perovskites allows for dielectric properties which includes ferromagnetism, piezoelectricity, ferroelectricity [9].

Most perovskites have symmetry that is less than a perfect cubic symmetry as can be seen in Figure 2.2 (b). There are 16 possible symmetries of the perovskite structure [10]. Where non-spherically symmetric ions are used, for example, an organic A cation (Figure 2.2 (a)) such as those found in methylammonium, it is possible to have more space-group symmetries [9]. In

addition, widely used organic components in the A site for hybrid perovskites change the perovskite geometry, so the symmetry is reduced in comparison to inorganic perovskites which are presented in the next section.

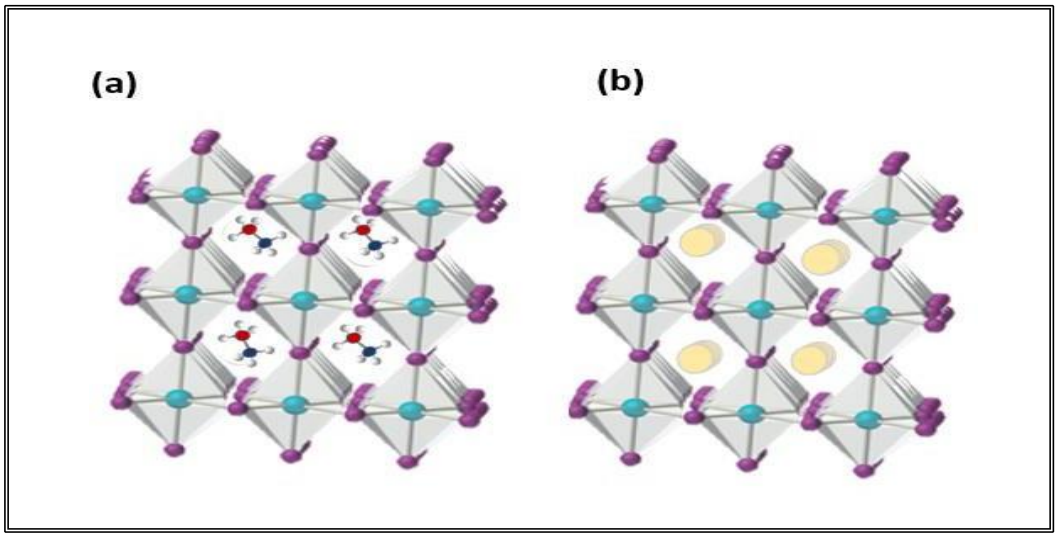

Figure 2.2.2.22: General structures of (a) organic-inorganic perovskites and (b) inorganic perovskite

It is also likely that octahedral tilts are a result of the smaller size of the A cation. Therefore, the geometrical conditions required to obtain a perfect packed perovskite structure can be estimated by using the Goldschmidt tolerance factor [11]. For this tolerance factor the following relation has to be achieved: t $=(r_A + r_B)/\sqrt{2}(r_B + r_X)$ (r_A, r_B and r_X are the ionic radii of '*A*', '*B*' and '*X*'). When the ratio (t),where there is a deviation from the Goldschmidt tolerance factor, there will be a lower symmetry of the A, B and X ions. For example, the stable structure of oxide perovskites exists in a range of 0.89 < t < 1. A lower value tolerance factor (t < 0.89 or 1.0 < t) leads to low symmetry [12]. Alternatively, a stable halide perovskite structure exists in the range of 0.85 < t < 1.1. For example, Methylammonium lead bromide perovskite ($MAPbBr_3$) has the cubic phase at room temperature, while the structure of lead iodide

perovskite ($MAPbI_3$) is in the tetragonal phase because of the large radii of halide (I^- (2.2 Å) and Br^- (1.96 Å)) [13].

Another consideration for a favoured symmetry is the BX_6 octahedron which is important in its own right as an individual identity, and the ratio $\mu=r_B/r_X$ also referred to as the *octahedral factor*, is required for a favoured symmetry. Empirical structure maps of $t-\mu$ indicate the formation window of a perovskite is limited to $\mu>0.414$ for oxide-perovskites and $\mu>0.442$ for halide-perovskites [14,7].

In order to achieve a stable perovskite structure, it is also necessary to calculate the electrostatic potential, thus, Madelung (electrostatic, coulomb) potential is a property of the crystal structure which depends on lattice energy and site electrostatic energies. For the halide perovskite stoichiometry, an electrostatic lattice energy is just –29eV/ unit cell, while the lattice energy for oxide perovskite is higher than 105 eV/cell as can be seen in the table below, depending on the charge imbalance between the A and B sites. Consequently, a relatively low electrostatic lattice energy of halide perovskite structure leads to their instability compared with oxide perovskites [8].

Table 2. 1:Lattice energy (eV/cell) and electrostatic potentials (in units of V) for each composition of stoichiometric perovskite oxide and halide (Cubic Lattice, a= 6 Å) [8].

		ABX_3		
Stoichiometry	Lattice energy(eV/cell)	V_A (V)	V_B (V)	V_X (V)
I-V-O_3	-140.48	-8.04	-34.59	16.66
II-IV-O_3	-118.82	-12.93	-29.71	15.49
III-III-O_3	-106.92	-17.81	-24.82	14.33
I-II-VII_3	-29.71	-6.46	-14.85	7.75

In the last decade, numerous reports have been published on the various structures of Organic-inorganic hybrid halide perovskite materials, characterisation of their fundamental properties and the development of their efficient applications. One such example of these efficient applications is the photovoltaic (PV) cell, reaching an efficiency of more than 22% [15] which competes with the other existing materials used in PV technologies. In addition, efficient optoelectronic properties of hybrid halide perovskite and easy and low-cost fabrication have caught the attention of chemistry and materials scientists in different fields, including photodetectors [16- 21], solar cells [21-24], LED's [25-27], x-ray detectors [28-30], lasers [31-33] and phototransistors [34]. However, for use in PV technologies there are serious concerns for its commercialisation because of potentially poor structural stability. This research is concerned with such stability under the operating conditions which would include consideration of the effects of current, heat and light.

2.3.1 Discovery of Halide Perovskite Materials

The first appearance of the halide in the perovskite structure was in 1958 by Moller [35]. It is notable that a variety of halide components allowed the properties of photoconductors in $CsPbX_3$ to be tuned [35]. Crystalline properties of hybrid perovskites were described by Weber in 1978 in his description of methylammonium lead halide, Mitizi et al. (1995) described the electrical properties and molecular structure of a hybrid metal halide perovskite (Sn-based) [36,37].

Since then these materials and the associated applications has been a rapidly developing area extending to a number of different research fields [38].

2.3.2 Crystal Compositions

As mentioned above, perovskites have a limited number of ions in the ABX_3 structure because the formal oxidation states of the two cations must be equal to three which means the anions can only come from group VII. It is possible for the A cation to be occupied by either an inorganic element such as Rubidium (Rb), Potassium (K), or Cesium (Cs) cations, or an organic compound such as RNH_3 which can be alkyl or phenethyl. Ethylammonium ($EA=CH_3CH_2NH_3$), Formamidnium ($FA=CH(NH_2)_2$), Methylammonium ($MA=CH_3NH_3$) are commonly used as organic compounds [39]. Most B cation is Lead (Pb) and sometimes it is occupied by Tin (Sn), Germanium (Ge), or Bismuth (Bi), and as for the X site it may be occupied Iodide (I), Chloride (Cl) or Bromide (Br) [40,41]. Furthermore, the site of A, B or X ions can be a mix of two or three elements instead of individual components, improving the properties of their structure. For example, MA with FA in $(MA)_X(FA)_{1-X}PbI_3$ can tune the band gap, while increasing Cs composition in $(Cs)_X(MA)_{1-X}PbI_3$ leading to improved stability [42].

There are a number of properties which make these semiconductors materials suitable for optoelectronic devices which include a direct band gap, long lifetime of the charge carrier, a high carrier mobility, as well as a high absorption coefficient to electromagnetic radiation [43-46].

2.3.3 Symmetry and Phases

The present research is concerned with the use of 3D perovskites. By the spatial arrangement of the octahedral inorganic units $[PbX_6]^{-4}$, the hybrid halide perovskite is able to form different dimensions at the molecular level including 3-dimensional (3D), 2-dimensional (2D), 1-dimensional (1D), and zero-dimensional (0D) networks. Each group of these materials exhibit interesting physical and chemical properties which make these compounds ideal for a variety of applications, particularly in optoelectronic devices, including photovoltaic cells, photodetectors and light-emitting diodes (LEDs) [42, 47-49].

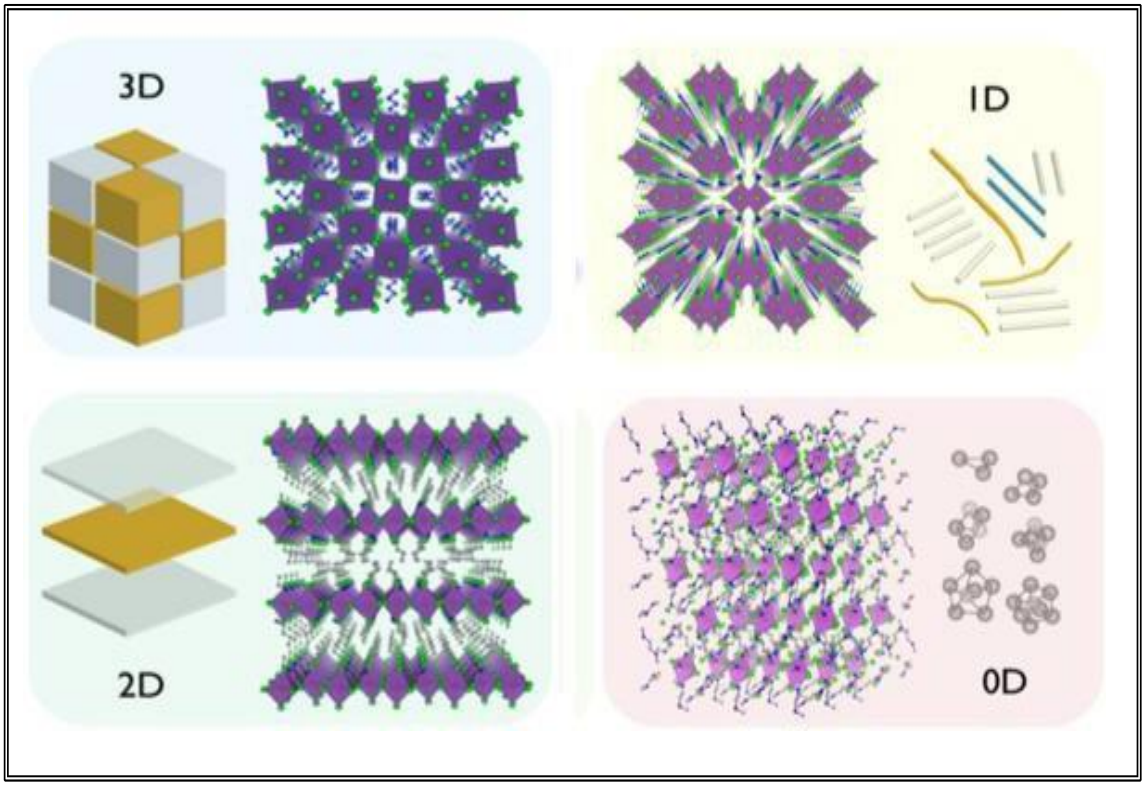

Figure2.3: Typical structures and their corresponding conventional materials for perovskite with different dimensionalities 3D (as bulk) , 2D (quantum wells), 1D (quantum wires), and 0D (clusters) , these images are reproduced after the permission from ACS Publications[49]

2.3.3

It necessary to point out that the size of A cation can be manipulated in order to get a variety of perovskite structures. For example, if the A site is occupied by a monovalent cation such as

Rb^+, Cs^+, $CH_3NH_3^+$, and $HC(NH_2)_2^+$, then a 3D framework is achieved [47] because the organic cations are of a size where they can fit into the inorganic octahedral cage. In other words, each inorganic octahedral is connected to six neighbouring halide ions forming a 3D perovskite [50,51]. However, if a larger organic cation occupies the A site, it will result in a 2D or 1D structure. Therefore, a large A cation leads to the 3D framework being destroyed. For 2D perovskite, each metal halide octahedra is connected with four neighbours of $CH_3CH_2NH_3^+$, forming a sandwich between two layers of organics, while a separate infinite chain forms a 1D network. This is a result of connecting the inorganic octahedra at two opposite corners with its neighbours whether sharing the face, edge or corner [8,47, 52, 53]. For the zero-dimensional network, inorganic octahedra, whether individual or as clusters, are isolated by the organic molecules [49]. Additionally, halide perovskites must adhere to allowable tolerances so that a required crystal symmetry is achieved. This structural dimensionality can be tuned in order to achieve the 0D, 1D, 2D and 3D structures, this is achieved through adjustments to the organic – inorganic molar fraction [54].

The normal structure of the parent perovskite ABX_3 is cubic. However, the structure of perovskite usually undergoes a variety of structural dynamics which are temperature dependent [42]. Since the organic cation cannot be steady in the lattice of inorganic octahedra at room temperature and it has low thermal fluctuations during its rotation, there are distinct positions for cation molecules with the coordinates x, y, z described depending on the resistance of the inorganic octahedron [55, 56]. Therefore, the interaction of hydrogen bonding, which is formed between the organic molecule and inorganic framework (X....H-N) is responsible for all geometrical changes inside the network [57]. At low temperature phases, cation molecules have preferred orientations, while highly disordered orientation is observed at high temperatures [55, 58]. Due to the conditions when preparing the perovskite sample, such as non-stoichiometry of the constituent ions in the precursor salts and rapid crystallisation, it is likely chemical defects

are introduced, and its concentration affects the temperature of phase transition. The existence of fewer defects leads to the crystal domains staying longer in a specific phase compared with a higher number of defects [59-61].

Weber was the first to describe the dynamic disorder in the hybrid halide perovskite structure ($MAPbX_3$, where X= I, Br or Cl) [55]. The perovskite structure has three structural phases, namely; the cubic phase, the tetragonal phase and the orthorhombic phase [42,55]. Although there are schemes suitable for describing phase transitions for perovskite materials that have inorganic cations [10,62], it is necessary to consider the order-disorder transitions of the MA cations as organic cations [48].

A pertinent question for the present study in relation to the structural phase transitions of $MAPbX_3$ is whether or not they affect photovoltaic performance. There have been studies that have investigated how the phase transitions affect thermal [63], optical [64], dielectric [65] and photovoltaic properties [66]. Experiments with $MAPbI_3$ to determine the electronic structures of each of the three phases have found that between the cubic and tetragonal phases the effects are relatively minor, but for the transition between the tetragonal and orthorhombic phases the effects are much larger [48]. In this study, I have investigated the formation and properties of Methylammonium Lead bromide Perovskite material as a single crystal structure.

2.3.4 Intrinsic Properties of Hybrid Halide Perovskite

Hybrid halide perovskite is semiconductor material, which is based on an interplay of organic and inorganic components at the molecular level. It is sequentially repeating, constructing a structural network. Thus, useful properties of organic and inorganic materials appear through

merging these materials together. Hybrid halide perovskites are non-covalent compounds (hydrogen bonding interactions), unlike common semiconductors such as Si, CdTe, GaAs, which are covalent compounds [57,67]. A combination of these materials provides the structural shape, stability and enhancement of the physical and chemical properties. Within each perovskite network, the organic molecule has remarkable properties allowing for cheap materials and low manufacturing cost; altering of chemical structure through tuning; lightweight materials, and high optical transparency. While the inorganic framework can provide interesting properties such as high electric transport, magnetic interactions, notable mechanical hardness and more environmental stability [68,69].

By using the same chemical formula (ABX_3), intrinsic multidimensional structures can form with different compositions of various components. This variety of structures affords variety in chemical and physical properties which make them suitable for various applications, particularly photonic devices. Additionally, these materials can be processed in a solution at low temperatures while at the same time keeping their high crystallinity, this is in addition to a low number of defects in the mesoscopic semiconductor films which further support their application in solar cells [70,71]. This processing allows various forms of perovskite materials, ranging from nanocrystals to single crystals to be produced. With respect to manufacture, the synthesis, which is solution based, is a cost-effective way of achieving crystalline films as opposed to high vacuum-based synthetic approaches which use a lot of energy [73]. It is the characteristic of the properties of perovskite materials that allow their phenomenal performances, of which includes their strong optical performance and adjustable band gap [74-76]. Furthermore, it is possible to tune the optical and electronic properties of hybrid perovskites [42].

2.3.4.1 Intrinsic Electronic Properties

To characterise perovskite materials electrically, it is essentially a quantitative determination of properties such as types of charge carriers, concentration of charge carriers and their mobility. All are dependent on the method used to prepare these materials [77]. The electronic properties of hybrid perovskites are related to their structure, specifically, the bond between B and X that is found in the inorganic framework. Although it is important to note that the A cation does not directly affect the electronic properties, the size of the A cation can contribute to distortion between the B – X bond which can have a negative effect on the symmetry [52,78,79] to such an extent that the 3D framework could be destroyed in addition to reduced dimensionality. In hybrid perovskite materials, the electronic levels in the BX_6 octahedral contribute to the electronic properties. In methylammonium Methylammonium lead bromide ($MAPbBr_3$), for example, the valence band (VB) consists of strong coupling between Br-4p and Pb-6s orbitals (lone pair), while the conduction band (CB) consists of a mixture of Pb-6p and others orbitals from the conduction band [17, 78, 80,67].

Concentration of chemical defects affects electronic properties since these defects act like trap states located somewhere between the conduction band and valence band. Defect density can be reduced by light which leads to improved electrical characteristics [59, 61].

The symmetry or cubic symmetry is important for perovskite materials because it allows for optimum properties, and there are a number of reasons for which a deviation tolerance could take place including size effects [42]. If crystal atoms are mismatched beyond what is acceptable it can lead to octahedral tilting which has an effect on the electronic properties of the material.

2.3.4.2 Intrinsic Optical Properties

Hybrid perovskites exhibit physical properties including a direct band gap and a high absorption coefficient which compares to semiconductor materials such as amorphous silicon (a-Si), single silicon (c-Si) and Gallium arsenide (GaAs). It can be seen that a thin layer of perovskite material (500 nm) has a higher absorption coefficient than others, obtaining good photocurrents.

The high absorption coefficient in hybrid halide perovskite is related to the high symmetry and hence a direct band gap and high probabilities of optical transition (p-p) where it is enabled by the Pbs orbital lone pair [39,67, 80,81].

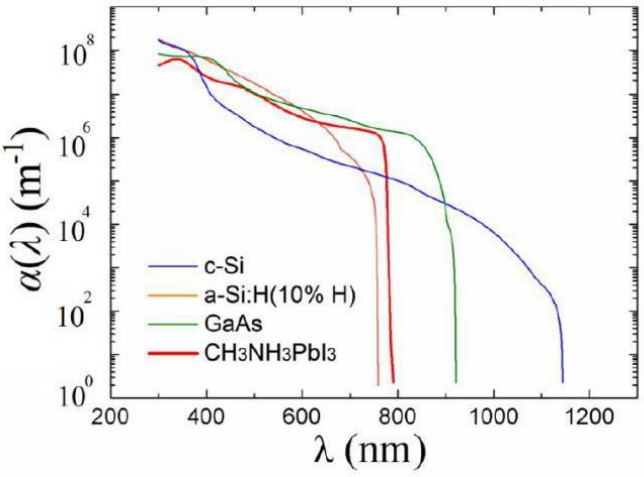

Figure2. 4: Absorption coefficient for various semiconductor materials namely; c-Si, a-Si:H, GaAs and perovskite , this figure is Reprinted with permission from ref 82

.

This strong optical absorbance allows for absorption across the visible light spectrum from a thickness of only 500nm of perovskite film. It is possible through the modification of hybrid perovskite materials to extend optical absorption performance which is an important property in designing optoelectronic devices. For example, the absorption spectra for $MAPbI_3$ and

$MAPbI_{(3-x)}Cl_x$ are virtually the same, with absorption onset at approximately 800 nm, however, $MAPbI_{(3-x)}Br_x$ gives an absorption onset at 700 nm [74, 83,84].

2.4 Preparation Methods of Hybrid Halide Perovskite

Hybrid perovskite-based materials can provide noteworthy properties when used in optoelectronic devices, such as broad absorption, tuneble optoelectronic properties, high charge mobility, and long carrier lifetime. Within a few years, many intensive investigations have been based on the preparation of high-quality perovskite devices. This is related to the fact that the efficiency of the devices is determined by the purity of polycrystalline perovskites, crystallisation and the morphology of the perovskite, which are controlled by the synthesis procedures.

Despite the fact that most reports have been focused on the perovskite in polycrystalline form, the single crystal is another form of perovskite that has exhibited as a single grain without the appearance of any grain boundaries. Generally, both types of perovskite are made from a solution process which is considered to be easy and low-cost. However, each form has specific techniques for fabrication. Here, these fabrication techniques are summarised.

2.4.1 Perovskite Thin Film Deposition

Lead halide perovskites have been produced by two popular methods namely, solution-processed technique and vapour deposition. Precipitation from a solution is a common technique because it uses simple and inexpensive equipment. However, deposition from the

vapour phase is known to provide better uniformity in the deposition layer compared to the solution processed technique.

2.4.1.1 Solution Processed Technique

Spin coating is the most common technique used for preparation of perovskite thin film compared to doctor-blade coating, spray coating and inkjet printing [85]. The one-step method uses spin coating for the deposition of the precursor solution of perovskite directly onto the substrate, then an annealing treatment is immediately carried out on the sample in order to form larger crystal grains [86]. To obtain more high-quality perovskite thin films, this technique was developed using a two-step solution process including the sequential solution deposition method and the vapor-assisted solution process. The sequential solution deposition method is a simple technique which consists of two steps. The first step involves spin coating only an inorganic component solution instead of the complete precursor solution. The second step involves dipping the substrate into the organic component [76]. After heating at a suitable temperature, perovskite is formed and crystallised into a thin film. Compared to the sequential solution deposition method, the vapour treatment is used in the vapor-assisted solution process. After depositing the inorganic component from the solution onto the substrate by using spin coating, the organic component vapor was spread out on the substrate. Finally, a perovskite thin film formed after heating the substrate [87]. Moreover, although the preparation methods seem to be different, they demonstrate that adjusting parameters in any steps such as temperature, treatment time, speed of spinning and the concentration of solutions are effective controllers to gain high quality film, hence high-performance devices.

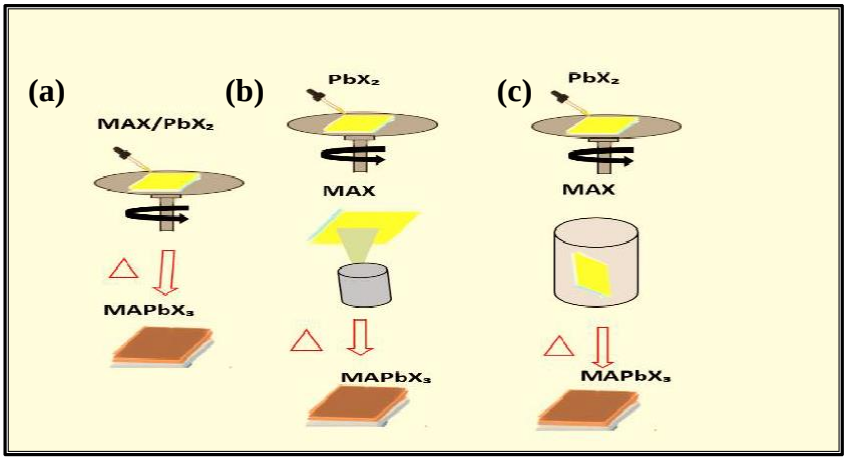

Figure2. 5 : Solution techniques for deposition of perovskite layer: (a) one-step method, (b) vapour-assisted solution method and (c) sequential deposition method

2.4.1.2 Vapour Deposition

Vapour deposition is a technique that uses condensation, or the reaction of vaporised materials in order to prepare perovskite thin films over the substrates. A high uniform perovskite film can be produced by one step (dual source vapor deposition) or two steps (vapor-assisted solution process and sequential vapour deposition). Dual source vapor deposition or vacuum deposition is a quick deposition technique in which the organic and inorganic source are co-evaporated and reacted onto the surface of the substrate in the vacuum system, forming a perovskite thin film with a uniform step coverage. Due to difficulty in monitoring the deposition rate of the organic source, sequential vapour deposition was developed, in which the vapour of the inorganic source was deposited first into the substrate, followed by deposition of the organic component vapor [88]. Although this method requires relatively high energy for film fabrication compared to the solution process, which was explained above, it provides better efficiency because of its high quality [89].

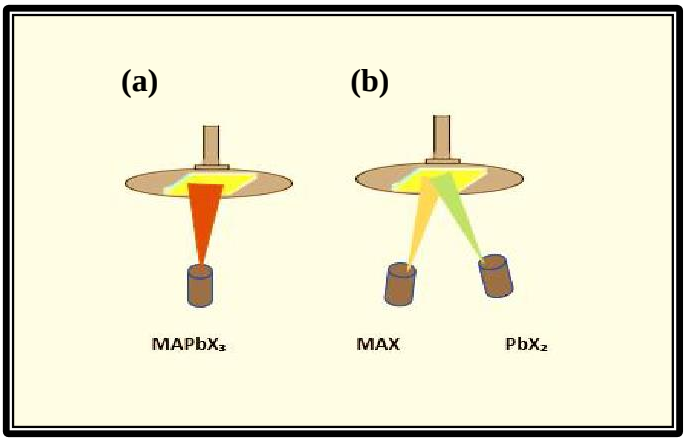

Figure2.6: Vapour techniques for deposition of perovskite layer: (a) one-step method, and (b) two-step method

.

2.4.2 Single Crystal Perovskite

It is known that the polycrystalline thin film can be produced by the solution method where the annealing procedure assists to gain better crystallisation and a highly uniform thin film. Similarly, the solution method is always used for growing hybrid halide perovskite single crystals [19, 90-92]. Generally, the term "crystal" refers to a solid object in which the constituent atoms, molecules, or ions are exhibit a regularly ordered, periodically repeating pattern in three dimensions [93].

High-quality hybrid halide perovskite single crystals answer a number of the disadvantages of polycrystals, this is because they have no grain boundaries due to a continuous crystal lattice and the fact that there are no defects which afford the single crystal structure its optical properties [94]. The superiority of the single crystal structure in hybrid perovskites has been reported in a number of studies [19,17, 90-92] whereby the optoelectronic properties are superior to the polycrystalline structure, this includes longer carrier lifetimes and mobilities and therefore, significantly longer diffusion lengths. [94-97].

Single crystal perovskites have consistently shown better results in terms of diffusion length, lifetime, mobility and trap density for $MAPbBr_3$ and $MAPbI_3$ respectively (see Table 2.2).

Table 2. 2: comparison between $MAPbBr_3$ and $MAPbI_3$ single crystal perovskites

	$MAPbBr_3$	$MAPbI_3$
Diffusion length	4.3 µm	10.0 µm
Lifetime	28 ± 5 ns	18 ± 6 ns
Mobility	24.0 cm^2/Vs	67.2 cm^2/Vs
Trap Density	3×10^{10} cm^{-3}	1.4×10^{10} cm^{-3}

They have been extensively studied as single crystal structures in comparison to polycrystalline structures [94;95;70; 98]. For example, the trap densities for hybrid perovskite single crystals have been shown to be lower than polycrystalline film. Specifically, single crystals appear to have a trap densities values of ~10^9 - 10^{10} cm^3 while polycrystalline films have trap densities value of ~10^{15} - ~10^{16} cm^{-3} . These very low to moderate trap densities are often observed in high quality semiconductors such as Silicon, whereby the single crystal structure yields a trap density of $10^9 – 10^{11}$ cm^{-3} compared to $10^{13} – 10^{14}$ cm^{-3} for the Silicon polycrystalline structure [91].

These low trap densities, low non-radiative recombination losses, high radiative efficiency, and long carrier diffusion lengths mean they have comparable performance with silicon and could have better optoelectronic performance overall [24, 99]. Beside tunable electrical and optical properties of hybrid halide perovskite, there are a number of properties that have been attributed to perovskite single crystals which include broad absorption from the near visible to near-infrared region of the light spectrum, lower charge scattering, ultra-low trap densities [100, 101].

Since the optoelectrical properties of hybrid halide perovskite materials, and their device efficiencies are directly affected by the microstructure of hybrid halide perovskite, perovskite single crystals offer the possibility to study the fundamental intrinsic properties of hybrid halide perovskites [102, 103].

2.4.2.1Single Crystal Growth

Since crystal growth is a controlled phase transformation, the process of forming single crystals from a homogenous medium has captured the interest of both people from industries and academic institutions due to the fact that the fabrication of devices from crystals critically depends on the homogeneity and quality of the single crystal. In addition, both separation and purification occur during a single operation which leads to gaining a crystalline solid with a high level of purity and low operating cost. Furthermore, the process of crystallisation can control the thickness and amount of crystals formed [19,90,91].

To grow hybrid halide perovskite single crystals, the supersaturation solution can be achieved by different methods. To date, mainly three different methods have been extensively reported which are the temperature-lowering method, anti-solvent vapour diffusion method and inverse temperature crystallisation method.

A. Temperature-Lowering Method

Temperature –lowering solution growth is widely used in the growth of bulk crystals because it is a relatively simple technique and produces good quality crystals. The basic principle of this method is to produce single crystal perovskite by cooling the precursor where the supersaturation is achieved by lowering the growth temperature [55, 104,105]. This method is

suitable for the preparation of crystals for materials having poor solubility in their solvents at room temperature, while the solubility of the substances increases with an increase the temperature.

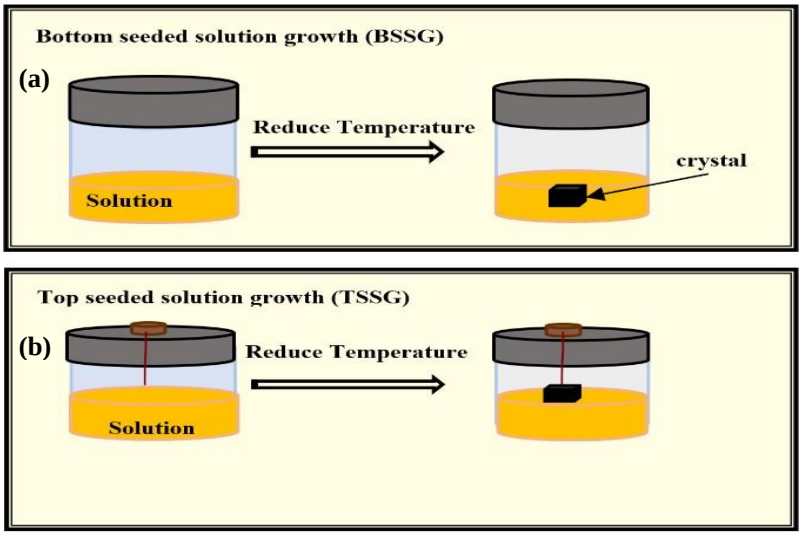

Figure2.7: a) Illustration of crystallisation of BSSG method showing the position of seed crystals, and b) illustration of crystallisation from TSSG.

The temperature lowering technique is used for the growth of large sized hybrid halide crystals with adjustable thickness [105,106]. After obtaining the small crystals from spontaneous nucleation, these crystals are selected as seeds and dropped back into the precursor solution, continuing with the temperature-lowering process. There are two ways employed based on a fixed position of the seeds which are the top seeded solution growth method (TSSG) and the bottom seeded solution growth method (BSSG). The principles of both processes have been illustrated in Figure 2.7. The top seeded solution growth method (TSSG) is the first version where seed crystals are placed at the coldest point of the solution and its growth stops when the solution becomes saturated. While the bottom seeded solution growth method (BSSG) is when seeds are put at the bottom of the medium [104,105]. However, these methods are highly time-

consuming. In order to gain a one-centimetre sized crystal, it might typically take more than two weeks, resulting to limits in its extensive use [105,107].

Additionally, these methods require applying a range of temperatures which is another disadvantage. Furthermore, there is a narrow temperature range that is suitable for growing crystals which means much of the solute dissolved in the solution remains without any benefit at the end of the grow period [108].

B. Anti-solvent Vapour Assisted Crystallisation Method (AVC)

Anti-solvent vapour (AVC) diffusion is the most typical method used to grow crystals and is suitable for those materials that are highly soluble in certain solvents but are poorly soluble in others [109]. Using the AVC method, a supersaturated solution can be achieved by slow diffusion of anti-solvent, which is usually a solvent with poor solubility of the perovskite, in a perovskite precursor solution. The size of the crystals is up to few millimetre. The working principle of this technique has been shown in Figure 2.8 [109,110].

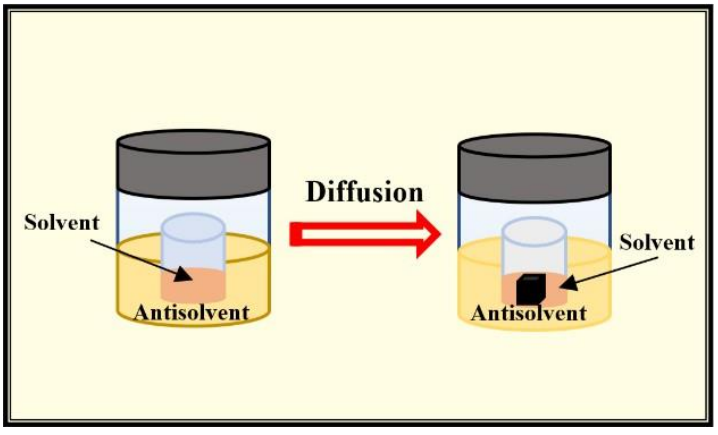

Figure2. 8:Schematic of the Anti-solvent vapour diffusion apparatus and Methylammonium lead bromide perovskite crystal growth

An anti-solvent vapour diffusion method was recommended for the small sized, high quality growth of perovskite single crystals. The Shi group (2015) argued that this method has high applicability and efficiency for the growth of single crystals for hybrid halide perovskites [91]. However, this method has rapid precipitation leading to the formation of small crystals. Hence, it is difficult to control particle characteristics including shape and size [111].

C. Inverse Temperature Crystallisation Method (ITC)

The Inverse Temperature Crystallisation (ITC) method is widely used for growing single crystals in which the precursor solution is not saturated and slowly becomes a supersaturated solution by evaporation of the solvent. It is usually heated up in an oil bath at a fixed temperature rather than cooling it down, resulting in obtaining perovskite crystals at the bottom of the solution. Compared to the temperature lowering method, it is suitable for substances that have a high solubility at room temperature in particular solvents, but the solubility decreases with an increase in temperature. For example, inverse temperature solubility behaviour is exhibited for $MAPbBr_3$, $MAPbI_3$, and $MAPbCl_3$ single crystal in the solvents DMF, GBL, and DMSO, respectively [17, 19, 100,121].

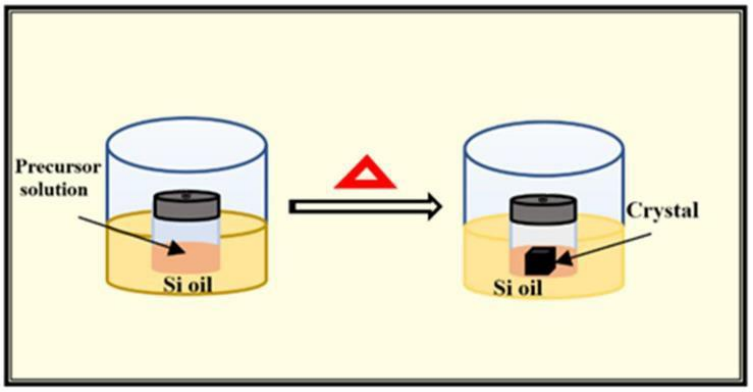

Figure2. 9: Schematic of the Inverse temperature crystallisation apparatus and Methylammonium lead bromide perovskite crystal growth

Additionally, the continuous enlargement of the crystals can be obtained by replacing the growth solution which depletes with the passage of time and using a template for controlling the shapes of the perovskite single crystals [113]. Importantly, a large-area and high-quality perovskite crystal film grown by using this method [114].

Distinctively, this method not only produces the large-sized (millimetres to centimetres) hybrid organo-halide perovskite single crystals at very fast rate, but it also maintains their carrier transport properties compared to other crystallisation methods [90,91,113, 115].

The ITC method has been chosen as a method of choice for the crystallisation of $MAPbBr_3$ for this research owing to particular advantages of this method compared to other crystallisation methods.

2.5 Summary

This chapter has provided an overview of perovskite materials, their types and characteristics. Specific attention has been shown towards the organic—inorganic hybrid halide perovskite towards an understanding of the instability process in perovskite materials used in photonic applications. The composition of hybrid halide perovskite, their symmetry and phases were discussed which directly impact on their optical and electrical properties. In addition, fabrication methods of hybrid halide perovskite are highlighted, including deposition of perovskite thin film and growth of perovskite single crystals.

2.6 References

[1] Y. Maeno et al., "Superconductivity in a layered perovskite without copper", *NATURE*, vol.732, pp. 532-534, 1994.

[2] Vonhippel, "Ferroelectricity Domain Structure, and Phase Transitions of Barium Titanate", *Reviews of modern physics*, vol. 22, 1950.

[3] J. Torrance, P. Lacorre, A. Nazzal, E. Ansaldo and C. Niedermayer, "Systematic study of insulator-metal transitions in perovskites RNi03 (R =Pr, Nd, Sm, Eu) due to closing of charge transfer gap", The American Physical Society, vol. 45, no. 14, 1992.

[4] A. Benedek and J. Fennie, "Why Are There So Few Perovskite Ferroelectrics?", *The journal of physical chemistry c*, vol. 10, 2013.

[5] G. Meyer, "THE SYNTHESIS AND STRUCTURES OF COMPLEX RARE-EARTH HALIDES", *Pergamon Press Ltd*, vol. 14, 1982.

[6] D. Megaw, "Crystal structure of double oxides of the perovskite type", *THE PROCEEDINGS OF THE PHYSICAL SOCIETY*, vol. 58, no. 326, 1946.

[7] C. Li, K. Soh and P. Wu, "Formability of ABO3 perovskites", *Journal of Alloys and Compounds*, vol. 372, no. 40-48, 2004.

[8] M. Frost, T. Butler, F. Brivio, H. Hendon, M. Schilfgaarde and A. Walsh, "Atomistic Origins of High-Performance in Hybrid Halide Perovskite Solar Cells", *American Chemical Society*, vol. 14, no. 2584-2590, 2014.

[9] K. Aleksandrov and J. Bartolome, "Structural distortions in families of perovskite-like crystals", *phase transitions: a multinations journal*, vol. 743, no. 255-335, 2001.

[10] A. Glazer, "The Classification of Tilted Octahedra in Perovskites", *CRYSTAL STRUCTURE OF PARPANIT*, vol. 28, no. 3384, 1972.

[11] B. Mitzi, "Templating and structural engineering in organic–inorganic perovskites", *The Royal Society of Chemistry*, vol. 1, no. 12, 2001.

[12] M. Johnsson and P. Lemmens, "Crystallography and Chemistry of Perovskites", *Handbook of Magnetism and Advanced Magnetic Materials*, vol. 4, 2007.

[13] J. Noh, S. Im, J. Heo, T. Mandal and S. Seok, "Chemical Management for Colorful, Efficient, and Stable Inorganic– Organic Hybrid Nanostructured Solar Cells", *American Chemical Society*, vol. 13, no. 17641769, 2013.

[14] C. Li, X. Lu, W. Ding, L. Feng, Y. Gao and Z. Guo, "Formability ofABX3(X= F, Cl, Br, I) halide perovskites", Acta Crystallographica Section B Structural Science, vol. 64, no. 6, pp. 702-707, 2008.

[15] N. Jeon et al., "A fluorene-terminated hole-transporting material for highly efficient and stable perovskite solar cells", *Nature Energy*, vol. 3, no. 8, pp. 682-689, 2018.

[16] J. Gao et al., "Single-crystalline lead halide perovskite wafers for high performance photodetectors", *Journal of Materials Chemistry C*, vol. 7, no. 27, pp. 8357-8363, 2019.

[17] G. Maculan et al., "CH3NH3PbCl3 Single Crystals: Inverse Temperature Crystallization and Visible-Blind UV-Photodetector", *The Journal of Physical Chemistry Letters,* vol. 6, no. 19, pp. 3781-3786, 2015.

[18] Y. Wang et al., "Solution-processed photodetectors based on organic–inorganic hybrid perovskite and nanocrystalline graphite", *Nanotechnology*, vol. 27, no. 17, p. 175201, 2016.

[19] M. Saidaminov et al., "High-quality bulk hybrid perovskite single crystals within minutes by inverse temperature crystallization", *Nature Communications*, vol. 6, no. 1, 2015.

[20] B. Sutherland et al., "Sensitive, Fast, and Stable Perovskite Photodetectors Exploiting Interface Engineering", *ACS Photonics*, vol. 2, no. 8, pp. 1117-1123, 2015.

[21] F. Palmstrom et al., "Enabling Flexible All-Perovskite Tandem Solar Cells", Joule, vol. 3, no. 1-12, 2019.

[22] P. Schulz, E. Edri, S. Kirmayer, G. Hodes, D. Cahen and A. Kahn, "Interface energetics in organo-metal halide perovskite-based photovoltaic cells", *Energy & Environmental Science*, vol. 7, no. 4, p. 1377, 2014.

[23] R. Friend, F. Deschler, L. Pazos-Out.n, M. Abdi-Jalebi and M. Alsari, "Back-Contact Perovskite Solar Cells", *Scientific Video Protocols*, vol. 1, no. 1, pp. 1-10, 2019.

[24] T. Leijtens, K. Bush, R. Prasanna and M. McGehee, "Opportunities and challenges for tandem solar cells using metal halide perovskite semiconductors", *Nature Energy*, vol. 3, no. 10, pp. 828-838, 2018.

[25] L. Gil-Escrig, A. Miquel-Sempere, M. Sessolo and H. Bolink, "Mixed Iodide–Bromide Methylammonium Lead Perovskite-based Diodes for Light Emission and Photovoltaics", *The Journal of Physical Chemistry Letters*, vol. 6, no. 18, pp. 3743-3748, 2015.

[26] Y. Kim, H. Cho and T. Lee, "Metal halide perovskite light emitters", *Proceedings of the National Academy of Sciences*, vol. 113, no. 42, pp. 11694-11702, 2016.

[27] X. Zheng, Y. Hou, H. Sun, O. Mohammed, E. Sargent and O. Bakr, "Reducing Defects in Halide Perovskite Nanocrystals for Light-Emitting Applications", *The Journal of Physical Chemistry Letters*, vol. 10, no. 10, pp. 2629-2640, 2019.

[28] S. Jiang et al., "Balance lead in solution-processed CH3NH3PbBrxCl(3−x) single crystals for high performance X-ray detection", *Materials Letters,* vol. 236, pp. 26-29, 2019.

[29] H. Gill et al., "Flexible perovskite-based X-ray detectors for dose monitoring in medical imaging applications", *Physics in Medicine*, vol. 5, pp. 20-23, 2018.

[30] H. Mescher, E. Hamann and U. Lemmer, "Simulation and design of folded perovskite x-ray detectors", *Scientific Reports*, vol. 9, no. 1, 2019.

[31] H. Yu et al., "Organic–inorganic perovskite plasmonic nanowire lasers with a low threshold and a good thermal stability", Nanoscale, vol. 8, no. 47, pp. 19536-19540, 2016. Available: 10.1039/c6nr06891j.

[32] L. Quan, B. Rand, R. Friend, S. Mhaisalkar, T. Lee and E. Sargent, "Perovskites for Next-Generation Optical Sources", *Chemical Reviews*, vol. 119, no. 12, pp. 7444-7477, 2019.

[33] Y. Wang et al., "Flexible Organometal–Halide Perovskite Lasers for Speckle Reduction in Imaging Projection", *ACS Nano*, vol. 13, no. 5, pp. 5421-5429, 2019. Available: 10.1021/acsnano.9b00154.

[34] X. Xu et al., "Dual-Band, High-Performance Phototransistors from Hybrid Perovskite and Organic Crystal Array for Secure Communication Applications", *ACS Nano*, vol. 13, no. 5, pp. 5910-5919, 2019. Available: 10.1021/acsnano.9b01734.

[35] C. K. Moller, "Crystal Structure and Photoconductivity of Caesium Plumbohalides," *Nature*, vol. 182, no. 4647, pp. 1436–1436, Nov. 1958.

[36] D. Weber, "CH3NH3PbX3, ein Pb (II)-System mit kubischer Perowskitstruktur / CH3NH3PbX3, a Pb(II)-System with Cubic Perovskite Structure", Zeitschrift für Naturforschung B, vol. 33, no. 12, pp. 1443-1445, 1978.

[37] D. Mitzi, S. Wang, C. Feild, C. Chess and A. Guloy, "Conducting Layered Organic-inorganic Halides Containing <110>-Oriented Perovskite Sheets", *Science*, vol. 267, no. 5203, pp. 1473-1476, 1995. Available: 10.1126/science.267.5203.1473.

[38] B. Park and S. Seok, "Intrinsic Instability of Inorganic–Organic Hybrid Halide Perovskite Materials", *Advanced Materials*, vol. 31, no. 20, p. 1805337, 2019. Available: 10.1002/adma.201805337.

[39] A. Mutalikdesai and S. Ramasesha, "Emerging solar technologies: Perovskite solar cell", *Resonance*, vol. 22, no. 11, pp. 1061-1083, 2017. Available: 10.1007/s12045-017-0571-1.

[40] K. Qin, B. Dong and S. Wang, "Improving the stability of metal halide perovskite solar cells from material to structure", *Journal of Energy Chemistry*, vol. 33, pp. 90-99, 2019.

[41] N. Park, M. Grätzel and T. Miyasaka, *Organic-inorganic halide perovskite photovoltaics*, 1st ed. Switzerland: Springer, 2016, pp. 1-17.

[42] Q. Chen et al., "Under the spotlight: The organic–inorganic hybrid halide perovskite for optoelectronic applications", *Nano Today*, vol. 10, no. 3, pp. 355-396, 2015. Available: 10.1016/j.nantod.2015.04.009.

[43] T. Baikie et al., "Synthesis and crystal chemistry of the hybrid perovskite (CH3NH3)PbI3 for solid-state sensitised solar cell applications", *Journal of Materials Chemistry A*, vol. 1, no. 18, p. 5628, 2013. Available: 10.1039/c3ta10518k.

[44] M. Safdari, A. Fischer, B. Xu, L. Kloo and J. Gardner, "Structure and function relationships in alkylammonium lead(ii) iodide solar cells", *Journal of Materials Chemistry A,* vol. 3, no. 17, pp. 9201-9207, 2015. Available: 10.1039/c4ta06174h

[45] J. Im, C. Lee, J. Lee, S. Park and N. Park, "6.5% efficient perovskite quantum-dot-sensitized solar cell", *Nanoscale*, vol. 3, no. 10, p. 4088, 2011. Available: 10.1039/c1nr10867k.

[46] C. Kagan, "Organic-Inorganic Hybrid Materials as Semiconducting Channels in Thin-Film Field-Effect Transistors", *Science*, vol. 286, no. 5441, pp. 945-947, 1999. Available: 10.1126/science.286.5441.945.

[47] T. Sum and N. Mathews, "Advancements in perovskite solar cells: photophysics behind the photovoltaics", *Energy Environ. Sci*., vol. 7, no. 8, pp. 2518-2534, 2014. Available: 10.1039/c4ee00673a.

[48] P. Whitfield et al., "Structures, Phase Transitions and Tricritical Behavior of the Hybrid Perovskite Methyl Ammonium Lead Iodide", *Scientific Reports*, vol. 6, no. 1, 2016. Available: 10.1038/srep35685.

[49] H. Lin, C. Zhou, Y. Tian, T. Siegrist and B. Ma, "Low-Dimensional Organometal Halide Perovskites", *ACS Energy Letters*, vol. 3, no. 1, pp. 54-62, 2017. Available: 10.1021/acsenergylett.7b00926.

[50] M. Green, A. Ho-Baillie and H. Snaith, "The emergence of perovskite solar cells", *Nature Photonics,* vol. 8, no. 7, pp. 506-514, 2014. Available: 10.1038/nphoton.2014.134.

[51] K. Matsuishi, T. Ishihara, S. Onari, Y. Chang and C. Park, "Optical properties and structural phase transitions of lead-halide based inorganic–organic 3D and 2D perovskite semiconductors under high pressure", *physica status solidi (b),* vol. 241, no. 14, pp. 3328-3333, 2004. Available: 10.1002/pssb.200405229.

[52] L. Dou et al., "Atomically thin two-dimensional organic-inorganic hybrid perovskites", *Science*, vol. 349, no. 6255, pp. 1518-1521, 2015. Available: 10.1126/science.aac7660.

[53] Z. Yuan et al., "One-dimensional organic lead halide perovskites with efficient bluish white-light emission*", Nature Communications*, vol. 8, no. 1, 2017. Available: 10.1038/ncomms14051.

[54] Chang, Y. H., Chul Hong Park, and Kiyoto Matsuishi. "First-principles study of the Structural and the electronic properties of the lead-Halide-based inorganic-organic perovskites (CH~ 3NH~ 3) PbX~ 3 and CsPbX3 (X= Cl, Br, I*).", Journal-Korean Physical Society*, vol. 44, pp.889-893, 2004.

[55] A. Poglitsch and D. Weber, "Dynamic disorder in methylammoniumtrihalogenoplumbates (II) observed by millimeter-wave spectroscopy", *The Journal of Chemical Physics*, vol. 87, no. 11, pp. 6373-6378, 1987. Available: 10.1063/1.453467.

[56] M. Becker, T. Klüner and M. Wark, "Formation of hybrid ABX3perovskite compounds for solar cell application: first-principles calculations of effective ionic radii and determination of tolerance factors", *Dalton Transactions*, vol. 46, no. 11, pp. 3500-3509, 2017. Available: 10.1039/c6dt04796c.

[57] P. Varadwaj, A. Varadwaj, H. Marques and K. Yamashita, "Significance of hydrogen bonding and other noncovalent interactions in determining octahedral tilting in the CH3NH3PbI3 hybrid organic-inorganic halide perovskite solar cell semiconductor", *Scientific Reports*, vol. 9, no. 1, 2019. Available: 10.1038/s41598-018-36218-1.

[58] D. Egger, A. Rappe and L. Kronik, "Hybrid Organic–Inorganic Perovskites on the Move", *Accounts of Chemical Research*, vol. 49, no. 3, pp. 573-581, 2016. Available: 10.1021/acs.accounts.5b00540.

[59] A. Dobrovolsky, A. Merdasa, E. Unger, A. Yartsev and I. Scheblykin, "Defect-induced local variation of crystal phase transition temperature in metal-halide perovskites", *Nature Communications*, vol. 8, no. 1, 2017. Available: 10.1038/s41467-017-00058-w.

[60] Y. Tian et al., "Mechanistic insights into perovskite photoluminescence enhancement: light curing with oxygen can boost yield thousandfold", *Physical Chemistry Chemical Physics*, vol. 17, no. 38, pp. 24978-24987, 2015. Available: 10.1039/c5cp04410c.

[61] D. deQuilettes et al., "Photo-induced halide redistribution in organic–inorganic perovskite films", *Nature Communications*, vol. 7, no. 1, 2016. Available: 10.1038/ncomms11683.

[62] K. Aleksandrov, "The sequences of structural phase transitions in perovskites", *Ferroelectrics*, vol. 14, no. 1, pp. 801-805, 1976. Available: 10.1080/00150197608237799.

[63] N. Onoda-Yamamuro, T. Matsuo and H. Suga, "Calorimetric and IR spectroscopic studies of phase transitions in methylammonium trihalogenoplumbates (II)†", *Journal of Physics and Chemistry of Solids*, vol. 51, no. 12, pp. 1383-1395, 1990. Available: 10.1016/0022-3697(90)90021-7.

[64] C. Quarti et al., "Structural and optical properties of methylammonium lead iodide across the tetragonal to cubic phase transition: implications for perovskite solar cells", *Energy & Environmental Science*, vol. 9, no. 1, pp. 155-163, 2016. Available: 10.1039/c5ee02925b.

[65] N. Onoda-Yamamuro, T. Matsuo and H. Suga, "Dielectric study of CH3NH3PbX3 (X = Cl, Br, I)", *Journal of Physics and Chemistry of Solids*, vol. 53, no. 7, pp. 935-939, 1992. Available: 10.1016/0022-3697(92)90121-s.

[66] H. Zhang et al., "Photovoltaic behaviour of lead methylammonium triiodide perovskite solar cells down to 80 K", *Journal of Materials Chemistry A*, vol. 3, no. 22, pp. 11762-11767, 2015. Available: 10.1039/c5ta02206a.

[67] A. Jena, A. Kulkarni and T. Miyasaka, "Halide Perovskite Photovoltaics: Background, Status, and Future Prospects", *Chemical Reviews*, vol. 119, no. 5, pp. 3036-3103, 2019. Available: 10.1021/acs.chemrev.8b00539.

[68] D. MITZI, *Progress in Inorganic Chemistry, vol.48*, 1st ed. Hoboken: John Wiley & Sons, Inc., 1999, pp. 1-20.

[69] A. Mohammad Bagher, "Comparison of Organic Solar Cells and Inorganic Solar Cells", *International Journal of Renewable and Sustainable Energy*, vol.3, no.3, p. 53, 2014. Available: 10.11648/j.ijrse.20140303.12.

[70] S. Stranks et al., "Electron-Hole Diffusion Lengths Exceeding 1 Micrometer in an Organometal Trihalide Perovskite Absorber", *Science,* vol. 342, no. 6156, pp. 341-344, 2013. Available: 10.1126/science.1243982.

[72] N. Jeon, J. Noh, Y. Kim, W. Yang, S. Ryu and S. Seok, "Solvent engineering for high-performance inorganic–organic hybrid perovskite solar cells", *Nature Materials*, vol. 13, no. 9, pp. 897-903, 2014. Available: 10.1038/nmat4014.

[73] W. Zhang, G. Eperon and H. Snaith, "Metal halide perovskites for energy applications", *Nature Energy*, vol. 1, no. 6, 2016. Available: 10.1038/nenergy.2016.48.

[74] A. Kojima, K. Teshima, Y. Shirai and T. Miyasaka, "Organometal Halide Perovskites as Visible-Light Sensitizers for Photovoltaic Cells", *Journal of the American Chemical Society*, vol. 131, no. 17, pp. 6050-6051, 2009. Available: 10.1021/ja809598r.

[75] M. Liu, M. Johnston and H. Snaith, "Efficient planar heterojunction perovskite solar cells by vapour deposition", *Nature*, vol. 501, no. 7467, pp. 395-398, 2013. Available: 10.1038/nature12509.

[76] J. Burschka et al., "Sequential deposition as a route to high-performance perovskite-sensitized solar cells", *Nature*, vol. 499, no. 7458, pp. 316-319, 2013. Available: 10.1038/nature12340.

[77] S. Brittman, G. Adhyaksa and E. Garnett, "The expanding world of hybrid perovskites: materials properties and emerging applications", *MRS Communications*, vol. 5, no. 1, pp. 7-26, 2015. Available: 10.1557/mrc.2015.6.

[78] P. Umari, E. Mosconi and F. De Angelis, "Relativistic GW calculations on CH3NH3PbI3 and CH3NH3SnI3 Perovskites for Solar Cell Applications", *Scientific Reports*, vol. 4, no. 1, 2014. Available: 10.1038/srep04467.

[79] K. Tanaka, T. Takahashi, T. Ban, T. Kondo, K. Uchida and N. Miura, "Comparative study on the excitons in lead-halide-based perovskite-type crystals CH3NH3PbBr3 CH3NH3PbI3", *Solid State Communications,* vol. 127, no. 9-10, pp. 619-623, 2003. Available: 10.1016/s0038-1098(03)00566-0.

[80] W. Yin, T. Shi and Y. Yan, "Unique Properties of Halide Perovskites as Possible Origins of the Superior Solar Cell Performance", *Advanced Materials*, vol. 26, no. 27, pp. 4653-4658, 2014. Available: 10.1002/adma.201306281.

[81] W. Yin, J. Yang, J. Kang, Y. Yan and S. Wei, "Halide perovskite materials for solar cells: a theoretical review", *Journal of Materials Chemistry A,* vol. 3, no. 17, pp. 8926-8942, 2015. Available: 10.1039/c4ta05033a.

[82] X. Ziang et al., "Refractive index and extinction coefficient of CH_3NH_3PbI_3 studied by spectroscopic ellipsometry", *Optical Materials Express*, vol. 5, no. 1, p. 29, 2014. Available: 10.1364/ome.5.000029.

[83] M. Lee, J. Teuscher, T. Miyasaka, T. Murakami and H. Snaith, "Efficient Hybrid Solar Cells Based on Meso-Superstructured Organometal Halide Perovskites", *Science*, vol. 338, no. 6107, pp. 643-647, 2012. Available: 10.1126/science.1228604.

[84] E. Mosconi, A. Amat, M. Nazeeruddin, M. Grätzel and F. De Angelis, "First-Principles Modeling of Mixed Halide Organometal Perovskites for Photovoltaic Applications", *The Journal of Physical Chemistry C*, vol. 117, no. 27, pp. 13902-13913, 2013. Available: 10.1021/jp4048659.

[85] Z. Shi and A. Jayatissa, "Perovskites-Based Solar Cells: A Review of Recent Progress, Materials and Processing Methods", *Materials*, vol. 11, no. 5, p. 729, 2018. Available: 10.3390/ma11050729.

[86] L. Chen, K. Lee and S. Lin, "Observation of Hybrid MAPbBr3 Perovskite Bulk Crystals Grown by Repeated Crystallizations*", Crystals*, vol. 8, no. 7, p. 260, 2018. Available: 10.3390/cryst8070260.

[87] Q. Chen et al., "Planar Heterojunction Perovskite Solar Cells via Vapor-Assisted Solution Process", *Journal of the American Chemical Society*, vol. 136, no. 2, pp. 622-625, 2013. Available: 10.1021/ja411509g.

[88] C. Ezike, G. Kana and A. Aina, "Progress and Prospect on Stability of Perovskite Photovoltaics*", Journal of Modern Materials*, vol. 4, no. 1, pp. 16-30, 2017. Available: 10.21467/jmm.4.1.16-30.

[89] D. Zhou, T. Zhou, Y. Tian, X. Zhu and Y. Tu, "Perovskite-Based Solar Cells: Materials, Methods, and Future Perspectives", *Journal of Nanomaterials*, vol. 2018, pp. 1-15, 2018. Available: 10.1155/2018/8148072.

[90] Q. Dong et al., "Electron-hole diffusion lengths > 175 μm in solution-grown CH3NH3PbI3single crystals", *Science*, vol. 347, no. 6225, pp. 967-970, 2015. Available: 10.1126/science.aaa5760.

[91] D. Shi et al., "Low trap-state density and long carrier diffusion in organolead trihalide perovskite single crystals", S*cience*, vol. 347, no. 6221, pp. 519-522, 2015. Available: 10.1126/science.aaa2725.

[92] Y. Zhang, F. Huang and Q. Mi, "Preferential Facet Growth of Methylammonium Lead Halide Single Crystals Promoted by Halide Coordination", *Chemistry Letters*, vol. 45, no. 8, pp. 1030-1032, 2016. Available: 10.1246/cl.160419.

[93] A. McPHERSON, "Current approaches to macromolecular crystallization", *European Journal of Biochemistry*, vol. 189, no. 1, pp. 1-23, 1990. Available: 10.1111/j.1432-1033.1990.tb15454.x.

[94] W. Peng, "Single Crystals of Organolead Halide Perovskites: Growth, Characterization, and Applications", *Doctor of Philosophy*, King Abdullah University of Science and Technology Thuwal, Kingdom of Saudi Arabia, 2017.

[95] T. Brenner, D. Egger, L. Kronik, G. Hodes and D. Cahen, "Hybrid organic—inorganic perovskites: low-cost semiconductors with intriguing charge-transport properties", *Nature Reviews Materials*, vol. 1, no. 1, 2016. Available: 10.1038/natrevmats.2015.7.

[96] M. Ahmadi, T. Wu and B. Hu, "A Review on Organic-Inorganic Halide Perovskite Photodetectors: Device Engineering and Fundamental Physics", *Advanced Materials,* vol. 29, no. 41, p. 1605242, 2017. Available: 10.1002/adma.201605242.

[97] J. Zhou and J. Huang, "Photodetectors Based on Organic-Inorganic Hybrid Lead Halide Perovskites", *Advanced Science*, vol. 5, no. 1, p. 1700256, 2017. Available: 10.1002/advs.201700256.

[98] J. Huang, Y. Shao and Q. Dong, "Organometal Trihalide Perovskite Single Crystals: A Next Wave of Materials for 25% Efficiency Photovoltaics and Applications Beyond?", *The Journal of Physical Chemistry Letters*, vol. 6, no. 16, pp. 3218-3227, 2015. Available: 10.1021/acs.jpclett.5b01419.

[99] Z. Song et al., "Perovskite Solar Cell Stability in Humid Air: Partially Reversible Phase Transitions in the PbI2-CH3NH3I-H2O System", *Advanced Energy Materials*, vol. 6, no. 19, p. 1600846, 2016. Available: 10.1002/aenm.201600846.

[100] J. Kadro, K. Nonomura, D. Gachet, M. Grätzel and A. Hagfeldt, "Facile route to freestanding CH3NH3PbI3 crystals using inverse solubility", *Scientific Reports*, vol. 5, no. 1, 2015. Available: 10.1038/srep11654.

[101] T. Zuo, X. He, P. Hu and H. Jiang, "Organic-Inorganic Hybrid Perovskite Single Crystals: Crystallization, Molecular Structures, and Bandgap Engineering", *ChemNanoMat*, vol. 5, no. 3, pp. 278-289, 2019. Available: 10.1002/cnma.201800618.

[102] P. Zhao et al., "Large-Size CH3NH3PbBr3 Single Crystal: Growth and In Situ Characterization of the Photophysics Properties", *The Journal of Physical Chemistry Letters*, vol. 6, no. 13, pp. 2622-2628, 2015. Available: 10.1021/acs.jpclett.5b01017.

[103] H. Fang et al., "Hybrid Perovskites: Photophysics of Organic-Inorganic Hybrid Lead Iodide Perovskite Single Crystals (Adv. Funct. Mater. 16/2015)", *Advanced Functional Materials*, vol. 25, no. 16, pp. 2346-2346, 2015. Available: 10.1002/adfm.201570107.

[104] Y. Fang, Q. Dong, Y. Shao, Y. Yuan and J. Huang, "Highly narrowband perovskite single-crystal photodetectors enabled by surface-charge recombination", *Nature Photonics*, vol. 9, no. 10, pp. 679-686, 2015. Available: 10.1038/nphoton.2015.156.

[105] Z. Lian et al., "High-Performance Planar-Type Photodetector on (100) Facet of MAPbI3 Single Crystal", *Scientific Reports*, vol. 5, no. 1, 2015. Available: 10.1038/srep16563.

[106] Y. Chen et al., "General Space-Confined On-Substrate Fabrication of Thickness-Adjustable Hybrid Perovskite Single-Crystalline Thin Films", *Journal of the American Chemical Society*, vol. 138, no. 50, pp. 16196-16199, 2016. Available: 10.1021/jacs.6b09388.

[107] Y. Dang et al., "Formation of Hybrid Perovskite Tin Iodide Single Crystals BTop-Seeded Solution Growth", *Angewandte Chemie*, vol. 128, no. 10, pp. 3508-3511, 2016. Available: 10.1002/ange.201511792.

[108] O. Sohnel, P. Novotny and Z. Solc, "Densities of aqueous solutions of 18 inorganic substances*", Journal of Chemical & Engineering Data*, vol. 29, no. 4, pp. 379-382, 1984. Available: 10.1021/je00038a004.

[109] Y. Yang et al., "Low surface recombination velocity in solution-grown CH3NH3PbBr3 perovskite single crystal", *Nature Communications,* vol. 6, no. 1, 2015. Available: 10.1038/ncomms8961.

[110] H. Zhou et al., "Antisolvent diffusion-induced growth, equilibrium behaviours in aqueous solution and optical properties of CH3NH3PbI3 single crystals for photovoltaic applications*", RSC Advances*, vol. 5, no. 104, pp. 85344-85349, 2015. Available: 10.1039/c5ra17579h.

[111] Y. Tidhar et al., "Crystallization of Methyl Ammonium Lead Halide Perovskites: Implications for Photovoltaic Applications", *Journal of the American Chemical Society*, vol. 136, no. 38, pp. 13249-13256, 2014. Available: 10.1021/ja505556s.

[112] L. Xie et al., "Understanding the Cubic Phase Stabilization and Crystallization Kinetics in Mixed Cations and Halides Perovskite Single Crystals", *Journal of the American Chemical Society*, vol. 139, no. 9, pp. 3320-3323, 2017. Available: 10.1021/jacs.6b12432.

[113] Y. Liu et al., "Two-Inch-Sized Perovskite CH3NH3PbX3(X = Cl, Br, I) Crystals: Growth and Characterization", *Advanced Materials*, vol. 27, no. 35, pp. 5176-5183, 2015. Available: 10.1002/adma.201502597.

[114] H. Rao, W. Li, B. Chen, D. Kuang and C. Su, "In Situ Growth of 120 cm2CH3NH3PbBr3Perovskite Crystal Film on FTO Glass for Narrowband-Photodetectors", *Advanced Materials*, vol. 29, no. 16, p. 1602639, 2017. Available: 10.1002/adma.201602639.

[115] Y. Dang et al., "Bulk crystal growth of hybrid perovskite material CH3NH3PbI3", *CrystEngComm*, vol. 17, no. 3, pp. 665-670, 2015. Available: 10.1039/c4ce02106a.

Chapter 3: Hybrid Halide Perovskite Applications and Stability

Chapter 3: Hybrid Halide Perovskite Applications and Stability

Perovskite solar cells have developed over a short period of time, and now compete with other photovoltaic technologies. A background of photovoltaic cells and photodetectors is introduced in this chapter, including a presentation of device structures and associated working mechanisms. Furthermore, due to a lack of perovskite stability, related to material compositions and device structures, the applications of lead halide perovskite solar cells are limited in this research study. Therefore, the chapter will also address these stability challenges that are faced by perovskite devices towards an understanding of relevant stability mechanisms for hybrid halide perovskite single crystal photovoltaic and photodetector devices.

3.1 Photonic Device

In reference to the application of hybrid perovskites in photonic devices it is necessary here to categorise these devices. Generally, such devices come under one of two categories namely; photovoltaic devices concerned with power generation , and photodetectors which convert optical energy into electrical signals.

3.2 Background of Photovoltaic Cells

The mechanism of the photovoltaic effect was first discovered in 1839 by Edmond Becquerel, using silver halides [1], to be later developed where the effect was seen in Selenium at the end of the 19^{th} Century [2] and later at the beginning of the 20^{th} Century where it was observed using Copper-Copper Oxide junction and Silicon [3].

Photovoltaics (PVs) is the process of converting light directly into electricity using solar cells [4]. Although the photovoltaic effect was discovered in the 19th Century, it was only scientific breakthroughs that took place later in the 20th Century that would allow this effect to be exploited; specifically, this included the development of quantum mechanics and semiconductor technology [4]. Because at that time production costs were high, and the use of photovoltaics was restricted to applications in locations where there is no electrical infrastructure. it is observed that space solar power technology have developed remarkably since the first solar-powered satellite was launched in 1950s. Space solar cell is a suitable application that fitted well with the nature of photovoltaics whereby there was a need for standalone systems, to avoid heavy energy resources and long term autonomous dependence on energy together with durability, reliability and efficiency and being a low-weight technology [5].

The current status of PV technology and possibilities for the future could be categorised into three generations, the first generation being the current situation, the second generation being amorphous or polycrystalline silicon, extending to the third generation in the future [6].

In reference to the current situation, or first generation, it is dominated by the use of single-crystal and multi-crystalline silicon as single junction solar cells. These devices which are based on a single junction silicon wafer were originally developed using a silicon ingot which was suitable for large scale production [7] where each wafer could produce an output of between 2 – 3 watts per square meter. They are commonly used due to their high efficiencies [8]. This first generation of solar cells can be divided according to one of two levels of crystallisation. Firstly, where the entire wafer is comprised of only one crystal it is referred to as a single crystal solar cell, and where it is comprised of crystal grains, it is referred to as a multi-crystal solar cell [6].

the efficiency of the single crystal solar cell is considered higher compared to the multi-crystal solar cell. However, the production of the multi-crystal solar cell is easier and more cost effective [8].

The second generation was based on the removal of unnecessary material through the use of thin film, while at the same time maintaining the efficiency of the first-generation PV devices [6]. Second generation PV technology used amorphous or polycrystalline silicon on glass substrates and were more efficient than single crystal [7]. Specifically, they were focussed on using a-Si thin film solar cells, copper indium selenide solar cell (CIS), copper indium gallium selenide solar cell (CIGS), and Cadmium telluride solar cell (CdTe). However, CIGS is expensive due to the rarity of indium and the structure may be difficult to manufacture and the Cadmium in CdTe is toxic. While the efficiencies of these materials were less they did cost less than the first generation and importantly, they had an aesthetic advantage in that they are applied directly to different surfaces [6]. Furthermore, it is possible to grow these thin films on flexible substrates on large surface areas of up to $6m^2$ as opposed to wafer based solar cells which are limited to wafer dimensions [8].

The second-generation PVs were much more economically viable and therefore, overcame the associated limitations of the first generation. However, it has been this trend of cost reduction which has driven the need for more efficient devices to meet the cost reduction trend [7]. This has seen the advent of a third generation of devices that have ultra-high efficiency for the same costs of production. The third generation of PV technology like Organic solar cells and hybrid solar cells takes advantage of the low-cost substrates and thin film concepts with the additional use of single crystals. Compared to other PV technology, perovskite solar cell has shown a quick development in the short time in the history of solar cell field.

3.2.1 Working Principles of Solar Cells

Perovskite-based solar cells essentially possess two main features in their structure. Firstly, perovskite material as the absorber layer possesses optical properties such as high absorption coefficient, large dielectric constant and low exciton binding energy. Secondly, charge carriers that can be effectively transported and selectively collected by the hole and electron transporting layers.

Although the working mechanism of perovskite solar cells is not very well understood until now, the common working principle of any solar cell has ability to convert solar energy into electricity involves four main processes, namely, absorption of incident photons, creation of free electron-hole pairs, free charge carrier transport and the collection of charge carriers at respective electrodes [9], each of which will be described in the following.

In reference to absorption of solar energy from the sun, it comes in the form of photons. It is possible for some photons to be absorbed by certain material which depends on the energy levels in the material itself (Band gap) and the quantum energy of the photon. Where the photon is absorbed the energy is taken by a carrier changing it from a ground state to a higher energy state and this carrier releases its energy, in numerous possible ways, so that it can return to its original ground state. Importantly, the time that the carrier is an excited state should be longer than the time required to extract the carrier. Furthermore, if the maximum of the valence band and the minimum of the conduction band have the same value of momentum, then it is referred to as a direct bandgap semiconductor. There are some semiconductor materials providing a low probability of absorption than the direct absorption. This is due to the momentum of maximum energy of the valence band not having the same momentum at the minimum in the conduction band energy, thus, they are called an indirect bandgap semiconductor.

The creation of electron-hole pairs involves the excited electron to be excited to the conduction band which results in an electron vacancy, referred to as a hole which is in the valence band. This electron-hole pair is attracted to each other due to Coulombic force which affords a stabilising energy to the electron-hole pair whose energy is slightly lower than the unbound electron in the valence band. As a result, an exciton is created which is a quasiparticle with a neutrally bound state due to the photon absorption. In a material this results in either a bound exciton or an unbound free charge, which is dependent upon the exciton in that particular material and the associated thermal energy which breaks the exciton. In the case of the researched materials($MAPbX_3$), electron-hole pairs which are weakly bound which leads to the generation of free charge carriers [10]

In reference to the transport mechanism, upon the creation of the free charge carriers, the charge has to be separated to its respective polarity in each electrode through the application of an electric field, forces the charges which have opposite polarity in opposite directions achieved using a Schottky junction or a p-n junction [9]. Using these approaches the fermi level would be equalised leading to the formation of a depleted region close to the junction which results in an increase in energy fields due to the band bending .

An important consideration in the transport mechanism is recombination, whereby the electron and holes recombine and return to the original ground state, this results in a reduction in the charge collection and thus current output. There are two type of recombination; namely band-band recombination which usually releases a radiative energy, and Shockley-Read-Hall (SRH) recombination where the amount of non-radiative energies depends on the number of trap states.

Now that the charges have been efficiently swept to the edge of the bulk they are now required to be collected at the electrode, this is possible through the formation of an ohmic contact

between the active semiconductor material and the electrode. Importantly, the collection of charge carries is controlled by the work function of electrodes. If the electrode has a higher work function than semiconductors, the electrode would be able to collect the holes. While, low work function should be used for collecting electrons.

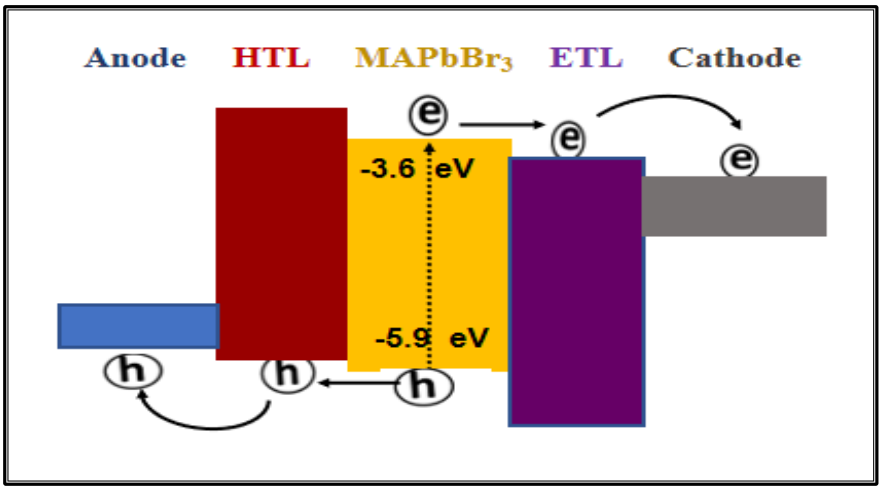

Figure3. 1:Schematic of ideal solar cell operation after absorbing incident light.

3.2.2 Hybrid Halide Perovskite Photovoltaic Cells

Perovskite solar cells use perovskite materials for light absorption for photovoltaic activity. They are an emerging family of materials for use in photovoltaic applications because of low cost, the abundance of raw materials, scalable fabrication, and especially the ability to efficiently convert light into electrical power [11]. Moreover, hybrid perovskites in photovoltaic applications possess unique optical and electrical properties which include high carrier mobility, quantum efficiency, efficient light harvesting, a high absorption coefficient and low trap density of states [12]. Among the qualities that are required for hybrid perovskites in solar applications, is that it would only require a thin layer of active material due to their efficient light harvesting [11].

The first application of organic-inorganic perovskites was in dye-sensitised solar cells in 2009 by Miyasaka and his colleagues. They used different perovskite materials, namely, methylammonium lead bromide ($MAPbBr_3$) and methylammonium lead iodide ($MAPbI_3$) perovskites. Despite the fact that both perovskite solar cells were not stable and their power conversion efficiencies (PCE) were 3.13% and 3.81% respectively [13], perovskite based solar cells have received extensive attention and have improved rapidly in a short period. Perovskite solar cells have demonstrated that they can be quite promising solar cell because of their high conversion efficiency, reaching beyond 22% without complicated structures or high cost.

3.2.3 Device Architectures of Perovskite Solar Cells

The overall performance of perovskite photovoltaic cells is highly dependent on their architecture including materials and preparation methods for deposition of the perovskite and other layers. The typical architecture of perovskite device usually contains a thin perovskite absorber layer which is designed to be between electron transporting layers (ETL) and hole transporting layers (HTL). Based on their structures, perovskite solar cells can be classed into five types, namely; mesoporous structure, planar (p-i-n and n-i-p) structures, ETL/HTL-free structure (including single crystal structure) and tandem cells.

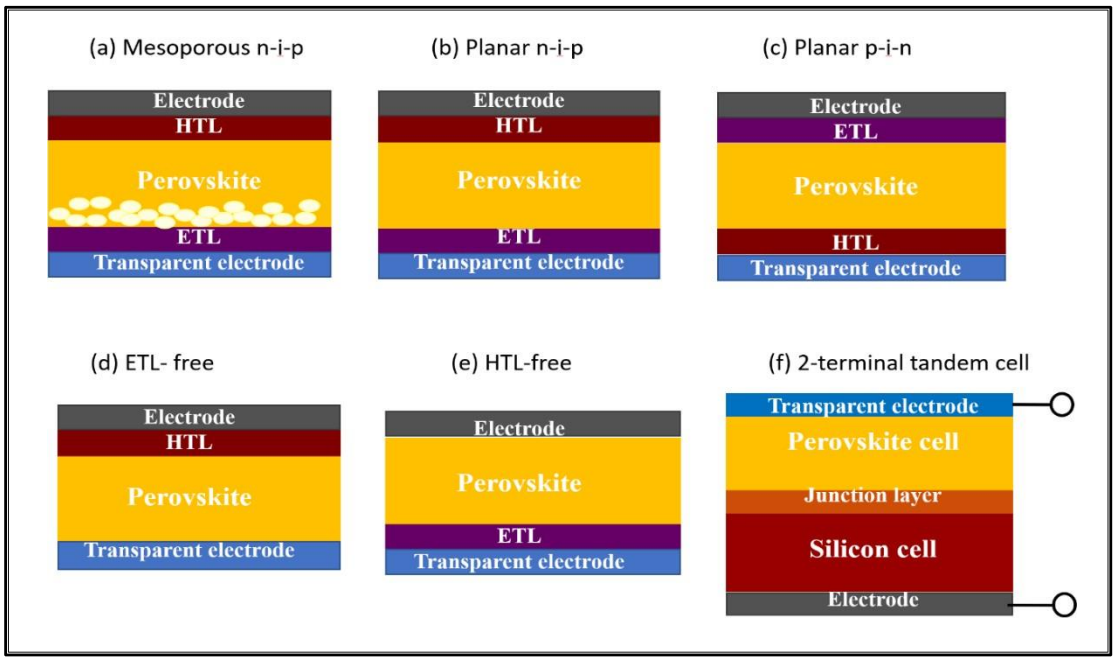

Figure3. 2: Common perovskite solar cell structures

3.2.3.1 Mesoporous Structured Solar Cell (MSSC)

Since the first mesoporous structured solar cell (MSSC) was reported in 2011, hybrid halide perovskite materials have gained significant attention in various photonic applications, particularly for perovskite solar cells. This structure usually consists of a thin layer of perovskite, a compact layer (typically TiO_2), a mesoporous TiO_2 or Al_2O_3 layer, a hole transport layer (HTL), and a metal electrode. Each layer in this structure has a specific function. For example, the mesoporous layer essentially increases light absorption inside the cell, and prevents contact between the compact layer and the hole transport layer [14], while metal oxide materials, such as TiO_2 ,SnO_2 and ZnO, as a compact layer can be used as an electron transport layer for preventing shunting and leakage currents under reverse bias [15]. Importantly, this

results in a high rate of charge extractions when using, for example, mesoporous TiO_2 scaffolds, as can be seen in table 3.1 [14,16,17]. However, a mesoporous TiO_2 layer causes a reduction in the stability of the device compared to other scaffold materials. This is attributed to form defects such as titanium interstitials and oxygen vacancies, which prevents electron transport [17].

Table 3. 1Mesoporous structured solar cell device structures (MSSC) and associated efficiency increase.

Device structure	PCE (%)
FTO/ Compact TiO_2/mp-TiO_2/quantum dot of $MAPbI_3$/redox liquid electrolyte/Pt	6.5 [16]
FTO/ Compact TiO_2/mp-TiO_2/ nanoparticles of $MAPbI_3$/spiro-OMeTAD/Au	9 [17]
FTO/ Compact TiO_2/mp-Al_2O_3/nanoparticle of $MAPbI_{3-x}Cl_x$/spiro-MeTAD/Ag	10.9 [18]
FTO/ Compact TiO_2/mp-TiO_2/ nanocrystal of $MAPbI_3$/spiro-OMeTAD/Au	15 [19]

3.2.3.2 Planar Heterojunction Solar Cells

Planar heterojunction solar cells are used in order to gain long-term stability with high efficiency. They usually consist of perovskite thin films which are sandwiched between the electron transport layer (ETL), and the hole transport layer (HTL) without containing mesoporous scaffolds [20]. The structure of planar heterojunction solar cells can be categorised as direct (n-i-p), or inverted architecture (p-i-n) based on the location of the transparent conducting substrate. In the n-i-p structure, for example, the incident light passes into the device starting from the ETL.

Since the first planar structure reported in 2013 by Jeng, most perovskite solar cells with the planar structure are achieved through making adjustments to this structure, such as modifying the configuration of the device and the morphology of the active absorber, as can be seen in Table 3.2. [21-23].

In consideration of the performance of perovskite solar cells, improved stability derived from the planar structure has been extensively reported. For example, Chen (2015) and his group demonstrated the power conversion efficiency (PCE) of the inverted planar structure of $MAPbI_3$ based on ZnO slightly decreased to 90% of initial device efficiency after 1000 hours of illumination [12].

Table 3. 2: Planar heterojunction solar cell device structures and associated efficiency increases

Device structure	PCE (%)
ITO/PEDOT: PSS/$MAPbI_3$ /C_{60} /BCP/Al	3.9 [27]
ITO/np-SnO_2/thin film of $MAPbI_3$/spiro-OMeTAD/Ag	13 [28]
FTO/Compact-TiO_2/$MAPbI_3$/ spiro-OMeTAD /MoO_3/Ag	15.2 [21]
FTO/Compact-TiO_2/$MAPbBr_3$/ spiro-OMeTAD/Ag	15.4 [23]
FTO/graphene-TiO_2/mp-Al_2O_3/ $MAPbI_{3-x}Cl_x$/ spiro-OMeTAD /Au	15.6 [29]
ITO/np-ZnO/ $MAPbI_3$/spiro-OMeTAD/Ag	15.7 [12]
FTO/Compact-TiO_2/mp-TiO_2/$(FAPbI_3)_{1-x}(MAPbBr_3)_x$/PTAA/Au	20.1 [21]
FTO/TiO_2/meso TiO_2: perovskite composite/perovskite /PTAA/Au	22.1 [30]

It is necessary to note that most planar heterojunction solar cells have an inverted architecture which exhibits a low hysteresis in J-V curves, originating from electronic defects and mobile ionic species rather than from ferroelectricity, which directly affects the efficiency and stability of the solar cell [24,22]. Additionally, inserting mesoporous TiO_2 (500nm) in the perovskite planar solar cell can also reduce the hysteresis by facilitating charge extraction and inhibiting accumulation at the interface [25]. Replacing the compact TiO_2 layer with an organic layer such as n-type in the perovskite solar cell can positively affect the hysteresis in J-V curves, in fact, negligible hysteresis can be achieved by using a fullerene organic layer [26].

3.2.3.3 HTL/ETL Free Solar Cell

HTL (hole transporting layer)-free solar cell means the metal electrode is deposited directly without the need for the HTL. This allows the layer of perovskite to work as an absorber and hole conductor, forming a heterojunction with ETL (electron transporting layer). The problem with this structure is that the metal electrode may react with the perovskite, especially halide ions, affecting the long-term stability of cells [22].

Table 3.3: HTL/ETL-free solar cell device structures and associated PCE increase

Device structure	PCE (%)
TiO_2/ $MAPbI_3$/Au	8.7 [31]
ITO/$MAPbI_3$/$PC_{61}BM$/$BisC_{60}$/Ag	11 [32]
ITO/$MAPbI_3$/P3HT/Ag	13.7 [33]
FTO/ $MAPbI_{3-x}Clx$/spiro-OMeTAD /Au	14 [34]

A HTL-free solar cell offers the opportunity to understand the working mechanism of perovskite solar cells [22].

The ETL is not necessary for perovskite solar cell structure because ITO, or FTO, which are usually used as a cathode, can act as the ETL layer. Furthermore, very low stabilised PCE in some ETL free solar cells is observed, although they do afford a high-power output [22]. Perovskite solar cells without these layers have been reported, as can be seen in Table 3.3.

3.2.3.4 Single Crystal Solar Cell

Hybrid halide perovskite single crystals have exhibited superior optoelectronic properties and are used in a number of different device applications. Here the use of these single crystals in solar cells is addressed. Moreover, most solar cell devices have been demonstrated using perovskite thin film, however, research about the use of perovskite single crystals in solar cells is still limited.

Perovskite monocrystalline (single crystal) solar cells were first demonstrated by Zhao et al. (2015). They observed that although there was a low photocurrent under illumination (12nA) in large-scale $MAPbBr_3$ single crystals, there is no current attenuation for all the regions of the single crystal that were measured, and the photocurrent was distributed equally over the surface of the crystal [35]. Importantly, Dong (2015) and his group reported that the diffusion of the charge carrier in a $MAPbI_3$ single crystal can be more than 175 micrometres under 1 sun of illumination, while it can exceed 3 mm under weak light [36]. Bakr's group (2016) obtained an ultra-stable perovskite device over 48 hours with a PCE above 5%. Additionally, it is also possible to increase the efficiency of hybrid perovskite solar cells by decreasing the thickness of the single crystal [37].

The results here prove that single crystals in these devices offer superior optoelectronic properties, and although the bulk size of the single crystal is difficult to fabricate as a solar cell, this problem has been overcome by Dong et al. (2016) who made a lateral structure using piezoelectric poling [36].

Table 3. 4: Single crystal solar cell device structure and associated PCE increases

Device structure	PCE (%)
ITO/TiO2/MAPbBr$_3$ /Au	5.49 [37]
FTO/TiO2/MAPbBr$_3$ /Au	6.5 [37]
ITO/PTAA/MAPbI3/PCBM/C60/BCP/Cu	17.8 [38]
ITO/ PTAA/MAPbI$_3$ single crystal/C60/BCP/copper (Cu)	21.09 [39]

The thickness of the perovskite single crystal should not exceed its carrier diffusion length (tens of micrometres), thus achieving high output power in solar cells. Therefore, considerable attention has been drawn to prepare methods for fabrication of thin single crystal solar cells. For example, Chen et al. (2017) improved the output power of single perovskite solar cells by growing thin $MAPbI_3$ single crystals directly onto the hole transport layer [38]. Alternatively, a $MAPbI_3$ single crystal of ~20 μm thick was

grown by using an inverse-temperature crystal growth method between PTAA substrates, and it yielded a cell with a power conversion of 21.09% [39].

To understand the working mechanism of perovskite single crystal solar cells and thoroughly investigate the stability of Methylammonium lead bromide perovskite single crystals, without

the need for numerous layers, a device structure was adopted in this research similar to that of HTM/ETM- free solar cells and single crystal solar cells.

3.2.3.5 Tandem Solar Cell

The value of open-circuit voltage affects the power output of single junction solar cells, and the open-circuit voltage is limited by the band gap of the absorber. A narrow band gap produces a low open circuit voltage, while a wide band gap can produce high open circuit voltage, but the short circuit current can be low because there are less photons to create photocurrent. However, connecting narrow band gap solar cells with wide band gap solar cells in series can improve all the parameters of the solar cell. This structure is known as the tandem structure of which there are two types of perovskite tandem solar cell, namely 4-terminal, and 2-terminal, whereby the 4-terminal device is made from stacking two 2-terminal devices on each other [22,14].

Mailoa (2015) and his group made a 2-terminal tandem solar cell which consisted of a semitransparent perovskite cell (top cell) and a Si or CIGS cell (bottom cell) connected by the Si tunnel junction. The PCE of this cell was 13.7 % which is lower than the efficiency of an individual cell of either Si or perovskite [40]. Alternatively, all perovskite tandem cells can improve the PCE because of their tunable band gap. Theoretically, a perovskite tandem solar cell consisting of $FAPbI_3$ (low bandgap) and $MAPb(I_{1-X}Br_X)_3$ (high bandgap) can achieve a PCE of 23.1% [22].

3.3 Photodetectors

Photodetectors are concerned with detecting optical signals and converting them to electrical signals. Photodetectors include a number of different devices such as photoconductors, photodiodes and phototransistors. Photodetectors are widely used in a number of applications and devices which include ambient sensors and image sensors used in wide variety of fields including biomedical imaging and spectrometry [41].

Photodetectors are designed to work for a particular wavelength associated with their particular function, as opposed to solar cells which are designed to detect light across the solar spectrum, specifically from the infrared (IR) region to the visible spectrum to the ultraviolet (UV) region [42]. Photodetection in the ultraviolet (UV) region has drawn an extensive attention because of the wide variety of UV photodetectors applications.

A high-performance photodetector (semiconductor materials) should meet the requirements which are high responsivity (the ratio of the photocurrent to the intensity of applied light), high response time (the time spent for charge carriers to cross the depletion region), high stability, and low electrical noise for reducing any errors [43]. An important attribute of photodetectors is the absorption coefficient [44] which is indicated by the depth of penetration of radiation [42]. Another important attribute of photodetectors is their response time, which is particularly important when the light radiation is received in pulses, this response time is dependent upon the carrier generation rate which needs to be faster than the arrival of the next radiation pulse [42].

There are four main types of photodetector. The first type is III-Nitride Semiconductor System, the most common components in this type photodetector are AlGaN and InGaN-based photodetectors. The former consists of AlGaN films which are usually deposited on GaN

templates, and widely used to detect UV radiation. The latter, InGaN-based photodetectors offer a potentially better approach for detecting optical energy in UV-A visible-blind (320–400 nm) better than Si photodetectors, due to their tunable direct bandgap. The second system is based on Silicon carbide (SiC), this type shows good potential for high-temperature, high-power, high-frequency, and radiation hardened applications. The third type, the Diamond photodetector, is another candidate in the photodetection field, it provides high-performance deep UV detectors with high thermal conductivity and mobility. The fourth system is the hybrid photodetector which is based on using organic semiconductor materials. Although attention has been paid to the manufacture of photodetectors that are high performance and inorganic material-based, including the use of materials such as silicon and gallium phosphide, their manufacture is both time consuming and expensive [44]. Specifically, the process uses expensive substrates, high temperatures, ultrahigh vacuum and rigorous fabrication [44].Therefore, there is a need to simplify and reduce the cost of the manufacturing process of photodetectors, this would require a strategy that is low temperature, solution-based and exploits hybrid materials [44]. However, photodetectors made using these approaches are beset with small responsivity [45], low specific detectivity [46], slow response time [47] and large dark current [48].

Furthermore, while all the photodetectors above are thermally stable detectors, the 1D nanostructure photodetectors are sensitive to the temperature due to their small dimension and strong surface states [43].

3.3.1 Working principles and Device Architectures of Photodetectors

The architectures of photodetectors are designed to meet different applications, however, generally, there are two main architectures for these devices, namely, lateral and vertical structures [49]. Lateral structured photodetectors include phototransistors and photoconductors, and those based on the vertical structure include photodiodes. Photoconductor and photodiode devices have a two-terminal structure with a cathode and an anode, and phototransistors have a three-terminal structure with a source, a drain and a gate [50]. Furthermore, the main parameters of photodetector's operation are responsivity and external quantum efficiency.

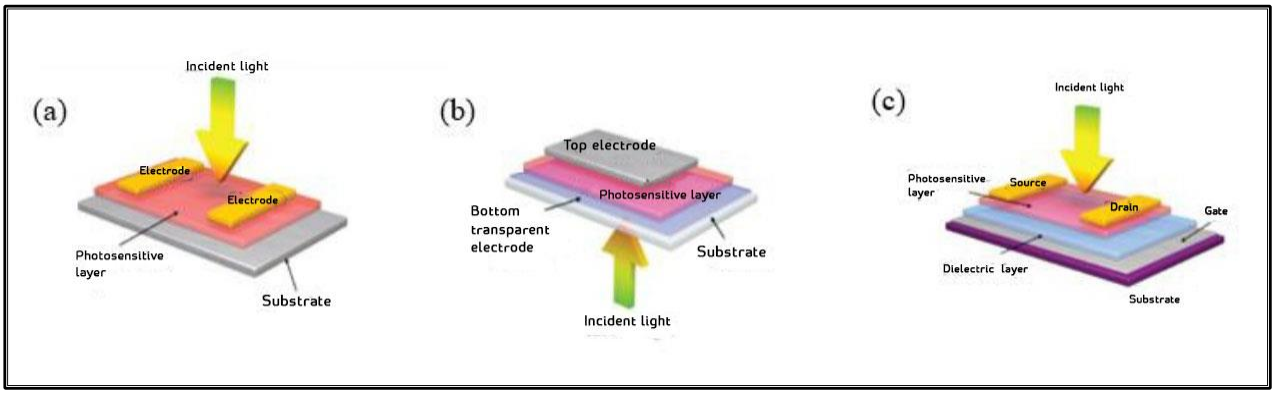

Figure3. 3: Schematics of (a) photoconductor, (b) photodiode with vertical structure, and (c) phototransistor , these images are reprinted after the permission from Heike Weller[51]

.

3.3.1.1 Photoconductors

Photoconductors, in contrast to photodiodes, show a slow response and a high driving bias. These attributes are a result of large electrode spacing required for a high photocurrent at the cost of response speed [51]. This ability of photocurrent amplification or gain affords high sensitivity, even in poor light conditions. The basic structure of photoconductors is comprised of the active material sandwiched between two electrodes to form an ohmic contact. The

specific mechanism involves a charge carrier being recirculated through the symmetrical contacts before it is recombined with the opposite charge [49]. The basic working principle of the photoconductor is to change the electrical conductivity as a function of the intensity of the light.

3.3.1.2 Photodiodes

The configuration of a photodiode can be either conventional or inverted and the presence of interface layers reduces dark current leading to high detectivity [49]. The different work function of each electrode controls the photogenerated carriers and a reverse charge is applied in order to increase the efficiency of the charge collection, as opposed to solar cells which function within a circuit receiving an external load [49]. Specifically, this external load is the application of forward bias on solar cells. There is a difference between the optimisation orientation of solar cells and diodes, however, they do possess a similar device structure [49]. Where photodiodes do work at a zero bias, they are self-powered photodetectors, similar to a solar cell when it is under a short circuit condition [52]. In contrast, since the total current is the sum dark current and photocurrent that passes through the device, the dark current in the photodiode should be reduced in order to increase their sensitivity.

3.3.1.3 Phototransistors

Phototransistors have a 3 terminal structure and a conductive channel. The terminal consists of drain electrodes on either side and the source on another side where electrons flow from drain to source. While a gate terminal controls the conductivity of the channel [49], it is possible to control channel conductance through light illumination. The gate, which is opto-electronically

modulated, is programmable and can facilitate or prevent charge transport while at the same time providing gain, thus it works as an amplifying switch [53].

3.3.2 Recent Developments in Hybrid Halide Perovskite photodetectors

Hybrid – organic-inorganic perovskite materials have also been applied in photodetectors. It is in fact the same optoelectronic properties that are found in other solar cell applications that make these materials suitable for photodetectors. Specific favorable properties of these materials have been found for this application and they include high responsivity, which is the number of electrons that can be harvested for each illuminated photon, high detectivity which refers to the lowest detectable light intensity and fast response speed [54]. These are achieved due to optical and electrical properties which include a high absorption coefficient, small excitonic binding energy, large carrier mobility and long electron and hole diffusion lengths [44]. Xie et al. (2014) reported the first photodetector based on $MAPbI_3$ perovskite thin film deposited on polyethylene terephthalate (PET) substrate patterned with ITO electrodes, it showed photo responsivity with an R of 3.49 A/W, 0.0367 A/W, an external quantum efficiency of 1.19×10^3 %, 5.84% at 365 nm and 780 nm respectively [55]. This report opened the path for a large amount of outstanding work.

Transistor type photodetectors that use perovskite materials have been reported [12]. The most common architectures are Metal–oxide–semiconductor transistors which usually consists of a gate, drain and a channel (photo active medium; perovskite) which is fabricated on the top of the device and contacted with an oxide layer and source electrodes (typically Au). However, these photodetectors still exhibit low performance because of the poor mobility of charge carriers in the channel where one type of free charge retains trapping in the channel, and the

other are accumulated in the channel [56]. Furthermore, the bilayer-structure which consists of a combination perovskite layers and inorganic semiconductors like graphene can improve the photo responsivity, hence increase their efficiency [57]. A necessary requirement of photodetectors is that they show a very fast response to incident radiation which is achieved using perovskite polycrystalline films, which offers high quantum yield and fast responses [12, 56,58].

The photodiode is another type of photodetector which was commonly reported in many studies because of its fast response time and high photoconductive gain characteristics [59]. However, it is important to note that achieving these devices with these materials requires complex structures and perhaps more importantly, the fact that perovskites are stability-restricted affecting device lifetime is another consideration.

3.3.2.1 Hybrid Halide Perovskites Single Crystal photodetectors

Although most of the demonstrated application areas for perovskites thin films have focused on solar cells, single crystal perovskites are more often found in photodetectors is more. This may be due to difficulty in attaining an appropriate thickness of perovskite single crystal for the structure of solar cells.

Wang et al., (2018) investigated the surface stability of the $MAPbBr_3$ single crystal under the environmental conditions of air and water, this was measured using XRD [60]. Lian et al. (2015) reported a photodetector based on methylammonium lead iodide as a perovskite single crystal which showed higher responsivity, approximately 100 fold, than the polycrystal structure of the same material[61]. Fang et al (cited in 62) found a narrow band photodetector using halide perovskite single crystal, this was due to a strong surface charge recombination,

this could be adjusted through tuning the molar ratio of the precursor in order to change the bandgap. A self-powered photodetector made by Fang (2016) and his group by combining the perovskite single crystal photodetector with a triboelectric nanogenerator, resulted in high responsivity without using an external electric field [62]. This was further developed by Ding et al. (2016) using a single crystal of methylammonium lead iodide with different metal electrodes [63]. Shaikh et al. (2016) developed a self-bias photodetector using a single crystal of methylammonium lead bromide together with Pt – Au electrodes [64].

Where the present study is different from these studies is in terms of what is measured to determine stability, how it is measured and the materials and their preparation. Wang et al.(2018) only considered surface stability and only measured stability using XRD [60], Murali et al. (2017) look at the stability of the whole of the $MAPbBr_3$ single crystal using PL intensity and Choi et al. (2019) tested the stability of the surface of the $MAPbBr_3$ as a single crystal in UHV (ultra-high vacuum)and dark conditions at room temperature[65,66]. Lian et al. (2015) used $MAPbI_3$ which was prepared differently to the present study and they used a different device structure and approaches to measuring stability[61]. Ding et al. (2016) used the same measurements as the present study including XRD and IV but for $MAPbI_3$ [63]. Fu et al. (2018) conduct a review on the progress of the long term stability of perovskite solar cells and cite numerous studies, none of which address $MAPbBr_3$ [67].

3.4 Stability of Hybrid Halide Perovskite

At present, there has been a significant improvement in terms of basic scientific understanding of perovskite materials achieving solar cell performance of 23% PCE [68,69]. In addition,

hybrid halide perovskites can be deposited on various substrates using solution-based processes. Semi-transparent perovskite solar cells can be fabricated [70-72]. Furthermore, planar perovskite solar perovskite solar cells have been experimented with by using an ultrathin layer of perovskite on the model plane [73]. In future, perovskite solar cells may be suitable for space applications because they are flexible and lightweight [22].

However, there are still issues that need to be resolved before they can be fully commercialised, one such issue is low stability, and unfortunately, there has been limited success in overcoming this problem [11]. Therefore, the stability of lead halide perovskite single crystals will be investigated in this research by studying these materials in isolation and in a solar cell device.

3.4.1 Intrinsic Stability for Hybrid Halide Perovskites Materials

In consideration of the properties of hybrid perovskites that have been addressed in chapter 2, it has been shown that it is possible to predict a stable structure of perovskite materials by measuring the geometric factors including the Goldschmidt tolerance factor and the octahedral factor. However, this established stable structure becomes unstable after fabrication, specifically, this relates to an instability related to the mobility of ions in the material [74].

There are many types of chemical defects (point defects) in organo-lead halide perovskite, like ion interstitials, ion vacancies or anti-site defects. Thus, the relative concentration of acceptor and donor states are directly related to the energies of defect formation. For example, the enthalpy of defect formation for $MAPbX_3$ (X=I, Cl) network is calculated to be higher when chloride is substituted with iodide on the electronic structure which improves their stability [75-78].

Fragmentation of organic molecules is another factor that impacts defect formation, this would include missing hydrogen atoms from the organic molecules. These hydrogen species like H^+, H^0, and H^- easily migrate to the inorganic lattice and interact with surrounding molecules. Thus, it is necessary to control the fragmentation of organic molecules and hydrogen migration [79,80]. Efficiency is no longer a primary concern, it is now important to address and improve stability of hybrid perovskites, including under various light and heat conditions [74].

As part of the overall development of the use of this material there have been considerable efforts in fabrication techniques for perovskite films, optimisation of cell structures and tailored chemical compositions [22]. In reference to the latter, composition engineering, there have been advances made to improve phase stability [81]. In general, long-term stability is associated with the sustainability of the crystal phase. To address the issue of stability in hybrid perovskites, Zhao and Park (2015) suggested that in order to improve the stability there should be an investigation of air stability, photo stability and heat stability. The thermal stability of hybrid perovskite materials, used in solar cells, is often addressed because the crystal phase transition together with ion migration as a result of temperature have an effect on the long-term stability of these materials [82]. Furthermore, there should also be consideration of photostability of hybrid perovskites in solar cell applications, which is due to the instability of these materials under AM 1.5 G (1 sun) irradiation which includes UV [83]. From previous studies, however, there is little research that addresses the effect of annealing and light on hybrid halide perovskite materials before incorporation into a device. This lack of information motivated this research to investigate the impact of annealing and light on hybrid halide perovskite materials.

The present study is concerned with the stability, in terms of heat and light stability, of a $MAPbBr_3$ single crystal and it is worth to note that crystalline structure will allow better elucidation of the mechanisms associated with long-term stability in terms of structure. The reason for this is that a polycrystalline structure has a high number of grain boundaries and

defects which make such elucidation difficult [84]. This issue is further compounded by the fact that there are unstable interfaces and importantly, because the quality of polycrystalline films is significantly affected by factors during preparation such as temperature and spin coating, leading to variations in quality, and thus, comparing results from different studies is unreliable [85-87]. These issues are eliminated in the study of the long-term stability of perovskite materials as a single crystal structure and therefore, this approach offers a more reliable way to investigate the intrinsic structural stability of this material which has a significant effect on light and thermal stability [84]. Furthermore, there is a lack of research of hybrid halide perovskite single crystals as a material alone not as a device, and a lack of $MAPbBr_3$ single crystal as a material alone in particular.

3.4.2 Stability of Hybrid Halide Perovskite Solar Cells

Solar cells that use polycrystalline perovskites are prone to degradation which affects their stability, this degradation has been attributed to a number of factors including phase transformations, chemical instability and exposure to light, oxygen, heat and moisture [88,89]. Stability has been something that has received less attention than performance of polycrystalline perovskite solar cells, this has been attributed to a lack of understanding of chemical and physical mechanisms in the solar device [89]. While solar perovskite cells generally demonstrate high performance, efficiency is not maintained, and degradation can take place in a relatively short space of time, on the other hand a solar cell with less efficiency often demonstrates better stability [68]. Therefore, it is essential to improve the stability of perovskite solar cells through understanding mechanisms of degradation and how this affects device performance [68]. Testing of stability should involve accelerated conditions of temperature and light [89].

There are a number of issues that contribute to the degradation of polycrystalline perovskites used in solar panel applications. One problem is related to perovskite materials itself; it contains salts which mean overtime they absorb moisture, leading to low formation energy and decomposition [89]. Importantly, weak bonds in the material are easily broken by exposure to light [88]. Another issue is that although decomposition of polycrystalline perovskite materials in solar cell applications decomposes at a slow rate under normal operating conditions, it does decompose rapidly under the temperatures which solar panels are packaged [89,90]. Both temperature and light are important considerations for degradation of polycrystalline perovskites because they react with all metals under moderate light and temperature conditions [91]. The present research is concerned with degradation under temperature and light conditions for single crystal perovskite.

There have been a number of efforts to improve stability of perovskite materials in these devices. Introduction of mixed halides or cations into perovskites can reduce the instability induced by light and heat. Ions migrate slowly when there is a partial substitution of cesium in lead halide perovskite materials such as $Cs_xFA_{1-x}Pb(Br_yI_{1-y})_3$, $Cs_xFA_{1-x}PbI_3$, and $Cs_x(MA_yFA_{(1-y)})Pb(I_{(1-y)}Br_y)_3$ [92-94].

In the above it has been shown that the stability of a device can be affected by the active material, namely, perovskites, however, the stability of a device, whether a solar cell or photoconductor, can also be related to the device structure and materials [88].

Specifically, this includes consideration of the modification of the interfaces between the perovskite material and the electron transport layer. For example, TiO_2 nanoparticles are used as a transport layer in solar cells because they improve the reaction rate of perovskites. However, with the use of TiO_2 the charge transfer can be unstable when exposed to UV light

due to the porous nature of this material [95]. To improve the stability of solar cells and reduce trap density, oxide materials such as ZnO and SnO_2 and organic materials such as [6,6]-phenyl-C61-butyric acid methyl ester (PCBM) and ICBA (indene C60 bis adduct), as well as carbon nanoforms such as fullerene C60, can be added to the transport layer of the solar cell instead of TiO_2 [14,88]. Therefore, modification of the interface is essential not only for performance but also for stability of the material [88].

Hole transporting materials (HTMs), including the use of organic and inorganic materials have been developed for solar cells such as polymer/carbon composites. They have hydrophobic properties to repel water, and importantly, a higher hole mobility [96]. However, the performance using these HTMs is lower than devices based on Spiro-OMeTAD which is also able to improve the interfacial contact between the electrode and the perovskite material due to the pinholes as a result of its ageing process [97]. In order to avoid these disadvantages of HTMs, a PbS buffer is applied to correct the orientation between the hole transport layer and the active layer, such devices exhibit a better photovoltaic performance as well as stability even at high humidity [88]. Despite the fact that HTMs are partially or even completely resistance to moisture, it might not be enough for protecting the perovskite materials from oxygen which is considered to be the greater concern compared to other gases in the atmosphere such as nitrogen. The surface of perovskite materials reacts with oxygen, forming superoxide ions which break down the perovskite [98,99]. Therefore, the development of perovskite compositions that have an insensitivity to oxygen through encapsulation that protects devices from oxygen-induced degradation and hydrophobic layers to protect against moisture, have been paramount. Therefore, degradation caused by moisture and oxygen has been a matter of great concern in perovskite applications, unlike instability resulting from temperature and light which is the focus of this research.

3.5 Summary

This chapter presented hybrid halide perovskite photovoltaic applications and associated stability. This included stability of hybrid halides generally and the resolution of identified stability issues which included achieving geometrical factors and replacing organic cations with organic - inorganic cation. An overview of photovoltaic devices was presented together with the relevant working principles of these devices. This included the various device architectures and their associated efficiencies. The research includes testing material as a photodetector device, and therefore, it was necessary to establish their device structure and working principles. For a more particular understanding of the materials considered in this research, hybrid halide perovskite-based and hybrid halide perovskite single crystal-based photodetectors were also presented. Importantly, towards a focussed understanding of stability mechanisms for the present study, the stability mechanisms of these particular devices, including hybrid halide perovskite solar cells was also presented.

3.6 References

[1] M. Grätzel, "Photoelectrochemical cells", Nature, vol. 414, no. 6861, pp. 338-344, 2001. Available: 10.1038/35104607.

[2] K. Tennakone, G. Kumara, I. Kottegoda, V. Perera and G. Aponsu, "Nanoporous n-/selenium/p-CuCNS photovoltaic cell", Journal of Physics D: Applied Physics, vol. 31, no. 18, pp. 2326-2330, 1998. Available: 10.1088/0022-3727/31/18/019.

[3] L. Grondahl, "The Copper-Cuprous-Oxide Rectifier and Photoelectric Cell", Reviews of Modern Physics, vol. 5, no. 2, pp. 141-168, 1933. Available: 10.1103/revmodphys.5.141.

[4] S. Wenham, Applied photovoltaics, 2nd ed. London: TJ International Ltd, Padstow, Cornwall, 2007, pp. 3- 38.

[5] P. Beauchamp, Solar Power Technologies for Future Planetary Science Missions, 1st ed. Pasadena, California: National Aeronautics and Space Administration, 2017, pp. 1-40.

[6] A. Mohammad Bagher, "Types of Solar Cells and Application", American Journal of Optics and Photonics, vol. 3, no. 5, p. 94, 2015. Available: 10.11648/j.ajop.20150305.17.Askari Mohammad Bagher12015

[7] D. Bagnall and M. Boreland, "Photovoltaic technologies", Energy Policy, vol. 36, no. 12, pp. 4390-4396, 2008. Available: 10.1016/j.enpol.2008.09.070.Bagnall and Boreland, 2008

[8] KIBRIA, Mohammad Tawheed, et al., " A Review: Comparative studies on different generation solar cells technology". In: Proc. of 5th International Conference on Environmental Aspects of Bangladesh, 2014.

[9] P. Joshi, "Understanding the photostability of perovskite solar cell", DOCTOR OF PHILOSOPHY, Iowa State University, 2016.

[10] v. von, "Stability and Properties of Methylammonium Lead Iodide Solar Cells", Master of Science in Physics, der Technischen Universität Berlin, 2017.

[11] J. Huang, Y. Yuan, Y. Shao and Y. Yan, "Understanding the physical properties of hybrid perovskites for photovoltaic applications", Nature Reviews Materials, vol. 2, no. 7, 2017.

[12] Q. Chen et al., "Under the spotlight: The organic–inorganic hybrid halide perovskite for optoelectronic applications", Nano Today, vol. 10, no. 3, pp. 355-396, 2015. Available: 10.1016/j.nantod.2015.04.009.

[13] A. Kojima, K. Teshima, Y. Shirai and T. Miyasaka, "Organometal Halide Perovskites as Visible-Light Sensitizers for Photovoltaic Cells", Journal of the American Chemical Society, vol. 131, no. 17, pp. 6050-6051, 2009. Available: 10.1021/ja809598r.

[14] U. Krishnan, M. Kaur, M. Kumar and A. Kumar, "Factors affecting the stability of perovskite solar cells: a comprehensive review", Journal of Photonics for Energy, vol. 9, no. 02, p. 1, 2019.

[15]J. Wang et al., "Low-Temperature Processed Electron Collection Layers of Graphene/TiO2Nanocomposites in Thin Film Perovskite Solar Cells", Nano Letters, vol. 14, no. 2, pp. 724- 730, 2013.

[16]J. Im, C. Lee, J. Lee, S. Park and N. Park, "6.5% efficient perovskite quantum-dot-sensitized solar cell", Nanoscale, vol. 3, no. 10, p. 4088, 2011. Available: 10.1039/c1nr10867k.

[17]H. Kim et al., "Lead Iodide Perovskite Sensitized All-Solid-State Submicron Thin Film Mesoscopic Solar Cell with Efficiency Exceeding 9%", Scientific Reports, vol. 2, no. 1, 2012. Available: 10.1038/srep00591.

[18]M. Lee, J. Teuscher, T. Miyasaka, T. Murakami and H. Snaith, "Efficient Hybrid Solar Cells Based on Meso-Superstructured Organometal Halide Perovskites", Science, vol. 338, no. 6107, pp. 643-647, 2012. Available: 10.1126/science.1228604.

[19]J. Burschka et al., "Sequential deposition as a route to high-performance perovskite-sensitized solar cells", Nature, vol. 499, no. 7458, pp. 316-319, 2013. Available: 10.1038/nature12340.

[20]Y. Shao, Y. Yuan and J. Huang, "Correlation of energy disorder and open-circuit voltage in hybrid perovskite solar cells", Nature Energy, vol. 1, no. 1, 2016.

[21]L. Yang, J. Wang and W. Leung, "Lead Iodide Thin Film Crystallization Control for High-Performance and Stable Solution-Processed Perovskite Solar Cells", ACS Applied Materials & Interfaces, vol. 7, no. 27, pp. 14614-14619, 2015. Available: 10.1021/acsami.5b01049.

[22]C. Zuo et al., "Advances in perovskite solar cells." Advanced Science 3, no. 7, pp. 1500324,2016.

[23]M. Liu, M. Johnston and H. Snaith, "Efficient planar heterojunction perovskite solar cells by vapour deposition", Nature, vol. 501, no. 7467, pp. 395-398, 2013. Available: 10.1038/nature12509.

[24]J. Beilsten-Edmands, G. Eperon, R. Johnson, H. Snaith and P. Radaelli, "Non-ferroelectric nature of the conductance hysteresis in CH3NH3PbI3 perovskite-based photovoltaic devices", Applied Physics Letters, vol. 106, no. 17, p. 173502, 2015. Available: 10.1063/1.4919109.

[25]W. Yang et al., "High-performance photovoltaic perovskite layers fabricated through intramolecular exchange", Science, vol. 348, no. 6240, pp. 1234-1237, 2015. Available: 10.1126/science.aaa9272.

[26]J. Heo, H. Han, D. Kim, T. Ahn and S. Im, "Hysteresis-less inverted CH3NH3PbI3 planar perovskite hybrid solar cells with 18.1% power conversion efficiency", Energy & Environmental Science, vol. 8, no. 5, pp. 1602-1608, 2015. Available: 10.1039/c5ee00120j.

[27]J. Jeng et al., "CH3NH3PbI3Perovskite/Fullerene Planar-Heterojunction Hybrid Solar Cells", Advanced Materials, vol. 25, no. 27, pp. 3727-3732, 2013. Available: 10.1002/adma.201301327.

[28]J. Song et al., "Low-temperature SnO2-based electron selective contact for efficient and stable perovskite solar cells", Journal of Materials Chemistry A, vol. 3, no. 20, pp. 10837-10844, 2015.

[29]J. Wang et al., "Low-Temperature Processed Electron Collection Layers of Graphene/TiO2 Nanocomposites in Thin Film Perovskite Solar Cells", Nano Letters, vol. 14, no. 2, pp. 724-730, 2013.

[30] W. Yang et al., "Iodide management in formamidinium-lead-halide–based perovskite layers for efficient solar cells", Science, vol. 356, no. 6345, pp. 1376-1379, 2017. Available: 10.1126/science.aan2301.

[31] J. Shi et al., "Hole-conductor-free perovskite organic lead iodide heterojunction thin-film solar cells: High efficiency and junction property", Applied Physics Letters, vol. 104, no. 6, p. 063901, 2014. Available: 10.1063/1.4864638.

[32] K. Tsai, C. Chueh, S. Williams, T. Wen and A. Jen, "High-performance hole-transporting layer-free conventional perovskite/fullerene heterojunction thin-film solar cells", Journal of Materials Chemistry A, vol. 3, no. 17, pp. 9128-9132, 2015. Available: 10.1039/c5ta01343g.

[33] D. Liu, J. Yang and T. Kelly, "Compact Layer Free Perovskite Solar Cells with 13.5% Efficiency", Journal of the American Chemical Society, vol. 136, no. 49, pp. 17116-17122, 2014. Available: 10.1021/ja508758k.

[34] W. Ke et al., "Efficient hole-blocking layer-free planar halide perovskite thin-film solar cells", Nature Communications, vol. 6, no. 1, 2015. Available: 10.1038/ncomms7700.

[35] P. Zhao et al., "Large-Size CH3NH3PbBr3 Single Crystal: Growth and In Situ Characterization of the Photophysics Properties", The Journal of Physical Chemistry Letters, vol. 6, no. 13, pp. 2622-2628, 2015. Available: 10.1021/acs.jpclett.5b01017.

[36] Q. Dong et al., "Electron-hole diffusion lengths > 175 μm in solution-grown CH3NH3PbI3single crystals", Science, vol. 347, no. 6225, pp. 967-970, 2015. Available: 10.1126/science.aaa5760.

[37] W. Peng et al., "Solution-Grown Monocrystalline Hybrid Perovskite Films for Hole-Transporter-Free Solar Cells", Advanced Materials, vol. 28, no. 17, pp. 3383-3390, 2016. Available: 10.1002/adma.201506292.

[38] Z. Chen et al., "Thin single crystal perovskite solar cells to harvest below-bandgap light absorption", Nature Communications, vol. 8, no. 1, 2017. Available: 10.1038/s41467-017-02039-5.

[39] Z. Chen et al., "Single-Crystal MAPbI3 Perovskite Solar Cells Exceeding 21% Power Conversion Efficiency", ACS Energy Letters, vol. 4, no. 6, pp. 1258-1259, 2019. Available: 10.1021/acsenergylett.9b00847.

[40] J. Mailoa et al., "A 2-terminal perovskite/silicon multijunction solar cell enabled by a silicon tunnel junction", Applied Physics Letters, vol. 106, no. 12, p. 121105, 2015. Available: 10.1063/1.4914179.

[41] G. Konstantatos, "Current status and technological prospect of photodetectors based on two- dimensional materials", Nature Communications, vol. 9, no. 1, 2018. Available: 10.1038/s41467-018- 07643-7.

[42] O., Franck et al. "Wide bandgap UV photodetectors: A short review of devices and applications." In Gallium Nitride Materials and Devices II, vol. 6473, pp. 64730E. International Society for Optics and Photonics, 2007.

[43] L. Sang, M. Liao and M. Sumiya, "A Comprehensive Review of Semiconductor Ultraviolet Photodetectors: From Thin Film to One-Dimensional Nanostructures", Sensors, vol. 13, no. 8, pp. 10482- 10518, 2013. Available: 10.3390/s130810482.

[44] H. Zhu et al., "Room-Temperature Solution-Processed NiOx: PbI2 Nanocomposite Structures for Realizing High-Performance Perovskite Photodetectors", ACS Nano, vol. 10, no. 7, pp. 6808-6815, 2016. Available: 10.1021/acsnano.6b02425.

[45] W. Wei, X. Bao, C. Soci, Y. Ding, Z. Wang and D. Wang, "Direct Heteroepitaxy of Vertical InAs Nanowires on Si Substrates for Broad Band Photovoltaics and Photodetection", Nano Letters, vol. 9, no. 8, pp. 2926- 2934, 2009. Available: 10.1021/nl901270n.

[46] M. Arnold et al.,"Broad Spectral Response Using Carbon Nanotube/Organic Semiconductor/C60 Photodetectors", Nano Letters, vol. 9, no. 9, pp. 3354-3358, 2009.

[47] J. Clifford, G. Konstantatos, K. Johnston, S. Hoogland, L. Levina and E. Sargent, "Fast, sensitive and spectrally tuneable colloidal-quantum-dot photodetectors", Nature Nanotechnology, vol. 4, no. 1, pp. 40-44, 2008. Available: 10.1038/nnano.2008.313.

[48] D. Shin et al., "Graphene/Si-Quantum-Dot Heterojunction Diodes Showing High Photosensitivity Compatible with Quantum Confinement Effect", Advanced Materials, vol. 27, no. 16, pp. 2614-2620, 2015. Available: 10.1002/adma.201500040.

[49] J. Miao and F. Zhang, "Recent progress on highly sensitive perovskite photodetectors", Journal of Materials Chemistry C, vol. 7, no. 7, pp. 1741-1791, 2019. Available: 10.1039/c8tc06089d.

[50] J. Miao and F. Zhang, "Recent Progress on Photomultiplication Type Organic Photodetectors", Laser & Photonics Reviews, p. 1800204, 2018. Available: 10.1002/lpor.201800204.

[51] G. Hernandez-Sosa, N. Coates, S. Valouch and D. Moses, "High Photoconductive Responsivity in Solution-Processed Polycrystalline Organic Composite Films", Advanced Functional Materials, vol. 21, no. 5, pp. 927-931, 2011. Available: 10.1002/adfm.201002518.

[52] I. Kim et al., "High-Performance, Fullerene-Free Organic Photodiodes Based on a Solution-Processable Indigo", Advanced Materials, vol. 27, no. 41, pp. 6390-6395, 2015. Available: 10.1002/adma.201502936.

[53] L. Ye, H. Li, Z. Chen and J. Xu, "Near-Infrared Photodetector Based on MoS2/Black Phosphorus Heterojunction", ACS Photonics, vol. 3, no. 4, pp. 692-699, 2016. Available: 10.1021/acsphotonics.6b00079.

[54] L. Dou et al., "Solution-processed hybrid perovskite photodetectors with high detectivity", Nature Communications, vol. 5, no. 1, 2014. Available: 10.1038/ncomms6404.

[55] X. Hu et al., "High-Performance Flexible Broadband Photodetector Based on Organolead Halide Perovskite", Advanced Functional Materials, vol. 24, no. 46, pp. 7373-7380, 2014. Available: 10.1002/adfm.201402020.

[56] J. Zhou and J. Huang, "Photodetectors Based on Organic-Inorganic Hybrid Lead Halide Perovskites", Advanced Science, vol. 5, no. 1, p. 1700256, 2017. Available: 10.1002/advs.201700256.

[57] Y. Lee et al., "High-Performance Perovskite-Graphene Hybrid Photodetector", Advanced Materials, vol. 27, no. 1, pp. 41-46, 2014. Available: 10.1002/adma.201402271.

[58] F. García de Arquer, A. Armin, P. Meredith and E. Sargent, "Solution-processed semiconductors for next-generation photodetectors", Nature Reviews Materials, vol. 2, no. 3, 2017. Available: 10.1038/natrevmats.2016.100.

[59] R. Dong et al., "High-Gain and Low-Driving-Voltage Photodetectors Based on Organolead Triiodide Perovskites", Advanced Materials, vol. 27, no. 11, pp. 1912-1918, 2015. Available: 10.1002/adma.201405116.

[60] C. Wang, B. Ecker, H. Wei, J. Huang and Y. Gao, "Environmental Surface Stability of the MAPbBr3 Single Crystal", The Journal of Physical Chemistry C, vol. 122, no. 6, pp. 3513-3522, 2018. Available: 10.1021/acs.jpcc.7b12740.

[61] Z. Lian et al., "High-Performance Planar-Type Photodetector on (100) Facet of MAPbI3 Single Crystal", Scientific Reports, vol. 5, no. 1, 2015. Available: 10.1038/srep16563.

[62] H. Fang et al., "A self-powered organolead halide perovskite single crystal photodetector driven by a DVD-based triboelectric nanogenerator", Journal of Materials Chemistry C, vol. 4, no. 3, pp. 630-636, 2016. Available:10.1039/c5tc03342j.

[63] J. Ding et al., "A self-powered photodetector based on a CH3NH3PbI3single crystal with asymmetric electrodes", CrystEngComm, vol. 18, no. 23, pp. 4405-4411, 2016. Available:10.1039/c5ce02531a.

[64] P. Shaikh et al., "Schottky junctions on perovskite single crystals: light-modulated dielectric constant and self-biased photodetection", Journal of Materials Chemistry C, vol. 4, no. 35, pp. 8304-8312, 2016. Available: 10.1039/c6tc02828d.

[65] B. Murali et al., "The Surface of Hybrid Perovskite Crystals: A Boon or Bane", ACS Energy Letters, vol. 2, no. 4, pp. 846-856, 2017. Available: 10.1021/acsenergylett.6b00680.

[66] J. Choi et al., "Atomic-scale view of stability and degradation of single-crystal MAPbBr3 surfaces", Journal of Materials Chemistry A, vol. 7, no. 36, pp. 20760-20766, 2019. Available: 10.1039/c9ta05883d.

[67] Q. Fu et al., "Recent Progress on the Long-Term Stability of Perovskite Solar Cells", Advanced Science, vol. 5, no. 5, p. 1700387, 2018. Available: 10.1002/advs.201700387.

[68] M. Asghar et al. "Device stability of perovskite solar cells–A review." Renewable and Sustainable Energy Reviews 77, pp. 131-146, 2017.

[69] A. Jena, A. Kulkarni and T. Miyasaka, "Halide Perovskite Photovoltaics: Background, Status, and Future Prospects", Chemical Reviews, vol. 119, no. 5, pp. 3036-3103, 2019.

[70] G. Eperon et al. "Neutral colour semi-transparent micro-structured perovskite solar cells." ACS nano 8, no. 1, pp. 591-598,2013.

[71] W. Zhang et al., "Highly Efficient Perovskite Solar Cells with Tunable Structural Color", Nano Letters, vol. 15, no. 3, pp. 1698-1702, 2015. Available: 10.1021/nl504349z.

[72] W. Subhani et al., "Anti-solvent engineering for efficient semi transparent CH3NH3PbBr3 perovskite solar cells for greenhouse applications", Journal of Energy Chemistry, vol. 34, pp. 12-19, 2019. Available: 10.1016/j.jechem.2018.10.001.

[73] M. Kaltenbrunner et al., "Flexible high power-per-weight perovskite solar cells with chromium oxide– metal contacts for improved stability in air", Nature Materials, vol. 14, no. 10, pp. 1032-1039, 2015. Available: 10.1038/nmat4388.

[74] B. Park and S. Seok, "Intrinsic Instability of Inorganic–Organic Hybrid Halide Perovskite Materials", Advanced Materials, vol. 31, no. 20, p. 1805337, 2019. Available: 10.1002/adma.201805337.

[75] G. Maculan et al., "CH3NH3PbCl3 Single Crystals: Inverse Temperature Crystallization and visible Blind UV-Photodetector" , The Journal of Physical Chemistry Letters, vol. 6, no. 19, pp. 3781-3786, 2015.

[76] P. Umari, E. Mosconi and F. De Angelis, "Relativistic GW calculations on CH3NH3PbI3 and CH3NH3SnI3 Perovskites for Solar Cell Applications", Scientific Reports, vol. 4, no. 1, 2014.

[77] W. Yin, T. Shi and Y. Yan, "Unique Properties of Halide Perovskites as Possible Origins of the Superior Solar Cell Performance", Advanced Materials, vol. 26, no. 27, pp. 4653-4658, 2014.

[78] A. Buin, R. Comin, J. Xu, A. Ip and E. Sargent, "Halide-Dependent Electronic Structure of Organolead Perovskite Materials", Chemistry of Materials, vol. 27, no. 12, pp. 4405-4412, 2015.

[79] D. Egger, L. Kronik and A. Rappe, "Theory of Hydrogen Migration in Organic-Inorganic Halide Perovskites", Angewandte Chemie, vol. 127, no. 42, pp. 12614-12618, 2015. Available: 10.1002/ange.201502544.

[80] R. Marom et al., "Quantum Tunneling of Hydrogen Atom in Dissociation of Photoexcited Methylamine†", The Journal of Physical Chemistry A, vol. 114, no. 36, pp. 9623-9627, 2010. Available: 10.1021/jp912107h.

[81] W. Peng, "Single Crystals of Organolead Halide Perovskites: Growth, Characterization, and Applications", Doctor of Philosophy, King Abdullah University of Science and Technology Thuwal, Kingdom of Saudi Arabia, 2017.

[82] A. Dobrovolsky, A. Merdasa, E. Unger, A. Yartsev and I. Scheblykin, "Defect-induced local variation of crystal phase transition temperature in metal-halide perovskites", Nature Communications, vol. 8, no. 1, 2017. Available: 10.1038/s41467-017-00058-w.

[83] J. Correa-Baena et al., "Promises and challenges of perovskite solar cells", Science, vol. 358, no. 6364, pp. 739-744, 2017. Available: 10.1126/science.aam6323.

[84] L. Chen et al., "Toward Long-Term Stability: Single-Crystal Alloys of Cesium-Containing Mixed Cation and Mixed Halide Perovskite", Journal of the American Chemical Society, vol. 141, no. 4, pp. 1665-1671, 2019. Available: 10.1021/jacs.8b11610.

[85] M. Xiao et al., "A Fast Deposition-Crystallization Procedure for Highly Efficient Lead Iodide Perovskite Thin-Film Solar Cells", Angewandte Chemie International Edition, vol. 53, no. 37, pp. 9898-9903, 2014. Available: 10.1002/anie.201405334.

[86] N. Ahn, D. Son, I. Jang, S. Kang, M. Choi and N. Park, "Highly Reproducible Perovskite Solar Cells with Average Efficiency of 18.3% and Best Efficiency of 19.7% Fabricated via Lewis Base Adduct of Lead(II) Iodide", Journal of the American Chemical Society, vol. 137, no. 27, pp. 8696-8699, 2015. Available: 10.1021/jacs.5b04930.

[87] Y. Zhao and K. Zhu, "CH3NH3Cl-Assisted One-Step Solution Growth of CH3NH3PbI3: Structure, Charge-Carrier Dynamics, and Photovoltaic Properties of Perovskite Solar Cells", The Journal of Physical Chemistry C, vol. 118, no. 18, pp. 9412-9418, 2014. Available: 10.1021/jp502696w.

[88] K. Qin, B. Dong and S. Wang, "Improving the stability of metal halide perovskite solar cells from material to structure", Journal of Energy Chemistry, vol. 33, pp. 90-99, 2019. Available: 10.1016/j.jechem.2018.08.004.

[89] C. Boyd, R. Cheacharoen, T. Leijtens and M. McGehee, "Understanding Degradation Mechanisms and Improving Stability of Perovskite Photovoltaics", Chemical Reviews, vol. 119, no. 5, pp. 3418-3451, 2018. Available: 10.1021/acs.chemrev.8b00336.

[90] Y. Yuan et al., "Photovoltaic Switching Mechanism in Lateral Structure Hybrid Perovskite Solar Cells", Advanced Energy Materials, vol. 5, no. 15, p. 1500615, 2015. Available: 10.1002/aenm.201500615.

[91] B. Conings et al., "Intrinsic Thermal Instability of Methylammonium Lead Trihalide Perovskite", Advanced Energy Materials, vol. 5, no. 15, p. 1500477, 2015. Available: 10.1002/aenm.201500477.

[92] K. Bush et al., "Compositional Engineering for Efficient Wide Band Gap Perovskites with Improved Stability to Photoinduced Phase Segregation", ACS Energy Letters, vol. 3, no. 2, pp. 428-435, 2018. Available: 10.1021/acsenergylett.7b01255.

[93] Y. Jiang et al., "Large-Area Perovskite Solar Modules: Combination of Hybrid CVD and Cation Exchange for Upscaling Cs-Substituted Mixed Cation Perovskite Solar Cells with High Efficiency and Stability (Adv. Funct. Mater. 1/2018)", Advanced Functional Materials, vol. 28, no. 1, p. 1870007, 2018. Available: 10.1002/adfm.201870007.

[94] M. Saliba et al., "Cesium-containing triple cation perovskite solar cells: improved stability, reproducibility and high efficiency", Energy & Environmental Science, vol. 9, no. 6, pp. 1989-1997, 2016. Available: 10.1039/c5ee03874j.

[95] T. Leijtens, K. Bush, R. Prasanna and M. McGehee, "Opportunities and challenges for tandem solar cells using metal halide perovskite semiconductors", Nature Energy, vol. 3, no. 10, pp. 828-838, 2018.

[96] S. Habisreutinger, T. Leijtens, G. Eperon, S. Stranks, R. Nicholas and H. Snaith, "Carbon Nanotube/Polymer Composites as a Highly Stable Hole Collection Layer in Perovskite Solar Cells", Nano Letters, vol. 14, no. 10, pp. 5561-5568, 2014. Available: 10.1021/nl501982b.

[97] A. Leguy et al. "Reversible hydration of CH3NH3PbI3 in films, single crystals, and solar cells." Chemistry of Materials 27, no. 9, pp. 3397-3407, 2015.

[98] H. Fang et al., "Ultrahigh sensitivity of methylammonium lead tribromide perovskite single crystals to environmental gases", Science Advances, vol. 2, no. 7, p. e1600534, 2016. Available: 10.1126/sciadv.1600534.

[99] N. Aristidou et al., "The Role of Oxygen in the Degradation of Methylammonium Lead Trihalide Perovskite Photoactive Layers", Angewandte Chemie, vol. 127, no. 28, pp. 8326-8330, 2015. Available: 10.1002/ange.201503153.

Chapter 4: Fabrication and Characterisation Techniques

Chapter 4: Fabrication and Characterisation Techniques

This chapter introduces an overview of fabrication and various characterisation techniques used in this research. In Section one, the technique used in the fabrication of single crystal perovskite devices is presented. Section two describes the techniques used in the characterisation of single crystal perovskites whilst section three presents the conventional parameters and measurement standards used to evaluate the performance of devices.

4.1 Fabrication Techniques

For the application of the of the metal electrodes to the single crystal for the lateral architecture two techniques were used in this research, namely; thermal evaporation (vacuum evaporation) and the brush technique.

4.1.1 Thermal Evaporation

One of the most common technique of physical vapor deposition (PVD) for coating is thermal evaporation (vacuum evaporation). For the preparation of a high-quality electrical contact on the single crystal perovskite, thermal evaporation was the only fabrication technique that was utilised due to its reasonable cost and ease of use.

In this research most of the selected metal electrodes, specifically; aluminium, silver, selenium, copper, gold, zinc, indium and tin were deposited using a vacuum evaporation to a thickness of 200nm.

Thermal evaporation is used to deposit thin film on the substrate by using one element or co-evaporation of a few elements. It offers efficient evaporation for a wide range of materials such as metal and some organic material [1].

Evaporation of a material and its subsequent condensation on a substrate is a simple technique where the transport of material to the substrate is affected by a physical driving mechanism, as shown in Figure 4.1. The materials and substrates are loaded into a vacuum chamber with a wire heater into which the material is placed. All baskets are made of materials that have high boiling points such as tungsten, tantalum or molybdenum. Based on the material's evaporation temperature, the shape of the basket should be selected, for instance a filament, a basket, a boat or a crucible. After a vacuum is created by using a pump, a large electrical current is passed through the basket heating the material to the desired temperature where evaporation occurs [1]. This means the solid or the liquid phase directly transforms to the vapor phase. Due to the low temperature of the substrates compared with the evaporation source, the material in vapor phase condenses on the substrate, forming a film.

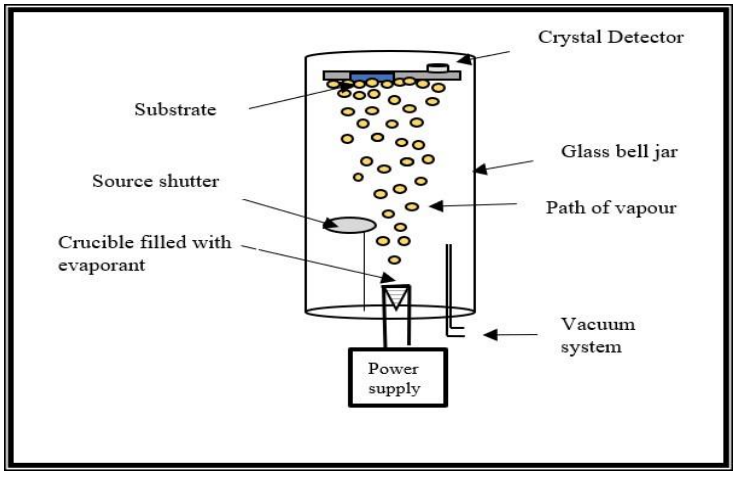

Figure4.1: Diagram of thermal evaporation process.

High vacuum and low pressure are important parameters to produce a high-quality deposited film. Therefore, evaporation in this work was kept at a pressure lower than 10^{-6} Torr. Atoms or molecules travel in straight lines from a thermal vaporisation source towards the substrate with minimum scattering or collision with surrounding residual gas molecules inside the evaporation chamber. Finally, the thickness of deposited electrodes (metal contacts)onto the perovskite single crystal was 200nm. It is usually controlled and monitored by using a shutter as well as a quartz crystal oscillator placed inside the Deposition chamber [1]. Edwards Auto 306 model thermal evaporator was used in this work.

4.1.2 Brush Painting Method

For aluminium-doped zinc oxide (AZO), carbon mixture, phenyl-C61- butyric acid methyl ester ($PC_{61}BM$) and Solution of poly (3,4-ethylenedioxythiophene): polystyrene sulfonate (PEDOT: PSS), were deposited using the brush painting method, described in the following.

Aluminium-doped zinc oxide (AZO) was deposited directly onto the surface of the crystal using a brush, followed by heating for 15 minutes at 120°C. The Carbon mixture was prepared by mixing carbon paste with silicone oil. The carbon mixture was deposited by brush on the surface of the crystal, followed by annealing at 100°C for 15 minutes.

Both of the abovementioned materials were deposited as a single layer. However, there were two materials that were required to be deposited as a bi-layer due to their low conductivity. Firstly, phenyl-C61-butyric acid methyl ester ($PC_{61}BM$) is usually introduced as an electron transport layer (ETL), 15 mg of $PC_{61}BM$ is dissolved in 0.5 ml of dichloride benzene and stirred on a hotplate for two hours at 70°C. This solution is deposited directly on one side of the $MAPbBr_3$ surface by using the brush and then heated for 15 minutes at 100°C. Secondly, a

solution of poly (3,4-ethylenedioxythiophene): polystyrene sulfonate (PEDOT: PSS) is usually used as a hole transporting layer. This solution was deposited using a brush and was annealed at 120°C for 15 minutes. Both these materials, deposited as a bilayer, are finished with a layer of silver deposited using vacuum evaporation.

4.2 Characterisation Techniques

Light and heat are utilised to determine the physical and chemical properties of materials. The working principle of associated techniques relies on observation of the changes in kinetic energy, phase, light intensity, direction of light beams, or electrical polarisation after interaction with the material being studied. Therefore, studying the physical and chemical properties of single crystal perovskites has played a major role in enhancing our understanding of material properties and mechanisms. In this work, Fourier Transform Infrared Spectroscopy ,UV-Vis Spectroscopy and Atomic Absorption Spectrometry (AAS) ,X-ray Diffraction Spectrometry (XRD), Scanning Electron Microscopy (SEM) , Electron Dispersive X-ray Spectroscopy (EDX), Thermal gravimetric analysis (TGA) and Differential scanning calorimetry (DSC) were used.

4.2.1 Fourier Transform Infrared Spectroscopy (FTIR)

Fourier transform infrared (FTIR) spectroscopy is used for solid, liquid and gas sample that is based on absorption or emission of infrared (IR) light of a range of wavelengths rather than a monochromatic light at each wavelength. Infrared spectroscopy is also known as vibrational spectroscopy.

When the infrared light strikes the sample, as seen in figure 4.2, some of radiation is absorbed and some of them pass through. The vibration energies in the molecules are a result of absorbed radiation in the sample. The frequency of vibration atoms in the sample rely on both the kind of bond, such as single, double, ionic and covalent bonds, and the type of molecule [2]. The light, which is not absorbed, is transmitted through the sample and falls on the detector. The number of absorption peaks in the absorption spectrum of the sample is indicative of the vibrational energy level at molecule, and intensity of the peaks refers to net changes in the dipole moment as result of molecule vibration. This infrared spectrum provided by FTIR offers information about the molecules in the sample including molecule structure and chemical bonding. The absorption spectra obtained from FTIR covers two regions in the range of 400-4000 cm^{-1}, representing a functional group and fingerprint regions [2].

The working mechanism of the FTIR benefits from the working principle of Michelson interferometer. When the source emits the light, the beam of light is split into two beams when it is passed through beam splitter. One of them reaches the constant mirror and is reflected. Part of the reflected light reaches the detector while the second part comes back to the source, passing through the splitter again. The second beam is reflected from a moving mirror which has only parallel movement. At the detector, the light intensity will be the combination from the two reflected beams. If the path length of both reflected lights is equal, the constructive interference will take place at the detector. However, if the signals of these beams are exactly opposite and out of phase, the destructive interference will occur at the detector [2].

Fourier Transformation is an algorithm that converts the interference pattern into the spectrum of transmittance/absorption in comparison with wave number calculated in cm^{-1} [2].

Bruker Alpha compact FTIR spectrometer was used in this study to identify the molecules of single crystal perovskite and determine changes in single crystal perovskite quality under different conditions.

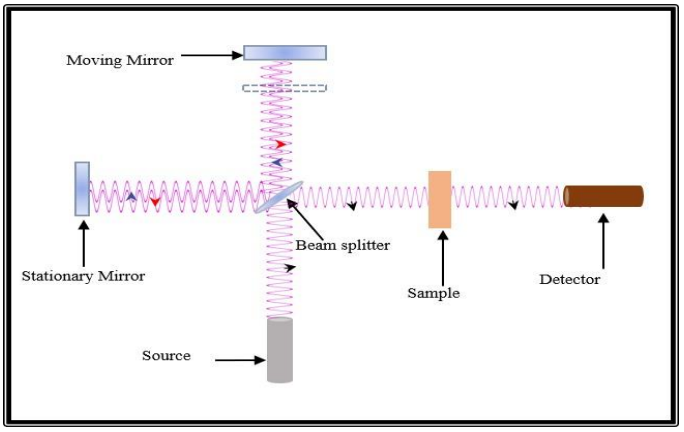

Figure4. 2: Diagram of Fourier transform infrared (FTIR) spectroscopy process.

4.2.2 Ultraviolet-Visible Spectroscopy (UV-Vis)

The purpose of using ultraviolet-visible (UV-Vis) spectroscopy is to investigate the absorption and transmission properties of the perovskite single crystal by measuring the maximum amount of absorbed light.

Due to absorption of the visible and ultraviolet (UV) radiation, electrons are excited, moving from lower to higher energy levels. Since each wavelength of light has an energy associated with it, a wavelength will be absorbed when its energy is enough to make one electronic transition. The large gap between the energy levels requires a great energy to excite the electron to move to the high energy level. Furthermore, there are two characterisations of the electron transition as either direct or indirect [3].

The working principle of UV-Vis spectroscopy is based on the absorption of the light at different wavelengths through the sample. In this spectrometer, a dual beam spectrometer, which splits the coming beam before it enters the measuring chamber, is used. A reference sample usually is placed in the reference slot so that measurements of samples can be compared with the values from the reference sample, and in order to eliminate the effects of substrate on the measurements from the sample. Before taking measurements of single crystal perovskite, the air was considered as a reference sample, so that it can be scanned, and background errors can be eliminated [3]. The spectral range was chosen between 190nm and 1100nm. Therefore, this work intends to measure the absorption or transmission of a material as a function of wavelength by using a Thermo Scientific Evolution 30UV-Vis Spectrometer.

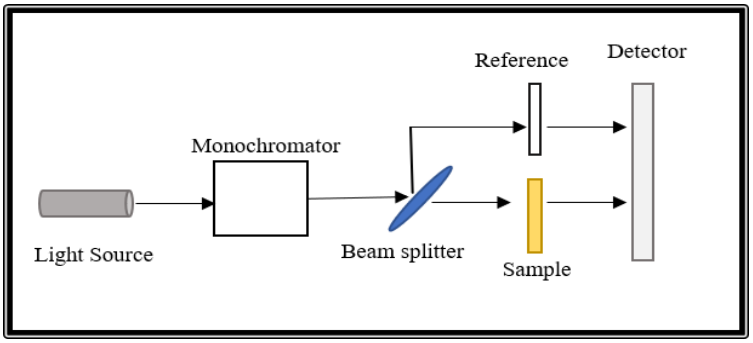

Figure 4.3: Diagram of UV-Vis spectroscopy characterisation

The percentage transmittance (T) is measured to determine the amount transmitted light through the crystal and is expressed by the following formula:

$$T = (I/I_0) \times 100\% \quad (1)$$

Absorption of the light can be measured by using the value of transmitted light in the following formula:

$$A = \log 10 \frac{1}{T} \quad (2)$$

$$A = \log 10 \frac{I_0}{I} \quad (3)$$

Where I_o and I are light intensities before and after transmitted by the sample and both A and T have no units [3].

For calculation of the optical band gap, it was calculated by using Tauc Plots. Since the electron transition in perovskite single crystal is a direct transition where electron-photon interactions occur , then the squared value of the product of photon energy and absorption coefficient ($\alpha h\nu$) is plotted versus the photon energy ($h\nu$) on the Y-axis and X-axis, respectively. The optical band gap was given by extrapolating the straight-line section in the graph to the X-axis. The relation between absorption coefficient and photon energy can be expressed using the following formula:

$$\alpha h\nu = A\,(h\nu - E_g)^n \quad (4)$$

Where A is constant, E_g is the band gap, h is Planck's constant, ν is frequency of vibration, n depends on the type of electronic transition; where n=2 for direct allowed transition and n= ½ for indirect allowed transition and α can be calculated by rearrangement of Lambert-Bouguer law [3]:

$$I = I_0 \exp(\alpha t) \quad (5)$$

$$\alpha = 1/t \ln[(1-R)^2 / T] \quad (6)$$

Where t is thickness of the sample, T and R refers to transmission and reflection, respectively. The value of the band gap can be calculated from this equation:

$$E_g = h\nu = 1240 / \lambda. \quad (7)$$

Where E_g is the band gap, h is Planck's constant, ν is frequency of vibration and λ is wave length.

4.2.3 Atomic Absorption Spectroscopy (AAS)

Atomic absorption spectroscopy measures the concentration of gas-phase atoms using light absorption. Perkin Elmer Analyst 400 Atomic Absorption Spectrophotometer was used in this study to confirm that a lead is the only element remain as the residual material after thermal decomposition of $MAPbBr_3$ crystal.

AAS uses a glass container which contains a cathode and an anode, the cathode is made of the same material that is under investigation, in this research lead, and the anode is a tungsten plate, the glass container is filled with argon at a low pressure. Between 500 and 1000 volts is applied to the electrodes it ionizes the atoms of the argon gas, positively charged ions remove atoms from the surface of the cathode which in turn collide with the energetic gas ions and become excited. This excitation emits characteristic radiation in the form of photons which is passed through a flame of the vaporised sample material under investigation, if this vaporisation contains lead then some of the emitted photons which have a wavelength specific to lead, will be absorbed. Thereafter, the radiation wavelength is passed through a monochromator to remove other light wavelengths found in visible light, before moving on to a detector as shown in figure 4.4. The detector measures the lead wavelength absorption,

the more of the wavelength that is absorbed, the higher the concentration of lead in the sample [5].

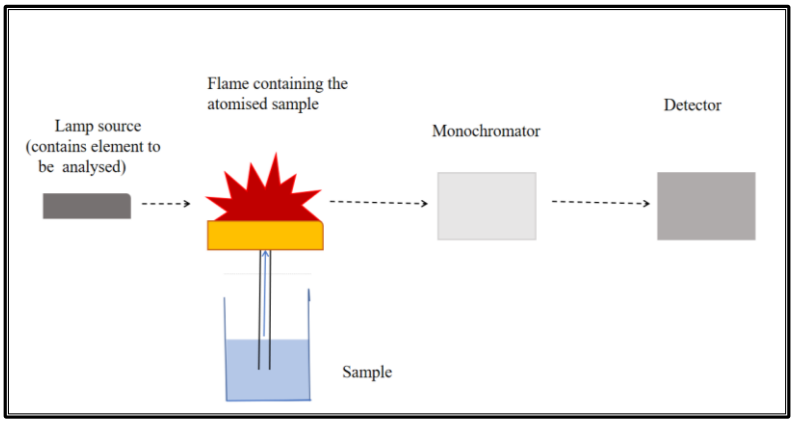

Figure4. 4:Schematic diagram on the process of an atomic absorption spectrometer(AAS)

4.2.4 X-ray Diffraction (XRD)

XRD is an analytical technique which provides detailed information regarding structural characteristics of crystalline solids. Measuring the diffracted waves by X-ray detector allows us to identify the distribution of atoms in a material. It relies on diffraction of X-rays which are generated upon the exposure of the metal target to the high energy electrons. Common metal targets used to generate X-rays involve Copper, Iron, Molybdenum and Chromium. In order to determine the structure of the desired samples, XRD is desirable option because of the quick delivery of results and convenience of use as the X-rays are not absorbed by the atmosphere [4].

X-rays were discovered in 1895 by Wilhelm Roentgen as electromagnetic radiation with short wavelengths. X-ray diffractometers consists of 3 elements as shown in Figure 4.5: X-ray tube, a holder of the sample, and an X-ray detector. In the X-ray tube, the electrons beam accelerates across a high voltage, which is usually measured in kilovolts, and hits the rotating or fixed solid

target. Upon collision with the target, two types of spectra are released from the X-ray tube. The first type, continuous spectra X-ray shown as a background of the radiation spectrum and has a range of minimum wavelengths and high intensity, depends on the voltage applied, and the material of target. The second type, characteristic spectra, have an intensity maximum at certain wavelength and are emitted from electronic transition states. When the energy of the electrons that accelerate to the target is high enough to remove the electron from the inner shell, the electron from the high energy shell will jump to the shell to take the place of a removed electron. It is necessary to mention that the intensity of characteristic spectra is higher than continuous spectra [4].

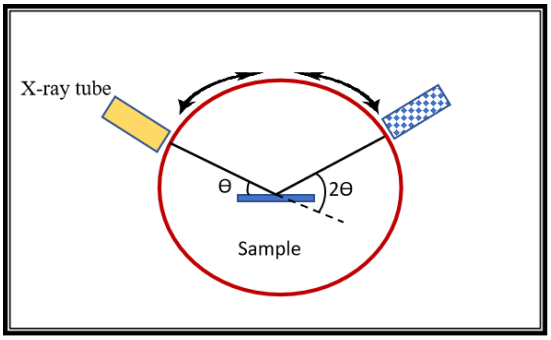

Figure4. 5: Diagram of X-ray diffraction process

When the incident beam of monochromatic X-rays strikes the sample in the form of perfect single crystal, the light is diffracted from the parallel planes separated by distance (d) measured by an angle "θ" with the surface of the plane. The beam reflected from the upper plane travels a shorter distance than the beam reflected from the lower plane. The intensity of reflected beams reaches their maxima, which is only possible if the path length difference corresponds to the integral number (n) of the wavelengths (λ). This relationship is given by the Bragg's law equation:

$$2dsin\theta = n\lambda \qquad (8)$$

Where d is the spacing between layers, θ is the angle between the incident ray and the surface, n is an integer and λ is the wavelength of electromagnetic radiation [4].

Moreover, the distribution of the atoms in the unit cell is described by the reflected beams. Since the highest density of electrons is found around atoms, the kind of atoms and their location can be determined by the reflections. Planes that pass through areas with low electron density will give weak intensities, while planes with high electron density will strongly reflect the beams. Due to periodic arrangement of atoms in a crystal, the size and shape of the unit cell are described by three lattice vectors (a, b, c) and the angles between them α, β, γ [4].

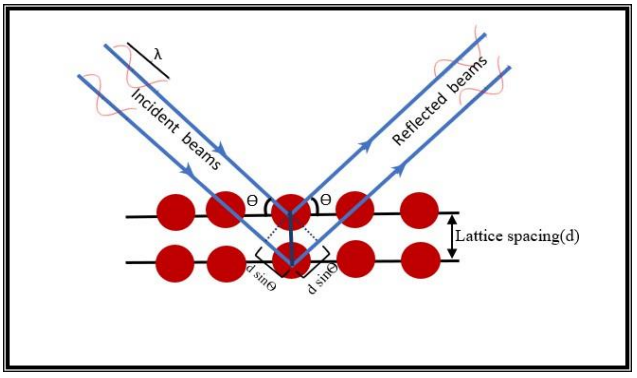

Figure4. 6: Diagram of the Bragg's law equation.

It is important to note that there is one family of peaks in the diffraction pattern generated for a single crystal perovskite. The XRD spectrometer is primarily used in this work to compare the structure of the single crystal hybrid perovskites at different light intensities as well as various temperatures. A structural characteristic was carried out in this work by using two XRD instruments which are Philips 1730 in the University of Leicester and Bruker 2D at De Montfort University.

4.2.5 Scanning Electron Microscopy (SEM)

A Scanning Electron Microscope (SEM) is a scientific tool which uses a focused beam of electrons generated by an electron gun to obtain detailed information by taking a top-view or cross-section images of specimens. It is utilised to extract information about the variations in the material's surface at a small-scale level, and to investigate the structural aspects of the sample. The high energy electrons scan the surface of the sample after passing vertically through a series of electromagnetic lenses and electrons are excited via ionization which are collected by suitable detectors.

Detectors convert the signal to a digital image where secondary electrons and backscattered electrons are the most collected signal[4].

There is the possibility of two types of scattering after the high energy electrons have hit the target material: Firstly, elastic scattering, in which kinetic energy, and velocity remain constant while the path of the electrons changes which are referred to as backscattered electrons. Secondly, inelastic scattering whereby lower-energy electrons resulting from an inelastic collision are known as secondary electrons where their energies are typically 50 eV or less [4].

The detailed image of the surface can be formed by secondary electrons, whereas the backscattering electrons detector is ideal for providing images that shows information on the sample's compositions. SEM in backscattering mode is also used to extract data about the atomic structure of the sample. However, the resolution of images in this mode is lower than that obtained in secondary electron mode due to a large generation region of backscattered electrons compared with the secondary electrons [4].

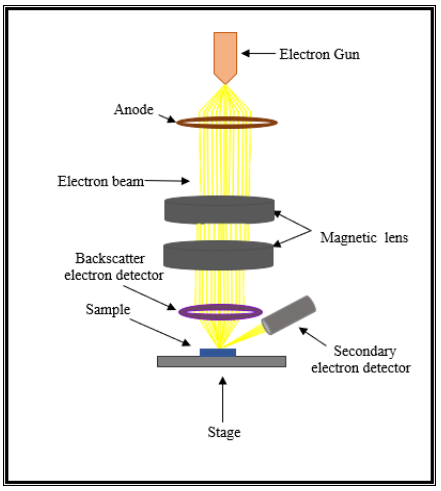

Figure4. 7:Diagram of Scanning Electron Microscope (SEM)

To obtain a high-quality image for the single crystal revealing the information about the surface structure or topography of the sample, SEM in a secondary electron mode was used. All SEM images in this work were taken using LEO 440SEM.

4.2.6 Electron Dispersive X-ray Spectroscopy (EDX)

Electron Dispersive X-ray Spectroscopy (EDX) spectroscopy is used to obtain elemental analysis by detecting the X-ray spectrum which is emitted from sample. It is important to mention that EDX can be used within SEM due to the fact that SEM provides the visual detail (images) while EDX provides the quantitative analysis. In EDX measurement, an electron beam bombards the sample, leading to inelastic colliding. Some of the electrons in the sample move out creating holes in the inner shell of the atom. These voids will be filled by the electrons from the outer shell which has higher energy [4]. For example, an electron of the M shell can fill a vacancy in the L shell, leading to the emission of Lα X-rays. Likewise, an electron from either the L shell or the M shell can fill a vacancy in the K-shell, resulting in the emission of K

α or K β X-rays, respectively. Since the probability of filling the K shell vacancy from an L shell electron is higher than that of an M shell electron, Kα X-rays has a higher intensity than that of Kβ X-rays.

The output of an EDX analysis are peaks showing levels of x-ray energy corresponding to specific elements, the intensity of these peaks refers to the quantity of the element as an wt percentage in the sample [4].

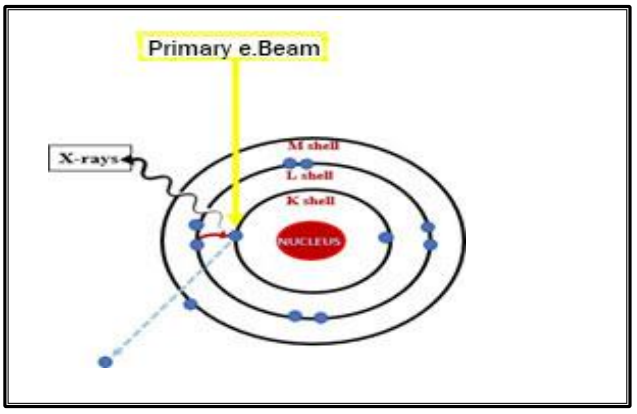

Figure4. 8: Diagram presents the principle for EDX

4.2.7 Thermal Gravimetric Analysis (TGA)

Thermal gravimetric analysis (TGA) is one of the extremely useful techniques, which provides information about any chemical or physical changes occurring in the sample such as oxidation, loss of solvent, loss of weight and moisture, as a result of changes in temperature (with a constant heating rate) or time (with constant temperature and/or constant weight) [2]. In this work, TGA was used to monitor the changes in mass of the sample as a function of temperature at a constant heating rate in order to detect the decomposition of sample materials. TGA curves are greatly influenced by properties of the sample, atmosphere of the chamber, heat rate and shape and nature of the sample pan. A sample is placed into the holder which is attached with

a sensitive microbalance. The holder is placed into the furnace. The balance allows to measure any change in the mass of the sample, and it is the most important part in the thermobalance instrument. The thermobalance instrument is used to record TGA data which consists of an electronic microbalance and associated temperature controller [4].

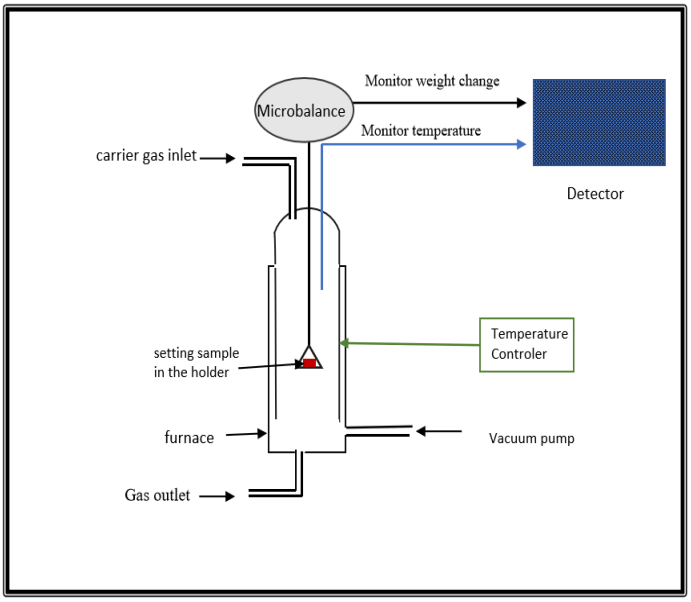

Figure4. 9:Schematic diagram of thermal gravimetric analysis set up.

In this research work, Perkin Elmer Pyris 1 TGA was used to perform TGA. All of experiments for collection of TGA data were conducted in the environment with constant nitrogen flow.

4.2.8 Differential Scanning Calorimetry (DSC)

Differential scanning calorimetry (DSC) is one of the most common thermo-analytical techniques that was developed by E.S. Watson and M. J. O'Neill in 1962. DSC provides useful information about phase changes taking place in a sample as a function of temperature. The DSC technique relies on measuring the amount of heat required to raise the temperature of a

sample as a function of temperature with respect to reference. In other words, measuring the amount of heat absorbed or released during heating or cooling of the sample can provide information like the exothermic and endothermic processes occurring in the sample, heat of phase changes and the crystallization and melting temperatures of the sample [4].

The DSC type which was used in this work is Heat flux DSC. In heat flux, a single furnace was used for heating both the sample and reference pans in order to provide a different temperature between them, which is used to get a required heat flow. An empty reference pan with its lid is commonly made up of an inert material like alumina. In order to avoid any reaction with them and resist the high temperatures, the sample pan, however, is made up of platinum, copper or gold. Different atmospheres can be applied and controlled in order to achieve a desired outcome. Both sample and reference are connected to a temperature sensor and a heater coil where temperature sensor monitors the temperature difference between the sample and reference while the heater coil heats them at a constant rate. Heat flow is directly proportional to the different temperature between the sample and a reference. Perkin Elmer Jade DSC was used to measure the phase transition of the Methylammonium lead bromide perovskite single crystal [4].

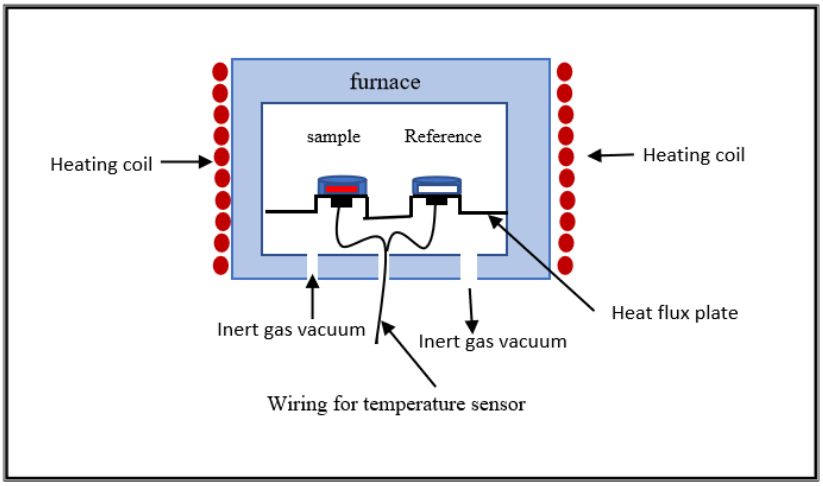

Figure 4. 10: Schematic diagram of a heat flux DSC.

4.3 Electrical Measurements

Many of electrical Characterisation techniques are used for research and manufacturing purposes. To evaluate solar cell performance, measurements such as current density of the cell as a function of voltage (J-V) for different light intensities as well as various applied temperatures, are used.

4.3.1 Current-Voltage Measurements

The Current-Voltage (I-V) or Current Density-Voltage (J-V) measurements are commonly used for understanding the photovoltaic cells operation; and its performances under standard illumination and dark without adding any additional load resistance. In this characterisation, a different bias voltage is applied across the device terminals sweeping the proper voltage range, while the current flow through the cell is measured. A simple equivalent circuit of PV cells is composed of current source arising from light illumination, diode, series resistor (R_s) and shunt resistor (R_{sh}) as shown below [6]. I–V characteristics were measured by HP4140B, that were controlled by Agilent Pro VEE software.

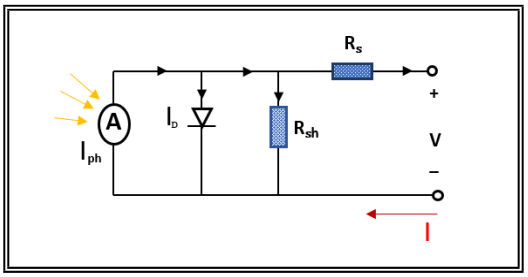

Figure4. 11:Diagram of ideal solar cell equivalent circuit.

From the equivalent circuit of solar cell:

$$I_{ph} - I_D - I_{sh} = I \quad (9)$$

Where I_{ph} is current generated by the solar cell, I_D is Diode current, I is the load current and I_{sh} is shunt current respectively [6].

4.3.1.1 Dark IV

The dark IV of device is shown as a diode, a large amount of current is passed through the device in forward bias while almost no current passes in reverse bias. Important parameters can be extracted such as ideality factor (n), dark saturation (I_O), Rectification ratio (RR), series resistance (R_s) and shunt resistance (R_{sh}).

$$J_D = J_o[\exp((qV_D)/nKT) - 1] \quad (10)$$

Where J_D,V_D and J_o are the current density passing through the diode, the voltage across the diode, and the dark saturation current density respectively, T, K and q are constants which are

the ambient temperature in Kelvin, Boltzmann constant and charge of an electron, respectively. An ideality factor (n) is a number between 1 and 2 which points out the type of charge carrier recombination, occurring inside the device. It is important to mention that the value of the ideality factor is inversely proportional to the fill factor which place important role in determining the efficiency of perovskite solar cell [2].

The second part of the equation can be ignored when applied voltage is above 50-100 mV.

$$J_D = J_o \exp\left((qV_D)/nKT\right) \quad (11)$$

By taking the log of both sides of the equation

$$\ln(J_D) = \ln(J_o) + (qV_D)/nkT \quad (12)$$

By plotting the $\ln(J_D)$ against the voltage at forward bias, the ideality factor and dark saturation current density are calculated from the slop [2].

The Rectification Ratio (RR) is calculated by the ratio of the forward bias to the reverse bias current density at a certain value of the applied voltage under a dark condition, as is presented by following equation. The rectification overall of the device is improved by reducing the reverse current density.

$$RR = J_F/J_R \quad (13)$$

Where J_F presents the majority carriers density from each depletion region across the junction, the minority carriers' density is presented by J_R. In addition, the value of RR in Schottky junctions is around $10^3 - 10^6$[7].

Resistivities' effects can reduce the efficiency of the solar cell by loss of power in the resistances. There are two kind of resistances in the equivalent circuit of solar cells which are a series and a shunt resistance. The series resistance is a result of movement of current through the diode material, as well as the contact resistance between the metal contact and semiconductors. Therefore, the series resistance should be a low resistance in order to achieve a high fill factor. Presence of a shunt resistance causes a loss of current at the edges of the device, which is a result of manufacturing defects, rather than poor design of the solar cell. Since the shunt resistance is connected in parallel to the device, it should be a high value in order to improve the fill factors and hence its performance. The values of R_s and R_{sh} can be calculated from the slopes of the linear parts of forward and reverse IV curves, respectively [6].

4.3.1.2 Light IV

The I-V curve shifts down into the fourth quadrant (positive x-axis and negative y-axis) as a result of illuminating the solar cell. Consequently, short-circuit current density (J_{SC}), open circuit voltage (V_{OC}), series resistance (R_s), shunt resistance (R_{sh}), the fill factor (FF) and power conversion efficiency (PCE) are the parameters that can be extracted from IV measurements. Current density-voltage characteristic of solar cells is described by the ideal diode equation under illumination as follows:

$$\mathrm{I} = \mathrm{I}_{ph} - I_D - I_{sh} \qquad (14)$$

$$\mathrm{I} = \mathrm{I}_{ph} - [\mathrm{I}_o(\exp((\mathrm{q}V_D)/\mathrm{nKT}) - 1)] - \frac{V_D}{R_{sh}} \qquad (15)$$

(16)

$$I = I_{ph} - [I_o(\exp(\frac{q(V+IR_s)}{nkT}) - 1)] - \frac{(V+IR_s)}{R_{sh}}$$

In an ideal circuit, the third term of the above equation is neglected because of lowest value of series resistance and highest value of shunt resistance. Consequently, both open circuit voltage and short circuit current can be calculated, and they are mainly used for determining the electrical performance of cells [6].

$$I = I_{ph} - [I_o(\exp(\frac{qV}{nkT}) - 1) \qquad (17)$$

The maximum voltage is provided by solar cell under illumination when load current is equal to zero (I = 0). Thus, open circuit voltage can be determined by the following equation:

$$V_{OC} = V \approx n\,V_T \ln(\frac{J_{ph}}{J_O} + 1) \qquad , V_T = \frac{kT}{q} \qquad (18)$$

Where V_T is thermal voltage .In addition, short circuit current can be calculated when putting V=0, where I_{SC} is usually equal to I_{ph} which they indicate to the maximum current produced by solar cell [6].

Fill factor is defined as the ratio between the maximum power and product of current and voltage. Since the output of maximum power is defined as product of maximum current and voltage, the equation for FF can be given where the value of P_{Solar} is always higher than P_{MAX}.

$$FF = \frac{P_{MAX}}{P_{solar}} = \frac{J_{MAX}V_{MAX}}{J_{SC}V_{OC}} \qquad (19)$$

The power conversion efficiency (PCE) is defined as a ratio of maximum electrical power output to total incoming light power as seen below [6]

$$PCE = \frac{P_{MAX}}{P_{in}} = \frac{V_{OC}\, J_{SC}\ FF}{P_{In}} \quad (20)$$

The light source in this work was an Oriel 96005 150W where the power of incident light was 85.8 W/m^2.

4.4 Summary

In summary, this chapter has presented the fabrication and characterisation techniques used in this study. Characterisation techniques were presented for both the devices and the single crystal perovskite to test for quality and performance. The fabrication included device fabrication; however, the fabrication of the single crystal perovskite is presented in detail in the following chapter.

4.5 References

[1] S. Campbell, Fabrication Engineering at the Microand Nanoscale, 3rd ed. New York: OXFORD UNIVERSITY PRESS, 2008.

[2] D. Schroder, Semiconductor material and device characterization, 3rd ed. Canada: John Wiley & Sons, 2006.

[3] T. Owen, Fundamentals of UV-visible spectroscopy. Germany: Hewlett-Packard Company, 1996.

[4] Y. Leng, MATERIALS CHARACTERIZATION Introduction to Microscopic and Spectroscopic Methods. Singapore: JohnWiley & Sons (Asia) Pte Ltd, 2008.

[5] R. Beaty and J. Kerber, Concepts, instrumentation and techniques in atomic absorption spectrophotometry. Shelton: PerkinElmer Instruments, 2002.

[6] J. NELSON, the physics of solar cells, 1st ed. LONDON: Imperial College Press, 2003.

[7] Z. Ahmad and M. Sayyad, "Electrical characteristics of a high rectification ratio organic Schottky diode based on methyl red", OPTOELECTRONICS AND ADVANCED MATERIALS–RAPID COMMUNICATIONS, vol. 3, no. 5, pp. 509-512, 2009.

Chapter 5: In Depth Investigation into the Growth of Methylammonium Lead Bromide Perovskite Single Crystals and their Structural, and Optoelectronic Properties

Chapter 5: In Depth Investigation into the Growth of Methylammonium Lead Bromide Perovskite Single Crystals and their Structural, and Optoelectronic Properties

Towards understanding the stability of methylammonium lead bromide perovskite single crystal, it is necessary to investigate their growth as well as their structural and optical properties. In this chapter, we begin by looking at the process of the growth of Methylammonium lead bromide perovskite single crystals including the materials and techniques, followed by the trial work on the growth of these crystals in this research. Thereafter, the factors affecting the crystals before and after their growth are described. Details of the crystal structure and intrinsic optoelectronic properties are explained.

5.1 Growth of Methylammonium Lead Bromide Single Crystals

All of the growth methods of hybrid halide perovskite single crystals described in chapter 2 are based on the principles of the crystallisation process, which is widespread in many industrial applications, including production materials such as food, chemical products and pharmaceutical products. The most common type of crystallisation is from a solution, in which the solution consists of two or more substances making a homogeneous mixture. There are three different types of solution depending on solubility concentration at a given temperature. The first type is a saturated solution which contains the maximum solute that can be dissolved. Whereas, undersaturated solution contains less concentration of solute than the solubility

concentration corresponding to the same temperature. The third type of solution is a supersaturated solution which is the basic feature of all crystallisation operations.

Supersaturated solutions contain more solute concentration than the solubility concentration corresponding to the same temperature, leading to crystallisation. The crystallisation process involves nucleation and growth is a result of the solution being supersaturated and not at an equilibrium. The nature of any system proceeding towards equilibrium, will be thermodynamically driven to minimise the free energy of the system, resulting in the formation of a crystal nucleus which will continue to grow until the system regains equilibrium [1,2].

Nucleation is the first order phase transition. The solute molecules leave the solution phase to form ordinary clusters of molecules bound together by their intermolecular interaction which is known as an embryo [3]. A new phase generated inside the large volume of solution has lower free energy than the solution phase where free energy can be defined as the amount of internal energy available to preform work. The embryos keep attracting the solute molecules dissolved in the solvent which leads to an increase in the embryos size [3].

A notable feature of the nucleation process is that free energy of the system changes during the formation of the nucleus. On the one hand, the free energy increases as a result of formation of the solid-liquid interface and the associated surface energy. For this reason, there is a possibility for becoming an unstable solid and the embryos tend to dissolve into the liquid phase instead of growing. On the other hand, the free energy decreases due to low free energy of the solid phase. Consequently, the embryos get large in all dimensions. To obtain stable

nuclei, there is an intermediate size at which there is a lowering of free energy and this is called the critical cluster size [1,3].

It is noteworthy to mention that both nucleation and crystal growth will continue to occur until their total free energy is in equilibrium with their surroundings which would be a minimum value. The single crystal is determined by formation of a perfect crystalline lattice [1].

5.1.1 Materials

Methylammonium lead bromide, as hybrid halide perovskite, has received significant attention due to photovoltaic efficiency [4]. $MAPbBr_3$, as a perovskite compound has shown very good conversion efficiency at 21.3%[4]. The single crystal structure of methylammonium lead bromide ($CH_3NH_3PbBr_3$) tested for optical absorption showed the same properties as polycrystalline thin films, however, single crystals were shown to have longer charge carrier lifetimes. As result, the higher diffusion lengths of $CH_3NH_3PbBr_3$ under a 1-sun-equivalent photon flux has been shown higher magnitude than thin film with only one degree [5,6,7]. However, $MAPbBr_3$ offers a more stable and compact structure in comparison to $MAPbI_3$ single crystal because there is a reduction in the lattice constants, and it affords a cubic phase. This is due to a much stronger hydrogen bond with halide where the larger I atom is replaced by the smaller Br atom [8].

5.1.2 Growth Technique

Organometal halide perovskite single crystals are separated from the solution. However, the choice of method for growing these crystals depends on the physical properties of the compound involved, the applications for which the crystals are designed and its economic

considerations. Hence, the proper design and control of crystallisation processes can have a noteworthy effect on the overall efficiency of crystal growth and the value of the final product. Therefore, the inverse temperature crystallisation (ITC) was chosen, in this study, as the crystallisation method because of a rapid growth process and a high quality crystal. Compared with other growth methods, the optical and transport properties of single crystals which are grown by ICT are similar [6,10]. Since higher quality is very much required for performance improvement of perovskite-based devices. Methylammonium Lead bromide perovskite single crystals were grown under various sets of conditions.

5.2 Synthesis of $MAPbBr_3$ Single Crystal

Lead bromide (98%) was purchased from Alfa Aesar Co, DMF (anhydrous, 99.99%) was purchased from Sigma Aldrich and MABr was purchased from Ossila Ltd. All salts and solvents used in this study were used according to the manufacturer's instructions. The experimental setup for the crystal growth was the same as that used in the inverse temperature crystallisation method. Briefly, perovskite precursor solution is a mixture of 0.498 g MABr and 1.642 g $PbBr_2$ which were dissolved in N, Ndimethylformamide (DMF, typically 6 mL) at room temperature. The solution was stirred until it became transparent (Figure 5.1 (a)). After that it was heated to 60°C for 15 minutes in order to enhance the solubility (Figure 5.1 (b)). To confirm there is no crystalline residue from MABr or $PbBr_2$ in the final precursor solution, all of the solutions were filtered using a Polytetrafluoroethylene (PTFE) membrane filters with 0.2-μm pore size prior to the growth of crystals before placing 6ML $MAPbBr_3$ precursor solution in a small beaker.

It is necessary to cover the beaker with foil which had 5mm^2 hole in the centre in order to control evaporation, as can be seen in Figure 5.1 (c). Then, it was kept in an oil bath at 80°C for 17 hours. When the perovskite solution reached a low supersaturation level, which was approximately estimated to be 6-9 hours in advance of the moment orange seed crystals came out of the solution (Figure 5.1 (d)). After 17 hours, orange single crystals of $MAPbBr_3$ are collected, then polishing is performed before drying using N_2 gas.

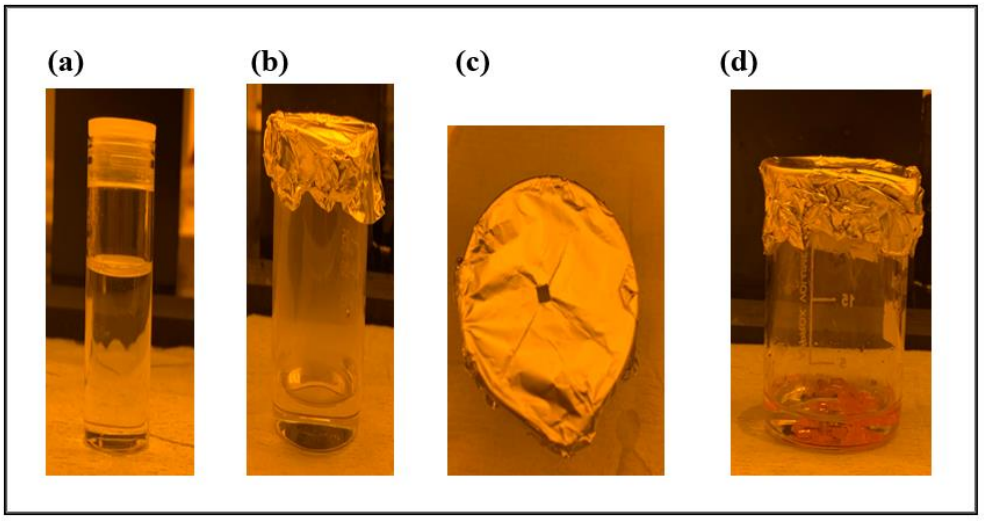

Figure5 1: photographs of crystallisation process of ICT method (a) Mixture before pre-heating.(b) after pre-heating at 60 C (c) the hole on the top of the foil. (d) large crystals grown.

Generally speaking, there are many techniques that exist for polishing a single crystal and removing the surface roughness including electropolishing, mechanical polishing and chemical mechanical polishing (CMP). Traditional mechanical polishing is typically done through the use of different grit files. Pieces of 240, 320, 1000 and 3000 grit files were used to polish the cubic crystal to obtain a perovskite crystal controlling its thickness and achieving smooth surfaces.

To polish the $MAPbBr_3$ single crystal and achieve a uniform flat surface, it is necessary to start with the coarsest file, 240 grit and finish with the finest file, 3000 grit. Each file was used to smooth the crystal by hand in a clockwise motion for two minutes and then again in an anticlockwise motion for a further two minutes. During the polishing process, DMF was used to wash away the ground perovskite powder completely before switching to a softer file, otherwise it can scratch the polished surface. It is important to note the DMF will dissolve the surface slightly, however, this will achieve a smother surface. In the last step, N_2 gas was used for drying the crystals.

It is important to mention that using a clean beaker is necessary in order to avoid some particles of dust which may cause nucleation sites or may prevent growth of the crystal. In addition, physical disturbance of the beaker during the experiment should be avoided. Furthermore, a vacuum desiccator is usually used to store all the crystals either before or after testing.

5.2.1 Factors Affecting the Growth of $MAPbBr_3$ Single Crystal

The success of crystallisation depends on experimentation and observation more than mathematical and physical calculations. In this section three experimental observation are presented.

The first observation was that the time and temperature required for crystallisation of $MAPbBr_3$, with the precursor solution at the desired concentration, varied depending on other factors such as the type of lid, the size of the hole and the size of the beaker used.

In the first experiments, small crystals were grown after a few hours, however, they were small. Therefore, it was obvious that even though all parameters in this experiment were constant such as salt, solvent, concentration, temperature and time, keeping the beaker in an oil bath on a hot plate without covering can lead to an increase in the concentration of solute species, providing tiny crystals. This can be attributed to a high supersaturation level, in which nucleation can dominate crystal growth [11]. Completely covering the top of the beaker, however, can prevent the solution reaching the supersaturation level and therefore, no crystals were formed.

The second observation is that leaving the crystal longer in the solution can negatively affect the quality of the crystal because of evaporation of all of the solution. Producing good quality crystals of a suitable size is the most important step in these experiments. As can be seen in photographic image (Figure 5.2 (d)), large sized crystals have a rough surface. The estimated size of $MAPbBr_3$ crystal after 17 hours heating at 80°C is in a range from between 1 to 10 mm^2, as can be seen in Figure 5.2 (c).

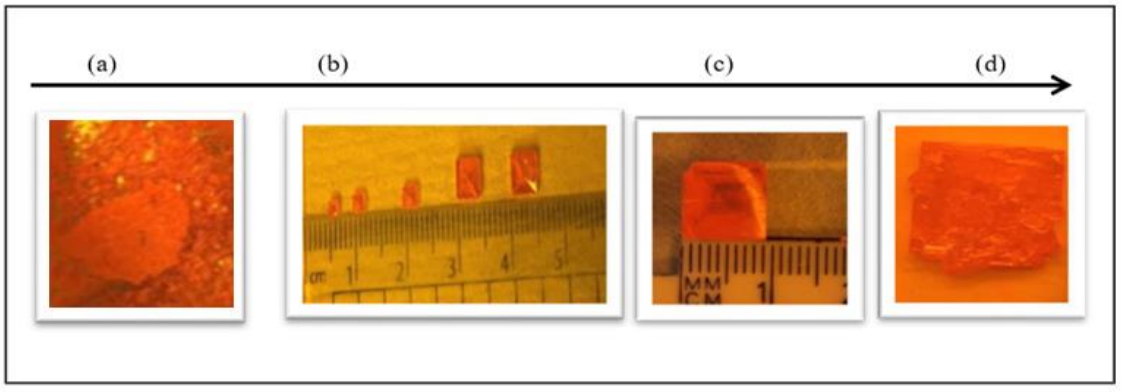

Figure5 2:Photographs for $MAPbBr_3$ single crystals grown via ITC method indicating that leaving the crystal longer in the solution can negatively affect the quality of the crystal.. (a) crystal seed (b) different crystal sizes (c)size of selected crystal, and (d) largest crystal after 17 hours growth

The third observation during the growth of $MAPbBr_3$ crystals was that the crystal grown from the freshly prepared solution was found to be of the highest quality in comparison to crystals grown from subsequent solutions recycled from the original solution as the concentration of constituents are already reduced . Few $MAPbBr_3$ single crystals (around 1-3 crystals) are usually taken out from 6ml of $MAPbBr_3$ precursor solution for each experiment, leaving behind the rest of solution. This solution was used to grow further crystals instead of discarding and wasting the solution and to save time compared to preparing a fresh solution for each growth process. The first step was to grow $MAPbBr_3$ crystals from the fresh solution that was placed in the beaker, $MAPbBr_3$ crystals were selected and taken out from the fresh solution. In order to get a clear precursor solution, the rest of the seeds were dissolved back into the solution and then the solution was filtered again and returned into an oil bath at the same temperature, which was 80°C. After 6 to 9 hours, the new single crystals were formed from the solution. These steps were repeated again.

In order to check the quality of the crystals in terms of its crystalline structure XRD was employed. Strong diffraction peaks were located at 14.92° and 29.88°, which corresponded to the (100) and (200) perovskite plane respectively, demonstrating no preferred orientation (weakly oriented) as can be seen from Figure 5.3 below [12]. However, the peak at 100 disappeared and a new peak in the second recycling was observed which may refer to a highly oriented perovskite crystal. Importantly, the width of the peaks observed in the first recycling were 0.15° and 0.16° FWHM for the 100 and 200 perovskite planes respectively and becomes broader in subsequent recycling. This indicates that the quality of the crystal deteriorates after repeated growth processes and becomes amorphous [14], in fact, by the third recycling no apparent peaks are observed (Figure 5.3) suggesting a less than amorphous structure. Similarly,

Chen et al. (2018) conducted the same XRD test on $MAPbBr_3$ and found similar results [12]. Therefore, these crystals from the secondary solution were of a lower quality compared to those from the freshly prepared solution and were not used in this study.

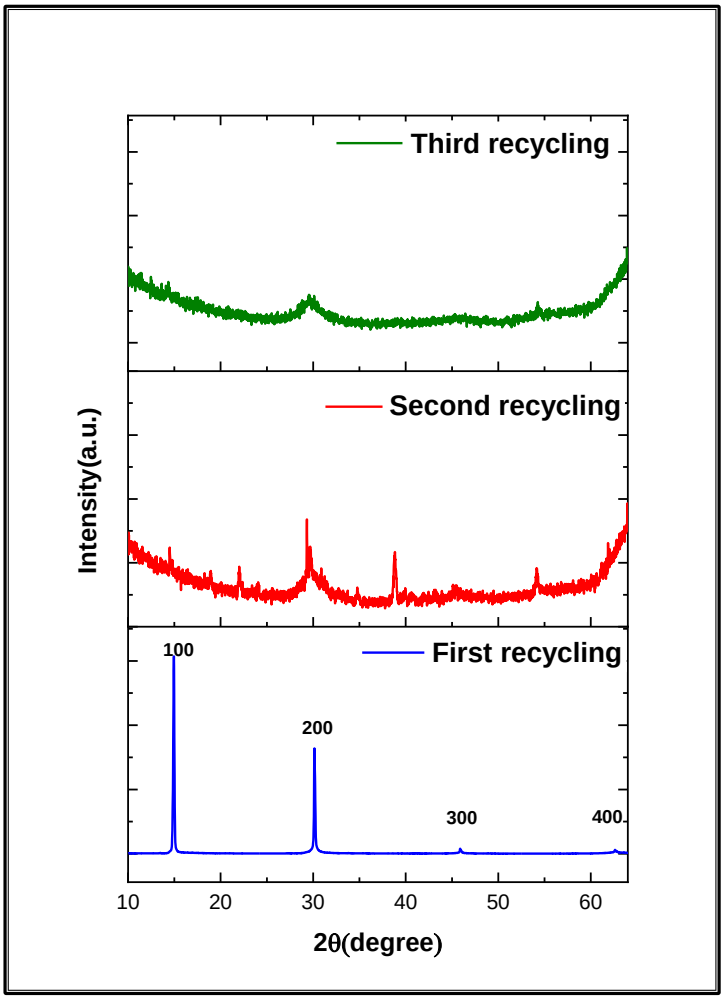

Figure5 3:XRD pattern of $MAPbBr_3$ bulk crystal formed after the repeating the crystallisation process indicating a deterioration in quality.

5.3 Single Crystal Structural Characterisation

The optical and electrical properties of Methylammonium lead bromide perovskite single crystal ($MAPbBr_3$) are attributed to its crystal structure. It presents a three-dimensional regular arrangement of ions in a crystalline lattice, which affords a structure free from grain boundaries. In this section the crystalline structure of $MAPbBr_3$ is presented in detail.

To estimate the formability and stability of the Methylammonium lead bromide perovskite single crystal structure, which consists of three elements, the geometrical factors are examined which were presented before in chapter 2. The geometrical factors are expressions for the Goldschmidt tolerance factor (t) and octahedral factor (μ) [15,16]. In consideration of the methylammonium (MA), it is an organic cation (non-spherical) and it is difficult to predict its radius in order to calculate the Goldschmidt Tolerance Factor for the $MAPbBr_3$ single crystal. Hence, Cheetham and co- workers (2015) solved this complexity by modifying the tolerance factor equation to use an effective radius of the organic cation. The organic cation in a perovskite structure is described as cylinders and assumed rotational freedom. Thus, the modified Goldschmidt Tolerance Factor is given by the following equation:

$$t = \frac{r_{A,eff} + r_X}{\sqrt{2}\,(r_B + r_X)} \qquad (1)$$

Where $r_{A,eff} = r_{mass} + r_{ion}$ [15,16].

The effective radius used for methylammonium $[CH_3NH_3]^+$ is 0.217 nm [16], the ionic radius of Pb^{+2} is 0.12 nm [17], and the radii of bromide Br^- is 0.196 nm [16]. Hence, it is found that the calculated Goldschmidt Tolerance Factor of the $MAPbBr_3$ crystal is 0.924. Since geometric strain and crystal distortions arise when the value of (t) is less than 1.11 or more than 0.85, the

$MAPbBr_3$ crystal has a stable crystal structure, therefore, the result of 0.924 indicates a stable structure.

Generally speaking, the halide perovskite structure is hard to form with unstable octahedra when the value of μ is less than 0.442 or higher than 0.90 [17]. However, the calculated octahedra factor of Methylammonium lead bromide perovskite is 0.61, thus $MAPbBr_3$ crystal is formed with a stable octahedron $[BX_6]^{-4}$.

The stable symmetry of $MAPbBr_3$ crystals provide the ideal electronic properties as a result of a high degree of ionic bonding [16-18] in which the ionic bond (Pb-Br) usually governs the electronic properties of perovskite more than the organic cation [18].

XRD measurements showed that all of the synthesised $MAPbBr_3$ crystals grown via the ICT technique, is crystalline with a cubic phase. The XRD analysis for the $MAPbBr_3$ single crystal as a bulk and powder is shown in Figure 5.4. The diffraction pattern of the powder crystals at room temperature revealed a cubic phase (*Pm3m*) with a lattice constant of 6.18°A. The X-ray 2Θ scan on the maximal facet of $MAPbBr_3$ single-crystal powder showed sharp peaks at 14.92°, 21.15°, 29.88°, 33.57°, 37.01°, 43.09°, 44.27°,45.80°, 53.45°, and 55.80°, corresponding to the (100), (110), (200), (210), (211), (220),(300), (310), (311), (320),and (321) planes of the cubic crystal structure respectively, which is in agreement with others [14,19- 24]. Furthermore, the XRD pattern of the bulk crystal shows only (100), (200), (300) and (400) diffraction peaks, indicating a predominantly well-structured $MAPbBr_3$ single- crystal. The full width at half maximum (FWHM) are 0.15°and 0.16° for the (100) and (200) peaks respectively, indicating a high-quality crystal structure of the $MAPbBr_3$ single crystal.

Importantly, the crystalline nature of the $MAPbBr_3$ single crystals is confirmed by a cross section SEM image after cutting the crystal.

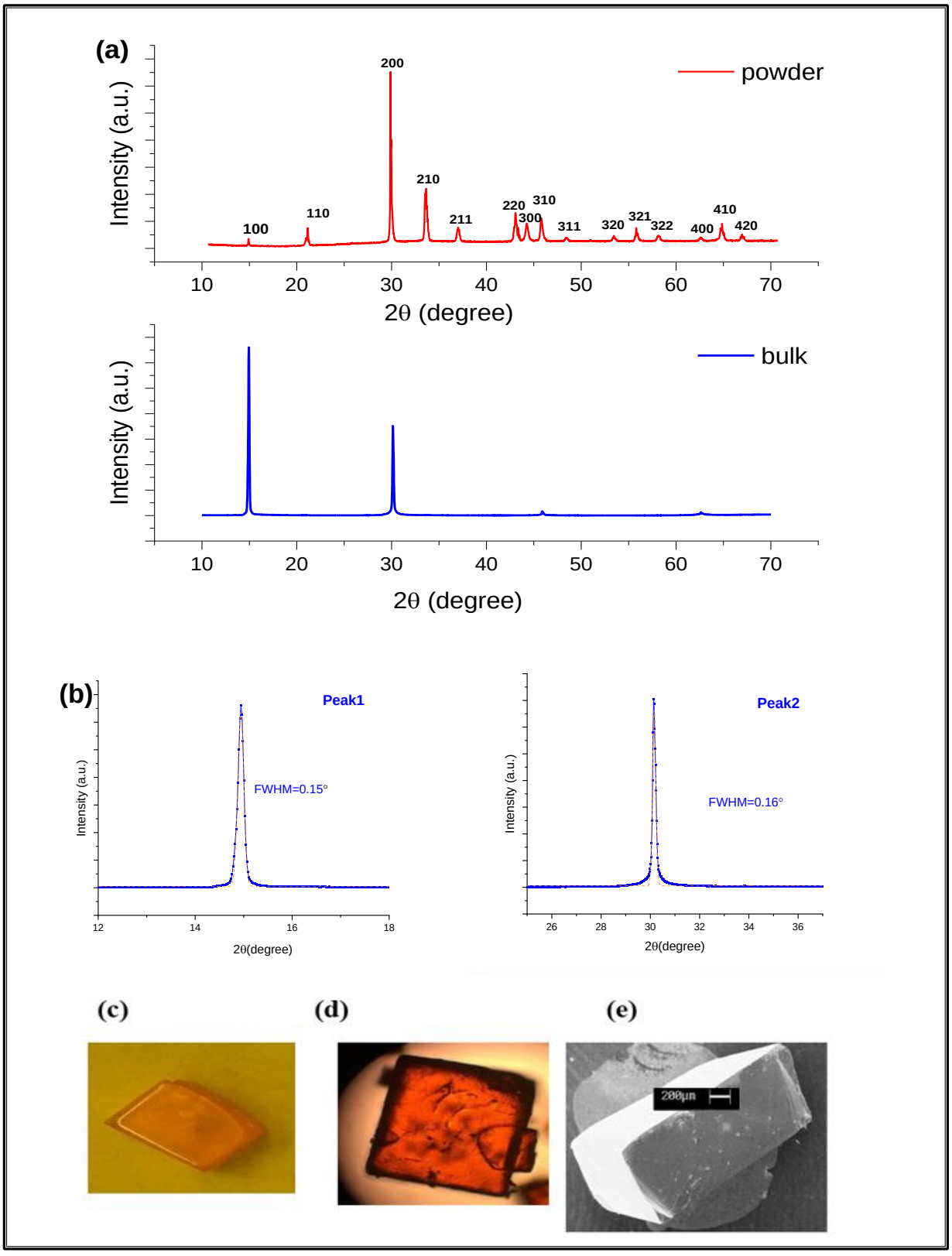

Figure5 4:(a) XRD diffraction pattern of $MAPbBr_3$ single crystal powder and bulk single crystal indicate cubic crystal structure (b) FWHM curve of the (0 0 1) and (0 0 2) diffraction peaks of the $MAPbBr_3$ single crystals indication the quality of crystal structure. (c and d) photograph and microscopic image of the $MAPbBr_3$ single crystal and (e) SEM cross section after cutting the crystal vertically.

5.4 Optical Characterisation

Since the nature of the energy band gap is an important implication on the optical properties of a semiconductor material, UV-Vis spectrophotometer is used to calculate the band gap of $MAPbBr_3$ single crystals. It is a powerful tool to collect transmission and reflectance spectra from the UV to near infra-red range of the spectrum. However, it is not the best choice to collect absorbance spectra in the mid and far infrared range which is essentially for studying and identifying $MAPbBr_3$ single crystals. Therefore, the optical properties of $MAPbBr_3$ single crystals in this section are investigated by using UV-Vis spectrometer and Fourier-transform infrared spectroscopy (FTIR) where absorption measurements were carried out in a range of wavelengths, 400 -1100 nm and 2500 -25000 nm, respectively.

The optical spectra are collected in transmission and absorption mode despite the large thickness of such crystals (typically 1mm), demonstrating their good optical quality. In Figure **5.5** (a) sharp behaviour of absorbance at 574 nm is clearly observed. However, the absorptance rapidly saturates as a result of the large optical density of the crystals. Considering that the absorptance is calculated from absorbance (A) = 1 - total transmittance (T_T)- total reflectance (R_T), the light in transmission mode is no longer detected below 574nm [25,26]. In order to estimate the energy band gap, the Tauc analysis was used to analyse the absorption spectra which was determined to be 2.1 eV. This value is smaller than the reported value which is a result of a single crystalline structure [6,25,26,27].

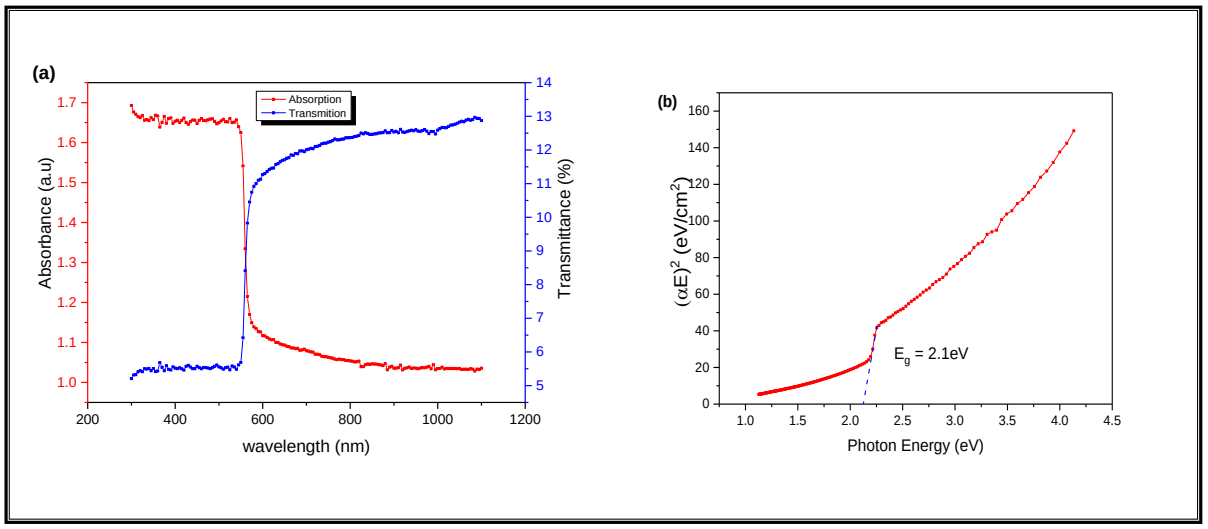

Figure5.5: (a) Absorbance and transmittance spectrum measured by UV-Vis spectrometer indicating the sharp of absorbance at 574nm (b) estimated band gap energy of a single crystal of MAPbBr3 from a Tauc plot at 2.1eV.

The absorption of IR radiation causes the various bonds in the molecules to stretch or bend with respect to one another, this means that infrared vibrational spectroscopy is an important tool for studying the bonds of perovskite structure. Therefore, measurement of the IR spectra of $MAPbBr_3$ single crystals was conducted at room temperature in dry air.

Our results show that there are seven significant peaks in the spectra of $MAPbBr_3$ single crystals which were grown at 80°C as seen in Figure 5.6. The wave numbers of $MAPbBr_3$ where absorption was observed were 906, 953.4, 1245.6, 1466, 1567.7,2920 and 3106 cm^{-1} which represents C-N rocking, C-N stretching, C-N rocking, NH_3 bending, NH_3 bending ,CH_3 stretching and N-H stretching vibration, which is in close agreement with others [28,29]. In addition, Pb-Br, and H-Br were not observed in the FTIR spectrum as the absorption was in the range of 300-500 cm^{-1}, hence, they do not show up in the spectra mode of $MAPbBr_3$.

The CH_3 related peak is weaker compared to corresponding NH_3 vibrations. This might be a result of the positive charge that is located on NH_3^+, enhancing the change in dipole moments related to vibrations of the ammonium group. In other words, there is a strong hydrogen bonding interaction between the amine group of the MA cation and the bromide atoms in the $MAPbBr_3$ single crystal (N+- H...Br) [28]. Both the contribution and the strength of the hydrogen bonds in the MABr salt increased in comparison to the perovskite crystal. This is related to a relative intensity ratio between the N–H stretching bonds in the MABr which is much higher than in $MAPbBr_3$. It was also observed that there is a narrower band at 2750-3250 cm^{-1} in the MA^+ salt compared to perovskite crystal, attributed to the strength of the hydrogen bond [29].

The crystal was found to be of high quality determined using FTIR, XRD, UV-Vis and EDX. This indicates an optimal composition of lead and organic compounds which affords optimal stability.

It can be observed from Figure 5.6 that the $MAPbBr_3$ single crystal is a pure crystal because indicated by the seven bonds in spectra modes. This result was confirmed by elemental map images and EDX elemental analysis as seen in Figure 5.7. While acknowledging the limitations of EDX analysis, it does provide the chemical composition of $MAPbBr_3$ single crystal and the distribution of each element across the same area which are carbon, bromine and lead.

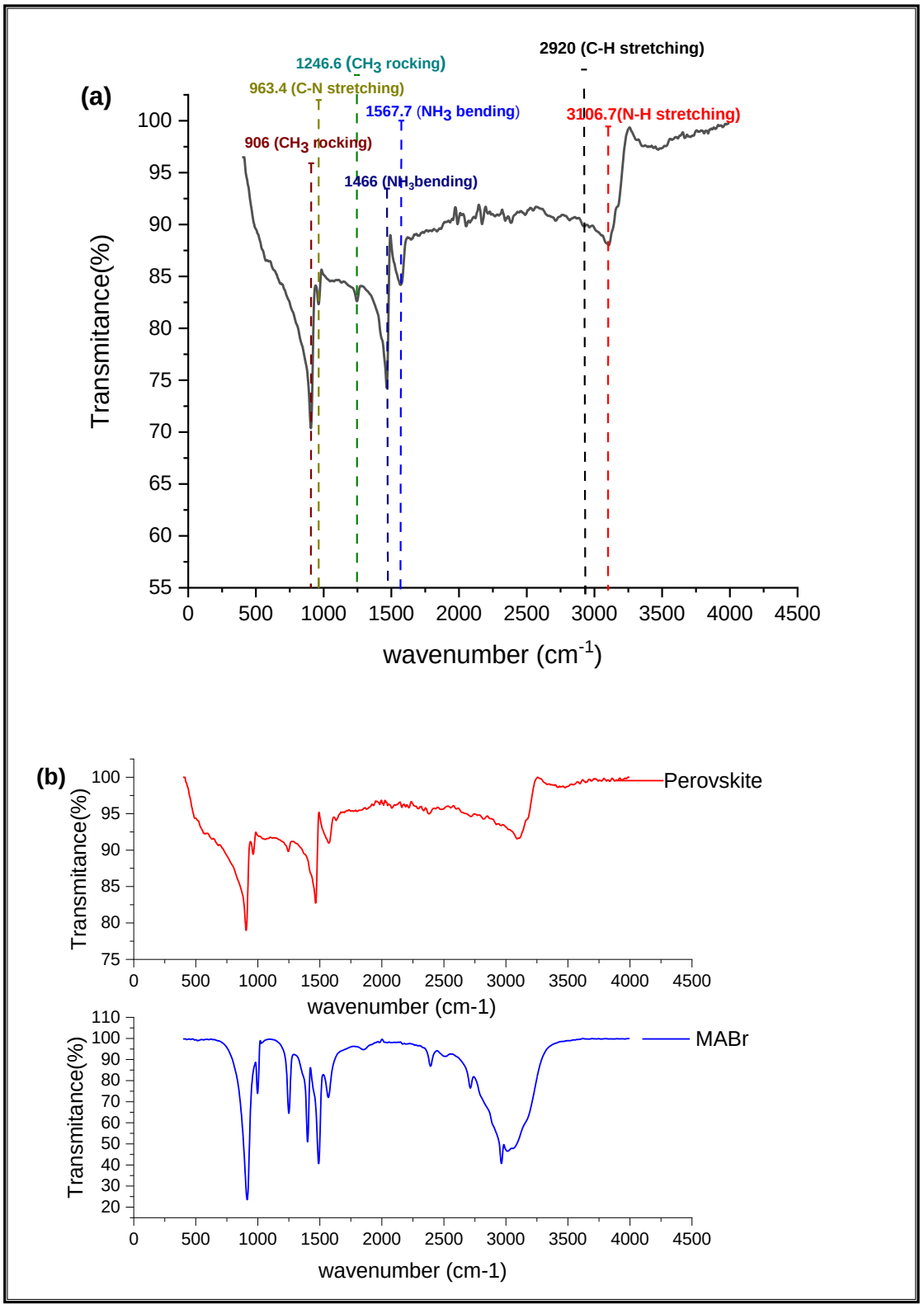

Figure5.6:(a) FTIR spectrum of $MAPbBr_3$ single crystals showing the seven bonds in the perovskite molecule (b) Comparison between FTIR spectra for $MAPbBr_3$ single crystals (RED) and MABr powder (blue), showing MABr to have stronger hydrogen bond.

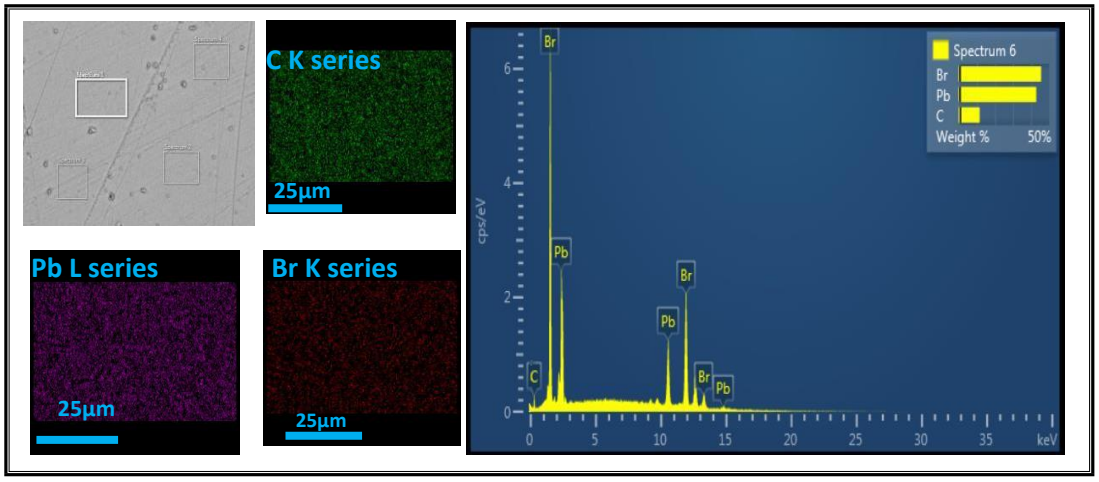

Figure5.7:Separate map images for each element in $MAPbBr_3$ single crystal with top view SEM image by EDX elemental analysis showing quantity element analysis for single crystal

5.5 Polishing Factors that Affect the Quality of $MAPbBr_3$ Single Crystals.

For the growth process of $MAPbBr_3$ single crystals, not only is the thickness of the crystal an important factor, surface quality of the substrate, such as roughness, damage, and stress, can also directly influence the properties of the crystal, reducing the performance of the device. Therefore, it is vital for producing $MAPbBr_3$ crystals with high quality to obtain the suitable thickness. In this section, how the optical and electrical properties of $MAPbBr_3$ single crystals are directly affected by surface quality, and how polishing techniques can improve this quality, is presented. The surface quality of $MAPbBr_3$ single crystals is investigated by structural, optical and electrical characterisation techniques.

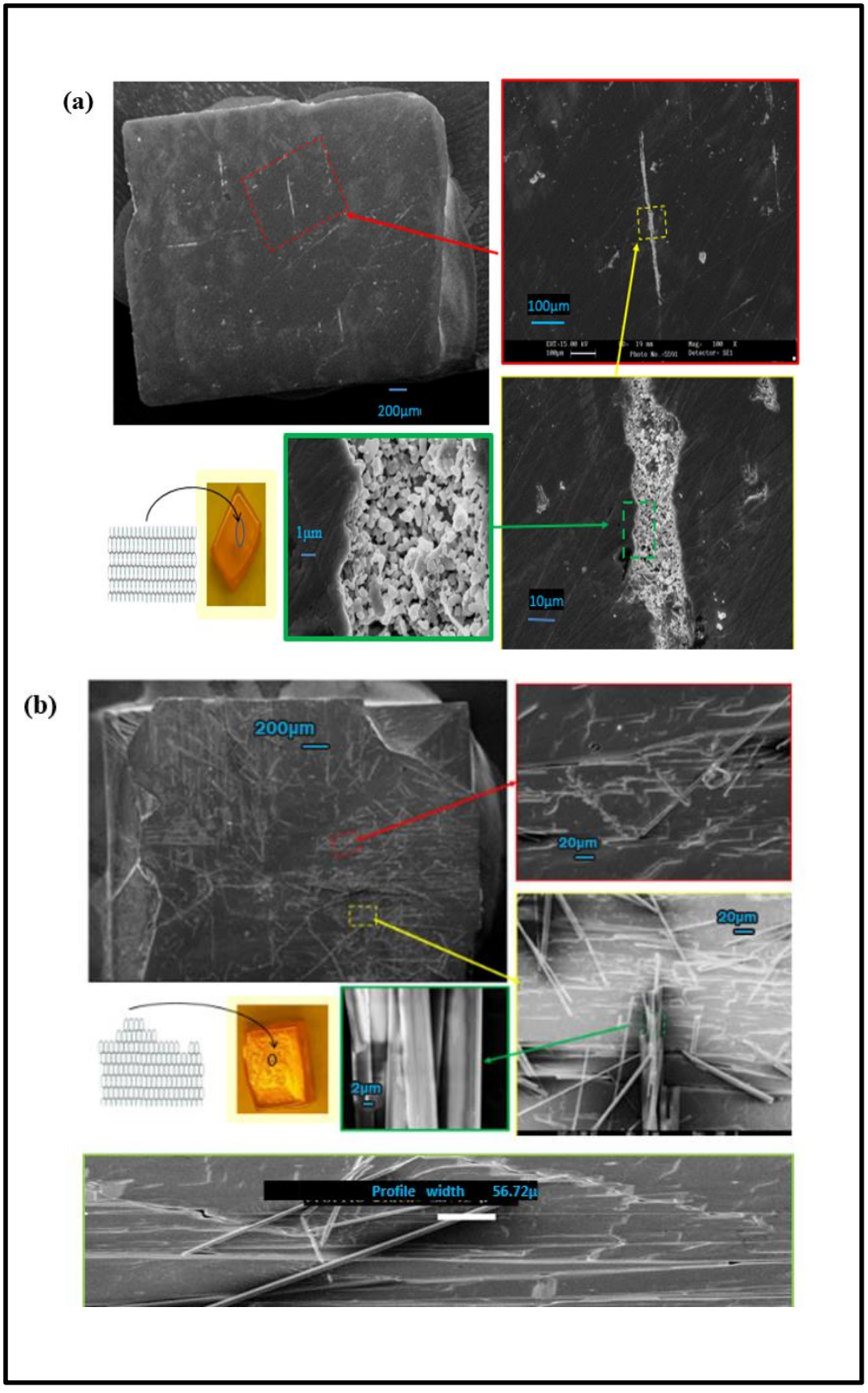

Figure5.8:Optical and Top view SEM images of polished and unpolished $MAPbBr_3$ crystal at different magnifications showing a flat region with scratches and residual particles (a and b)

Top view SEM images were obtained before and after polishing the surface as shown in Figure 5.8. The polished surface shows a flat region with some scratches and residual particles on the surface. However, the unpolished crystal has a rougher surface than the polished crystal. It is observed on the surface of the unpolished crystal the presence of needles, plenty of nuclei and multilayer stacks.

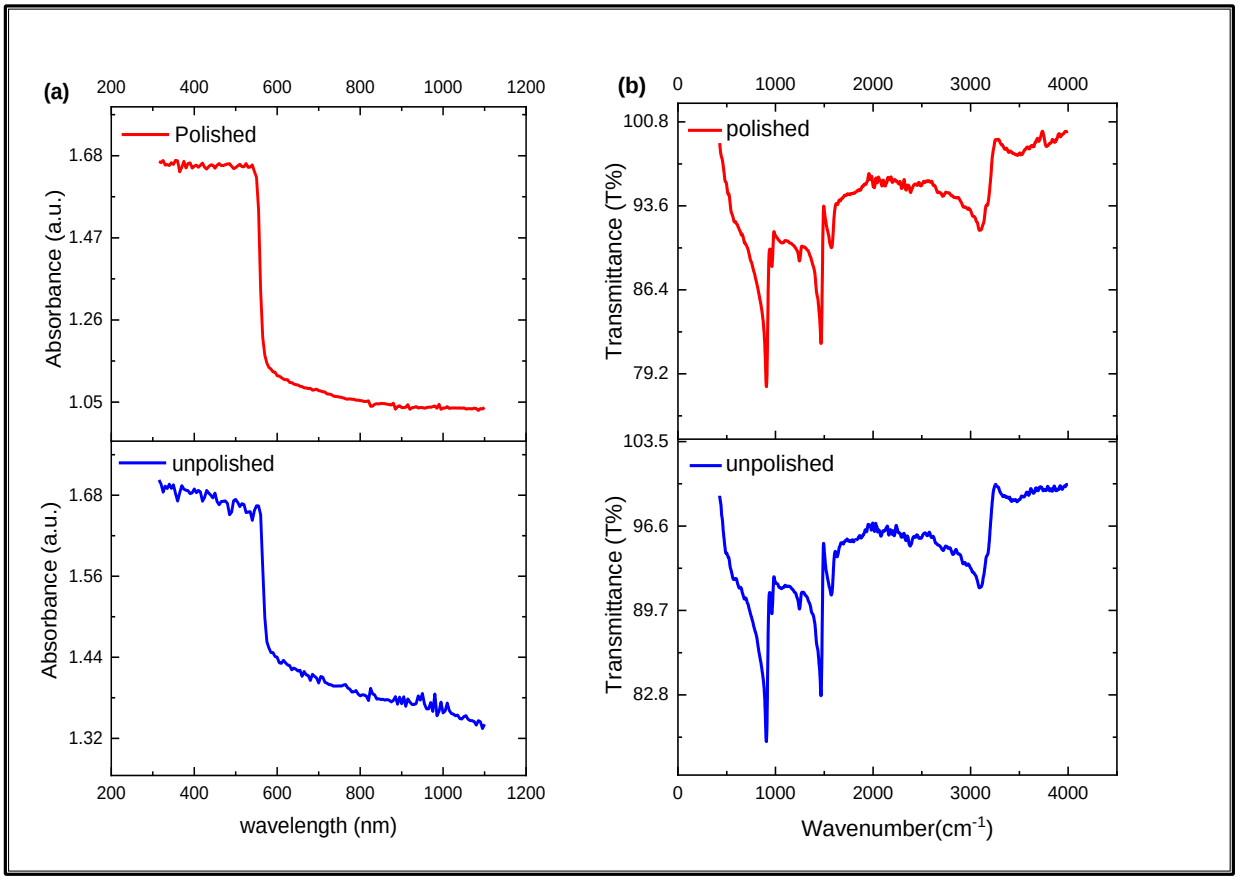

Figure5.9: Optical measurements for comparison between unpolished and polished $MAPbBr_3$ single crystal (a) UV-Vis showing no variation between polished and unpolished crystals (b) FTIR at 1mm thickness

However, there were no composition changes in the $MAPbBr_3$ crystal as evidenced by FTIR. UV-Vis did not show any variation between the polished and unpolished crystals, as seen in Figure 5.9.

Electrical measurements show the effect of polishing the $MAPbBr_3$ single crystal surface roughness. In order to determine surface roughness, several electrode strips (silver) were deposited through evaporation on top of the $MAPbBr_3$ single crystal at the same geometry but at different distances at 100, 200, 300, 400 μm between any two series electrodes as can be seen in the image in Figure 5.10. Dark I-V curves showed that the current flow decreased disproportionally as the spacing between two electrodes in series increased in the unpolished crystal compared to the polished crystal. Additionally, despite the potential difference (V) and the current (I) curves in the unpolished crystal showing a straight line, they are not symmetric curves compared with the polished crystal because the polished crystal has a flatter surface than the unpolished crystal. Therefore, the results for the polished crystal demonstrated the importance of the smoothness of the crystal surface and the associated polishing technique for achieving greater contact with the electrode. Thus, non-uniform of electric field, which is shown in the IV measurements, may be caused from the rough interface contact. This can display unexpected electrical behaviour.

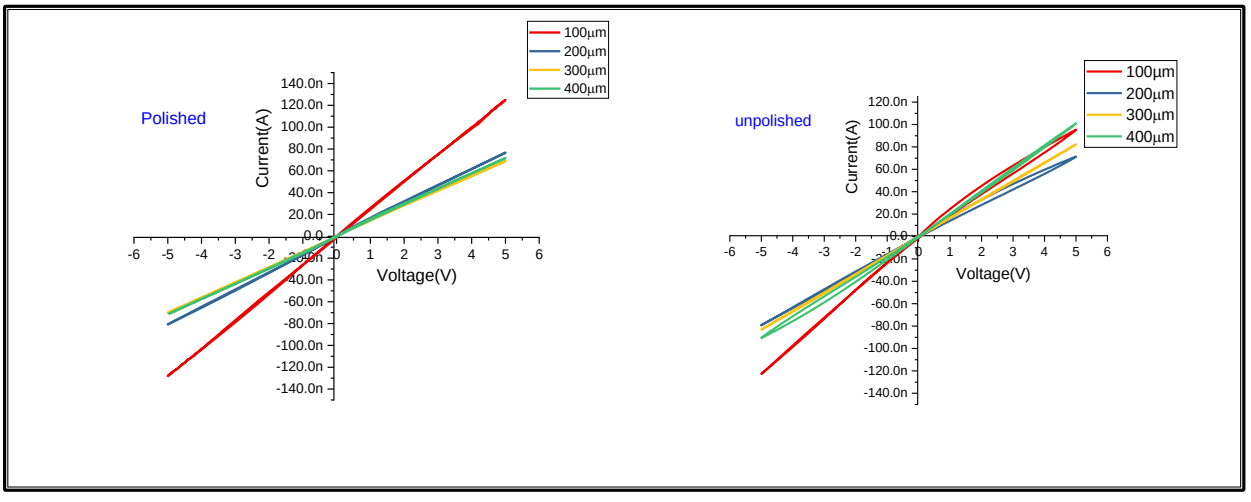

Figure5.10: IV curves for polished and unpolished $MAPbBr_3$ crystal indicating difference in surface flatness

5.6 Summary

This chapter showed how the $MAPbBr_3$ single crystal was fabricated including the factors that affect crystal growth. This chapter presented both the optoelectrical and structural characterisations. These characterisations were essential in ensuring the overall quality of the crystal for experimental purposes, which was also ensured and demonstrated through polishing the single crystal, affording greater conductivity in application as a new contribution of this study.

5.7 References

[1] G. Coquerel, "ChemInform Abstract: Crystallization of Molecular Systems from Solution: Phase Diagrams, Supersaturation and Other Basic Concepts", *ChemInform*, vol. 45, no. 21, p. no-no, 2014. Available: 10.1002/chin.201421248.

[2] A. McPHERSON, "Current approaches to macromolecular crystallization", *European Journal of Biochemistry*, vol. 189, no. 1, pp. 1-23, 1990. Available: 10.1111/j.1432-1033.1990.tb15454.x.

[3] D. Camacho Corzo, C. Ma, V. Ramachandran, T. Mahmud and K. Roberts, Crystallisation Route Map. Dordrecht: Springer, 2017, pp. 179-213.

[4] Z. Chen et al., "Single-Crystal MAPbI3 Perovskite Solar Cells Exceeding 21% Power Conversion Efficiency", ACS Energy Letters, vol. 4, no. 6, pp. 1258-1259, 2019.

[5] T. Brenner, D. Egger, L. Kronik, G. Hodes and D. Cahen, "Hybrid organic—inorganic perovskites: low-cost semiconductors with intriguing charge-transport properties", *Nature Reviews Materials*, vol. 1, no. 1, 2016. Available: 10.1038/natrevmats.2015.7.

[6] M. Saidaminov et al., "High-quality bulk hybrid perovskite single crystals within minutes by inverse temperature crystallization", Nature Communications, vol. 6, no. 1, 2015.

[7] M. Zhang, H. Yu, M. Lyu, Q. Wang, J. Yun and L. Wang, "Composition-dependent photoluminescence intensity and prolonged recombination lifetime of perovskite CH3NH3PbBr3−xClxfilms", *Chem. Commun.*, vol. 50, no. 79, pp. 11727-11730, 2014. Available: 10.1039/c4cc04973j.

[8] J. Chen et al., "Recent progress in stabilizing hybrid perovskites for solar cell applications", *Journal of Power Sources*, vol. 355, pp. 98-133, 2017.

[9] J. Huang, Y. Yuan, Y. Shao and Y. Yan, "Understanding the physical properties of hybrid perovskites for photovoltaic applications", *Nature Reviews Materials*, vol. 2, no. 7, 2017. Available: 10.1038/natrevmats.2017.42.

[10] G. Maculan et al., "CH3NH3PbCl3 Single Crystals: Inverse Temperature Crystallization and Visible-Blind UV-Photodetector", The Journal of Physical Chemistry Letters, vol. 6, no. 19, pp. 3781-3786, 2015.

[11] D. Bonn, and N. Shahidzadeh. "Multistep crystallization processes: How not to make perfect single crystals." *Proceedings of the National Academy of Sciences 113*, no. 48, pp. 13551-13553, 2016.

[12] A. Ishii, A. Jena and T. Miyasaka, "Fully crystalline perovskite-perylene hybrid photovoltaic cell capable of 1.2 V output with a minimized voltage loss", *APL Materials*, vol. 2, no. 9, p. 091102, 2014. Available: 10.1063/1.4895039.

[13] Y. Liu et al., "Low-temperature-gradient crystallization for multi-inch high-quality perovskite single crystals for record performance photodetectors", *Materials Today*, vol. 22, pp. 67-75, 2019. Available: 10.1016/j.mattod.2018.04.002.

[14] G. Kieslich, S. Sun and A. Cheetham, "An extended Tolerance Factor approach for organic–inorganic perovskites", *Chemical Science*, vol. 6, no. 6, pp. 3430-3433, 2015. Available: 10.1039/c5sc00961h.

[15] F. Sani, S. Shafie, H. Lim and A. Musa, "Advancement on Lead-Free Organic-Inorganic Halide Perovskite Solar Cells: A Review", *Materials*, vol. 11, no. 6, p. 1008, 2018.

[16] J. Zhou and J. Huang, "Photodetectors Based on Organic-Inorganic Hybrid Lead Halide Perovskites", *Advanced Science*, vol. 5, no. 1, p. 1700256, 2017.

[17] Q. Chen et al., "Under the spotlight: The organic–inorganic hybrid halide perovskite for optoelectronic applications", *Nano Today*, vol. 10, no. 3, pp. 355-396, 2015.

[18] W. Peng et al., "Solution-Grown Monocrystalline Hybrid Perovskite Films for Hole-Transporter-Free Solar Cells", *Advanced Materials*, vol. 28, no. 17, pp. 3383-3390, 2016. Available: 10.1002/adma.201506292.

[19] A. Poglitsch and D. Weber, "Dynamic disorder in methylammoniumtrihalogenoplumbates (II) observed by millimeter-wave spectroscopy", *The Journal of Chemical Physics*, vol. 87, no. 11, pp. 6373-6378, 1987.

[20] Y. Zhang, Y. Liu, Y. Li, Z. Yang and S. Liu, "Perovskite CH3NH3Pb(BrxI1−x)3 single crystals with controlled composition for fine-tuned bandgap towards optimized optoelectronic applications", *Journal of Materials Chemistry C*, vol. 4, no. 39, pp. 9172-9178, 2016. Available: 10.1039/c6tc03592b.

[21] M. Cao, J. Tian, Z. Cai, L. Peng, L. Yang and D. Wei, "Perovskite heterojunction based on CH3NH3PbBr3 single crystal for high-sensitive self-powered photodetector", *Applied Physics Letters*, vol. 109, no. 23, p. 233303, 2016. Available: 10.1063/1.4971772.

[22] J. Tisdale et al., "Precursor purity effects on solution-based growth of MAPbBr3 single crystals towards efficient radiation sensing", *CrystEngComm*, vol. 20, no. 48, pp. 7818-7825, 2018.

[23] P. Tsai, J. Chen, E. Ercan, C. Chueh, S. Tung and W. Chen, "Uniform Luminous Perovskite Nanofibers with Color-Tunability and Improved Stability Prepared by One-Step Core/Shell Electrospinning", *Small*, vol. 14, no. 29, 2018. Available: 10.1002/smll.201802153.

[24] P. Nayak et al., "Impact of Bi3+ heterovalent doping in organic–inorganic metal halide perovskite crystals." *Journal of the American Chemical Society 140*, no. 2, pp. 574-577,2018.

[25] M. Saidaminov et al.,"Inorganic Lead Halide Perovskite Single Crystals: Phase-Selective Low-Temperature Growth, Carrier Transport Properties, and Self-Powered Photodetection". Advanced Optical Materials, 5(2), p.1600704, 2016.

[26] X. Liu et al., "Charge Transport Behavior in Solution-Grown Methylammonium Lead Tribromide Perovskite Single Crystal Using α Particles", The Journal of Physical Chemistry C, vol. 122, no. 26, pp. 14355-14361, 2018.

[27] X. Zhao et al., "Capillary-written single-crystalline all-inorganic perovskite microribbon arrays for highly-sensitive and thermal-stable photodetectors", Nanoscale, vol. 11, no. 5, pp. 2453-2459, 2019.

[28] X. Huang, T. Paudel, P. Dowben, S. Dong and E. Tsymbal, "Electronic structure and stability of the CH3NH3PbBr3 (001) surface", *Physical Review B*, vol. 94, no. 19, 2016. Available: 10.1103/physrevb.94.195309.

[29] T. Glaser et al., "Infrared Spectroscopic Study of Vibrational Modes in Methylammonium Lead Halide Perovskites", *The Journal of Physical Chemistry Letters*, vol. 6, no. 15, pp. 2913-2918, 2015. Available: 10.1021/acs.jpclett.5b01309.

[30] L. Xie et al., "Organic–inorganic interactions of single crystalline organolead halide perovskites studied by Raman spectroscopy", *Physical Chemistry Chemical Physics*, vol. 18, no. 27, pp. 18112-18118, 2016.

Chapter 6: In Depth Investigation into the Electrical Properties of Methylammonium Lead Bromide Perovskite Single Crystals in applications

Chapter 6: In Depth Investigation into the Electrical Properties of Methylammonium Lead Bromide Perovskite Single Crystals in Application

This chapter presents the fabrication details and the intrinsic electronic properties through characterisation towards achieving an optimal device for investigating thermal and photo stability. Furthermore, the process of determining the optimal material for the electrodes involved testing for stability. Investigating the electrical properties revealed an insight into mechanisms related to degradation and instability of the active material. In this research, two device structures, a solar cell and a photodetector, for $MAPbBr_3$ single crystals are presented.

6.1 Background

The performance of devices, including their stability, can be affected by the device structure including materials and number of layers and the fabrication techniques used to form these layers. Specifically, more complex structures involve more materials and layers, increasing the possibility of interfering with internal processes within the crystal or at the crystal / electrode interface and returning unreliable results pertaining to stability. Since the aim of this study is to investigate the stability of the Methylammonium Lead Bromide Perovskite single crystal, a simplification of their device structures is required. Moreover, device complexity should not be considered the only factor for device stability, the choice of electrode materials may also have an effect thus, affecting results. Therefore, the next step is to determine the simplest structure

with the most effective materials in terms of stability and performance through electrical characterisation of the $MAPbBr_3$ single crystal and electrodes as a device.

6.2 Device architecture

The device structure used in this study is comprised of a HTL (hole transporting layer)-free solar cell whereby the electrode is deposited directly without the need for the HTL and the perovskite single crystal works as the absorber and hole conductor which forms a heterojunction with the ETL (electron transporting layer).

However, due to issues, such as making a crystal of a few micrometres thick, both electrodes, anode and cathode, are placed apart on one surface. An electron and/or hole transport layers is required for charge extraction. Ideally, the electrical characterisation of the $MAPbBr_3$ single crystals for the below-mentioned electrode configuration should be a simple quasi-ohmic contact.

Since the edges of the valence and conduction bands for $MAPbBr_3$ are to be 5.9 eV and 3.6 eV respectively [1], selecting suitable electrodes for electron and hole collecting should be based on the required energy band. The driving force for the efficient collection of charge carriers (electrons at the cathode and holes at the anode) is dependent on a built-in electric potential which is created between the charge collecting layers, and the work function of the perovskite layer.

In a perovskite solar cell, a quasi-ohmic contact is required for decreasing the injection energy barriers at the interface. This means the difference between the work function of electrodes and the maximum of the valence band of the perovskite layer should be small, as well as the difference between the minimum of the conduction band of the perovskite layer and the work function of electrodes.

An N-type semiconductor can form a Schottky contact or ohmic contact, if the work function of the contact metal is high or low respectively. Likewise, a P-type semiconductor can form a Schottky contact or ohmic contact, if the work function of the contact metal is low or high respectively [2]. The successful choice of the electrode materials employed in this study, either metals or organic material, is presented in Figure 6.1.

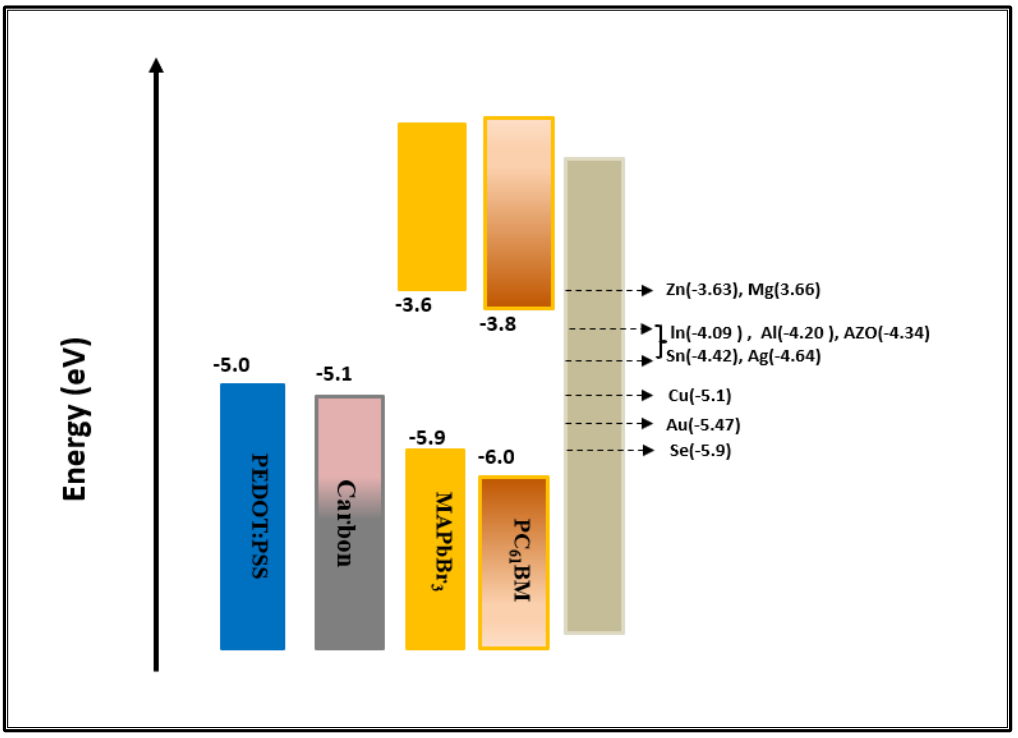

Figure 6 .1:Schematic view of work function for some materials tested in this study including hole selective materials, electron selective materials and metal electrodes.

6.2.1 Electrode Material Selection

The appropriate work function is an important consideration in the successful selection of electrode materials; however, there are other properties which can improve the device PCE such as low resistance, being free from hysteresis and electrode stability. The hysteresis behaviour, which could be caused by the effects of polarisation, ionic migration or trapping and de-trapping processes, can have an effect on the device parameters of perovskite solar cells.

Previous research has addressed these issues, Diang and Yan (2017) test with Gold, Gallinium and Platinum for electrode materials for a photodetector device structure [3]. Similarly, Peng et al. (2016) tested Indium Tin Oxide and Gold for a photodetector device[4]. A much closer experiment was conducted by Tisdale et al. (2018) who presented the hysteresis due to the electrode interface as the present study, however, with different electrode materials [5].

In the present study the ohmic contact of more materials are tested including aluminium, silver, selenium, copper, gold, zinc, indium and tin (see Figure 6.2) are demonstrated by using dark I-V curves. It was found that indium, silver, tin, copper, gold and selenium had a high work function, and aluminium and zinc showed high oxidation (Figure 6.2). Silver was found to be the most appropriate electrode for the cathode for the $MAPbBr_3$ single crystal device because of its stability and low resistance.

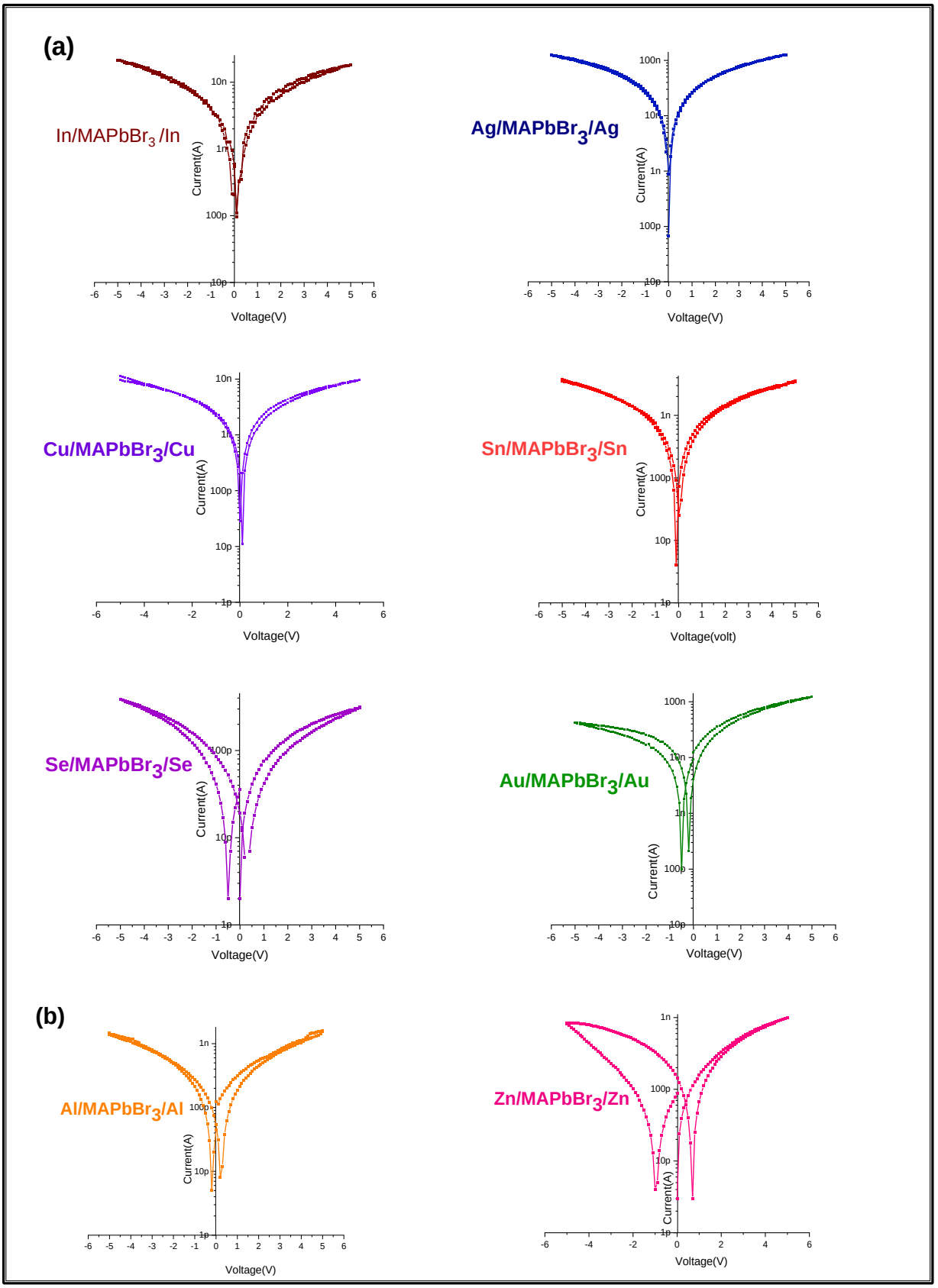

Figure 6 2:IV curves for different metal electrode materials which were used for $MAPbBr_3$ single crystal device structure Showing (a) high work function for indium, silver, tin, copper, gold, selenium and (b) shows high oxidation for aluminium and zinc. Silver was selected because the results show there was low resistance and low hysteresis .

Although aluminium, selenium, copper, gold, indium and tin also displayed symmetric linear behaviour in the I-V curves which is an indication of the ohmic nature of the contact, only silver afforded low resistance (high conductivity). To demonstrate this, the value of current was 127nA at 5 volts for the silver as an electrode, while it was 1.6nA, 0.313nA, 9.7nA, 59nA, 18.5nA , and 0.316nA for Al, Se, Cu, Au, In and Sn respectively. Importantly, gold is shown as a second choice after silver comparing with other electrodes as contact metals, however it displayed a low current (59 nA at 5 volt). This is related to higher work function of the gold than that of perovskite which cause high barrier towards the charge carriers transfer. It also was eliminated due to high cost leading to a high cost of device fabrication.

In consideration of the device fabrication, the stability of the electrode material is essential. Although aluminium electrodes are used as cathodes in perovskite devices, because of their low work function and low cost, they are eliminated in this study. It was observed that the layer of Al was not present a few minutes after its deposition. This may be attributed to its quick oxidation and diffusion into the perovskite crystal compared to other metals [6] a process which could affect the stability of the crystal, thus potentially affecting the results in the investigation of thermal and photo stability. The zinc electrode is rejected in this study because of an obtained hysteresis behaviour which reduces the efficiency of solar cell, as can be seen in Figure 6.2.

Although the use of silver for the cathode in the perovskite device is considered as the best choice because of its low resistance, and the difference between the work function of the $MAPbBr_3$ single crystal and the silver is small, it was found in this study to offer little improvement in terms of the rate of charge extraction. Consequently, a bilayer of two different materials is used in order to achieve a high rate of charge extraction. In Figure 6.3 (a), the two layers are comprised of phenyl-C61-butyric acid methyl ester ($PC_{61}BM$) with silver is also

tested as the use of an organic compound as the electron transport layer (ETL) can accelerate the transferring of charger carriers. However, there was a further decrease in the rate of charge extraction.

Since $PC_{61}BM$ is an organic material it is possible that its stability will be affected under certain thermal and light conditions, in consideration of the fact that the crystal contains organic compounds, the results for stability of the crystal could therefore, be affected and was thus, this bi-layer combination was rejected.

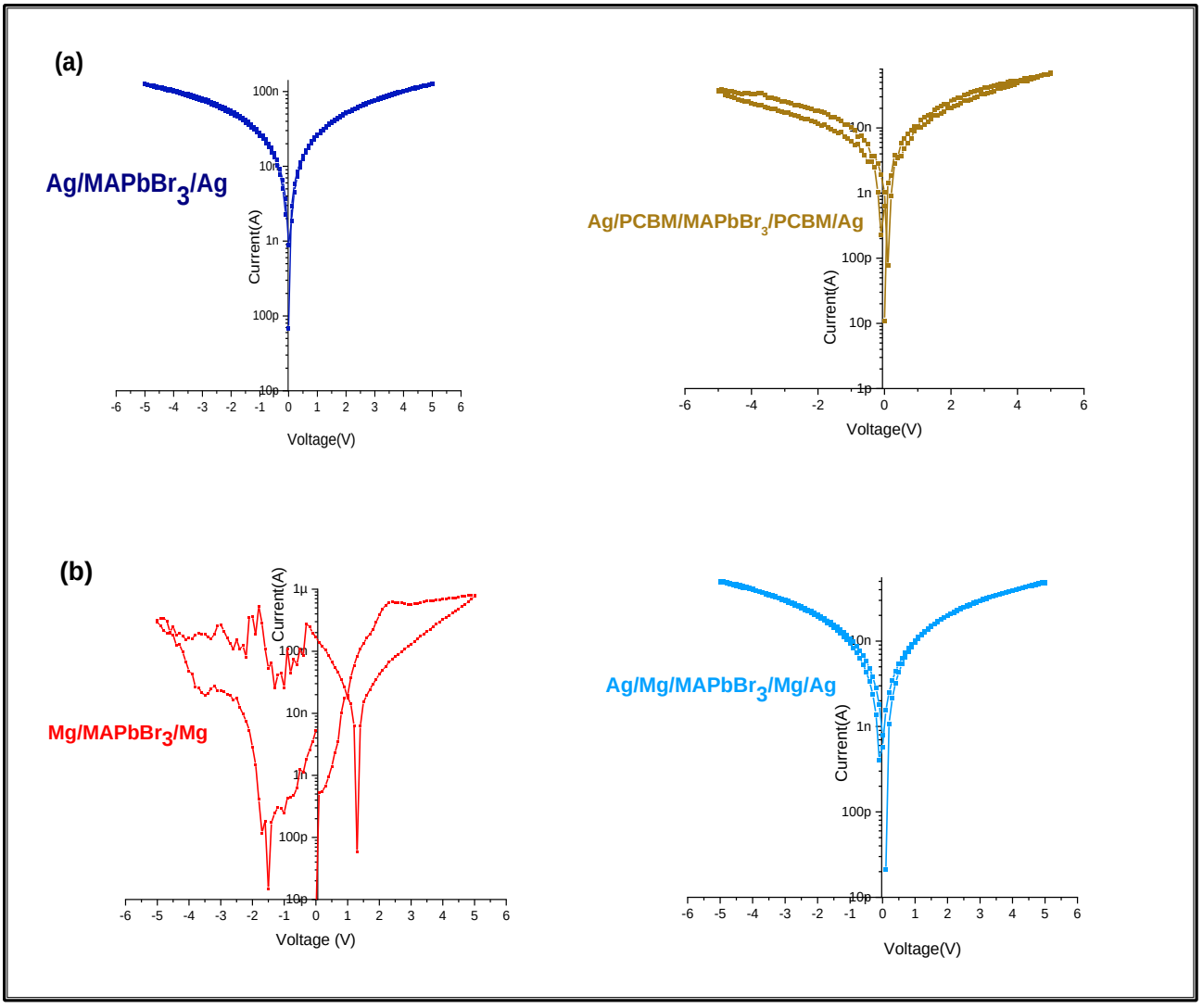

Figure 6 3:IV curves for (a) silver as a single layer and silver with PCBM as a bilayer and (b) magnesium as a single layer and magnesium with silver as a bilayer, all were used in the $MAPbBr_3$ single crystal device structure.

The use of magnesium as a single layer exhibited a high hysteresis (Figure 6.3 (b)) in order to achieve a hysteresis-free IV measurement silver was added as a capping onto the magnesium to form a bilayer (magnesium 5nm and silver 200nm). The results showed that this significantly reduced the hysteresis (Figure 6.3 (b)), however, it was still higher than silver as a single layer. Therefore, silver as a single layer was selected because as a bilayer with PCBM there was no improvement in charge extraction. Furthermore, silver as a single layer exhibited lower hysteresis than magnesium as a single layer and magnesium as a bilayer with silver.

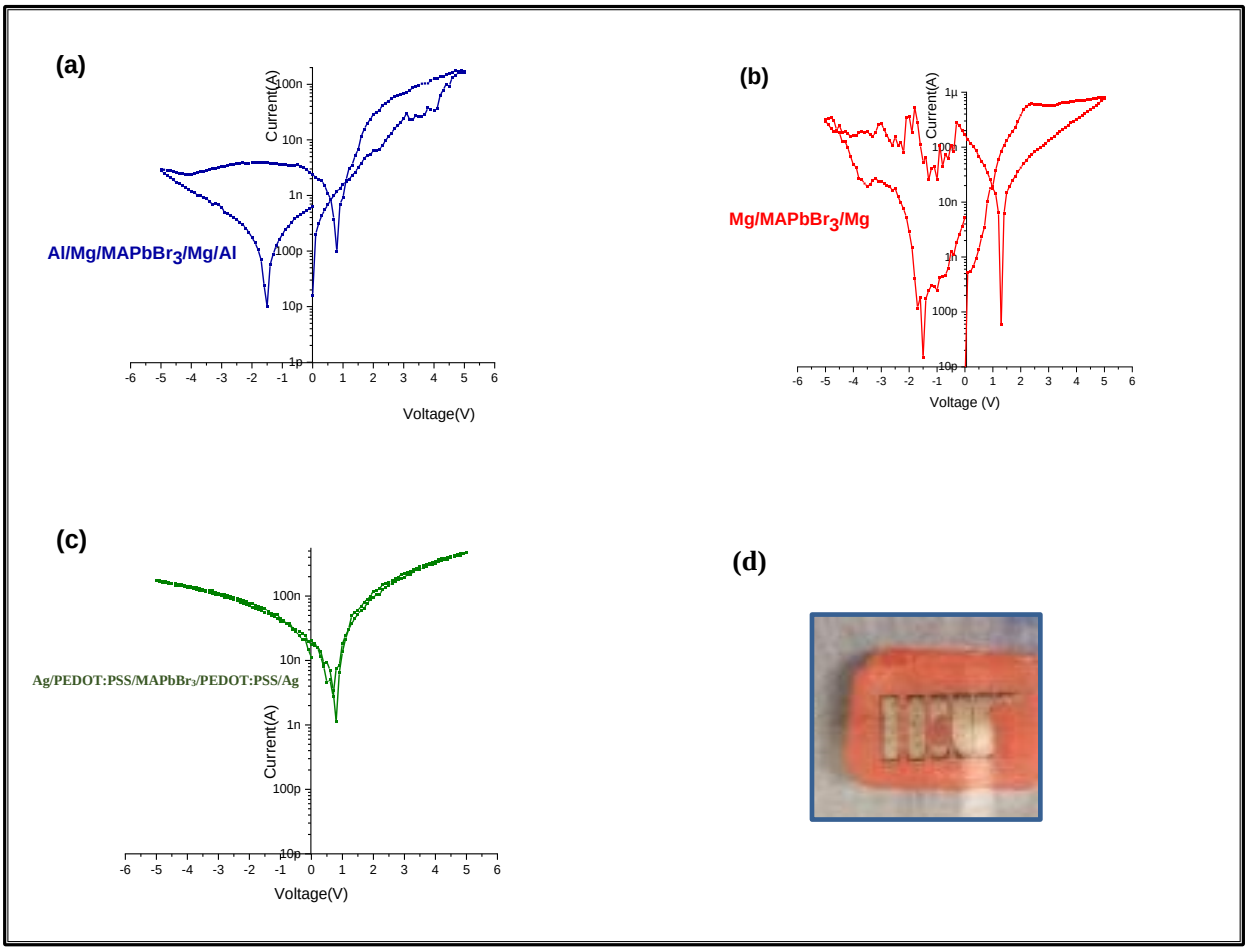

Figure 6 4:IV curves for (a) magnesium as a bilayer with aluminium,(b) magnesium as single layer (c) silver as a bilayer PEDOT : PSS , all used on the surface of $MAPbBr_3$ single crystal as electrodes. (d) Image showing dissipation of aluminium and magnesium. Magnesium as a single layer and as a bilayer with aluminium were rejected because of high hysteresis and diffused into the crystal. Although bilayer of silver with PEDOT: PSS showed low hysteresis, it was rejected because it is organic material susceptible to instability

For the anode five electrode materials were found to be suitable in the $MAPbBr_3$ device. In this study, carbon mixture, aluminium-doped zinc oxide (AZO), magnesium, a bi- layer of PEDOT: PSS/Ag and a bi-layer of magnesium and aluminium are experimentally applied with a corresponding cathode of the same materials in order to determine the most suitable material for the required Schottky contact.

Although magnesium displayed a Rectifying-contact behaviour and high current, it also showed hysteresis (Figure 6.4 (a)) and it could be due to a fast oxidation of Mg when evaporated on the surface of the crystal and thus was overruled from further consideration in this study. In order to protect the magnesium, 200nm of aluminium was deposited on the top of 5 nm of Magnesium as seen in figure 6.4 (b). The hysteresis decreased compared with magnesium alone, however, it was rejected because the aluminium did not offer protection for the magnesium, in fact, it was observed that both the aluminium and the magnesium diffused into the crystal see image in Figure 6.4 (d).

Regarding the bilayer of PEDOT: PSS/Ag, although it showed good Schottky behaviour with almost zero hysteresis, shown in Figure 6.4(c), it is eliminated as result of its organic materials whereby it is possible the stability of PEDOT: PSS/Ag will be affected under experimental conditions. Furthermore, because the crystal contains organic compounds, the results for stability of the crystal could be affected, therefore, PEDOT: PSS/Ag was rejected as a material for the anode.

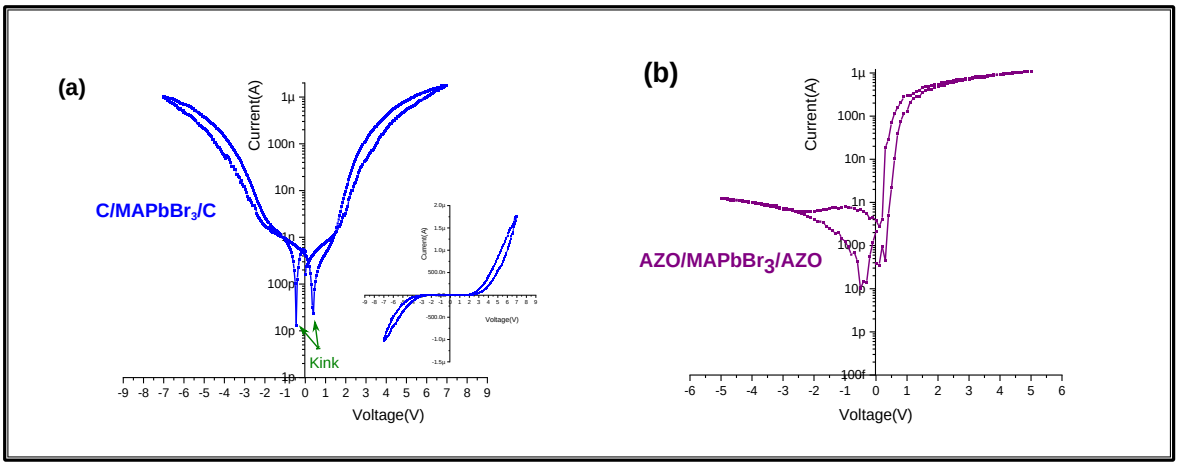

Figure 6.5:(a) linear and log scale of IV for Carbon paste by using C/ $MAPbBr_3$/C structure, and (b) log plot IV for AZO which were deposited on $MAPbBr_3$ single crystal by using AZO/ $MAPbBr_3$/AZO structure.

Aluminium-doped zinc oxide (AZO) and the carbon paste were used for the first time in this study for the anode. However, after several experiments with a number of devices, AZO was proven to be an unacceptable option because it did not demonstrate a double Schottky as was the case for the carbon mixture (Figure 6.5(a)). For more details about this experiment refer to section 6.3.2. As for carbon, it is usually explored as a cathode because it is an sustainability material available in a diverse range, is easily modified, and has high electrical conductivity [7], and it is adopted for the anode in this study. From Figure 6.5(a), it is observed that carbon mixture has double Schottky curves with low hysteresis behaviour compared to Mg and Mg/Al. This result showed that the carbon mixture exhibited double Schottky, high current (1.8 μA at 7 volt) and low hysteresis which makes it the best choice for this study.

6.2.2 The selection process of materials

In this section, both carbon paste and AZO were examined on glass substrate in order to select the best material for the electrical contact before using them on the surface of Methylammonium Lead Bromide Perovskite single crystal.

6.2.2.1 Aluminium-doped Zinc Oxide (AZO)

The aluminium doped zinc oxide was deposited on glass before putting on to the $MAPbBr_3$ single crystal in order to determine electrical properties. The brush technique was used for the deposition of AZO, followed by annealing at 120ºC for 15 minutes. Thereafter, silver with a thickness 200 nm was evaporated on the top of the AZO using a gap mask. TLM (transmission line measurement) is used to calculate the sheet resistance of semiconductor (R_{sh}), contact resistance (Rc), and Transfer length. The TLM made up of multiple electrodes that have the same length and width geometry but vary in the distances (L) from each other.

When the current is flowed through the semiconductor from the contact 1 to the contact 2, The total resistance consists of resistance of semiconductor and resistance of metal/semiconductor interface is given as:

$$R_T = R_{semi} + 2R_c \qquad (1)$$

$$R_T = \frac{R_{sh}}{W} L + 2R_c \qquad (2)$$

The above equation is used to obtain the plot for extraction of the sheet resistance value, Where width of contact (W= 0.1cm), different contact separation (L= 100, 250, 500 and 1000µm), and slope = $\frac{R_{sh}}{W}$ as can be seen in Figure 6.6 (a and b).

From TLM curve, The contact resistance sheet resistance of AZO coated by using the brush technique is 0.31 $\times 10^{12}$ Ω/square, contact resistance is 0.019 $\times 10^{12}$ Ω, and the transfer length is 0.002cm.

The AZO which is a degenerately doped semiconductor material, is an unacceptable option for the anode for the Methylammonium lead bromide perovskite single crystal device structure, it has a high sheet resistance, and thus acts as an insulator.

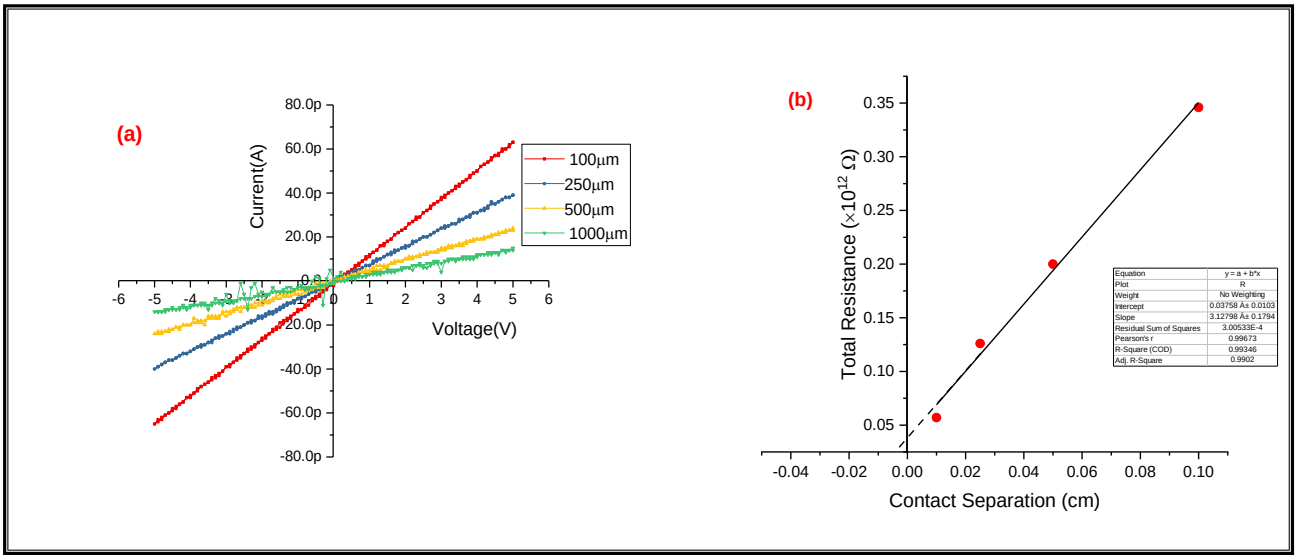

Figure 6 6: Calculation of sheet resistance of AZO I-V curves of AZO coated with different pad spacings of silver metal.

6.2.2.2 Carbon Paste

The black carbon paste, which is a type of carbon material, was used for the anode in this experiment. Initially, the carbon paste was tested by using two methods in order to determine the best preparation for achieving optimal conductivity for the electrical contact, these methods included testing a carbon paste as a mixture with different solvents, and upon determining the optimal mixture, it was then tested at different temperatures.

A- Carbon mixture

The carbon mixture was prepared by using two methods. First, carbon paste was dissolved in Isopropyl alcohol (IPA) and thermally stirred for 10 minutes at 100°C forming a solution. The second method was a mixture of the carbon paste with different ratios of silicone oil (see Figure 6.8). The silicone oil was chosen for its purity and low resistance. In both methods, the carbon paste mixture was deposited by brush on the surface of the glass, followed by annealing at 100°C for 15 minutes.

The IV curves in Figure 6.7 show that the second method (carbon paste – silicone oil mixture) has a higher current than the first method (IPA). This means that silicone oil has improved the conductivity of carbon paste even though it does not evaporate at 100°C. Moreover, it was noted that 0.05 ml of silicone oil is the best ratio to produce the highest conductivity possible for the carbon paste.

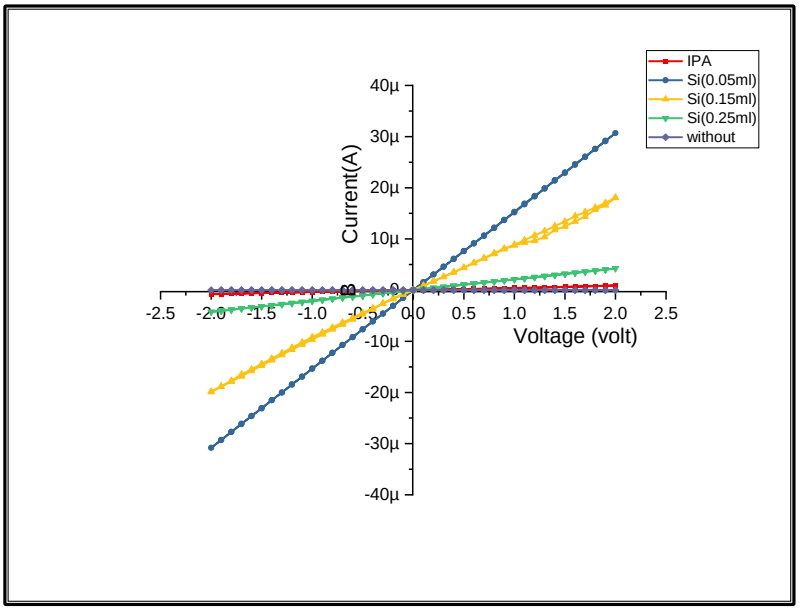

Figure 6.7: IV measurements for different mixtures of carbon paste showing 0.05ml of silicone oil was best ratio for the higher current.

B- Testing of Carbon Paste with Silicone Oil at Different Temperatures

A mixture of carbon paste with 0.05ml of silicone oil was experimentally tested on the surface of glass at different temperatures for 10 minutes as shown in Figure 6.9. The low current and fluctuation in the curve (hysteresis) were most apparent without heating. I- V testing at 50, 75, 100 and 125°C showed similar results, however, 100°C exhibited low hysteresis and high current.

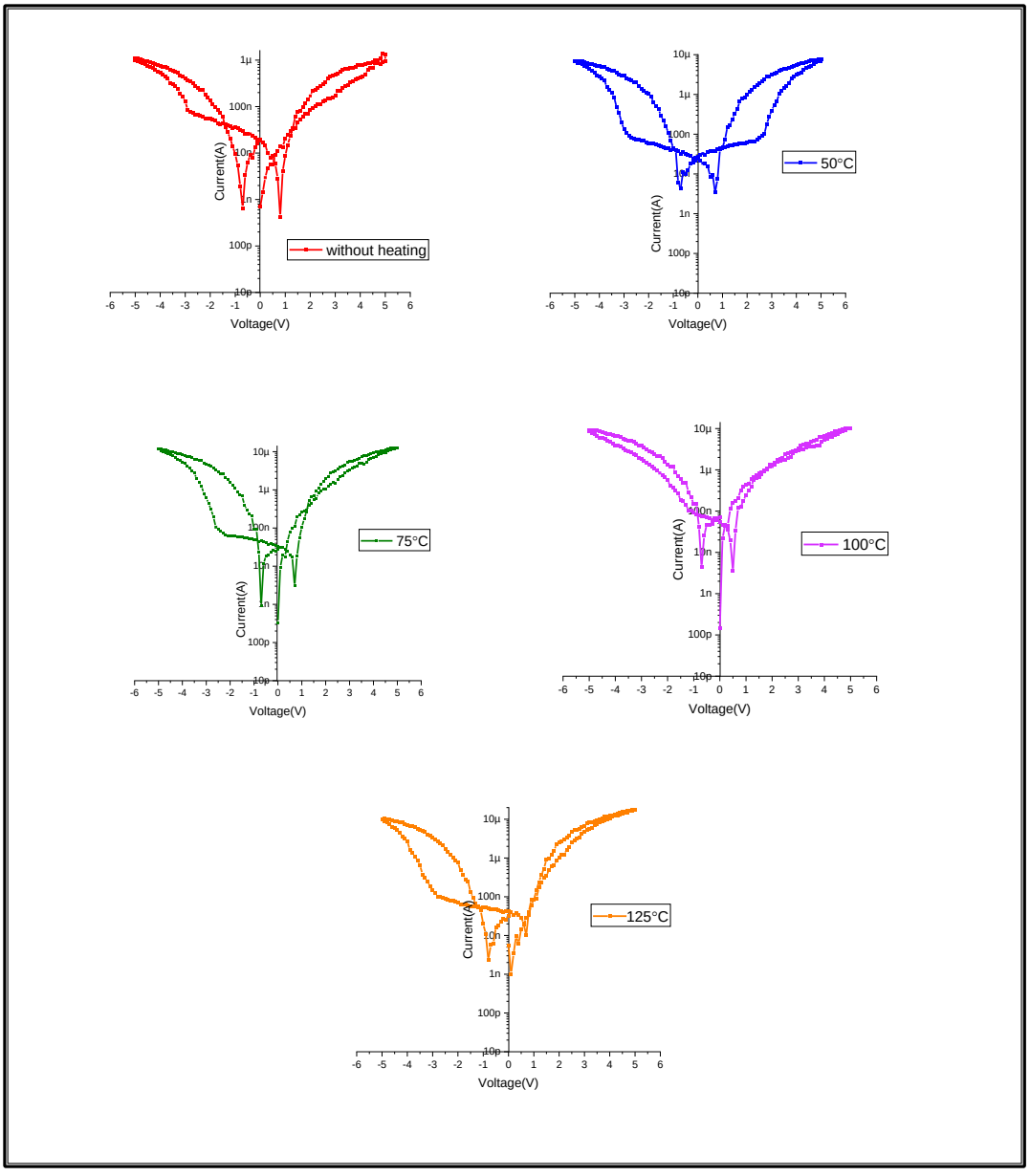

Figure 6 3 : IV measurements for carbon paste / silicone oil solution at different temperatures

6.3 Mechanisms for Hysteresis in $MAPbBr_3$ Single Crystal Device

Results in the previous section show that hysteresis or no hysteresis was observed for the different electrode materials.

6.3.1 Charge Trapping

One possible consideration for the observed hysteresis is charge carrier trapping at the defect sites (electronic defect) which are found at the surface of the material [10]. A possible explanation is that upon application of the external electric field there are more charge carriers, these will move to the defect sites and then to the metallic electrode before being replaced with other charge carriers and creating a continuous flow [9-11]. While this is a possible explanation for the observed hysteresis it does not offer an explanation for differing hysteresis observed for the different electrode materials.

This is the only variable in all of the experiments and given the different results for each material in term of hysteresis or I– V without hysteresis, it would suggest that the attributes of individual metals are responsible. The explanation for such variation should be explored through potential mechanisms that would include processes that are related to these metals. Metals and perovskites have different work functions. The energy levels at the interface between the electrode and the perovskite material have to match in order for the charge carriers to transfer into the electrode, however, if there is a difference between the work functions the charge carriers will accumulate leading to hysteresis [12].

Given the location of these electronic trap sites, at the surface of the material, and the location of the electrodes, it can be said that the cause of hysteresis is located at the active material / electrode interface [9,10,13,14]. An explanation for the differing hysteresis could lie in the mechanism of extraction whereby the charge carriers drift from the electronic trap site to the lectrode, therefore, there is a need to consider the electrode materials. The rate of this extraction is determined by the type of metal and therefore, has a differing effect on hysteresis which has been observed. This mechanism is further supported by the idea that the perovskite layer cannot solely be responsible for hysteresis, if this was the case then I -V hysteresis could be observed in all devices that have perovskites [15]. Therefore, the effect on hysteresis of the trap sites at the surface of the $MAPbBr_3$ single crystal is mediated by the extraction rates of the different electrode materials.

While electronic trapping and the associated mechanism of extraction do offer a possible explanation for the observed hysteresis, $MAPbBr_3$ single crystal has been shown to have low defect density at the surface. Therefore, ionic defects should be considered in addition to, or in conjunction with electronic defects, as possible causes of charge carrier trapping and the associated hysteresis.

6.3.2 Scan Rates of IV Measurement

The electric field in the device is supplied by the voltage source and is controlled by the direction and scan rate of the sweeping current. Variation in scan rate has been attributed to different hysteresis [10]. It has been shown in the literature that where there are electronic defects they are located near to the surface or interface between the perovskite and metal electrode, and that under a fast scan rate the electron would move directly to the metallic

electrode [16]. Likewise, under a low scan rate an increased hysteresis has been shown [17] as a result of a build-up of electrons.

For the experiment here, the applied external current was between +5 and -5 v applied at a consistent scan rate of 100 mV/s, and the results showed different hysteresis for the same scan rate was observed. Given that different scan rates show different hysteresis, it would be expected that a consistent scan rate would show the same hysteresis, however, this was not the case (see Figures 6.2, 6.3, 6.4 and 6.5). Therefore, this supports the idea that the electrode material, as another variable, is responsible for the different hysteresis observed in these experiments.

Under a short circuit condition, where no external bias is being applied and there is no current flow, the electronic traps sites will empty through diffusion and combine with the respective opposite charges at the surface of the contacts, creating an equilibrium in the material [9,10,14,15,18]. Therefore, if the traps sites are empty there will be low hysteresis at this point which was observed in the experiments.

6.3.3 Ion Migration

Upon application of an external electric field the bonds between the ions in the crystal structure are broken releasing the ion allowing it to migrate and accumulate at the interface, creating ionic defects [18-21].

As another explanation for this ion migration, related to the results in the above that a higher or lower work function is observed together with greater hysteresis, where such a work function of the electrode is present, there will be a build-up of electrons in the active material, these electrons increase the charge which result in breaking of the ionic bonds in the active material resulting in ion migration. Therefore, electronic defect density is related to hysteresis because these defects provide the opportunity for the ions found in the bulk of the perovskite material to migrate towards the electrodes [22] leading to hysteresis.

In addition to the accumulation of ions at the interface, another consequence of ion migration is that the ions break away from the structure leaving a vacancy, this vacancy may be filled by another ion or it may be left vacant, in the case of the latter the overall material structure will lose stability.

As has been mentioned in the literature, ion migration alone, or together with charge trapping has been shown to be responsible for hysteresis [10,18,23,24]. Specifically, as an explanation for the phenomenon observed in the results of this study, the ions, both negative and positive migrate to the electrodes depending on the respective polarity and become accumulated at the electrode interfaces. This creates ionic defect trap sites which trap charge carriers leading to hysteresis. However, it is important to note that the level of hysteresis is mediated by the rate of extraction of the specific electrode material. A greater rate of extraction would mean less charges in the bulk material leading to a lower hysteresis and vice versa.

Further evidence for ion migration is the observation of a kink in the I -V curve in this study. Specifically, the migration of ions under a forward or reverse bias at some point will stop where

the distribution of ions is at an equilibrium. At this point there is no ion migration and a balanced drift-diffusion [10,13], which is an explanation for the kink observed in the hysteresis as can be seen in Figure 6.6 and 6.9.

Another possible mechanism is more directly associated with instability of the $MAPbBr_3$ single crystal material as a result of ion migration. It is possible for the ions, such as silver to combine with other ions, such as bromide, forming new compounds, such as AgBr at the interface [25]. Given that ions are either positive or negative they will migrate to their respective electrode under application of an external field, however, upon a reverse of the bias some heavy ions will not be able to migrate to their respective electrode in time due to a lower mobility, for example, Pb^+ has low mobility and a low concentration of these ions will remain near the negative electrode when it changes to the positive electrode, thus being available for combination with the highly concentrated negative ions [25], for example with Br^- resulting in the compound PbBr, thus different compounds will form at each of the electrodes depending on polarity and concentration of positive and negative ions. In fact, $PbBr_2$ has been observed in subsequent experimentation of the present research as a result of heating $MAPbBr_3$ single crystal (see Chapter 7 section 7.1) It is important to note it is the formation of these compounds that is responsible for the observed hysteresis.

It has been shown here theoretically that the hysteresis could be due to ion migration, however, that alone does not offer an explanation for the observed hysteresis being different for each type of electrode material. There is a need to consider the possibility of ion migration, or more specifically, ions reacting with electrode metals to form new compounds that constitute a new layer between the perovskite material and the electrode which may affect the results as another

potential mechanism. There is the possibility that because such compounds contain metal then they could modulate the extraction of charge carriers at the interface [13,26]. Specific evidence for the role of the electrode in the hysteresis is that the electrode material has been shown to react with Br^- which has a modulating effect on the capacitive current [27] leading to hysteresis.

Thus, it is important to determine which ions are responsible for the hysteresis observed here in the $MAPbBr_3$ single crystal. One possibility is H^+ ions, however, because methylammonium has weak acidity maintaining a high concentration of H^+ ions is difficult, and therefore, their role would be minor in comparison to other ionic defects [28]. MA^+ ions are another possibility where it has been shown that MA^+ ions become redistributed as a result of the applied external electric field [29]. It has been shown that MA^+ are driven and aligned to accumulate at the electrode interface, due to the application of an external field, resulting in hysteresis [30]. However, how much the migration of MA^+ ions contributes to hysteresis is something that is still debated [31], whereby the value of the diffusion coefficient of MA^+ was found to be four to five orders of magnitude lower than halide ions and should be considered as a potential possibility for the observed hysteresis [31]. In fact, this is supported by evidence which suggests that halide ion migration is the main reason for hysteresis [31,32].

6.4 Structural Instability

The strength of the electric field will result in different degrees of degradation, initially an increasing electric field will increase the length of the covalent bonds between the A sites cations and Br sites anions [33], effectively stretching these bonds by increasing the lattice parameters thus increasing lattice distortion [33] leading to a reduction in stability.

A larger electric field will result in reduced stability whereby there is ionic migration, specifically, ion migration involves the jumping of ions from one molecule to another affecting the orientation of ions which result in overall instability [34].

The greatest concentration of ionic vacancy defects occurs at the surface of the perovskite which can also travel into the bulk of the material through ion migration in the z direction that can lead to hysteresis and material degradation in another part of the material, however, this mechanism is unclear and is not a well understood phenomenon of ion migration in perovskite solar cell [14].

6.5 HTL and ETL Free Device Structure to Understand Electrical Properties of $MAPbBr_3$ Single Crystal

Two device structures were studied in this research. The first structure comprised the $MAPbBr_3$ single crystal sandwiched between two silver layers as the cathode and anode, forming the metal/semiconductor/metal (M-S-M) structure. However, this structure cannot be used for a solar cell device and is demonstrated here for the purposes of understanding a perovskite photo detector device. The second structure will be used to demonstrate the perovskite solar cell device and is comprised of a Carbon/ $MAPbBr_3$ / Ag structure.

6.5.1 Ag/ $MAPbBr_3$ /Ag Structure

The $MAPbBr_3$ single crystal is demonstrated as a M–S–M device in this section. It was fabricated using 1mm thick $MAPbBr_3$ single crystal sandwiched between two layers of silver with a thickness of 200 nm. This structure was investigated under light and dark conditions for photoconductivity and resistivity respectively, whereby light was directed at the side of the device at the crystal's surface.

6.5.1.1 Photoconductivity

A photoconductor is a material that is able to create electron-hole pairs after absorbing light, the separation and collection of these charges to the biased contacts are required in photodetector applications.

In order to measure photoconductivity in the single crystal I–V measurements were conducted using the Ag/ $MAPbBr_3$ /Ag structure for four samples under dark and light conditions. The results showed that the measured device was a photoconductor (see Figure 6.9). Importantly, the value of the photocurrent was equal to around four to five times than that of the dark current despite the fact presence of traps in the metal-semiconductor interfaces or defects as a result of the process of growing the perovskite single crystal. An explanation for this is that where the device is under the light condition, some of the photogenerated charge carriers will be trapped at the defect sites. Upon application of the reverse bias, the trap rate increases which depends on current in the device and empty trap site density [35].

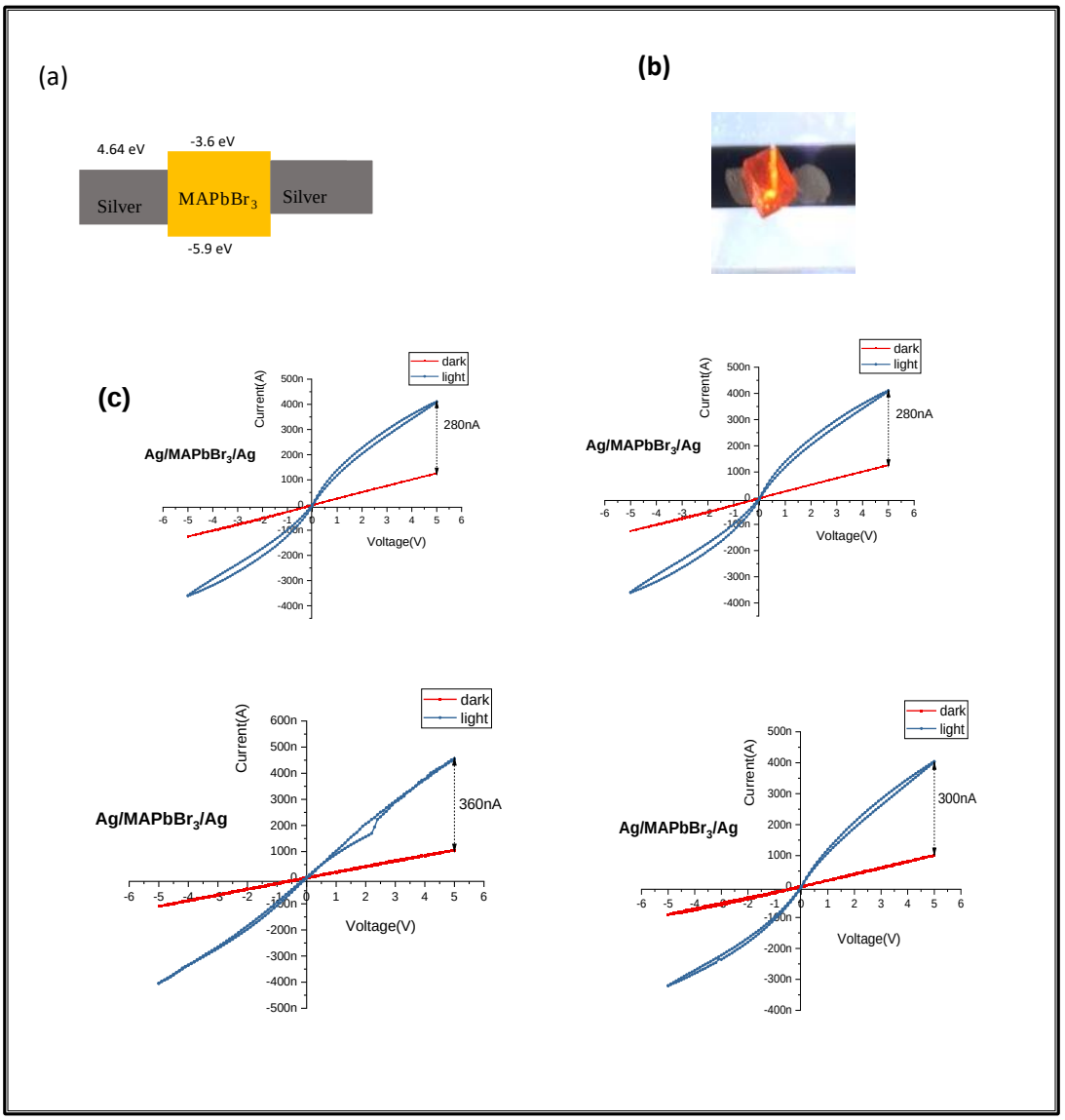

Figure 6.9: Photoconductivity of Methylammonium lead bromide perovskite single crystals , (a)Device structure , (b) image of device where single crystal placed in the gap between 2 silver electrodes. and (c)IV measurement under dark and light condition (taken from 4 devices) indicating that photocurrent was equal to around four to five times the dark current.

6.5.1.2 Sheet Resistance of $MAPbBr_3$

In order to measure the resistivity of the $MAPbBr_3$ crystal it was first necessary to measure the sheet resistance of this crystal. The Transmission Line Model (or Transfer Length Method) (TLM) was employed.

TLM structure was fabricated by evaporating silver metal on the perovskite single crystal with the same geometry of length (L) and width (W) and varying distances. I-V measurements were carried out by a sweeping voltage between -5 and 5 volts and measuring the current across each resistor at a varied separation between the electrodes which were 100, 200, 300, 400, 500 and 600 µm (see Figure 6.10).

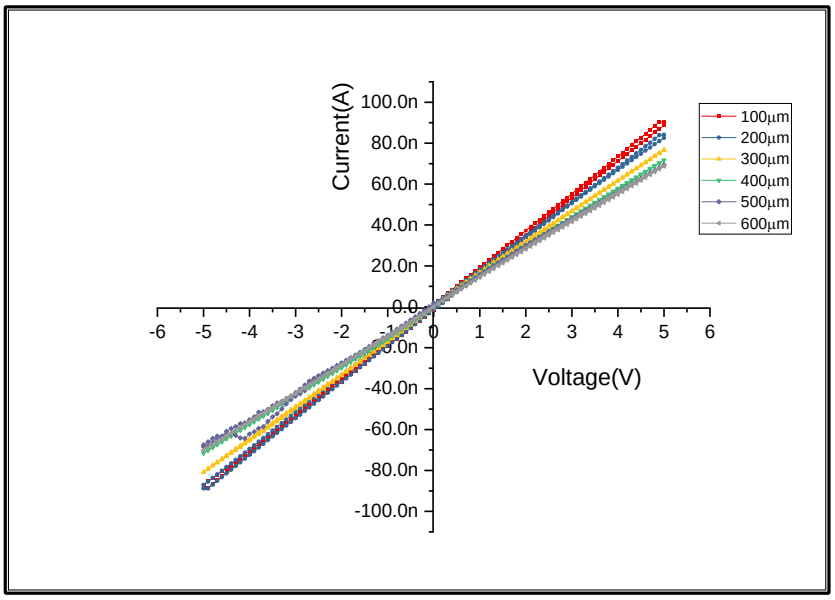

Figure 6.10: I-V curves of Methylammonium lead bromide perovskite single crystals at different pad spacings

From TLM analysis, The inverse of the slope of each individual curve is the resistance and total resistance is plotted as a function of the pad spacing to extract sheet resistance, contact resistance and transfer length (see Figure 6.11) by using the equation below:

$$R_T = \frac{R_{sh}}{W} L + 2R_c \qquad (3)$$

Where width of contact (W= 1cm), different contact separation(L=100, 200, 300, 400, 500and 600µm). sheet resistance Can calculate by known slope = $\frac{R_{sh}}{W}$. From figure 6.11, sheet resistance is 0.35×10^9 Ω/square, contact resistance is equal to 26 ×10^6 Ω, and the transfer length is 703 µm. The resistivity of $MAPbBr_3$ single crystal can be calculated by multiplying the sheet resistance (R_{sh}) , by the thickness of $MAPbBr_3$ single crystal (t=0.1cm). Thus, the resistivity of of $MAPbBr_3$ single crystal is 0.35×10^8 Ω.cm. This result is similar to other studies [36,37].

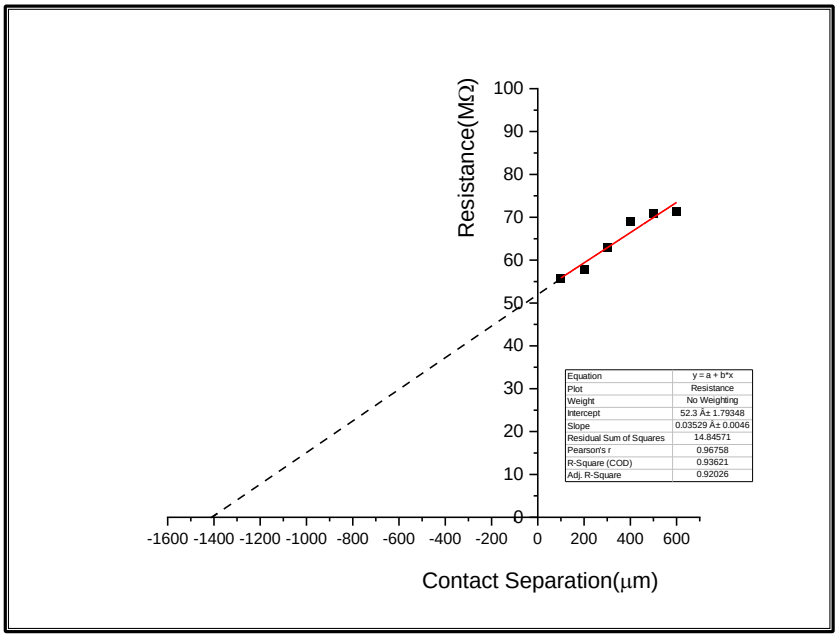

Figure 6.11:TLM fitting curve of $MAPbBr_3$/Ag ohmic contact calculating sheet resistance

6.5.2 Carbon/ $MAPbBr_3$/ Ag Structure

The carbon paste, which is a type of carbon material, is used as an anode whereas silver is used as the cathode for a photodetector single crystal. Since the selection of materials for device structure can affect the performance and stability of perovskite devices, regular n-i-p based

perovskite photodetector were fabricated using C/MAPbBr$_3$/Ag in order to optimise the photodetector device and to understand the degradation process inside them.

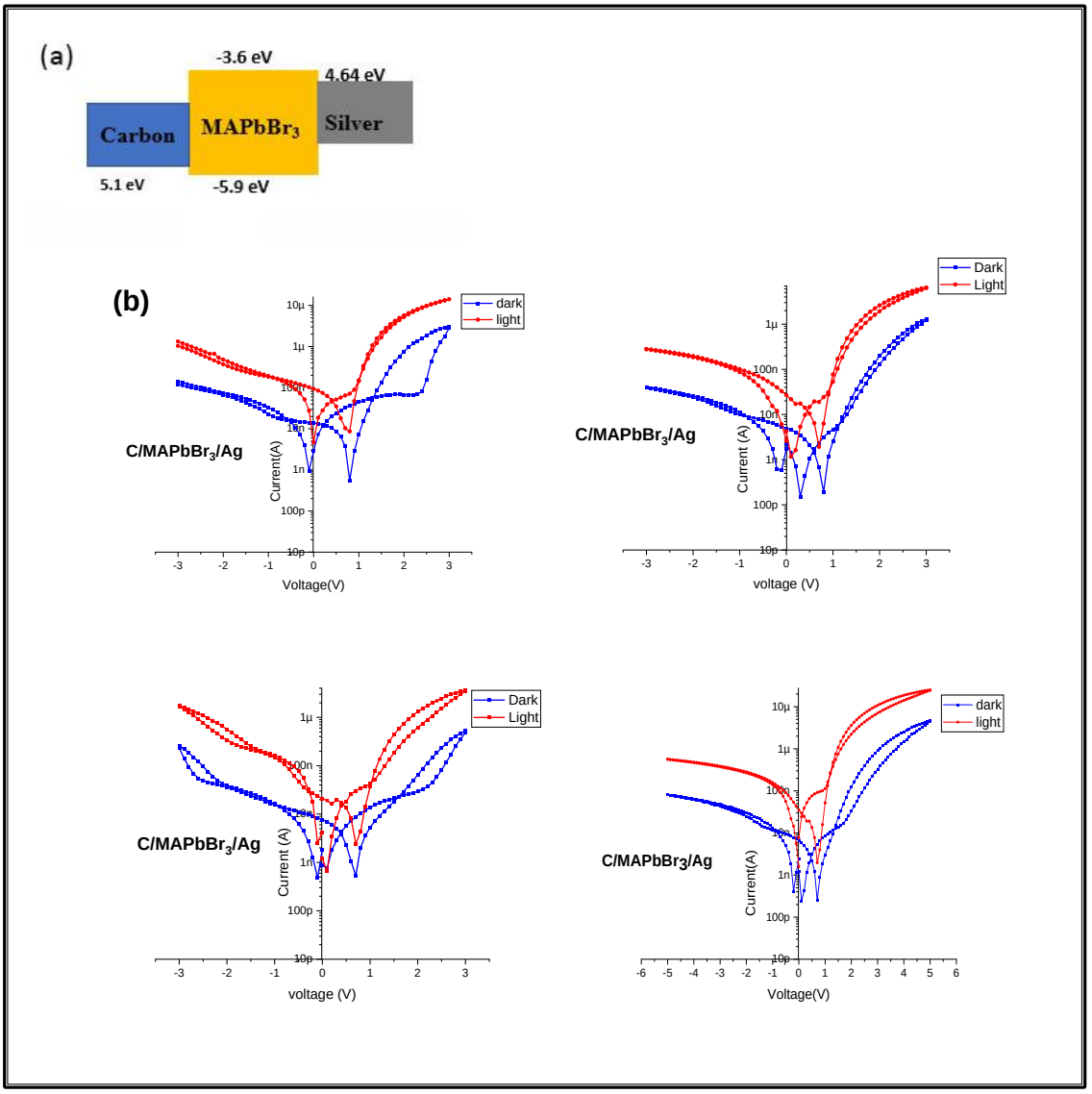

Figure 6.12:(a) Device structure of C/ MAPbBr$_3$/Ag and its band diagram, and (b) I-V curves of C/ MAPbBr$_3$/Ag (4 devices) Showing decreased hysteresis for light condition compared to the dark condition

The current-voltage experiment was conducted with the C/MAPbBr$_3$/Ag under dark and light conditions. The results revealed that for both conditions charge trapping and detrapping was observed at the interface, however, hysteresis was observed to be increased under the dark condition.

Possible explanation as to the reason for this observation requires revisiting the abovementioned mechanism. Under both conditions there will be an increase in charge carriers at the interface. Under the dark condition the charge carriers will accumulate in the material because they do not have enough energy to jump the interface barrier and therefore, they become trapped in the trap sites at the interface, this mechanism provides an explanation for the observed hysteresis (see Figure 6.12). Under the light condition there is an increase in the number of electrons, however, they will have enough energy to cross the interface barrier and consequently accumulation of charge carriers trapped at the interface will be less.

6.6 Summary

As part of device development for the selection of electrode material, this chapter presented the investigation of electrical properties of $MAPbBr_3$ single crystal under light and dark conditions. As part of this development there was an explanation of the observed hysteresis for different electrode materials and considered mechanisms including charge trapping. However, while this charge trapping was a possible explanation for the hysteresis, it did not offer an explanation for the different hysteresis for different electrode materials. However, these observed differences indicate to the differing roles played by different electrode materials. Silver was determined to the best material for the electrodes where it showed no hysteresis and therefore, was suitable for identifying attributes of the perovskite, $MAPbBr_3$, that would be responsible for hysteresis.

The results indicated involvement of the interface for identified possible mechanisms for hysteresis. This was evidenced by the involvement of charge extraction rates at the interface for different electrode materials. Another explanation for the observed hysteresis was an

interaction of ions with electrode materials forming a new material layer between the bulk and the electrode which could contain metals modulating extraction of charge carriers. The chapter revealed three possible mechanisms for hysteresis which will be considered in further experimentation involving temperature and light which are reflective of operating conditions.

6.7 References

[1] P. Schulz, E. Edri, S. Kirmayer, G. Hodes, D. Cahen and A. Kahn, "Interface energetics in organo-metal halide perovskite-based photovoltaic cells", Energy & Environmental Science, vol. 7, no. 4, p. 1377, 2014. Available: 10.1039/c4ee00168k.

[2] A. Uhl, Metal Counter Electrodes for Perovskite Solar Cells, 1st ed. Switzerland: byWiley-VCH Verlag GmbH & Co, 2018, pp. 422-446.

[3] J. Ding and Q. Yan, "Progress in organic-inorganic hybrid halide perovskite single crystal: growth techniques and applications", Science China Materials, vol. 60, no. 11, pp. 1063-1078, 2017. Available: 10.1007/s40843-017-9039-8.

[4] W. Peng et al., "Solution-Grown Monocrystalline Hybrid Perovskite Films for Hole-Transporter-Free Solar Cells", Advanced Materials, vol. 28, no. 17, pp. 3383-3390, 2016. Available: 10.1002/adma.201506292.

[5] J. Tisdale et al., "Dynamic Impact of Electrode Materials on Interface of Single-Crystalline Methylammonium Lead Bromide Perovskite", Advanced Materials Interfaces, vol. 5, no. 18, p. 1800476, 2018. Available: 10.1002/admi.201800476.

[6] L. Zhao et al., "Redox Chemistry Dominates the Degradation and Decomposition of Metal Halide Perovskite Optoelectronic Devices", ACS Energy Letters, vol. 1, no. 3, pp. 595-602, 2016.

[7] M. Jørgensen, K. Norrman and F. Krebs, "Stability/degradation of polymer solar cells", *Solar Energy Materials and Solar Cells*, vol. 92, no. 7, pp. 686-714, 2008.

[8] Y. Cai, L. Liang and P. Gao, "Promise of commercialization: Carbon materials for low-cost perovskite solar cells", Chinese Physics B, vol. 27, no. 1, p. 018805, 2018.

[9] J. Lee, S. Kim, J. Yang, Y. Yang and N. Park, "Verification and mitigation of ion migration in perovskite solar cells", APL Materials, vol. 7, no. 4, p. 041111, 2019.

[10] C. Li, A. Guerrero, Y. Zhong and S. Huettner, "Origins and mechanisms of hysteresis in organometal halide perovskites", Journal of Physics: Condensed Matter, vol. 29, no. 19, p. 193001, 2017.

[11] D. Kim et al., "Probing Facet-Dependent Surface Defects in MAPbI3 Perovskite Single Crystals", The Journal of Physical Chemistry C, vol. 123, no. 23, pp. 14144-14151, 2019.

[12] K. Qin, B. Dong and S. Wang, "Improving the stability of metal halide perovskite solar cells from material to structure", Journal of Energy Chemistry, vol. 33, pp. 90-99, 2019.

[13] A. Rizzo et al., "Understanding lead iodide perovskite hysteresis and degradation causes by extensive electrical characterization", Solar Energy Materials and Solar Cells, vol. 189, pp. 43-52, 2019.

[14] C. Stecker et al., "Surface Defect Dynamics in Organic–Inorganic Hybrid Perovskites: From Mechanism to Interfacial Properties", ACS Nano, vol. 13, no. 10, pp. 12127-12136, 2019.

[15] G. Xing et al., "Interfacial Electron Transfer Barrier at Compact TiO2/CH3NH3PbI3Heterojunction", Small, vol. 11, no. 29, pp. 3606-3613, 2015.

[16] H. Snaith et al., "Anomalous Hysteresis in Perovskite Solar Cells", The Journal of Physical Chemistry Letters, vol. 5, no. 9, pp. 1511-1515, 2014. Available: 10.1021/jz500113x.

[17] W. Tress, N. Marinova, T. Moehl, S. Zakeeruddin, M. Nazeeruddin and M. Grätzel, "Understanding the rate-dependent J–V hysteresis, slow time component, and aging in CH3NH3PbI3 perovskite solar cells: the role of a compensated electric field", Energy & Environmental Science, vol. 8, no. 3, pp. 995-1004, 2015.

[18] M. Futscher et al., "Quantification of ion migration in CH3NH3PbI3 perovskite solar cells by transient capacitance measurements", Materials Horizons, vol. 6, no. 7, pp. 1497-1503, 2019.

[19] Y. Lin et al., "Excess charge-carrier induced instability of hybrid perovskites", Nature Communications, vol. 9, no. 1, 2018.

[20] D. Meggiolaro, E. Mosconi and F. De Angelis, "Formation of Surface Defects Dominates Ion Migration in Lead-Halide Perovskites", ACS Energy Letters, vol. 4, no. 3, pp. 779-785, 2019.

[21] J. Shi et al., ”Interplays between charge and electric field in perovskite solar cells: charge transport, recombination and hysteresis”, arXiv preprint arXiv:1604.02819,2016.

[22] A. Guerrero et al., "Interfacial Degradation of Planar Lead Halide Perovskite Solar Cells", ACS Nano, vol. 10, no. 1, pp. 218-224, 2015. Available: 10.1021/acsnano.5b03687.

[23] I. Dharmadasa, Y. Rahaq and A. Alam, "Perovskite solar cells: short lifetime and hysteresis behaviour of current–voltage characteristics", Journal of Materials Science: Materials in Electronics, vol. 30, no. 14, pp. 12851-12859, 2019.

[24] H. Khassaf, S. Yadavalli, O. Game, Y. Zhou, N. Padture and A. Kingon, "Comprehensive Elucidation of Ion Transport and Its Relation to Hysteresis in Methylammonium Lead Iodide Perovskite Thin Films", The Journal of Physical Chemistry C, vol. 123, no. 7, pp. 4029-4034, 2019.

[25] Y. Luo et al., "Direct Observation of Halide Migration and its Effect on the Photoluminescence of Methylammonium Lead Bromide Perovskite Single Crystals", Advanced Materials, vol. 29, no. 43, p. 1703451, 2017. Available: 10.1002/adma.201703451.

[26] T. Wu, M. Ahmadi and B. Hu, "Giant current amplification induced by ion migration in perovskite single crystal photodetectors", Journal of Materials Chemistry C, vol. 6, no. 30, pp. 8042-8050, 2018.

[27] J. Carrillo et al., "Ionic Reactivity at Contacts and Aging of Methylammonium Lead Triiodide Perovskite Solar Cells", Advanced Energy Materials, vol. 6, no. 9, p. 1502246, 2016.

[28] J. Frost and A. Walsh, "What Is Moving in Hybrid Halide Perovskite Solar Cells?", Accounts of Chemical Research, vol. 49, no. 3, pp. 528-535, 2016.

[29] Y. Yuan et al., "Photovoltaic Switching Mechanism in Lateral Structure Hybrid Perovskite Solar Cells", Advanced Energy Materials, vol. 5, no. 15, p. 1500615, 2015.

[30] C. Eames, J. Frost, P. Barnes, B. O'Regan, A. Walsh and M. Islam, "Ionic transport in hybrid lead iodide perovskite solar cells", Nature Communications, vol. 6, no. 1, 2015.

[31] Z. Xiao et al., "Giant switchable photovoltaic effect in organometal trihalide perovskite devices", Nature Materials, vol. 14, no. 2, pp. 193-198, 2014. Available: 10.1038/nmat4150.

[32] N. Ahn et al., "Trapped charge-driven degradation of perovskite solar cells", Nature Communications, vol. 7, no. 1, 2016. Available: 10.1038/ncomms13422.

[33] D. Ji et al., "Role of an external electric field on hybrid halide perovskite CH3NH3PbI3 band gaps", Scientific Reports, vol. 8, no. 1, 2018.

[34] K. Kim and D. Siegel, "Correlating lattice distortions, ion migration barriers, and stability in solid electrolytes", Journal of Materials Chemistry A, vol. 7, no. 7, pp. 3216-3227, 2019.

[35] S. Chakrabarty, G. Das, M. Ray and S. Hossain, "Optically enhanced trap assisted hysteretic I-V characteristics of nanocrystalline silicon-based p-i-n heterostructure", Journal of Applied Physics, vol. 127, no. 8, p. 085708, 2020. Available: 10.1063/1.5127653 [Accessed 23 December 2020].

[36] H. Wei and J. Huang, "Halide lead perovskites for ionizing radiation detection", Nature Communications, vol. 10, no. 1, 2019.

[37]Y. Liu, Z. Yang and S. Liu, "Recent Progress in Single-Crystalline Perovskite Research Including Crystal Preparation, Property Evaluation, and Applications", Advanced Science, vol. 5, no. 1, p. 1700471, 2017.

CHAPTER 7: Investigation of Thermal Stability of Methylammonium Lead Bromide Perovskite Single Crystals

CHAPTER 7: Investigation of Thermal Stability of Methylammonium Lead Bromide Perovskite Single Crystals

Photovoltaic devices in use are often under extreme weather conditions, in particular heat. As part of investigating the degradation of $MAPbBr_3$ single crystal the influence of temperature on the crystal properties is provided in this chapter.

The three-dimensional regular arrangement of ions in the crystalline lattice of Methylammonium lead bromide perovskite single crystal was presented in Chapter 4. From the literature the Madelung electrostatic potential shows that halide perovskites have exceptionally low lattice energy values of just (-29.71 eV/cell) at room temperature, this is because the halide belongs to the VII group of anions [1]. Consequently, it is easy to break the bonds between the ions, and low ionization potential for halide perovskite is expected. Hence, some physical and chemical properties are affected by its low lattice energy meaning that the bond between the ions in compound is weak which makes it easier to break the bond and separate ions.

In Chapter 5, the Goldschmidt tolerance factor and octahedral factor provided guidelines for describing Methylammonium lead bromide perovskite formability and stability at room temperature. Here it is determined how temperatures can affect the structure of the $MAPbBr_3$ single crystal through testing the single crystal as a material and within a device structure. Thermogravimetric analysis (TGA) and Differential scanning calorimetry (DSC), FTIR, XRD, SEM and UV –Vis spectroscopy are used to test the single crystal as a material. For electrical

testing IV and CV measurements are used to test the material in a device structure, specifically, a Ag/ $MAPbBr_3$/Ag structure.

7.1 Thermal Properties of $MAPbBr_3$ and its Components

Even if the perovskite applications was made with a structurally stable Methylammonium lead bromide perovskite single crystal, it is not guarantee that the crystal will remain stable under external conditions such as heat. In this section, the thermal properties of $MAPbBr_3$ as a material are extensively studied because it is important to understand the thermal response of the individual components of this material before investigating the thermal stability of its crystal form. Therefore, the thermal behaviour of the organic (MABr) and inorganic ($PbBr_2$) materials and $MAPbBr_3$ single crystal material were examined by using the Thermogravimetric analysis (TGA) and Differential scanning calorimetry (DSC). These were also conducted by Liu et al. (2015), however, using DSC they only tested the organic component, whereas the present study tested both the organic and inorganic components using DSC[2].

7.1.1 Thermogravimetric Analysis (TGA)

TGA was used to investigate the decomposition process of the Methylammonium lead bromide perovskite single crystal material and its individual components, namely, organic (MABr) and inorganic ($PbBr_2$) components separately, under the application of heat. All the TGA data was collected at a 5°C/min heating rate as shown in Figure 7.1.

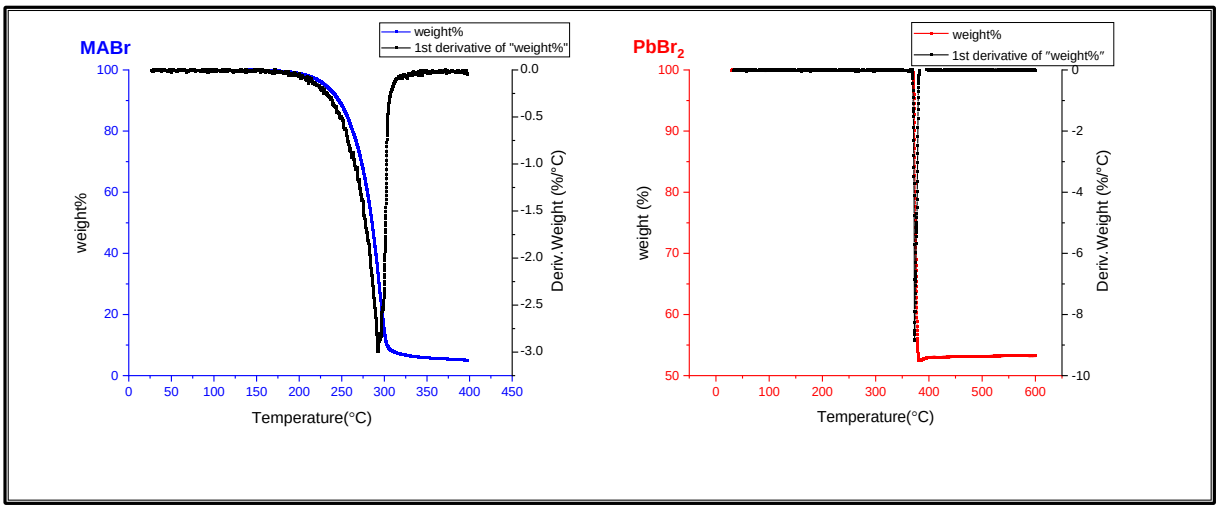

Figure7.1: Thermogravimetric analysis showing the weight loss and derivative weight loss of MABr and PbBr2 as a function of temperature between 24-600°C. MABr shows 95% weight loss in a single step and PbBr2 showed 50% mass loss at 370˚C.

The organic component (MABr) of the $MAPbBr_3$ material showed a 95% weight loss in a single step, the onset of which started near 180°C, which was mainly due to the sublimation of MABr. These results were supported by other studies [3,4]. Similarly, the TGA curve for the inorganic component, lead bromide, demonstrated 50% mass loss at 370°C which is close to the established degradation temperature for $PbBr_2$ at 373°C. This degradation and subsequent loss of mass was caused by the sublimation of bromide as indicated by the sharp transition in the differential TGA curve. At 400°C there was a complete loss of bromide from inorganic component due to the aforementioned sublimation which is consistent with the data provided by some other studies [4,5,6].

The TGA curves of $MAPbBr_3$ single crystal material at heating rates of 5°C/min and 20°C/min are presented in Figure 7.2. Results show different behaviour for each rate in the two thermograms due to different heating rates in the single crystal perovskite material during the decomposition process.

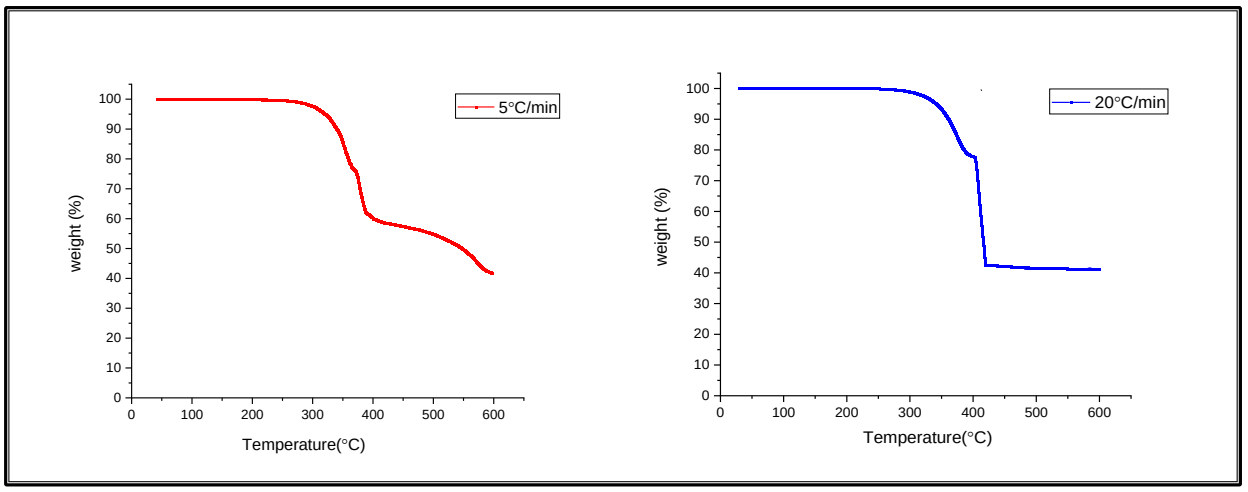

Figure7.2: TGA of weight loss as a function of temperature for crystals at different scanning rate 5°C/min and 20°C/min showing effect of heating rate on reaction

At 20°C/min it was observed that the weight loss of 57 % occurred approximately between 300°C and 400°C. For this decrease in mass it was observed from the TGA curve that it occurred in two steps (see Figure 7.2). In order to investigate these steps, formula weights were to determine the relative weights of products and reactants in a chemical reaction.

Through this calculation it was determined that the first step of the mass decrease was attributed to thermal decomposition of the organic component of the perovskite material, specifically CH_3NH_3Br. As for the second step, the formula weights calculation showed that it was related to a loss of Bromine from the inorganic component, which left behind a black solid residue, identified as lead, as seen in Figure 7.3. These findings are in agreement with findings reported in other studies [7-13] and were derived from the following formula weights equation for the present study:

$CH_3NH_3PbBr_3$ (s) = CH_3NH_3Br + $PbBr_2$ (s) step 1

= 23.3%

$CH_3NH_3PbBr_3$ (s) = CH_3NH_3Br (g) + Br_2 (g) + Pb(s) step 2

= 23.38% + 33.36 % + 43.3%

During the temperature increase from 400°C to 600°C, no weight loss could be observed from the TGA curve.

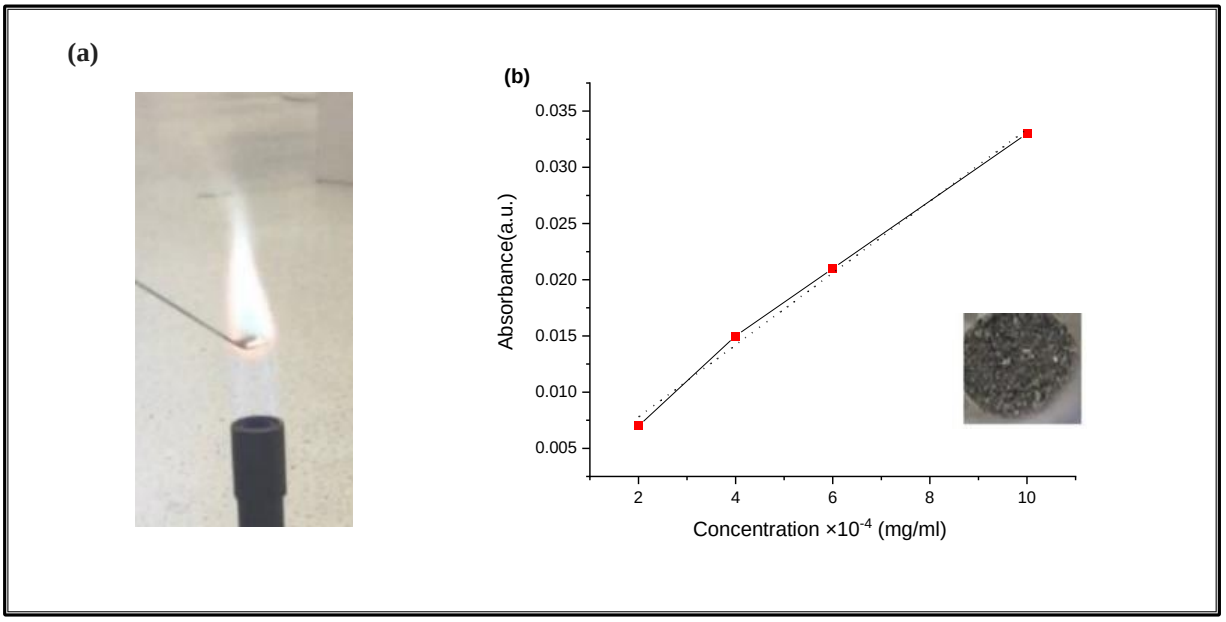

Figure7.3:(a) flame test of residues of $MAPbBr_3$ crystal, (b) calibration curve of AAS, both used to determine lead as the black solid residue.

In reference to the black solid residue, as seen in Figure 7.3, a flame test and Atomic Absorption Spectroscopy (AAS) were performed to show that the residue was lead. The flame test was used to identify the presence of certain elements such as Cobalt, Iron and Sodium based on the colour

appearing in the flame. It can be seen in Figure 7.3 (a) showed a white flame upon application of the MAPbBr3 residue, thereby confirming the presence of lead as the residual material. AAS was performed using a solution of the residue the results showed that lead was present in a high concentration in the solution. The concentration of the lead is estimated by using the standard calibration plot that was obtained by AAS from a range of 0 -1 mg/l of lead. As seen in Figure7.3 (b), this equation is y = 0.0325 x, where 0.0325 is the slope of the line, and the value of determination coefficient (R^2) is 0.978. By correlating its absorbance, the concentration of the lead was estimated to be 0.862 mg/l.

In Figure 7.3, TGA analysis was used to prove that the decomposition process of Methylammonium lead bromide perovskite single crystal at 5°C/min took longer heating duration compared to a heating rate of 20°C/min. This indicate that Methylammonium lead bromide perovskite single crystal could be heated at 5°C/min in order to reduce the sublimation process. In future application, it is recommended that when use Methylammonium lead bromide perovskite single crystal to keep the heating rate at 5°C/min.

7.1.2 Differential Scanning Calorimetry (DSC)

After understanding the heat-induced degradation of MAPbBr3, MABr and $PbBr_2$ through weight loss and Differential Scanning Calorimetry (DSC) was used to understand the thermal degradation of $MAPbBr_3$ single crystal. DSC provides information about phase changes of a sample that occur as a function of temperature. Specifically, this is determined from a sample that is heated at a specific heating rate, this approach is referred to as non-isothermal.

The MAPbBr3 crystals remained stable when heated between 30-300°C as can be seen in Figure 7.4. No glass transition was recorded because of its pure crystallinity between these temperatures which means no phase change took place. Therefore, it was necessary to obtain the DSC curve after heating the crystalline perovskite from 300 – 420°C for different heating rates (5°C/min, 10°C/min, 15°C/min, and 20°C/min). It was observed that the instability in the composition of the MAPbBr3 was noticeable between 300 to 400°C for all heating rates.

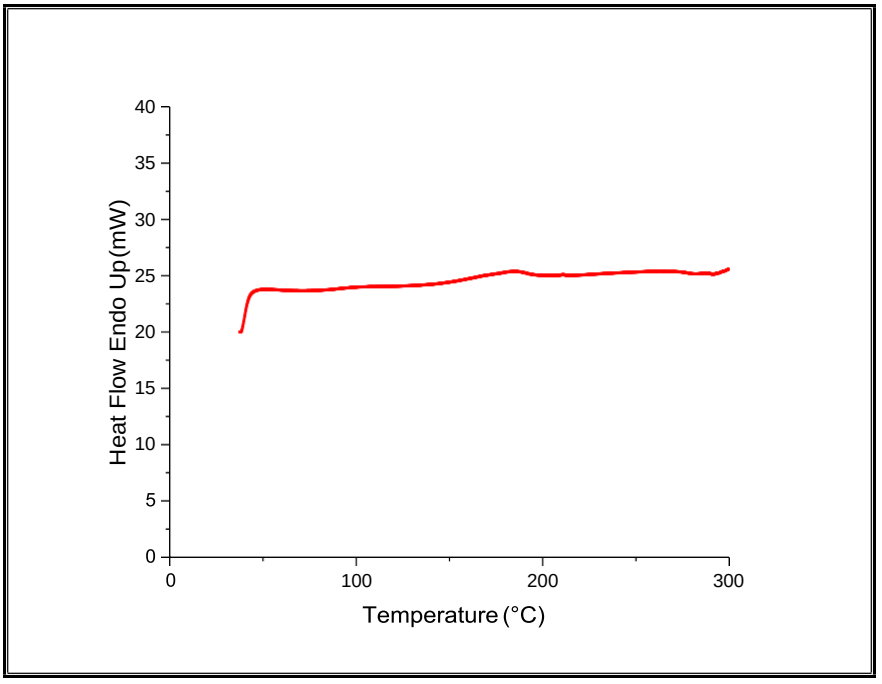

Figure7.4: DSC curve of $MAPbBr_3$ crystals obtained after heating from 30-300°C indicating stability and no phase changes

Long sharp exothermic peaks were observed for all four heating rates. However, it is important to note that the peaks, that represent thermal decomposition of MAPbBr3 due to structural change from the cubic to the tetragonal phase [14,15], occurred at different temperatures, specifically; 5°C/min at 373°C, 10°C/min at 385°C, 15°C/min at 395°C and 20°C/min at 400°C. Thus, it is observed that a lower heating rate leads to decomposition at a lower temperature.

A lower heating rate means that the sample is under the influence of heat for a longer period of time which may have an effect on the structure. Further evidence for this idea is that although it is expected that a higher temperature rate would lead to decomposition earlier, the results show it does not, this suggests that temperature rate has a greater effect because heat is being applied for a longer period of time. In fact this is supported by [16] who in using DSC for characterising complex materials, said that transitions are kinetic events and are therefore, a function of time and temperature, thus a transition will occur at a higher temperature when heated at a higher rate because it has had less time at a particular temperature. The exact inverse of this phenomenon has been observed here, where a longer exposure to temperature, from a lower heating rate resulted in phase changes occurring at lower temperatures [16]. In consideration of these findings, the attributable factor appears to be length of time that the samples are exposed to heat, thus a possible explanation for this observation is that longer exposure to heat means, i.e. lower scan rate, more time that structural bonds are exposed and thus lead to decomposition at a lower temperature.

It was also observed that for 10°C, 15°C, and 20°C/min there were fluctuations close to the large exothermic peak, indicating that phase changes were disordered for these temperatures. However, for 5°C/min there was no such phenomena indicating a more ordered cubic structure at low temperature [17] (see Figure 7.5). Therefore, we recommend that $MAPbBr_3$ should be heated at 5°C/min in order to obtain a stable transition phase, as a higher rate may result in unstable intermediate transitions of $MAPbBr_3$.

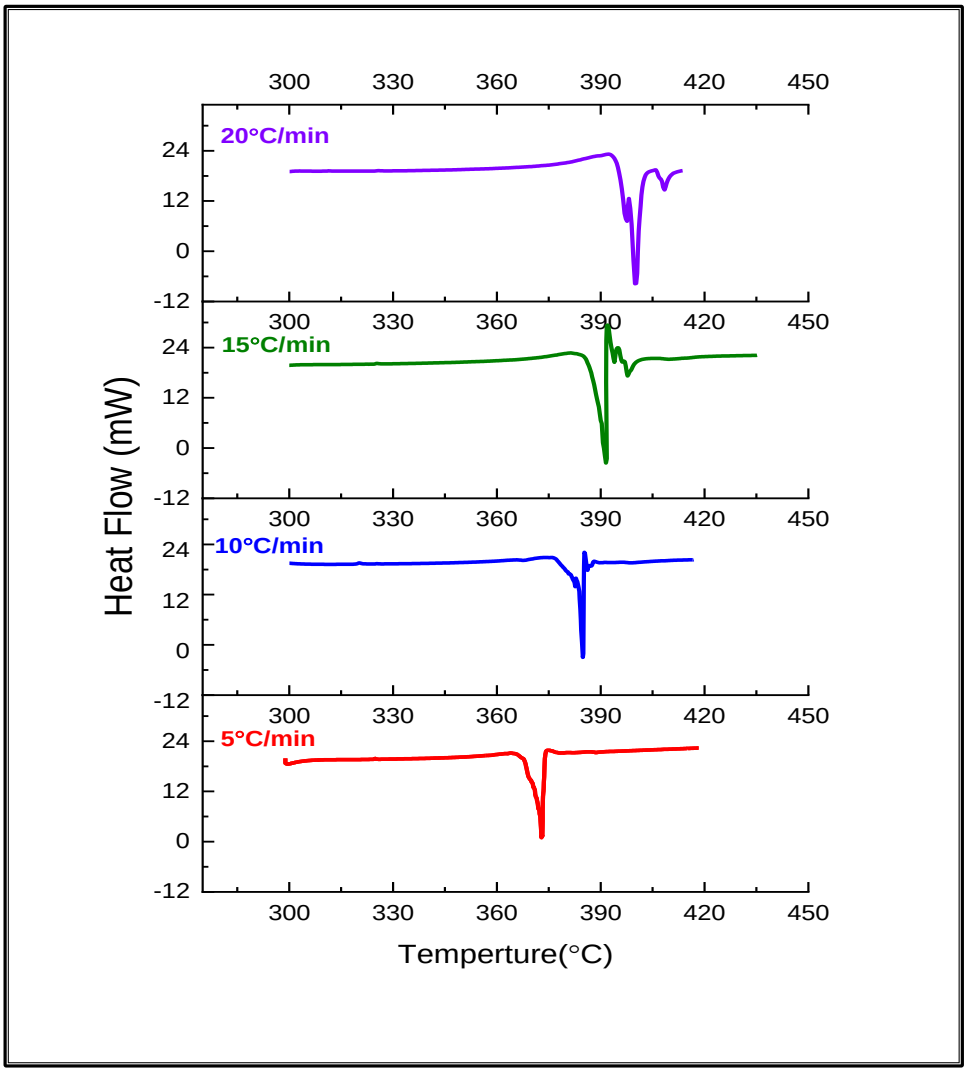

Figure7.5: DSC curve of $MAPbBr_3$ single crystal different scanning rates: 5, 10, 15, and 20°C/min showing that a lower heating rate leads to decomposition at a lower temperature.

Another indication of decomposition, in addition to the abovementioned phase changes, is the activation energy of the $MAPbBr_3$ single crystal. To calculate the activation energy the non-isothermal differential scanning calorimetry (DSC) measurements and popular non-isothermal mathematical models, such as Kissinger and Ozawa methods, are often used to study the activation energy E_a which is the most important kinetic parameter of energetic materials. Kissinger's method is described as an important kinetic parameter to show the shape and temperature of the reaction at exothermic peaks [18].

Using Kissinger's equation (equation 1), the activation energy was calculated using inverse temperature and ln(β/T^2), and the plotted gradient of the line was used to estimate the activation energy as seen in Figure 7.6 (a). The activation energy of the crystallised material was found to be 166.9 KJ/mol (1.74 eV).

Using Ozawa's established theory of kinetic method by assuming that the reaction order is a constant value, can be seen in equation 2. Ozawa provides the equation which is a simple relationship between heating rate and peak temperature where the gradient plot is represented by the activation energy as seen in Figure 7.6(b) [19]. The value of activation energy is 168.7 KJ/mol (1.757eV) which shows a close agreement with the value obtained from the Kissinger Method.

$$\ln\left(\frac{\beta}{r_P^2}\right) = \ln\left(\frac{AR}{E_a}\right) - \frac{E_a}{RT_P} \quad (1)$$

$$\ln(\beta) = constant - 1.052\frac{E_a}{RT_P} \quad (2)$$

Where β is the heating rate, Tp is the peak temperature, A is the pre-exponential factor, Ea is the activation energy and R is the gas constant (8.14 J/mol. k). In order to allow the MAPbBr3 molecules to transition from a stable cubic structure to a tetragonal structure, the minimum activation energy should exceed 167.85 KJ/mol.

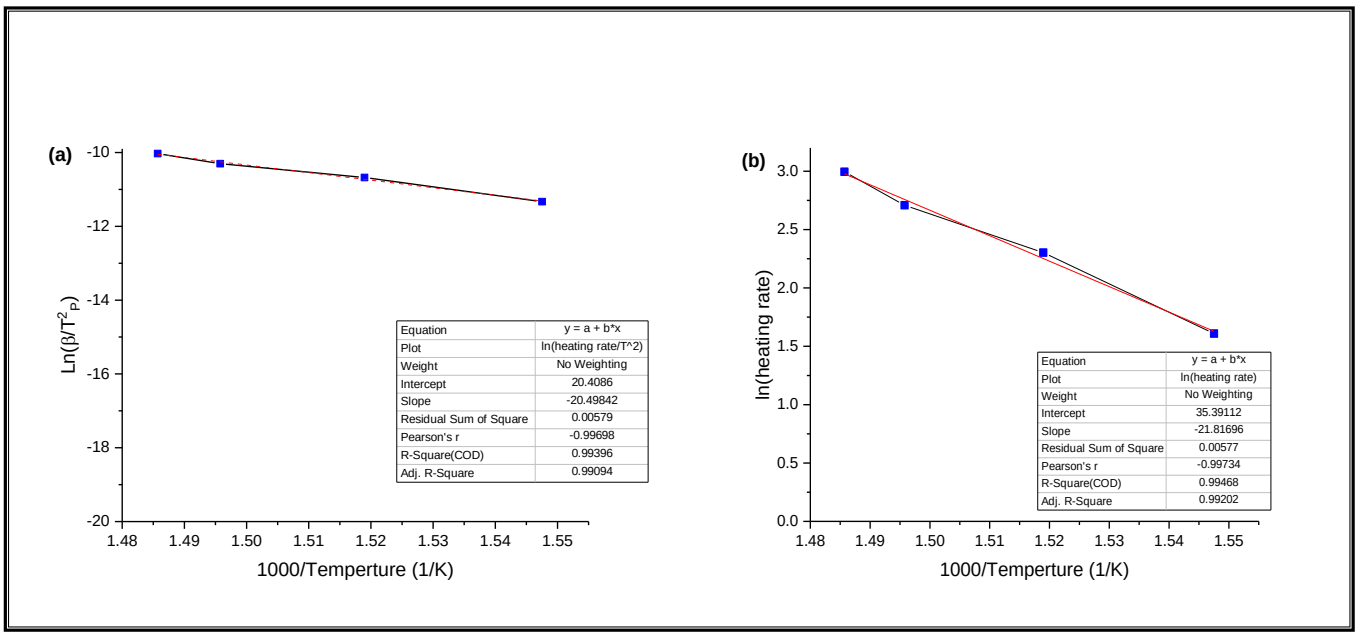

Figure7.6:Activation energy calculations (a)Kissinger's plot for $MAPbBr_3$crystal, and (b) Ozawa's plot for $MAPbBr_3$ crystal, both showing minimum activation energy was found at 167.85 KJ/mol.

7.2 Thermal Stability of $MAPbBr_3$ Single Crystal at Constant Temperature

Perovskite photoconductive halide materials are prone to degradation under various environmental conditions such as humidity, oxygen, UV light, heat and other factors. Therefore, effort addressing the stability of perovskite photoconductive towards the development of enhancement strategies while maintaining high performance, is a necessary endeavour.

The present research is concerned with photoconductive devices in which $MAPbBr_3$ exists as a single crystal. In this section the thermal stability of the single crystal is presented, firstly, as a single crystal using UV-Vis spectrometry, XRD, FTIR, EDX, and SEM, and secondly, as device structure using dark current voltage.

For the single crystal alone, thermal stability is examined at various temperatures 50, 80, 120, 170 and 220°C at a constant over 360 minutes using the aforementioned optical characterisation techniques. The single crystal as a device structure is investigated at temperatures starting from temperatures from 24°C to 220°C with increments of around 25°C in order to reveal activation energy using Arrhenius equation to reveal activation energy.

Thermal stability is an important factor for stability of perovskite applications. Operation of photocurrent under direct sunlight can cause an increase in device temperature, higher than ambient temperature. Therefore, stability of perovskite photocurrent continues to be a challenge. In this section, we systematically studied the thermal stability of $MAPbBr_3$ single crystal with 1mm thickness fabricated from the inverse crystallisation temperature (ICT) method under ambient air conditions.

7.2.1 Band Gap and Temperature

UV-Vis spectrometry was used to measure the band gap as an indicator of structure. Despite the fact that the band gap of Methylammonium lead bromide perovskite single crystal is around 2.1eV as seen in Chapter 5 (Figure 5), the energy band gap was found to decrease gradually with an increase in the duration of applied temperature at a constant. Notably, decreasing absorbance is clearly observed as the duration of heating increases from 120°C and 170°C. In contrast the energy band gap remains the same during the heating of the $MAPbBr_3$ single crystal at 50°C and 80°C evidenced by no change in absorbance during the annealing of the crystal at these temperatures. These findings confirm that the $MAPbBr_3$ single crystal has a greatly enhanced thermal stability

over a period of six hours at 80°C. At an even higher temperature, 220°C the band gap disappears, and the semiconductor properties cease (Figure 7.7).

What the results therefore show, is that an increased temperature results in a corresponding decrease in the band gap dependent on duration. However, in application as a solar this decrease in the bad gap would not be an issue as normal operating temperatures would not be this high, however, the results presented here are relevant to other applications such as photo detectors in high temperature environments.

Therefore, conclusion is longer exposure mechanisms is dependent on temperature only works at a certain point. It is observed that under the higher temperature the decrease in the band gap takes place from the outset of the heating process (for example 220 ºC), therefore, would suggest that temperature, as opposed to length of time exposure to temperature is the significant factor.

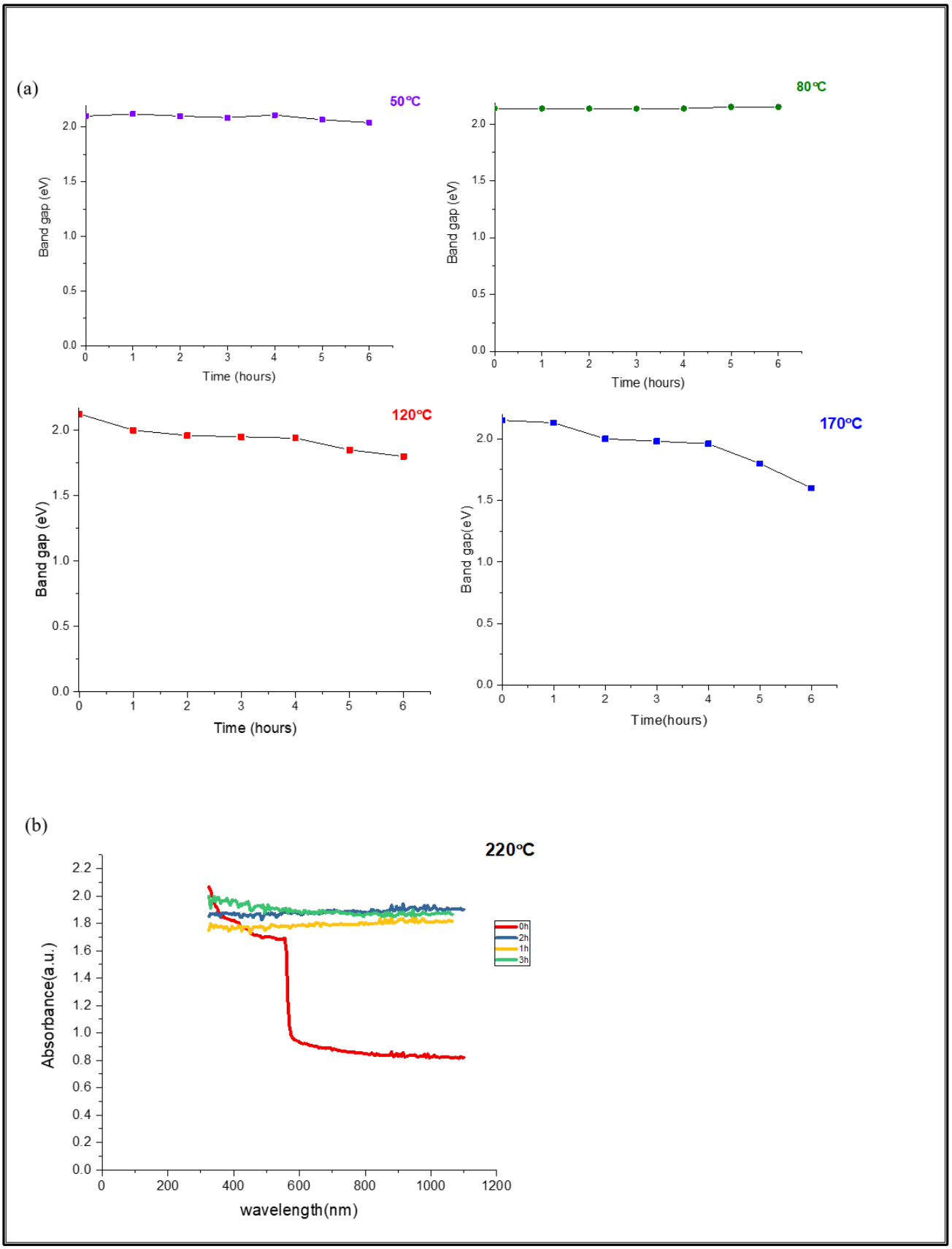

Figure7 7: (a) UV-Vis spectroscopy for bandgap over time for perovskite crystal under high temperatures 50,80, 120 and170˚C over 0,1,2,3,4,5,6 hours, showing decreasing absorbance for 120˚C and 170˚C, and (b) UV-Vis spectroscopy for absorbance over wavelength at 220 ˚C over 0,1,1 and 3 hours showing the band gap disappears after one hour heating.

.

7.2.2 Bond Strength and Temperature

It was observed visually that the direction of decomposition was from the surface of the crystal to the bulk. Therefore, this prompts investigation of surface degradation as well as the structure of Methylammonium lead bromide perovskite single crystal in relation to thermal stability using heating induced degradation experiments. Towards understanding this structure under various temperatures FTIR spectra are used in order to compare the transmittance spectra of Methylammonium lead bromide perovskite single crystal after every hour up to six hours of annealing at different temperatures.

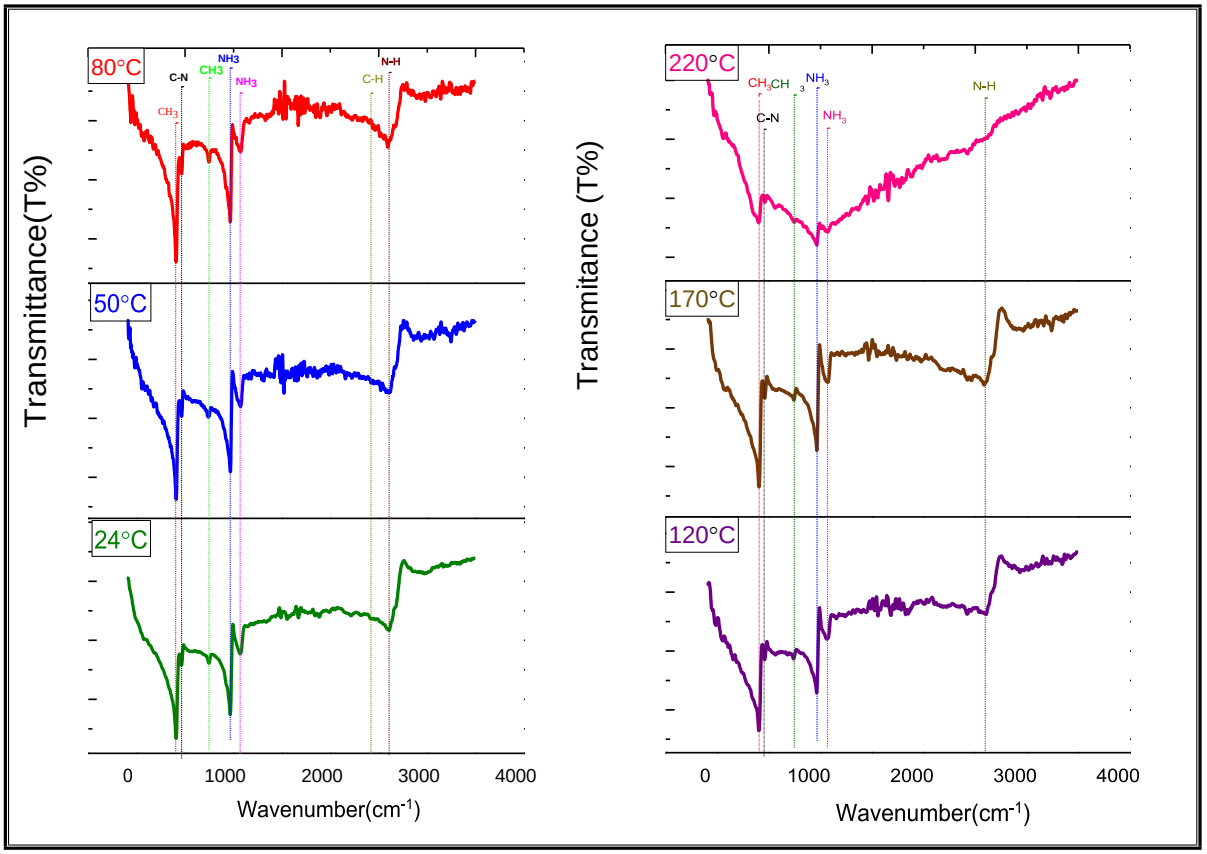

Figure7.8: FTIR analysis of perovskite single crystal at 24, 50, 80, 120,170 and 220°C after 6 hours annealing showing That For 50˚C and 80˚C no bonds are missing, forming or shifting, for 120˚C and 170˚C the strength of the bond decreases over time and for 220˚C N-H is missing

It was observed that there are no bonds missing, forming or even shifting during the full six hours heating time at 50°C and 80 °C, this is in contrast to other higher temperatures, as seen in Figure 7.8, whereby although there are no bonds missing or forming for 120°C and 170°C, the strength of these bonds reduces over the period of six hours.

At 220°C the N-H bond is missing after heating Methylammonium lead bromide single crystal for 4 hours (see figure7.9), which means the perovskite is starting to decompose to gases HBr and CH_3NH_2 due to degradation of the organic molecule MA, which is an explanation for the observed reduction in mass of the perovskite [5].

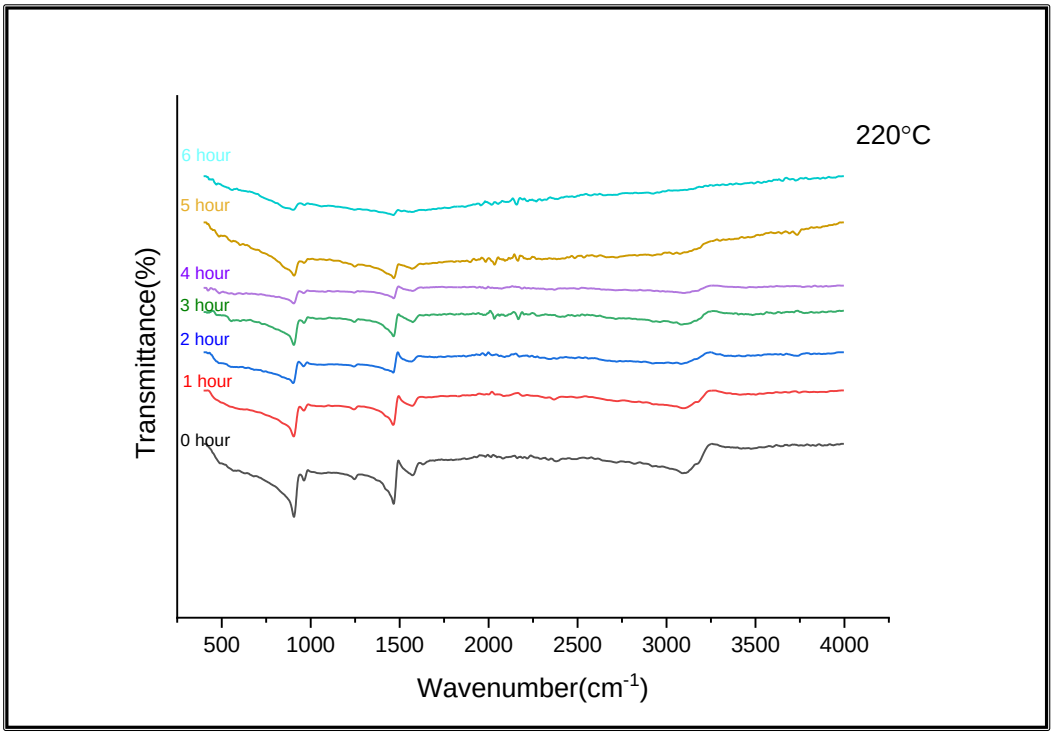

Figure7.9: FTIR analysis of perovskite crystal at 220°C at different durations of heating time 0,1,2,3,4,5,6 hours showing missing N-H bonds

.

Furthermore, the aforementioned surface degradation was observed after six hours of heating at 220°C evidenced by a full change in the surface colour to white, although this process did start at 170°C (see Figure 7.10). Thus, there is a surface-dominated reaction, which was not observed in the surface after 6 hours of annealing at 50°C, 80°C, and 120°C. The degradation process continues until all of the bulk degrades. Importantly, this change in the colour from orange to white is a result of the release of MA from the perovskite bulk via sublimation leaving the lead bromide behind. Specifically, $PbBr_6$ is transformed to $PbBr_2$ whereby the weak bonds are broken, thereafter, $PbBr_2$ relaxes into its energetic structure and the white- colored lead bromide ($PbBr_2$) is shown as a product of this decomposition. FTIR spectrum was not used here as Pb-Br and H-Br were not observed in this spectrum because the absorption was in the range of 300 – 500cm^{-1}, therefore, they will not be seen in the spectra mode of $MAPbBr_3$. Further evidence for this process is the EDX pattern which shows that at 220°C after six hours PbBr remains (see Figure 7.11).

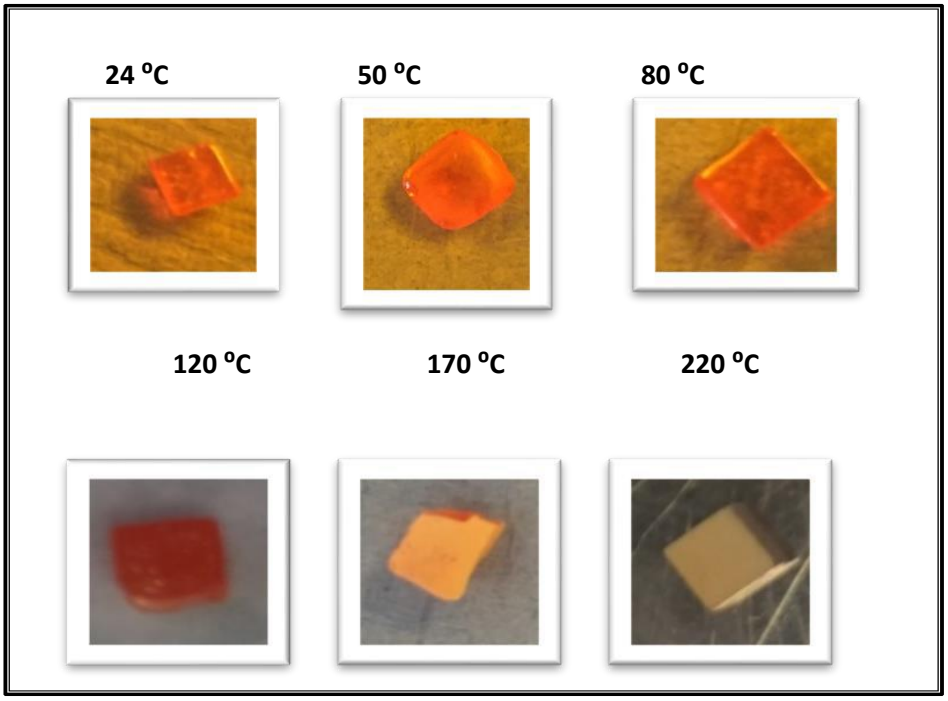

Figure7.10: photographs of $MAPbBr_3$ after annealing for 6 hours at 24, 50, 80, 120, 170 and 220°C showing change in surface colour from orange to white at higher temperatures indicating the release of MA from perovskite.

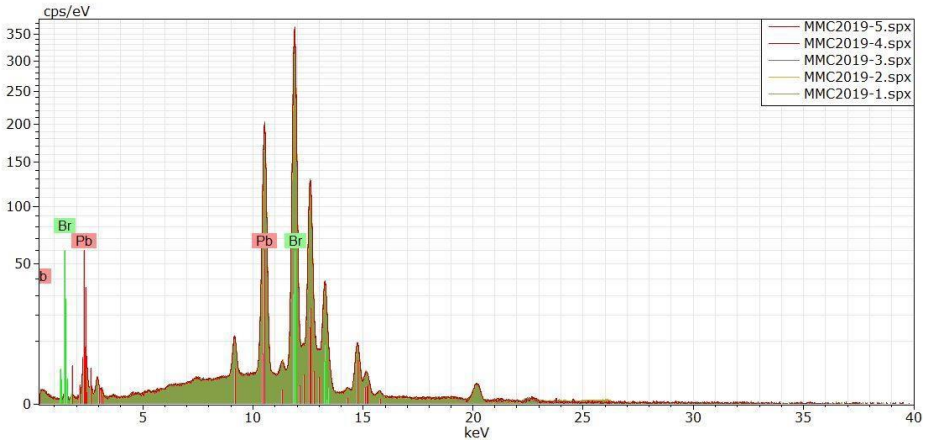

Figure7.11: EDX patterns of the single perovskite crystal after six hours at 220°C showing lead bromide as a product of decomposition of perovskite

7.2.3 Phase Transition and Temperature

It is clear that the structural stability determines whether the crystalline structures, i.e. cubic and tetragonal, are stable for a wide range of external factors such as heat, light and moisture. Therefore, after checking the optical and structural properties of $MAPbBr_3$ single crystal at various temperatures and durations in the above, it is now necessary to illustrate the change in XRD patterns for perovskite single crystals at different temperatures after six hours of heating. Similar research was conducted to test the thermal stability of $MA_{1-x}Cs_xPbBr_3$ as a single crystal using XRD [20].

As seen from figure 7.12, most of the peaks related to perovskite cubic structure are present in the diffraction pattern after six hours heating. The behaviour of these peaks changes with an increase in temperature. After six hours exposure of the crystal to 50°C or 80°C, the intensity of the peaks change, however, the presence of these peaks still means that the structure of the $MAPbBr_3$ is cubic although the difference in the intensity (as seen in figure 7.12) in the XRD pattern after six hours exposure to 120°C, 170°C and 220°C shows a transition to the tetragonal phase as indicated by a splitting in the peaks at these temperatures, see Figure 7.12. For example,

splitting within the peak (200) is in an indication of phase transformation to a lower symmetry [20]. In other words, the structure of the Methylammonium lead bromide perovskite single crystal underwent several structural transitions after six hours of annealing at these temperatures. Further indication of a shift to the tetragonal phase is an observed shift in main peaks towards a lower theta value with an increasing temperature, this confirms that the crystal structure underwent elongation, an attribute of the tetragonal phase, where the dimension of the simple unit cell is expanded.

As noted in the above, it was visually observed that the crystal started to turn white at 170°C and completely white at 220°C due to the lead bromide ($PbBr_2$) left behind, this would represent a structural change from the tetragonal to the trigonal phase [21].

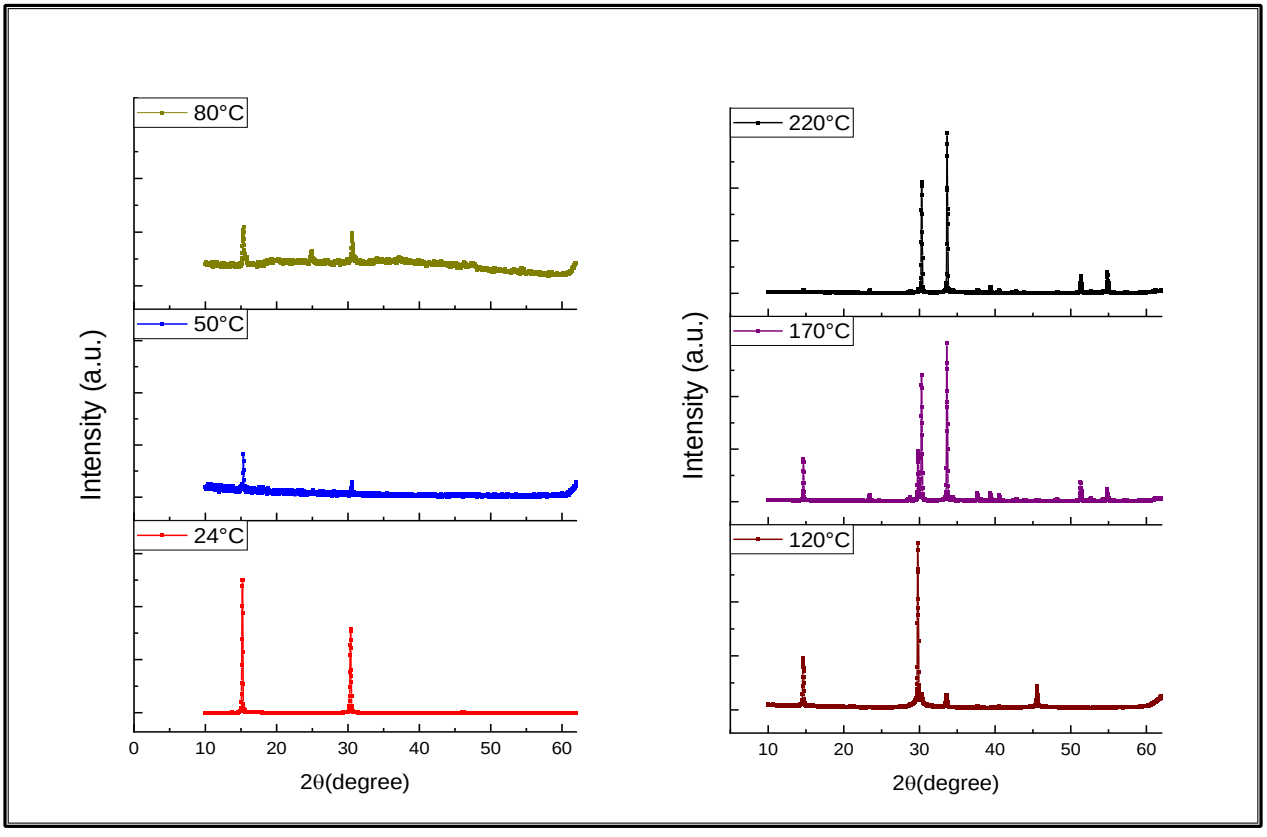

Figure7.12: XRD patterns of the single perovskite crystals under different temperatures at 24,50,80, 120,170 and 220°C for six hours showing phase changes.

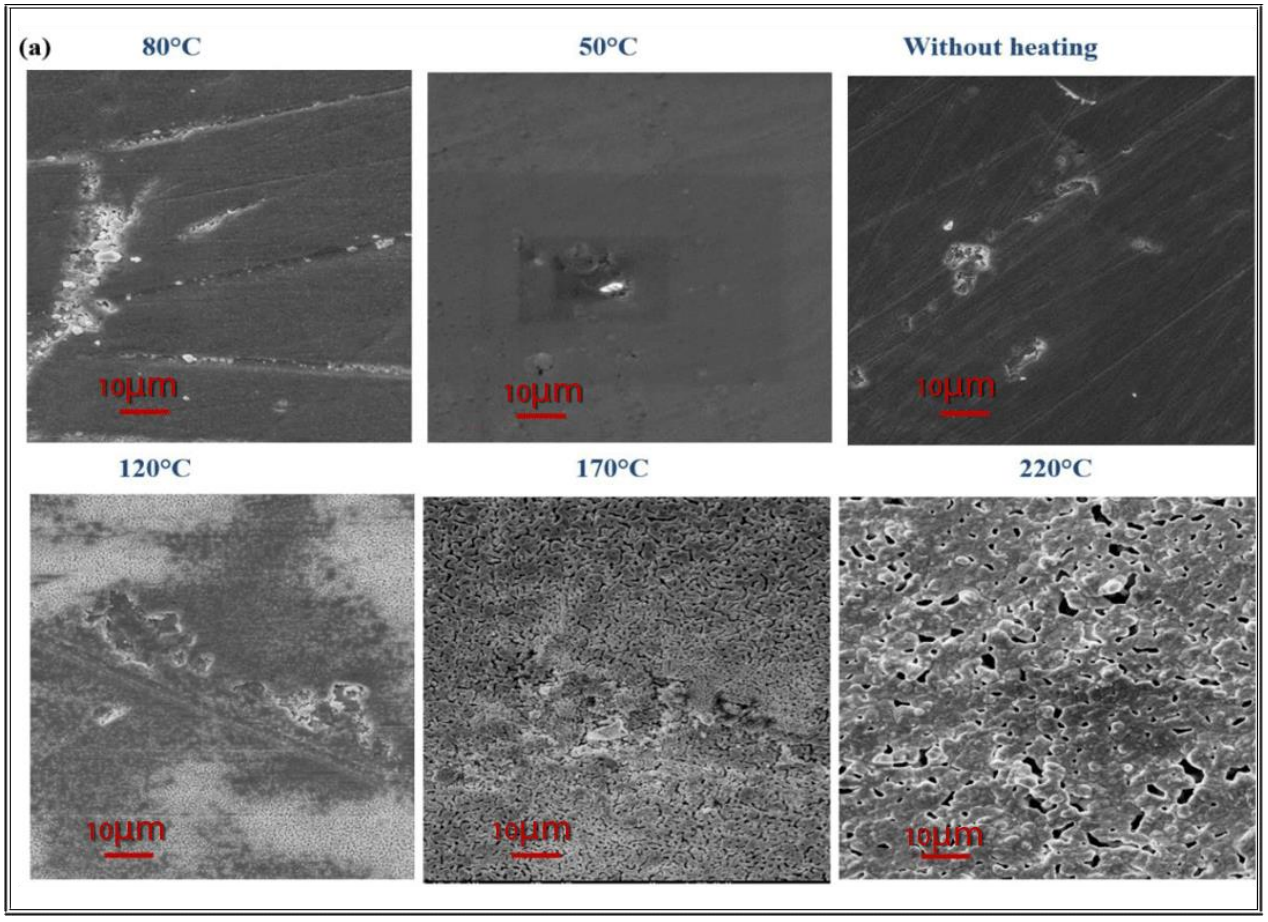

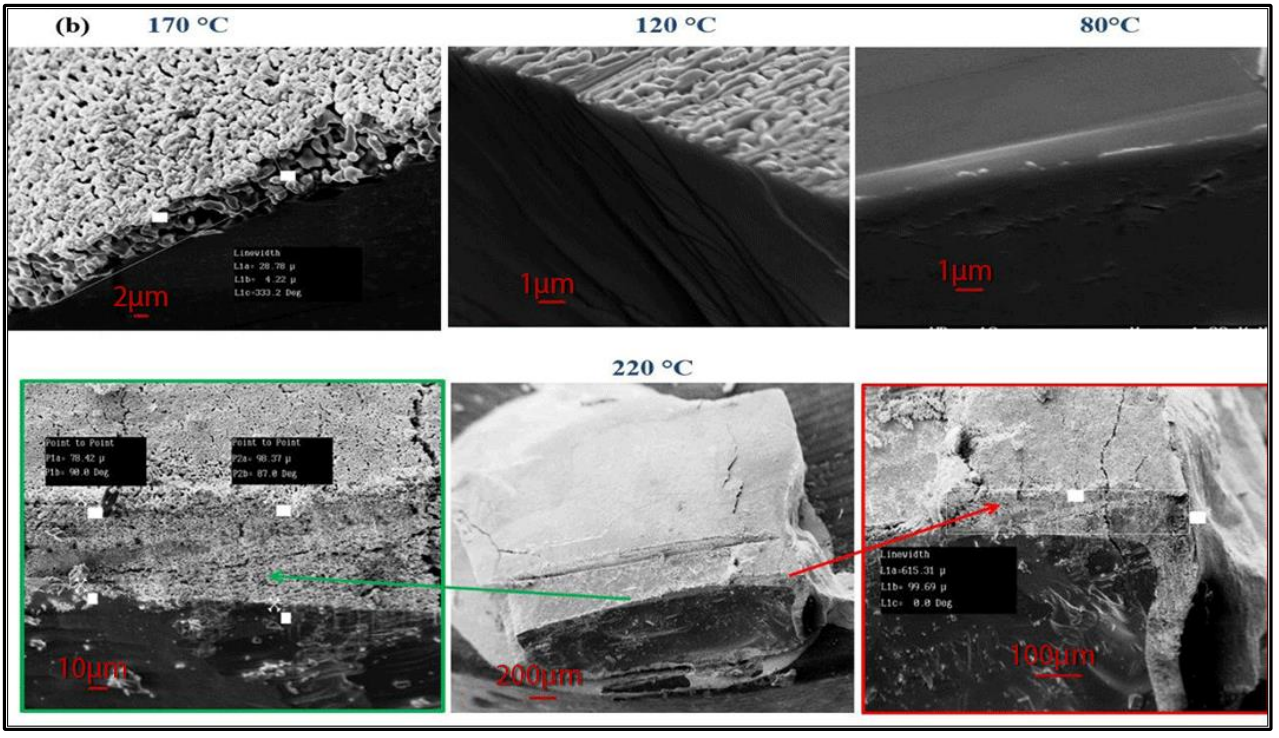

Figure7.13: SEM images for $MAPbBr_3$ after their annealing for 6 hours at 24, 50, 80, 120, 170 and 220°C (a) at the surface, and (b) vertical cross section. Images indicate changes on crystal surface become thicker for each subsequent temperature increase.

In the above (see Figure 7.12) it has been shown that there are phase changes evident for each temperature. Furthermore, in the pictures below there is a visually observed process of whitening of the surface of the crystal that is thicker for each subsequent higher temperature. Therefore, there is a link between this observed whitening of the crystal and the phase changes

Given that it has been established in the above that the whitening is a result of sublimation of the organic compound leaving behind lead bromide and that this also indicates, to a certain extent, the process of a phase change to the trigonal phase [21], it would stand to reason that at the stage the observed whitening at 120°C (Figure 7.13 (a)) sublimation is taking place and therefore, trigonal is observed together with tetragonal, the latter evidenced by a split in the peak at 120°C and the former evidenced by the start of the whitening of the surface at the same temperature (Figure 7.13 (b)). At the next higher temperature 170°C further whitening takes place, while at the same time there is a tetragonal phase, further evidence that the tetragonal and trigonal phases are existing simultaneously [23]. Finally, at 220°C the whitening is even more evident and there is a change to trigonal phase (Figure 7.13 (b)).

7.2.4 Dark Current Activation and Temperature

Dark IV curves were measured at various temperatures from 24°C to 220°C with increments of around 25°C in order to reveal activation energy, as shown in Figure 7.14 below. It was revealed that the dark current curves at different temperatures showed an ohmic linear nature, the dark current increases with an increase in the temperature as well as an increase in applied voltage. In Figure 7.14 (a), these specific effects are shown over this temperature range. The dark current remains stable below 100°C for all applied voltages.

To determine the activation energy in the $MAPbBr_3$ crystal, the Arrhenius equation was used in which the dark resistance presents as logarithmic dependence on $(k_B T)^{-1}$[24]

$$R_{dark} = R_0 \exp\left(-\frac{E_a}{T\,K_B}\right) \qquad (3)$$

Where R_{dark} and R_0 are dark resistance and the pre-exponential factor respectively, E_a is the activation energy, T is the temperature in kelvin and $K_B = 8.617\times10^{-5}\ K^{-1}.eV$ which is the Boltzmann constant

In Figure 7.14 (b), the graph is divided into two regions; the activation energy of $MAPbBr_3$ is 0.22eV at the low temperature region (24°C - 100°C), while it increases to 0.8 eV at the high temperature region (120-220°C). Increase in the activation energy is related to thermal band-to-band (intrinsic) kinetics [22]. The activation energy in organic materials is an indication of the energy difference between the Fermi level and transport level [23]. An increase in temperature causes the carriers to become thermally excited and they jump to the conduction band which leads to decreased resistivity and a current flow that is linked to temperature [25]. Furthermore, the observation that there is an increase in the activation energy associated with an increase in temperature is attributed the fact that increasing temperature narrows the band gap.

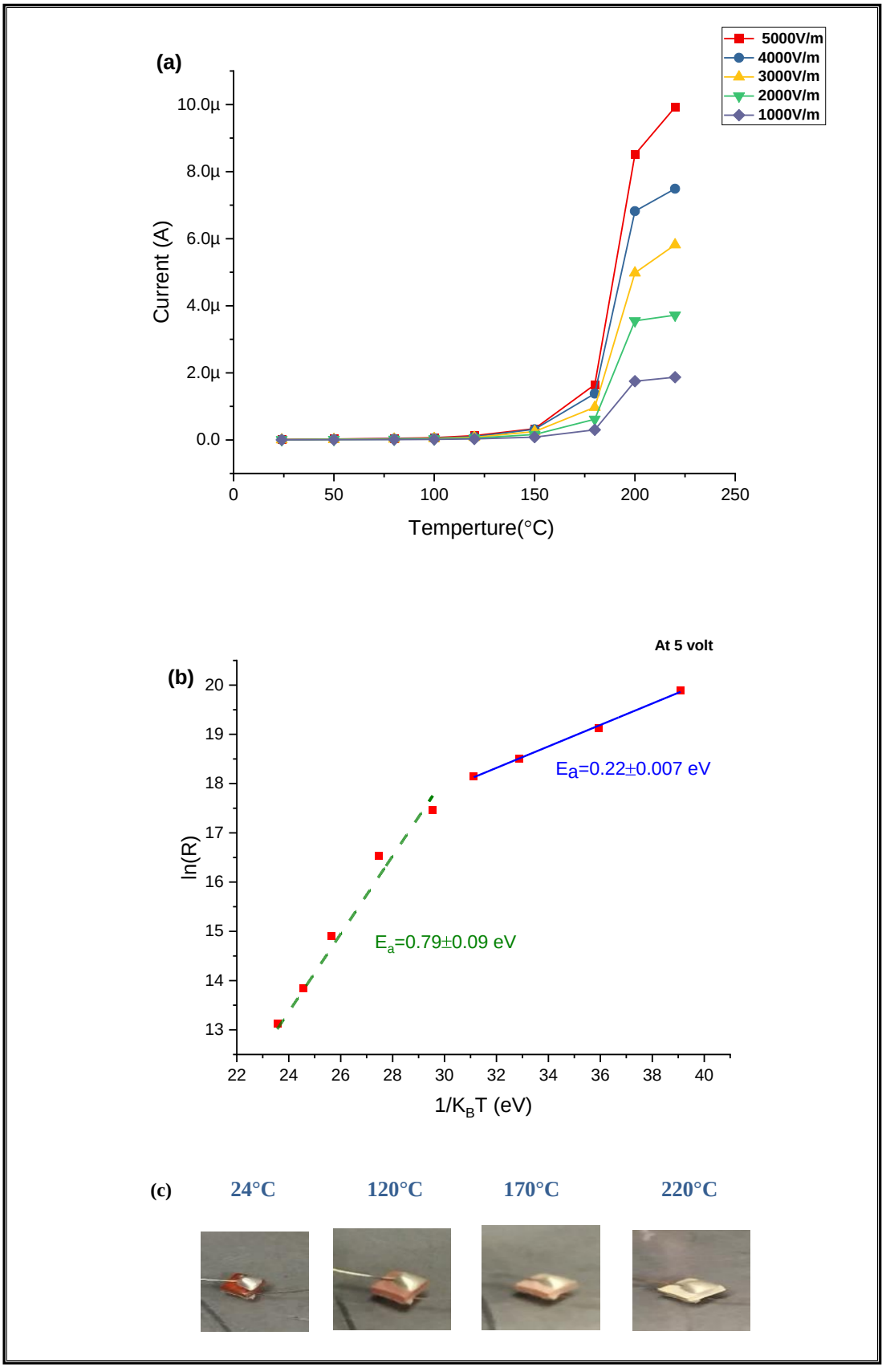

Figure7.14: single perovskite crystals annealed at different temperatures: 24,50,80,100,120,150,180 200 and 220°C (a) current vs. temperature at different electric fields showing current remaining stable below 100˚C for all voltages, (b) Arrhenius plot at 5 volts to calculate activation energy ,and (c) photographs of $MAPbBr_3$ after annealing

7.3 Summary

This chapter has presented the investigation of the effect of temperature of the stability of the $MAPbBr_3$ single crystal. This was achieved through testing the single crystal and as a device structure, specifically, through the various techniques there was extensive testing of the thermal properties. The results revealed that temperature had an effect on material stability in a number of ways. TGA revealed a loss of mass through the sublimation of the organic component of $MAPbBr_3$ and a loss of inorganic bromine associated with increasing temperatures, leaving behind lead residue which was confirmed by AAS and a flame test. DSC was used to determine associated phase changes in the material which were observed at different temperatures, however, the rate of heating was found to be significant in this process, whereby it was found that for a lower heating rate decomposition took place at a lower temperature due to the material being exposed longer to heat. DSC also determined that it is recommended to heat $MAPbBr_3$ at a rate of 5°C /min to a achieve stable transition phase. Phase changes were also observed with increasing temperature by XRD and that these phase changes can occur through elongation and sublimation and a trigonal phase was achieved, evidence by sublimation of the organic compound, a process that increased with increasing temperatures. This was observed visually whereby a white layer, as a result of lead bromide left behind through this sublimation, increase in thickness with increasing temperatures. Therefore, increasing temperature was instrumental in the observed surface degradation of the single crystal

Furthermore, it was revealed that higher temperatures were required for material decomposition, evidenced by a lack of structural change at 50°C and 80°C, over a heating period of six hours using optical characterisations, whereby degradation was observed at 120°C, 170°C and 220°C.

The application of DSC together with Kissinger's and Ozawa's non-isothermal mathematical models were used to calculate activation energy. This was supported by electrical characterisation which found higher activation energies for high temperatures attributed to a decreasing band gap. Further evidence of this phenomenon is that using UV-Vis and IV dark current a relationship between temperature and band gap, specifically, higher temperature resulted in a narrowing of the band gap, even to a point where it disappears, was revealed. Using UV-Vis it was observed that the band gap started to narrow at 120°C after a period of six hours heating. This phenomenon is also supported by the results of the IV dark currents which showed an increase in the activation energy, an indicator of a decreasing band gap, also at 120°C. This is a contribution of the research whereby changes in the band gap, associated activation energy and structural degradation were observed at these temperatures.

7.4 References

[1] M. Frost, T. Butler, F. Brivio, H. Hendon, M. Schilfgaarde and A. Walsh, "Atomistic Origins of High-Performance in Hybrid Halide Perovskite Solar Cells", *American Chemical Society*, vol. 14, no. 2584-2590, 2014.

[2] Y. Liu et al., "Two-Inch-Sized Perovskite CH3NH3PbX3(X = Cl, Br, I) Crystals: Growth and Characterization", Advanced Materials, vol. 27, no. 35, pp. 5176-5183, 2015. Available: 10.1002/adma.201502597.

[3] A. Dualeh, P. Gao, S. Seok, M. Nazeeruddin and M. Grätzel, "Thermal Behavior of Methylammonium Lead-Trihalide Perovskite Photovoltaic Light Harvesters", Chemistry of Materials, vol. 26, no. 21, pp. 6160-6164, 2014.

[4] B. Brunetti, C. Cavallo, A. Ciccioli, G. Gigli and A. Latini, "On the Thermal and Thermodynamic (In)Stability of Methylammonium Lead Halide Perovskites", Scientific Reports, vol. 6, no. 1, 2016.

[5] M. Kulbak et al., "Cesium Enhances Long-Term Stability of Lead Bromide Perovskite-Based Solar Cells", The Journal of Physical Chemistry Letters, vol. 7, no. 1, pp. 167-172, 2015.

[6] T. Berhe et al., "Organometal halide perovskite solar cells: degradation and stability", Energy & Environmental Science, vol. 9, no. 2, pp. 323-356, 2016.

[7] N. Tiep, Z. Ku and H. Fan, "Recent Advances in Improving the Stability of Perovskite Solar Cells", Advanced Energy Materials, vol. 6, no. 3, p. 1501420, 2015.

[8] J. Navas et al., "Revealing the role of Pb2+ in the stability of organic–inorganic hybrid perovskite CH3NH3Pb1−xCdxI3: an experimental and theoretical study", Physical Chemistry Chemical Physics, vol. 17, no. 37, pp. 23886-23896, 2015.

[9] C. Qin, T. Matsushima, T. Fujihara, W. Potscavage and C. Adachi, "Degradation Mechanisms of Solution-Processed Planar Perovskite Solar Cells: Thermally Stimulated Current Measurement for Analysis of Carrier Traps", Advanced Materials, vol. 28, no. 3, pp. 466-471, 2015.

[10] S. Ahmad, P. Kanaujia, W. Niu, J. Baumberg and G. Vijaya Prakash, "In Situ Intercalation Dynamics in Inorganic–Organic Layered Perovskite Thin Films", ACS Applied Materials & Interfaces, vol. 6, no. 13, pp. 10238-10247, 2014.

[11] Q. Fu et al., "Recent Progress on the Long-Term Stability of Perovskite Solar Cells", Advanced Science, vol. 5, no. 5, p. 1700387, 2018. Available: 10.1002/advs.201700387.

[12] G. Abdelmageed et al., "Mechanisms for light induced degradation in MAPbI3 perovskite thin films and solar cells", Applied Physics Letters, vol. 109, no. 23, p. 233905, 2016.

[13] G. Niu, X. Guo and L. Wang, "Review of recent progress in chemical stability of perovskite solar cells", Journal of Materials Chemistry A, vol. 3, no. 17, pp. 8970-8980, 2015. Available: 10.1039/c4ta04994b.

[14] K. Wang, L. Li, M. Shellaiah and K. Wen Sun, "Structural and Photophysical Properties of Methylammonium Lead Tribromide (MAPbBr3) Single Crystals", Scientific Reports, vol. 7, no. 1, 2017. Available: 10.1038/s41598-017-13571-1.

[15] I. Swainson, C. Stock, S. Parker, L. Van Eijck, M. Russina and J. Taylor, "From soft harmonic phonons to fast relaxational dynamics inCH3NH3PbBr3", Physical Review B, vol. 92, no. 10, 2015. Available: 10.1103/physrevb.92.100303.

[16] L. Thomas, "Use of multiple heating rate DSC and modulated temperature DSC to detect and analyze temperature-time-dependent transitions in materials", American Laboratory, vol. 33, no. 1, pp. 26-31, 2001. [Accessed 18 February 2020].

[17] R. Worhatch, H. Kim, I. Swainson, A. Yonkeu and S. Billinge, "Study of Local Structure in Selected Organic–Inorganic Perovskites in thePm3̄mPhase", Chemistry of Materials, vol. 20, no. 4, pp. 1272-1277, 2008.

[18] P. Roura and J. Farjas, "Analytical solution for the Kissinger equation", Journal of Materials Research, vol. 24, no. 10, pp. 3095-3098, 2009.

[19] N. Koga, "ChemInform Abstract: Ozawa's Kinetic Method for Analyzing Thermoanalytical Curves - History and Theoretical Fundamentals", ChemInform, vol. 44, no. 48, p. no-no, 2013.

[20] H. Kaslasi, Y. Feldman, Y. Rakita, D. Cahen and G. Hodes, "Single-Crystal Growth and Thermal Stability of (CH3NH3)1–xCsxPbBr3", Crystal Growth & Design, 2020. Available: 10.1021/acs.cgd.0c00122.

[21]T. Ava, A. Al Mamun, S. Marsillac and G. Namkoong, "A Review: Thermal Stability of Methylammonium Lead Halide Based Perovskite Solar Cells", Applied Sciences, vol. 9, no. 1, p. 188, 2019.

[22]S. Reynolds, A. Houghton and D. Keeble, "Carrier transport in methylammonium lead iodide perovskite single crystals studied by dark current, steady state and transient photocurrent measurements", Journal of Physics: Conference Series, vol. 1186, p. 012035, 2019. Available: 10.1088/1742-6596/1186/1/012035.

[23]L. Mao, H. Ning, C. Hu, Z. Lu and G. Wang, "Physical Modeling of Activation Energy in Organic Semiconductor Devices based on Energy and Momentum Conservations", Scientific Reports, vol. 6, no. 1, 2016.

[24]M. Wimmer, M. Kaes, C. Dellen and M. Salinga, "Role of activation energy in resistance drift of amorphous phase change materials", 2014.

[25]C. Lin et al., "Metal contact and carrier transport in single crystalline CH3NH3PbBr3 perovskite", Nano Energy, vol. 53, pp. 817-827, 2018. Available: 10.1016/j.nanoen.2018.09.049.

Chapter 8: Investigation the Photostability of Methylammonium Lead Bromide Perovskite Single Crystals

Chapter 8: Investigation the Photostability of Methylammonium Lead Bromide Perovskite Single Crystals

In the previous chapter it has been shown that heat alone did have an effect on the stability of the single crystal, suggesting that electrodes may not necessarily be solely responsible for observed instability. Therefore, there is a need to test the single crystal at room temperature, not as a device, under light conditions using optical and structural measurements, to check for instability that may attributed to light alone. After that, $MAPbBr_3$ single crystals were tested as photodetector under different light conditions where consideration of electrodes would be relevant.

8.1 Effect of the Light Intensities on the $MAPbBr_3$ Single Crystal

$MAPbBr_3$ single crystals are examined under different light conditions provided by a xenon lamp which is emitting continues spectrum from ultraviolet to infrared regions covering visible region in order to determine if there is an effect on material stability. Three different light intensities are applied over a period of 100 minutes to the $MAPbBr_3$ single crystals which were without filter (85.8 W/m^2), ND2 (42.9 W/m^2), and ND4 (21.45 W/m^2) and stability was investigated using XRD, FTIR and SEM.

Using XRD for all three light intensities, the crystal structure of $MAPbBr_3$ was remained in a cubic phase, as indicated by the position of the peaks in the XRD pattern being the same (see Figure 8.1 (b)) which indicates to structural stability of these crystals.

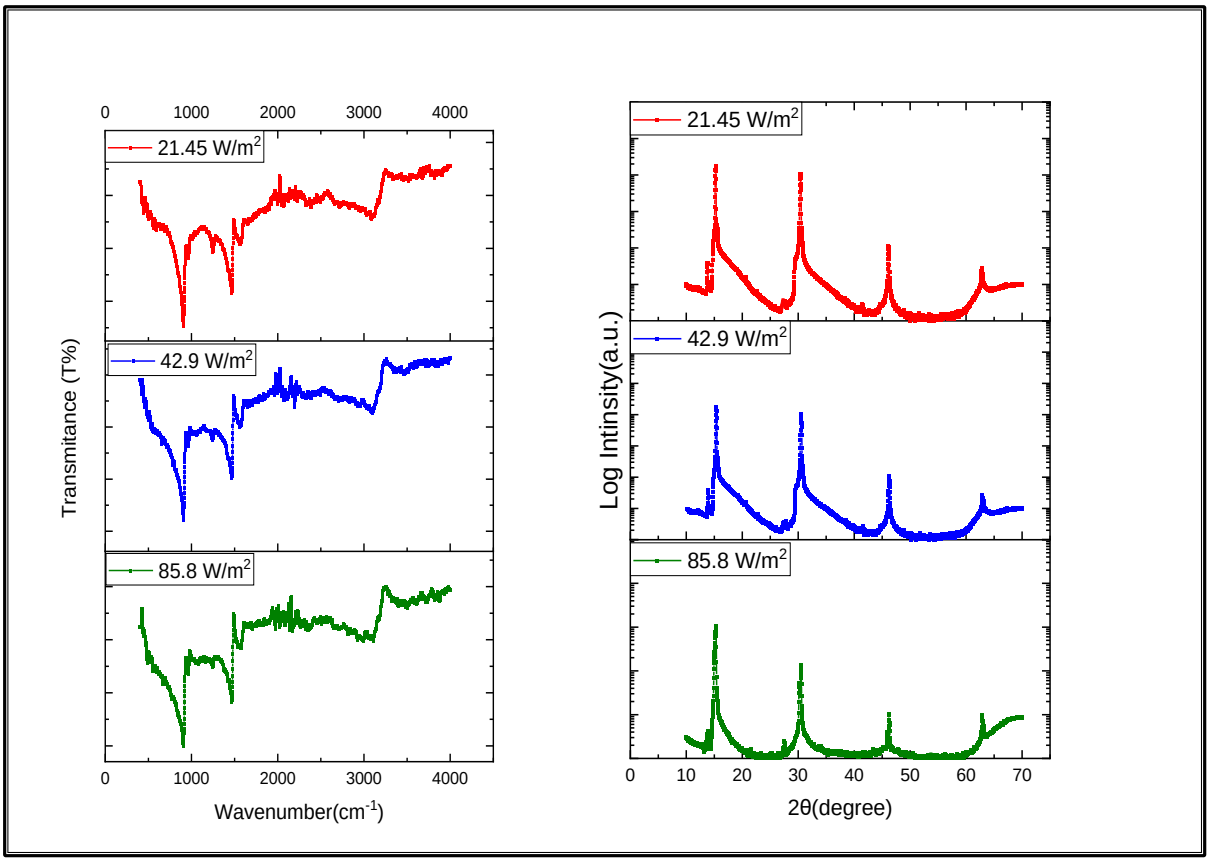

Figure 8.1: (a) FTIR analysis, and (b). Semi-log plot of XRD diffraction pattern for $MAPbBr_3$ single crystal after expose to different light intensity over 100 minutes, both indicating no change in the crystal structure

Furthermore, the results for the FTIR also confirm that there was no structural instability in the $MAPbBr_3$ single crystal for all three light intensities, as indicated from a comparison between samples exposed to the different light intensities for a period of 100 minutes (see Figure 8.1 (a)). It was observed that there are no bonds missing, forming or even shifting during the full 100 minutes after expose to different light intensities. Further experiments, using SEM images were performed on the crystal before and after exposure to light without a filter (85.8 W/m^2).

It was observed that no material degradation took place (see Table 8.1). While full solar irradiation can degrade perovskite materials in the ambient condition, there was no observable change on $MAPbBr_3$ perovskite single crystal bulk using FTIR, XRD and SEM when the crystal was exposed to light for 100 minutes.

Table 8.1: SEM images for $MAPbBr_3$ single crystal before and after exposure to unfiltered light (85.8 W/m^2) over100 minutes showing no difference in surface appearance.

Light	Before expose to the light	After exposing
Without filter	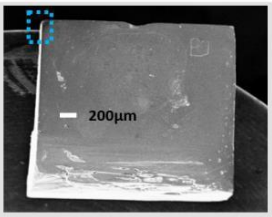	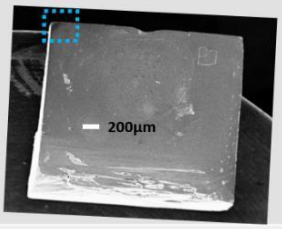
	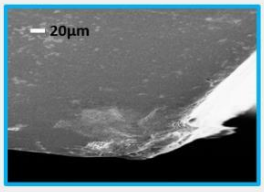 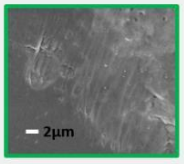	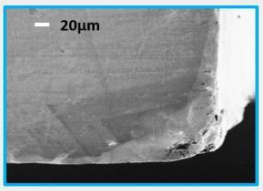 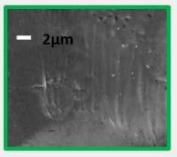

8.2 Photocurrent Transients

Photocurrent transient will show the effect of both light and dark conditions being applied intermittently; the idea is to reveal the recovery of the material, in reference to stretching and recovery of bonds, under the dark condition by using Ag/MAPbBr3/Ag as a device structure.

This transient measurement can reveal mechanisms including the generation of current and the recombination of charges in perovskite materials [1].

Three light intensities were switched on and off over a period of time at a constant bias of 5 volts. The light intensities were 21.45, 42.9 and 85.8 W/m^2 which were provided by using the filters ND4 and ND2, and without a filter, respectively. The intermittent timings for switching the light on and off were 4 minutes, 2 minutes and 30 seconds. This has previously been tested by Shaikh (2016) who tested photocurrent transients for a photodetector device with $MAPbBr_3$ single crystal, and Fang et al. (2015) who did the same with $MAPbI_3$ single crystal[2,3]. However, white light was used for both studies, in the present research a solar simulator was used.

The results show that in the case of a high-power light intensity (85.8 W/m^2), the photocurrent is consistently high for all three on-and-off light time intervals. However, there are observed differences in the shape of the peaks; for the 4 minute on-and-off interval there was an observed decrease in the photocurrent density at each subsequent peak under the light condition (see Figure 8.2 (a)), where the time was decreased to 2 minute on-and-off intervals the photocurrent density remained stable for each peak under the same light condition (see Figure 8.2 (b)). At the 0.5-minute time interval, again under the light condition, there was a gradual increase in photocurrent density for each peak. For the first peak there was and observed sudden peak, indicated in Figure 8.3 (c). An explanation for the anomalous transient photocurrent behaviour is trapping/detrapping at the interface between metal and active layer. Upon application of the light. there is an accumulation of charge as a result of a non-equilibrium of transport of charge carriers in the device, leading to an accumulation of charge which redistributes the electric field [4-10]. As the illumination continues the concentration of charge carriers at the interface will continue until the rate of this migration is balanced by the rate of transfer across the interface

and recombination (charge trapping and de trapping), creating a steady state concentration [4-10]. When the light is switched off suddenly there is a rapid decrease in the flow of charge carriers, however, extra charge carriers continue to migrate to the surface and could become trapped, and because there is no light the magnitude of the de-trapping process could be decreased, and it is the resulting trapped carriers that cause the cathodic current overshoot [4-10].

Where there was a longer exposure to light, (4-minute intervals) each of the observed peaks showed a decrease in the current. In consideration of the mechanism described in the above, a longer exposure to light would produce more hole and electrons which would accumulate at the surface, the corresponding rate of extraction would not be sufficient to achieve the aforementioned steady state concentration, therefore, there will be an accumulation of these charge carriers at the interface which would lead to the observed decrease in photocurrent density for each peak (see Figure 8.2 (a)). Where there is a decrease in the light exposure time to 2-minute intervals, an increase in the current is observed which then stabilises, reflecting achievement of a steady state concentration. This can also be attributed to the abovementioned process, less exposure to light means less accumulation of charge carriers at the interface allowing the extraction rate of the electrode to achieve the steady state, in other words the extraction and recombination of charge carriers in the electrode is equal to the rate of arrival of these charges at the interface.

Under the shortest light exposure, at half minute intervals, there is a distinctive shape observed in the curve which reflects an exponential increase in the photocurrent density. One observation of this phenomena is that whatever the cause is, it takes place before the optimal photocurrent

density is achieved, as opposed to the other two photocurrent transients (4 minutes and 2 minutes) where the respective phenomena occurred after the optimal photocurrent density was achieved.

This would suggest that the applied current and light created conditions that subsequently led to those phenomena, however, in the case of the half-minute photocurrent transients the phenomenon, i.e. the exponential increase in photocurrent density, occurred before the optimal photocurrent was achieved. Therefore, this could be attributed to conditions that were present before the application of current and light. An explanation for this observation is related to the period of darkness, under the half-minute photocurrent transit the period of darkness is less (i.e. 0.5 minutes as opposed to 2 or 4 minutes) and there would be less time for the charge carriers to de-trap through the process of drift whereby the charge carriers drift from the trap sites to the electrode. This would mean that not all of the charge carriers would have drifted and would remain accumulated at the interface, when the light is switched on the presence of these charge carriers will initially cause a decreased photocurrent density until they transfer to the electrode. This idea is supported by the fact that although there can be a fast recovery of light-activated trap states in the dark at less than one minute [11], this is not a full recovery which suggests that some charge carriers do not fully dissipate.

There is the observation that no matter the length of the photocurrent transit exposure, the optimal photocurrent density will always be reached. For the ND2 light intensity the peaks showed the same patterns for all three photocurrent transients which means that the abovementioned mechanisms also apply. However, for the lowest light intensity, ND4, the peaks revealed very little increase in photocurrent density. It is important to note that for all three peaks for each photocurrent transit there was an observed sudden peak before the curve

settled to a steady state. An explanation for this observation is that the presence of generated charge carriers is represented by the initial peak in the current, specifically, the charge carriers, albeit fewer in number, combine with the opposite charge carriers creating electron / holes pairs causing the increase in current. However, this increase is short-lived because of the fewer number of charge carriers and therefore, the observed steady state is achieved immediately afterwards, when the light is applied for the next photocurrent the process is repeated.

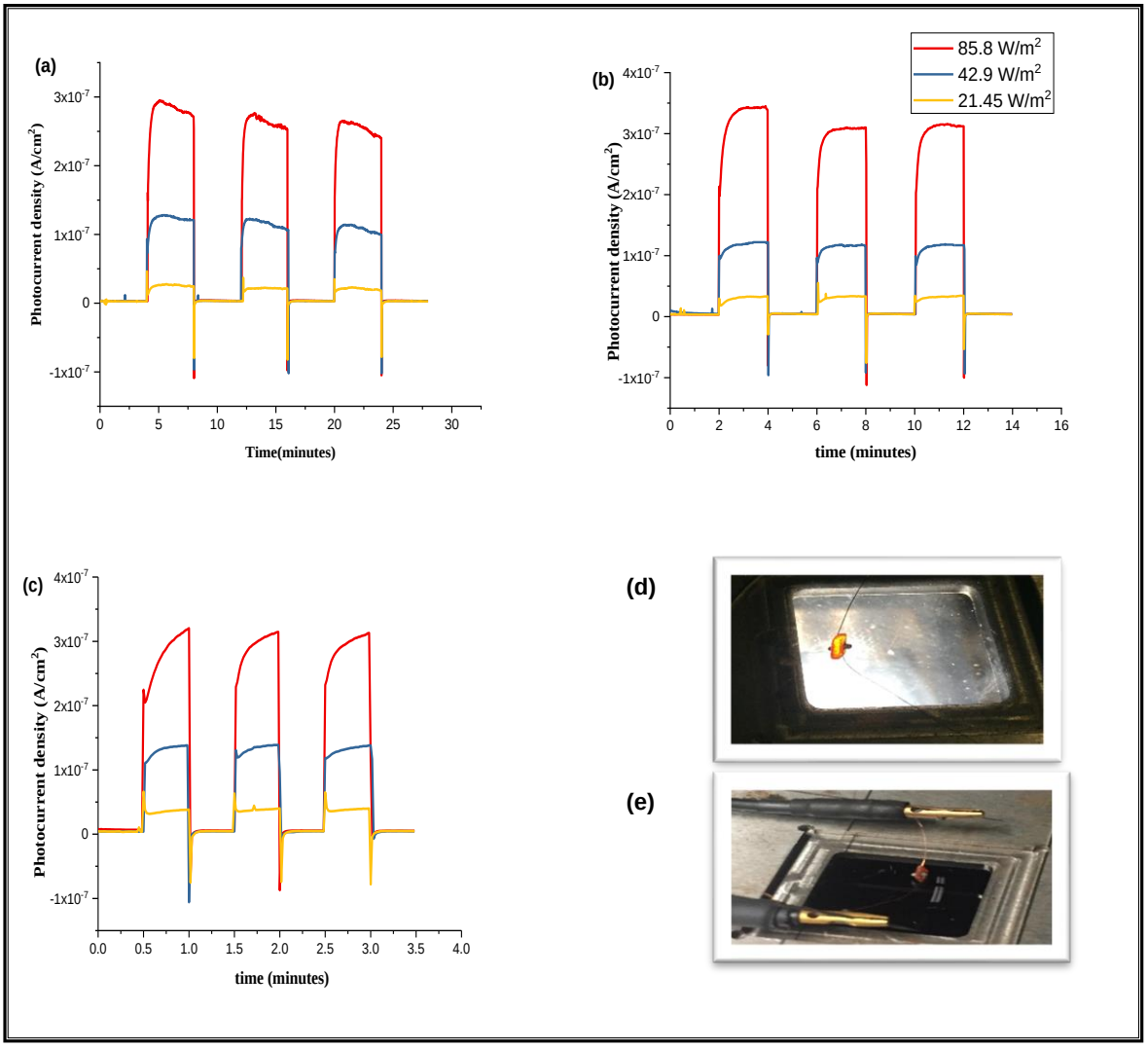

Figure 8.2:Photocurrent transients for different light intensities 21.45,42.9 and 85.8 W/m^2 (a) 4 minutes, (b) two minutes, and (c) 30 second time intervals showing higher light intensity results in higher current, and that the steady state is achieved when trapping and detrapping reaches equilibrium (d) device under light condition, and (e) device under dark condition

An additional observation from the results is that for the higher and medium light intensity the time exposure has an effect on the mechanism, evidenced by differences in the shape of the peaks and the associated mechanisms, however, the peaks for lower light intensity are not affected by time exposure to light as evidenced by consistent shape for all three photocurrent transit times. This means that a lower light has a greater effect on the mechanism than time of exposure.

8.3 Photocurrent at Constant Light Exposure

Measuring the photocurrent density response for a constant exposure over time leads to understanding the effect of light intensities on the behaviour of the current in the $MAPbBr_3$ crystal by using the same architecture structure (Ag/$MAPbBr_3$/Ag). Exposure to light has been tested for a photodetector device structure with a $MAPbBr_3$ single crystal using IV measurements, however, this was limited to full solar radiation, the present research extends on this to include three different light intensities.

Under the highest light intensity as expected an increase in the external electric field correlated with an increase in the current (see Fig 8.3 (a)). It was observed that over the 2 hours' time period there was a gradual decrease in the current observed for all applied voltages and the pattern of this decrease was almost identical between them, this would suggest that the process of degradation is the same for all voltages. However, the current output was not correlated proportionally with the electric field input, whereby an increase in the electric field was associated with a slower increase in the current (see Figure 8.3 (a)).

For the ND2 and ND4 there was an observed steady state achieved at the lowest applied voltage. As has been stated before, a steady state is achieved when there is an equilibrium between the extraction rate and generated charge carriers. This would suggest that at a certain level of light intensity it is no longer possible to achieve a steady state, this is further evidence of the effect of light intensity on the photo instability of the single crystal.

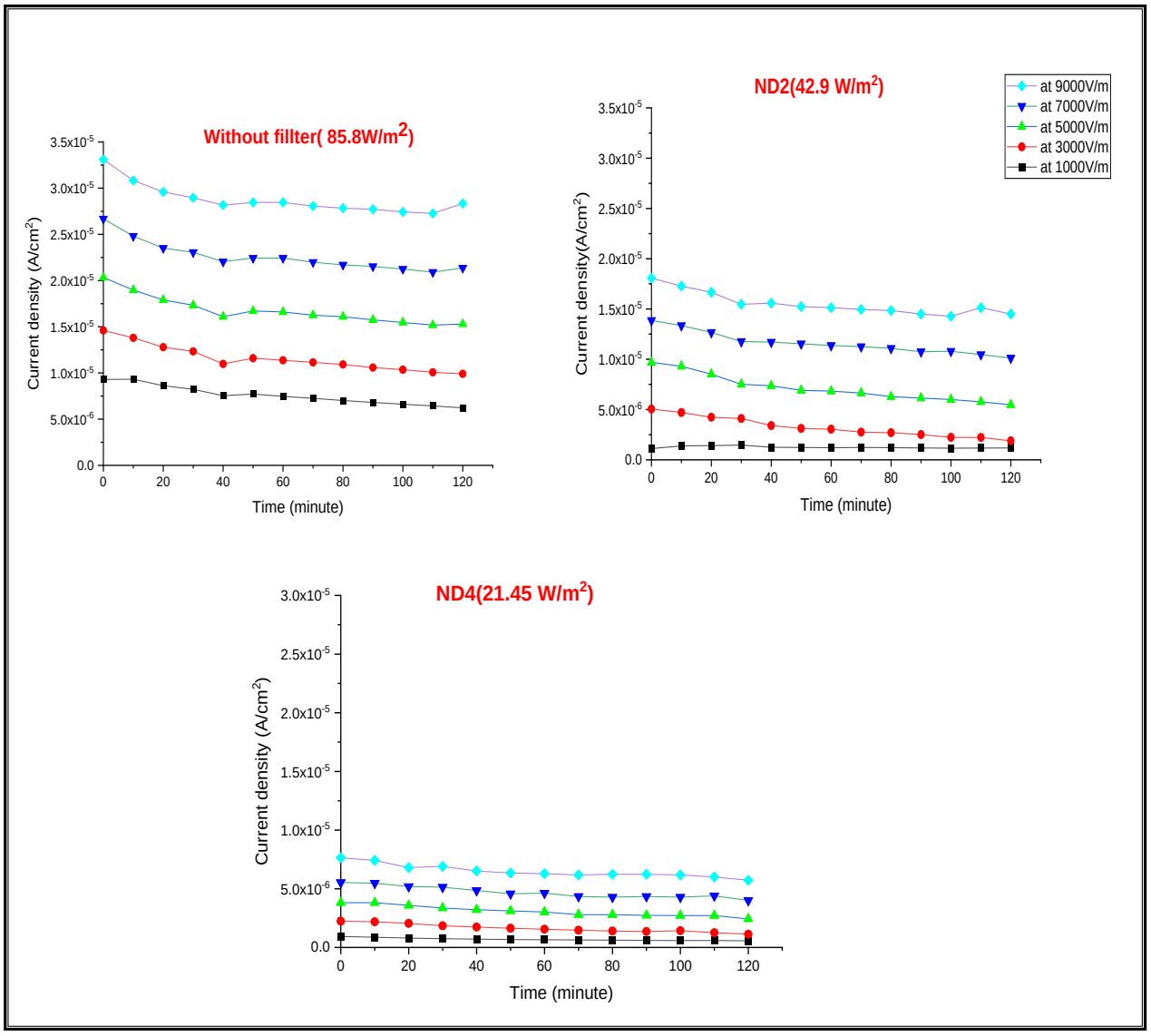

Figure 8.3: Photocurrent density for two hours exposing to different light intensities (a) without filter, (b) ND2, and (c) ND4 using solar Simulator at different electric fields (1000, 3000, 5000, 7000 and 9000 V/m) showing a lower light intensity results in a steady state

In these experiments it has been shown that both the applied external current and the applied light, under various intensities and various time periods, have an effect on the photo instability of the single crystal. Specifically, the contribution of light to photo instability has been shown by the differing results for each light intensity in terms of the rate of increase of resistance, shown for different applied voltages for different light intensities, and the fact that light intensity has been shown to have an effect on the achievement of a steady state.

8.4 Summary

In Chapter six hysteresis was revealed as a result of mechanisms associated with the electrodes, in Chapter 7 heat alone was found to have an effect on hysteresis and thus stability. Here the photostability of the perovskite was examined under differing light conditions, using solar simulator of light intensity 85.8 W/m^2. Using optical and structural measurements no structural instability was found. However, where photocurrent transients were applied a notable pattern occurred suggesting recovery mechanisms that took place during dark periods. Light was also shown to have a mediating effect on stability against the inputted current. Overall, light contributed to instability of the device in operating conditions due to its effect on charge carriers resulting in hysteresis. Therefore, the chapter has revealed that light has an effect on perovskite stability and on the overall functionality of perovskite $MAPbBr_3$ as a photoconductor device.

8.5 References

[1] R. Gottesman et al., "Dynamic Phenomena at Perovskite/Electron-Selective Contact Interface as Interpreted from Photovoltage Decays", Chem, vol. 1, no. 5, pp. 776-789, 2016.

[2] P. Shaikh et al., "Schottky junctions on perovskite single crystals: light-modulated dielectric constant and self-biased photodetection", Journal of Materials Chemistry C, vol. 4, no. 35, pp. 8304-8312, 2016. Available: 10.1039/c6tc02828d.

[3] H. Fang et al., "A self-powered organolead halide perovskite single crystal photodetector driven by a DVD-based triboelectric nanogenerator", Journal of Materials Chemistry C, vol. 4, no. 3, pp. 630-636, 2015.

[4] P. Calado et al., "Evidence for ion migration in hybrid perovskite solar cells with minimal hysteresis", Nature Communications, vol. 7, no. 1, 2016.

[5] N. Alwadai et al., "High-Performance Ultraviolet-to-Infrared Broadband Perovskite Photodetectors Achieved via Inter-/Intraband Transitions", ACS Applied Materials & Interfaces, vol. 9, no. 43, pp. 37832-37838, 2017.

[6] L. Peter, A. Walker, T. Bein, A. Hufnagel and I. Kondofersky, "Interpretation of photocurrent transients at semiconductor electrodes: Effects of band-edge unpinning", Journal of Electroanalytical Chemistry, vol. 872, p. 114234, 2020.

[7] L. Hu, X. Liu, S. Dalgleish, M. Matsushita, H. Yoshikawa and K. Awaga, "Organic optoelectronic interfaces with anomalous transient photocurrent", Journal of Materials Chemistry C, vol. 3, no. 20, pp. 5122-5135, 2015.

[8] S. Karak et al., "A perovskite based plug and play AC photovoltaic device with ionic liquid induced transient opto-electronic conversion", Journal of Materials Chemistry A, vol. 4, no. 23, pp. 9019-9028, 2016.

[9] S. Chakrabarty, G. Das, M. Ray and S. Hossain, "Optically enhanced trap assisted hysteretic I-V characteristics of nanocrystalline silicon based p-i-n heterostructure", 2020. .

[10] L. Peter, "Energetics and kinetics of light-driven oxygen evolution at semiconductor electrodes: the example of hematite", Journal of Solid State Electrochemistry, vol. 17, no. 2, pp. 315-326, 2012.

[11] W. Nie et al., "Light-activated photocurrent degradation and self-healing in perovskite solar cells", Nature Communications, vol. 7, no. 1, 2016. Available: 10.1038/ncomms11574.

Chapter 9: Conclusion and Future Work

This research has emphasised the benefits of hybrid halide perovskites for use in photonic devices and specifically, $MAPbBr_3$ as a single crystal for such devices including photodetectors. With increasingly cost-effective approaches for optoelectronic devices and the need to produce more efficient materials, this has led to the third generation of photovoltaic materials and devices including organic and hybrid devices. However, in addition to efficiency there is also the need to understand the stability of these new materials since they will operate under conditions that include exposure to heat and light as part of their operation.

Hybrid halide perovskites have been shown to have a favoured symmetry and the optical absorption properties required for PV devices. However, the stability of these materials has not been fully investigated which has led to a lack of understanding of the mechanisms of stability in these materials as photonic devices. Initially, a description and justification of the use of halide perovskites, specifically hybrid halide perovskites as a single crystal for use in PV devices was presented in this research before moving on to investigation material stability.

The literature has shown that the electrical properties of hybrid halide perovskites, as a functional attribute of photonic devices, are affected by the structural stability of the material, which provided further justification for examining structural stability of the $MAPbBr_3$ single crystal. Towards understanding material stability, the research considered established mechanisms of material degradation related to heat and light conditions and proposed new mechanisms for instability based on the results of experimentation.

The thesis started with an introduction to semiconductors generally and perovskites specifically, as intrinsic semiconductors before a more detailed description was provided of metal halide perovskites as the material tested in this study, namely, the $MAPbBr_3$ single crystal. The chapter on growth and characterisation offered an insight into the stability of the single crystal, it mainly served to justify the use of the single crystal in applications through presentation of its intrinsic properties. In addition, single crystals were introduced, and their optoelectronic properties as a justification for investigation of their material stability under heat and light conditions was provided.

Although there are a number of different mechanisms offered for the I-V hysteresis observed for the $MAPbBr_3$ single crystal, there was a need for explanation of different hysteresis for the different electrode materials used. Electrodes, and specifically electrode material, can have an effect on the mechanisms within a photonic device, specifically, this manifests as different hysteresis for different electrode materials. There was a need to select a suitable electrode material in terms of consistency in results and the least amount of hysteresis in order to minimise the obscuring of electrical mechanisms taking place within the perovskite material and at the electrode interface, both of which were relevant to material stability. Therefore, a number of different electrode materials and material combinations were tested for hysteresis. Specifically, towards an understanding of the stability and degradation mechanisms that take place in the device, it was necessary to select a material for the electrodes that had low resistance, low hysteresis and be stable. However, the process of selecting the right material from a number of choices in itself revealed the mechanisms that took place within the single crystal, which could be affected by the work function of the electrode material and the interactivity of the material with that of the single crystal, all of which gave insight into interface mechanisms in such devices. The differences in I-V hysteresis for the different

electrode materials and an understanding of the associated mechanisms led to the choice of silver as an electrode material because of low hysteresis in I-V measurements. This process of selection served to offer a better understanding of the possible mechanisms within the crystal itself. Therefore, a contribution of this research was an understanding of how different electrode materials had an effect on charge extraction and other interface mechanisms. An associated contribution of the present research was a comparison between a number of different electrode materials in terms of current and I-V hysteresis.

The result of experimentation for electrical properties revealed the involvement of the interface charge as a mechanism for the hysteresis. In fact, subsequent experimentation revealed that the events that took place at the interface were instrumental in the performance and associated stability and degradation of the material. This not only addressed the intrinsic mechanisms within the material itself but also the role of the electrode as part of the interface. The interface was instrumental in observed hysteresis and material degradation in a number of different ways which included extraction rates, trapping and de-trapping of charge carriers and recombination of ions forming new compounds at the interface.

Furthermore, the surface was significant where it was observed in the crystal alone that there was surface degradation as a result of high temperatures causing sublimation, and increasing temperatures led to an increase of this degradation into the bulk of the material. However, evidence of material instability was only observed at much higher temperatures. This suggests that instability that occurred at much lower temperatures in the device structure was attributed to mechanisms that are a result of this structure, particularly those that involve the interfaces between the active material and the electrodes. What is relevant, and has been contributed in this research, is the device structure and associated electrode materials as factors for material

instability, found at much lower temperatures, is pertinent to the single crystal in application as a photonic device.

Temperature was found to have a significant effect on the stability of the $MAPbBr_3$ single crystal in a number of different ways. This was evidenced by sublimation through a loss of the organic component of $MAPbBr_3$ as well as inorganic bromine and phase changes.

The research contributes to revealing phase changes at high temperatures for $MAPbBr_3$ single crystal. Phase changes indicated the effect of heat on material stability where it was found that the length of exposure to heat was significant in effecting phase changes, even for lower temperatures. While this mechanism has been established for other materials the contribution of the present research is identification of heat degradation phenomena for the $MAPbBr_3$ single crystal. Another contribution related to the rate of heating and longer exposure to heat is that at 5°C/minute there is an ordered phase change, as opposed to 10, 15 and 20°C /min which exhibited disordered phase changes. This has implications for applications where it is recommended that the crystal not be heated at a higher rate than 5°C/ min. Furthermore, understanding phase changes and temperatures contributed to recommendations for heating for the achievement of a stable transition phase.

Experimentation with temperature included the single crystal alone and revealed surface degradation, pointing further to the significance of the surface layer. Significant evidence of the effect of heat on material stability at the surface was the sublimation of MABr from the crystal resulting in a 95 % weight loss of the material. The specific process of how this occurred was determined to be an initial decomposition of the organic component CH_3NH_3Br followed by a loss of bromine from the inorganic component leaving lead behind. A contribution of this

research was a verification of the lead residue through flame test and Atomic Absorption Spectroscopy (AAS).

As a contribution of this research, degradation was observed at a much lower temperature, 120 ˚C over a period of six hours, using UV-Vis, FTIR, XRD, SEM and I-V measurements. Heat was shown to have an effect on the band gap. Longer exposure to heat having an effect on stability was also found using UV-Vis, where a constant temperature was applied over a six-hour period a decrease in the band gap was observed. It was revealed that there was a relationship between temperature and band gap, whereby an increase in temperature led to a narrowing of the band gap. Furthermore, the activation energy increased with an increase in temperature leading to degradation due to a break in the energy barrier at the interface and an associated flow of electrons. This was attributed to increasing temperatures leading to a decrease in the bandgap. Therefore, a contribution of this research is that this structural degradation was observed at these temperatures.

Another contribution of the study was a comparative understanding of different light intensities on material instability for both structural and electrical properties of $MAPbBr_3$ single crystal. Through optical and structural measurements, it was shown that light did not have an effect on material stability for different light intensities. As a contribution, the lack of effect on material stability was also found for solar simulator, in contrast to other studies for perovskite materials as a device structure.

Generally, longer exposure to light was found to have an effect on the stability of the material evidenced by a decrease in current, this was evident for all applied voltages. While this confirmed other studies, the additional contribution of this research, through the application of

different light intensities, showed that these light intensities had different effects on material stability, this was found to be the case for photocurrent transient and constant light exposure. Therefore, this raises a question about what is responsible for the instability in this case, it may be the interaction at the electrode interface, or it may be the different effect of light on the flowing of charge carriers inside the crystal, this could be resolved in future research.

9.1 Future Research

In reference to the fact that there can be a combination of ions forming new compounds at the interface, it has been suggested in this study that this could be a possible cause of hysteresis. The combination of ions observed in this research resulted in new compounds, a future study could investigate if there is relationship between IV hysteresis and a new molecules were formed.

Given that the material used for the electrodes was significant in the instability mechanisms mentioned in this research. Even though silver was found to be optimal, carbon was not sufficient for the device structure. Future research could investigate further electrode materials that would give optimal stability to the single crystal device structure. This could include experimentation with multiple layers of different materials to consider the effect on work function, chemical reaction and interactivity at the interface.

The single crystal alone showed that there was significant surface degradation at higher temperatures due to the sublimation of the organic component MA leaving behind a lead bromide residue. Future research could remove this surface residue and test the exposed crystal

below in order to determine if there is material degradation beyond the visibly observed degradation. This could provide insight into the process of degradation within the surface of the crystal and could be achieved through a comparison of results with a pristine sample.

Appendices

10.1 Appendix A – List of Chemical Acronyms

$MAPbBr_3$ ..... Methylammonium lead bromine(lead bromide perovskite)

$MAPbI_3$ ..... lead iodide perovskite

DMF .....N, N- dimethylformamide

PTFE…..... Polytetrafluoroethylene membrane filters

AZO… .....Aluminium-doped zinc oxide solution

C……... Carbon solution

$PC_{61}BM$…..... phenyl-C61-butyric acid methyl ester

PEDOT: PSS..... poly (3,4-ethylenedioxythiophene): polystyrene sulfonate solution

10.2 Appendix B – List of Acronyms

PVs ..... photovoltaic cells

LEDs ..... light-emitting diodes

TSSG…..... Top seeded solution growth method

BSSG…..... Bottom seeded solution growth method

AVC ..... Anti-solvent Vapour Assisted Crystallisation Method

ITC… ..... Inverse Temperature Crystallisation Method

MSSC ..... Mesoporous structured solar cell

ETL ..... Electron transporting layer

HTL…..... Hole transporting layer

FWHM… ..... Full width at half maximum

PCE… ..... Power conversion efficiency

FTIR ..... Fourier-transform infrared spectroscopy

UV-Vis ..... Ultraviolet–visible spectroscopy

SEM… ..... Scanning electron microscope

AAS..... Atomic Absorption Spectroscopy

EDS ..... Electron Dispersive X-ray Spectroscopy

XRD… ..... X-Ray Diffraction

TLM ..... Transmission Line Model (or Transfer Length Method

I-V…..... Current-Voltage

TGA… ..... Thermal gravimetric analysis

DSC..... Differential scanning calorimetry

10.3 Appendix C – Supplement Data.

Calculation the $MAPbBr_3$ perovskite as powder plane regarding to XRD diffraction peaks

2θ	θ	$\sin^2\theta$	$\sin^2\theta/\sin^2\theta$	$h^2+k^2+l^2$	hkl	$a^2=\lambda^2\times(h^2+k^2+l^2)/4\sin^2\theta$	a	$d=a/\sqrt{h^2+k^2+l^2}$	θ rad	to be sure calculte d=λ/2 sinθ
14.915	7.4575	0.015309	1	1	100	2.377764	6.231333	6.231333088	0.124049	6.231241033
21.152	10.576	0.031517	2.05872363	2	110	4.755528	6.141818	4.342921128	0.178477	4.342895277
29.881	14.9405	0.063458	4.14514338	4	200	9.511056	6.121265	3.060632516	0.254652	3.060630221
33.566	16.783	0.080029	5.22757855	5	210	11.88882	6.094186	2.725402707	0.28681	2.725403072
37.009	18.5045	0.097082	6.34152459	6	211	14.26658	6.061216	2.474481014	0.316856	2.474481518
43.08743	21.54372	0.130698	8.53735711	8	220	19.02211	6.03204	2.132648308	0.3699	2.132648539
44.27277	22.13639	0.13775	8.99797505	9	300	21.39988	6.232034	2.077344738	0.380045	2.078376232
45.80932	22.90466	0.147122	9.61015089	10	211	23.77764	40.4046851	6.356468	2.010091667	0.39338	2.011415193
48.451	24.2255	0.163823	10.7010974	11	311	26.1554	39.91409636	6.31776	1.90487643	0.416706	1.904876686
53.454	26.727	0.197381	12.8931217	13	320	30.91093	39.15139162	6.257107	1.7354093	0.460365	1.735409354
55.803	27.9015	0.213949	13.975374	14	321	33.2887	38.89793362	6.236821	1.666860471	0.480864	1.666862282

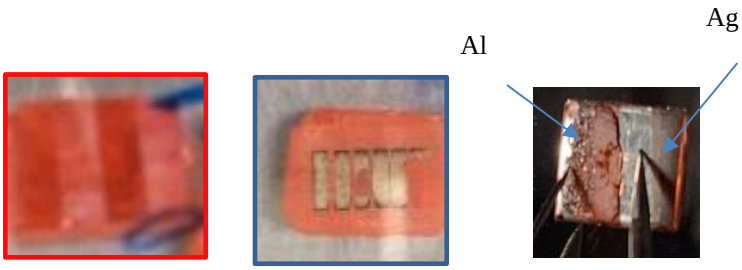

Samples used to test IV measurements (a) Mg, (b) bilayers of Mg/Al,.(c) Al/ $MAPbBr_3$/Ag

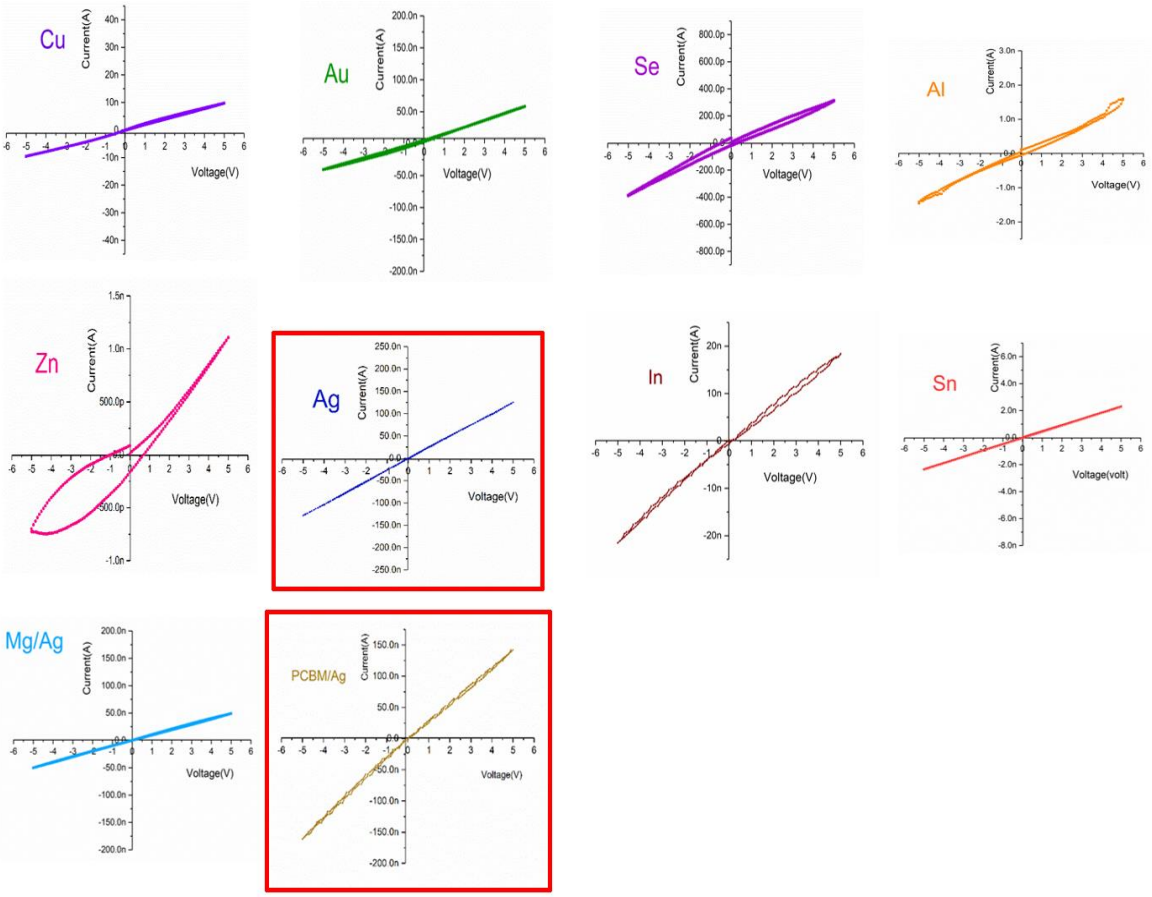

IV curves in linear plot for different metal electrodes which were used for $MAPbBr_3$ single crystal including silver, selenium, tin, zinc, copper, gold, indium, aluminium, Magnesium/silver, and PCBM/silver.

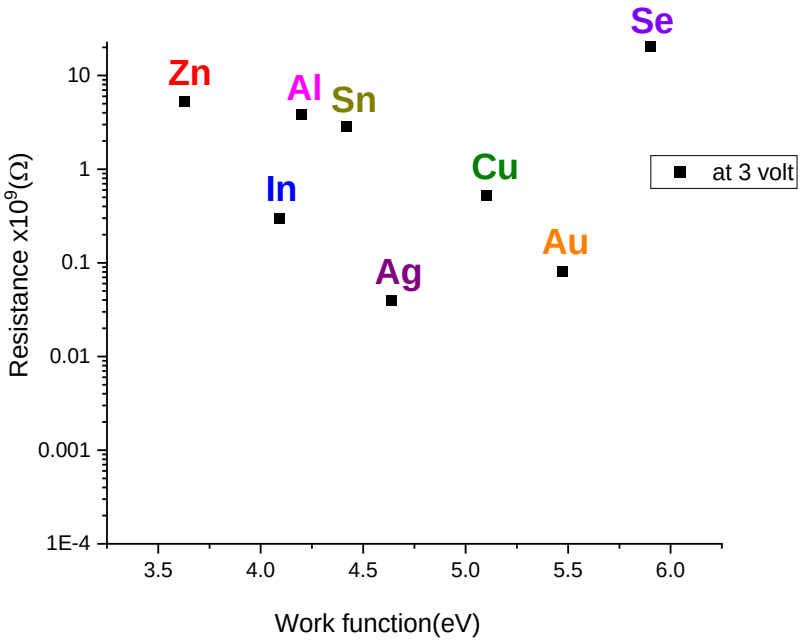

plot curve between work function for different metal electrodes which were used for $MAPbBr_3$ single crystal for and their Resistance at 3 volt

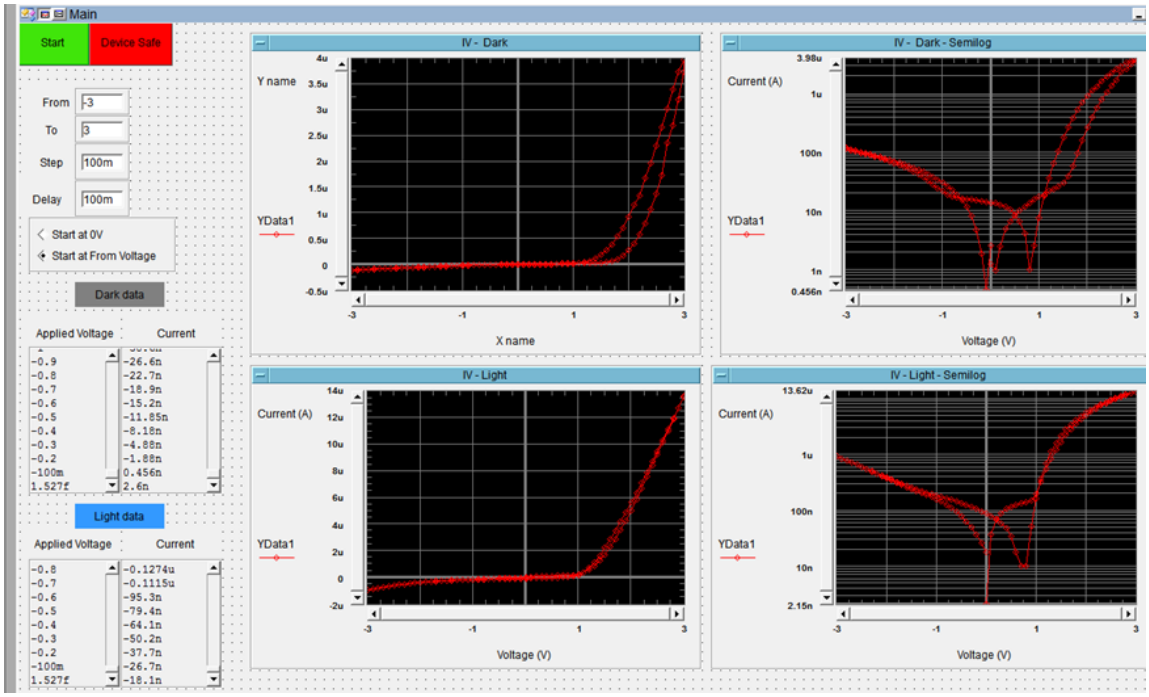

IV curves in linear and log plot for C/$MAPbBr_3$/Ag

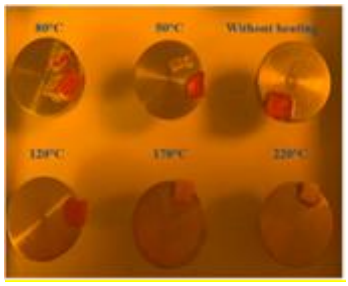

Sample used to record the SEM images for $MAPbBr_3$ after annealing for 6 hours at 24, 50, 80, 120, 170 and 220°C, and more SEM images related to thermal stability

At 50°C

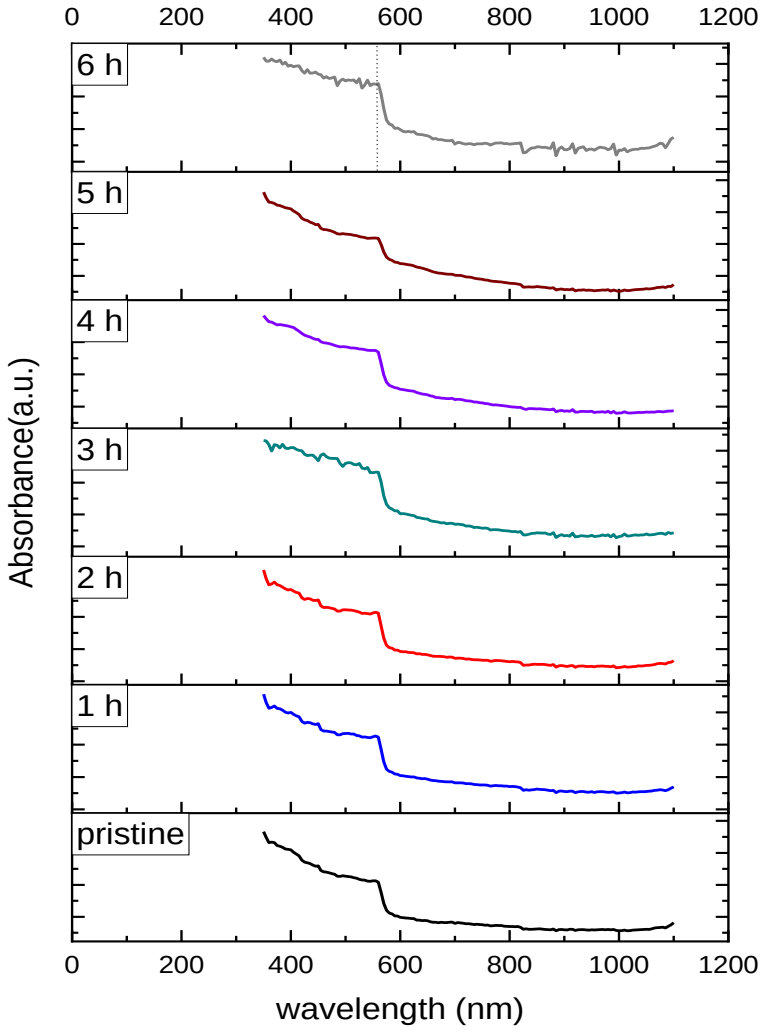

UV-vis analysis of perovskite crystal at 50°C at different duration of heating time 0,1,2,3,4,5,6 hours

At 80°C

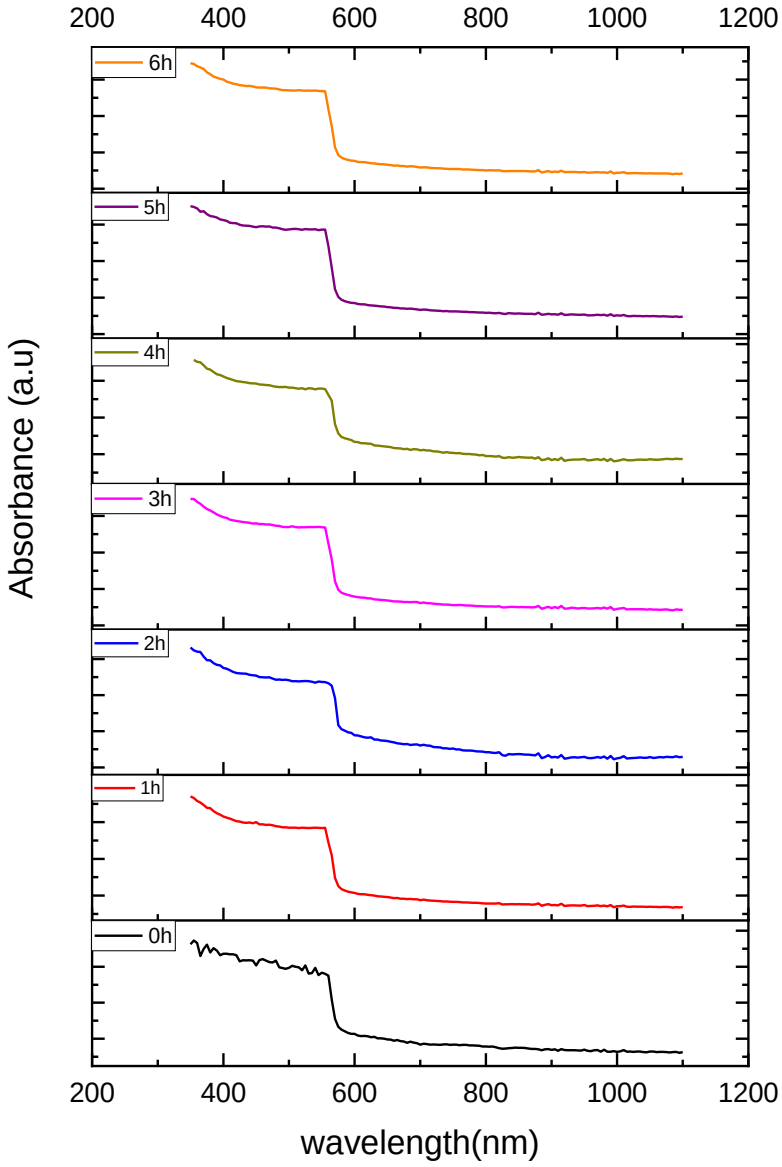

UV-vis analysis of perovskite crystal at 80°C at different duration of heating time 0,1,2,3,4,5,6 hours

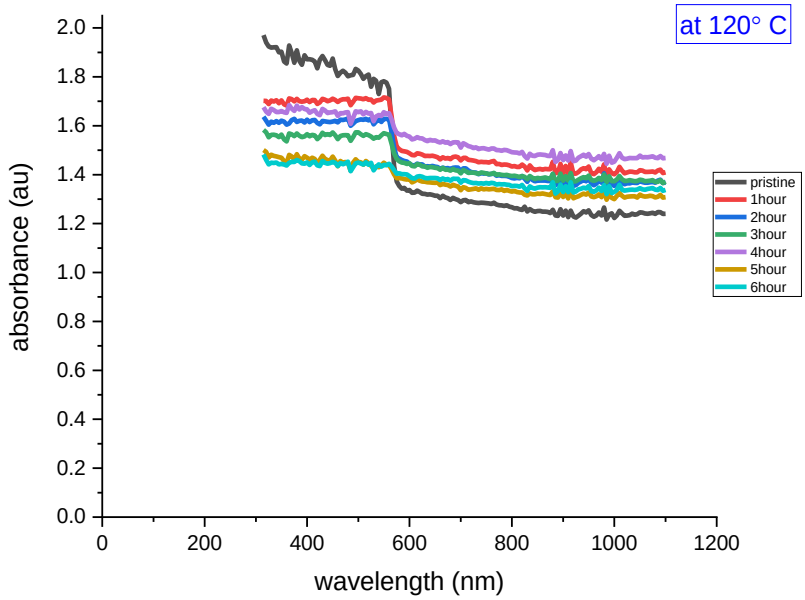

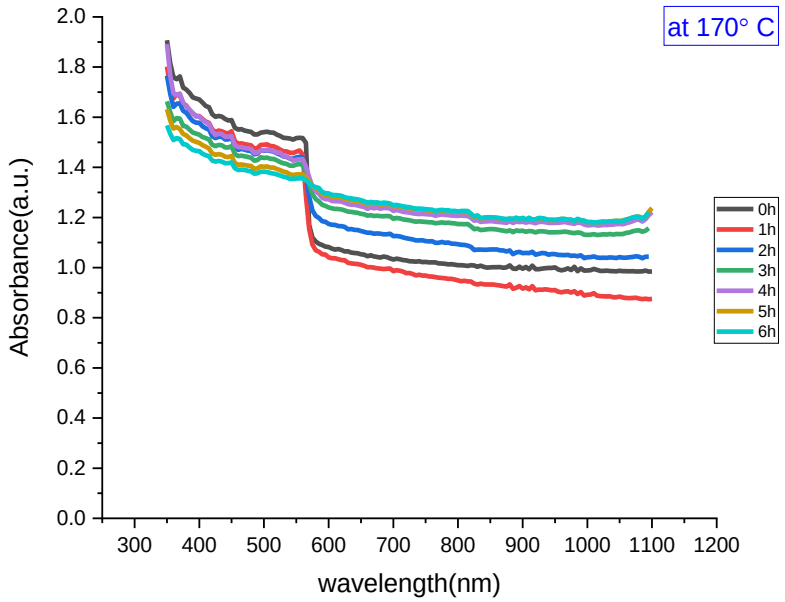

UV-Vis analysis of perovskite crystal at 120 and 170 °C at different duration of heating time 0,1,2,3,4,5,6 hours

At 220°C

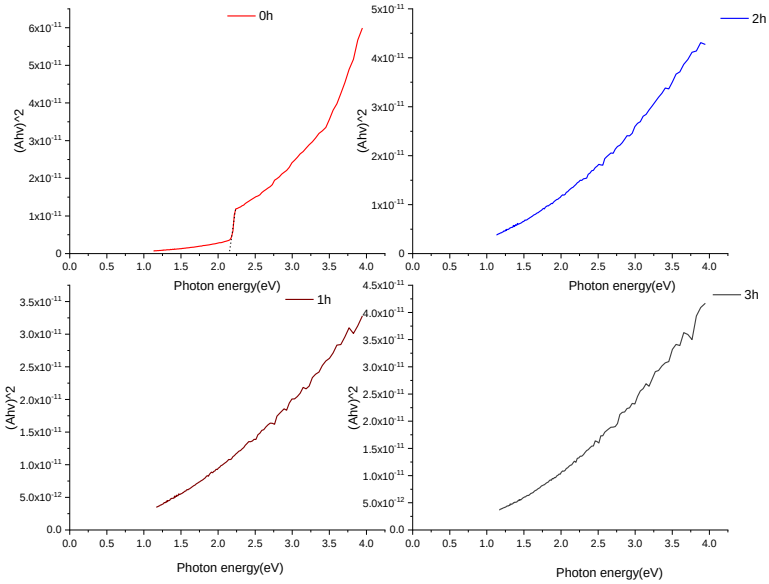

UV-Vis analysis of perovskite crystal at 220°C at different duration of heating time 0,1,2,3,4 hours

---

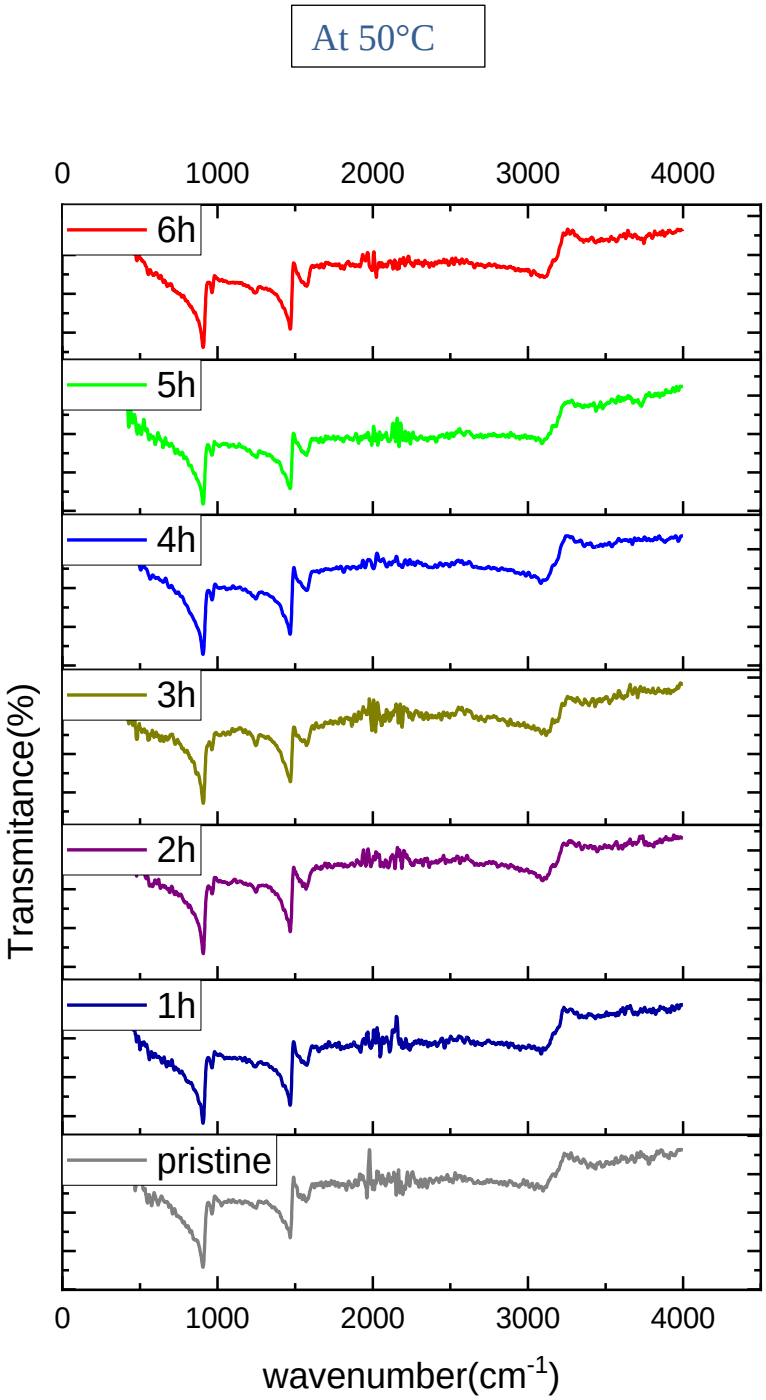

FTIR analysis of perovskite crystal at 50°C at different duration of heating time 0,1,2,3,4,5,6 hours

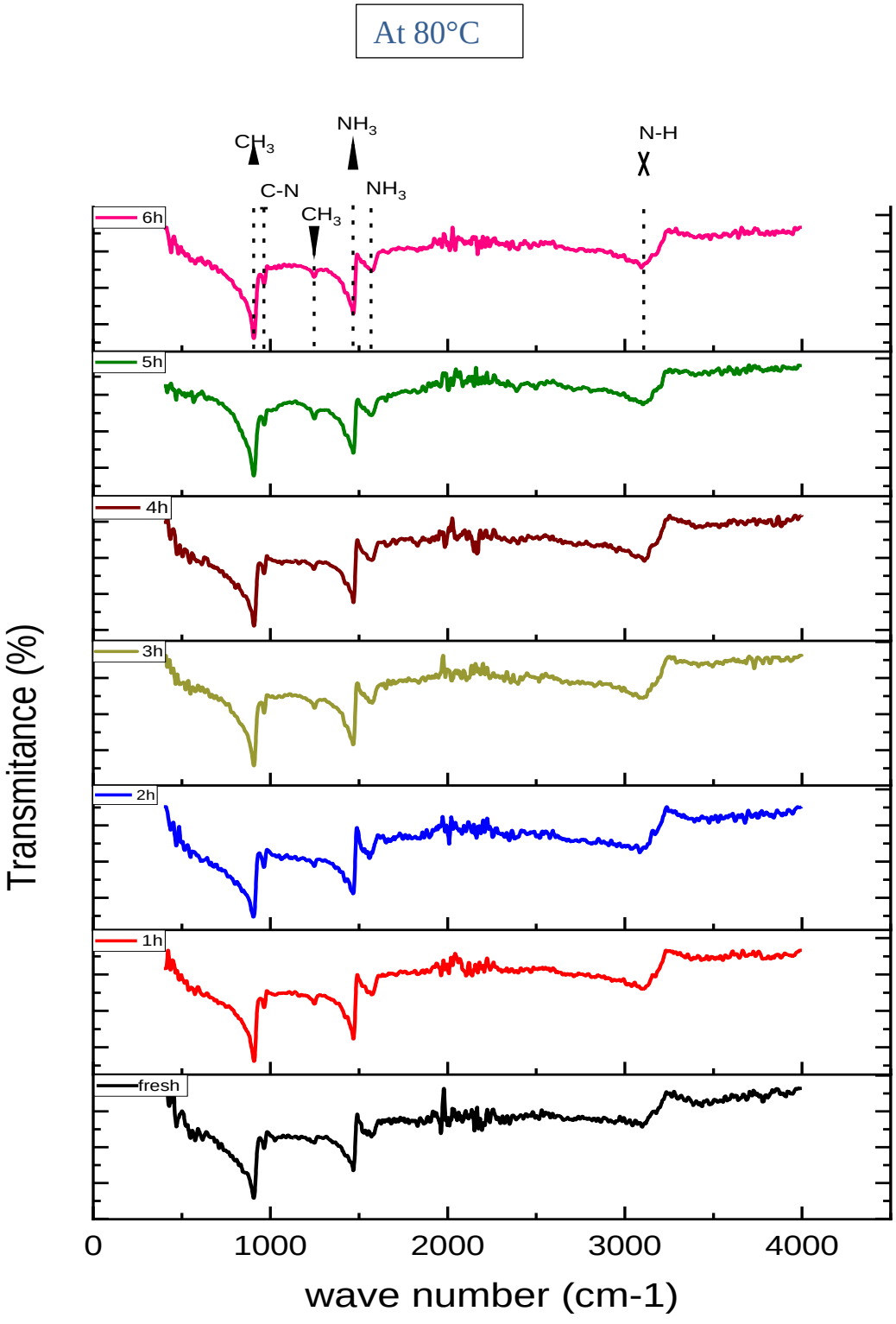

FTIR analysis of perovskite crystal at 80°C at different duration of heating time 0,1,2,3,4,5,6 hours

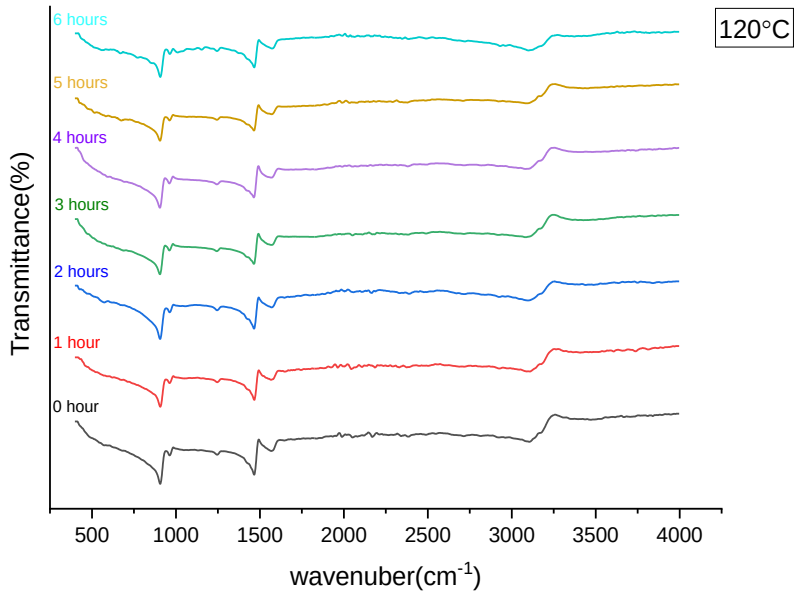

FTIR analysis of perovskite crystal at 120°C at different duration of heating time 0,1,2,3,4,5,6 hours

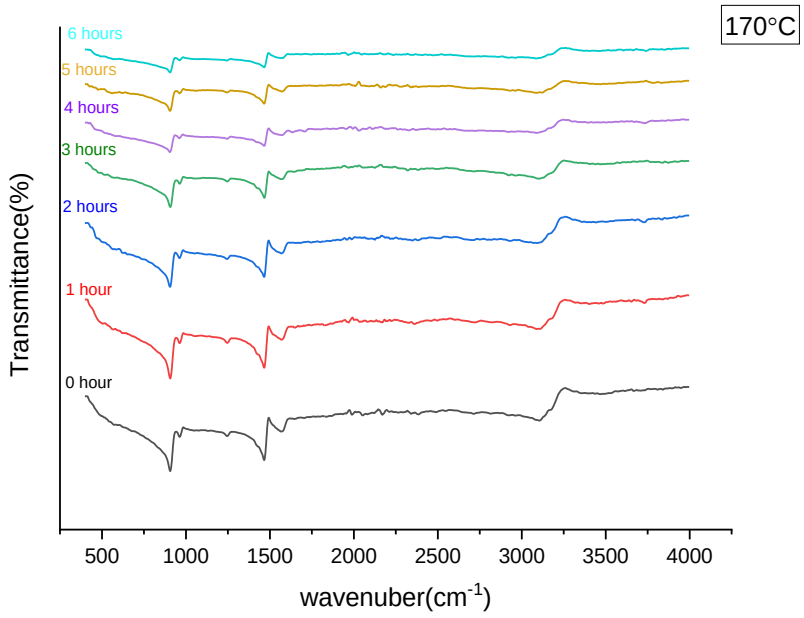

FTIR analysis of perovskite crystal at 170°C at different duration of heating time 0,1,2,3,4,5,6 hours